Roles of cortical tension and cell-cell adhesion during gastrulation of *Xenopus laevis*

David Rozema

Department of Biology

McGill University, Montreal

October 2021

A thesis submitted to McGill University in partial fulfillment of the requirements of the degree of Doctor of Philosophy

Contents

Acknowledgements

First and foremost, I would like to thank my supervisor François. The past seven years of working with you have truly been a pleasure. From your constant willingness to drop anything you were doing to discuss data or answer (at times bad) questions, to your 'pathological optimism', there was never a time where I felt unsupported in the lab. You trusted me to give me the space I needed to grow as a scientist, and I can't thank you enough for the time and effort you have invested in my development as a researcher. I hope this experience was even a fraction as rewarding for you as it was for me. To Leily, you were always a great friend in the lab, and I'm so grateful how gracious you were in trusting me with finishing off the ectoderm-mesoderm transition project. Azam, I don't think I have ever spent so much time with anyone who wasn't a direct family member as I have with you. Your constant willingness to listen to me complain about all aspects of my life and laugh at some terrible jokes, you may be one of the most patient people I have ever met. To all of my lab mates, past and present, thank you for the conversation, the jokes, and any support you have given me. From Montreal, Laura, Nazanin, and Eleyine; from Montpellier, Lina, Guillaume, Laura (a different one), Elise, Valentine, Marie, Marie (a different one), and Rim.

I also thank Craig Mandato, Claire Brown for serving as my committee members and my co-supervisor Paul Lasko for offering invaluable advice throughout these last seven years. I also need to thank the staff of the MRI for all their help with microscopes over the years, and to Marc and Philippe of the animalerie for taking care of our frogs.

Over the past seven years I have been lucky to meet so many incredible people that I can now call my friends (in part thanks to the 3–4 year turnover of PhD students in France…). So, in chronological order. Kathleen, Mark, and Rowan, my fellow first year PhD students at McGill. Thank you for helping me navigate the early stages of this PhD (and extra thanks to Kathleen for still acting as my therapist all this time later). My first French crew, Alicia (British, but close enough), Fanny, and Etienne (who translated my abstract), thank you for making me feel welcome at the CRBM and in Montpellier. Next, Adham, Jesus, Igor, and Lorene, thank you for the lazy hangouts at my place that made me feel like a teenager again. They were always a great

escape. To Fatimat and Kevin for always being ready to have a pint. The Lebanese gang, Adham (same one), Fabie, Baraah, Amani, Jona, and Jacinthe (my adoptive mother), thank you for welcoming me into your little family and being some of the kindest people I have ever met. Yolanda, getting to know you these past few months has been a welcome distraction. There are so many more to mention, but to be brief, if we have ever talked in the hall or had a drink together at a pot, thank you.

Finally, to my family. You have always made me feel so supported and loved. You have provided me with such a large safety net that I have never felt like I couldn't take risks in my life and my career, thank you for this immense privilege. Dad, you were my first scientific mentor, you sitting me at the kitchen table in the fifth grade and teaching me how to form and test a hypothesis was one of the most formative moments of my childhood. Mom, your unconditional love has given me so much confidence I have never felt like I could fail. To the rest of you, thank you for all being smart, reasonable, non-dramatic people. Lee and Rosalie, Marc and Amanda, Josh and Randi, and Eric and Diedre (I won't list all the nieces and nephews due to space constraints and just in case a new one comes around and one day reads this just so they don't feel left out). If anyone reads this and feels like they deserved a shout-out they didn't receive, I'm sorry, I'm sure you did.

Abstract

Morphogenesis is the process by which unstructured embryos generate complex shape from their constituent tissues. This is accomplished by a combination of cellular processes: cell division, cell growth and shape change, cell death, and cell rearrangements. In mesenchymal models of morphogenesis, cell rearrangements are driven by differential cell migration. Using the *Xenopus laevis* gastrula as a model, we first sought to better understand how the migratory properties of cells that drive morphogenesis are controlled. We found that the highly motile mesoderm expresses two negative regulators of RhoA, Shirin and Rnd1, that are absolutely required for development. We then show that overexpression of these regulators in the non-migratory ectoderm is sufficient to induce a migratory switch through down regulation of cortical tension, which we term the 'ectoderm-to-mesoderm transition'. Similar effects are seen at the tissue scale, with both Shirin and Rnd1 overexpression in ectoderm explants decreasing tissue surface tension and provoking migration. I next aimed to examine how mesoderm cells remodelled their cell-cell contacts in response to forces applied by differentially migrating cells. I uncovered that two mechanisms contribute to remodelling: at early stages, the contact is smoothly disassembled through dissociation of cadherin trans bonds, while at late stages, as residual cadherin has condensed and resists dissociation, the final detachment requires rupture of the cytoplasmic link between the cadherin-catenin complex and the actin cytoskeleton. Finally, I show levels of cortical tension can influence how the cell-cell contact is remodelled. Overall, this thesis explored the intimate interplay of cortical tension and cell-cell adhesion in key aspects of morphogenesis in a mesenchymal model.

Résumé

La morphogénèse désigne le processus par lequel un embryon génère une forme complexe depuis les tissus qui le constituent. Ce processus est accompli par une combinaison de processus cellulaires : division cellulaire, croissance cellulaire, modification de la forme, mort cellulaire et réarrangement cellulaire. Dans les modèles mésenchymiaux de la morphogénèse le réarrangement cellulaire est la conséquence de l'hétérogénéité des migrations cellulaires environnantes. Utilisant la gastrulation de Xenopus laevis comme modèle nous avons cherché à mieux comprendre comment les propriétés migratoires des cellules qui conduisent la morphogénèse sont contrôlées. Nous avons montré que le mésoderme (dynamique) exprime deux régulateurs négatifs de RhoA : Shirin et Rnd1 qui sont absolument nécessaire au développement. Nous avons par la suite montré que la surexpression de ces régulateurs dans l'ectoderme (non-migrant) est suffisante pour déclencher la migration grâce à la baisse de la tension corticale, ce que nous désignons par « transition ectoderme vers mésoderme ». Des effets similaires sont observés à l'échelle du tissu, où la surexpression de Shirin et Rnd1 dans des explants d'ectoderme décroit la tension superficielle et provoque la migration. J'envisage par la suite d'examiner comment les cellules du mésoderme remodèlent leurs contacts intracellulaires en réponses aux forces induites par les migrations environnantes. J'ai découvert deux mécanismes contribuant au remodelage de l'adhésion cellulaire : la dissociation des liaisons trans-cadhérines dans les premières phases, et plus tard, quand les cadhérines résiduelles se condensent et opposent une résistance à la dissociation, la rupture des jonctions cytoplasmiques entre complexes cadhérine-caténine et cytosquelette d'actine, étape qui apparaît nécessaire à la dissociation finale. Finalement j'ai montré que les différents niveaux de tensions corticales peuvent influencer la façon dont les contacts inter-cellules sont remodelés. De manière générale, cette thèse explore les interactions entre tension corticale et adhésion intercellulaire pendant la morphogénèse dans un modèle mésenchymateux.

Contributions

Chapter I

I prepared and wrote the entirety of this chapter with the guidance of François Fagotto.

Chapter II

This chapter was published in Plos Biology, where I am the co-first author: Kashkooli, L.*, **Rozema, D.***, Espejo-Ramirez, L., Lasko, P. and Fagotto, F. (2021). Ectoderm to mesoderm transition by down-regulation of actomyosin contractility. *PLOS Biology* 19(1): e3001060. Leily Kashkooli initiated the study and observed the initial phenotype when treating ectoderm with Y27632. She then performed the screen for negative regulators of RhoA, identifying Shirin and Rnd1. She contributed to the initial characterizations of the single cell phenotypes. Specifically, she collected and analyzed some of the data in Figure 2.1., 2.2, 2.3A, 2.4, 2.5 and 2.7. Lina Espejo helped collect and analyze data in Figures 2.1, 2.4, and 2.5, and analyze 2.8. François Fagotto, in addition to conceptualization and design of the study at all stages, collected and analyzed data in Figures 2.1, 2.2, 2.4, 2.5, 2.6, 2.7, and analyzed 2.8. My main contributions were in the conceptualization/design and data collection/analysis for Figures 2.9 and 2.10, though I also collected/analyzed the data in Figure 2.3B-F, performed all the experiments in Figure 2.8, collected some of the data in Figure 2.5, helped perform the experiments in Figure 2.6, and did the western blots in Figure S2.6H. All corresponding supplementary figures were contributed by those who contributed to the main figures. François and I wrote the manuscript with help from Paul Lasko.

Chapter III

This chapter is currently in preparation to be submitted to a journal for publication. Along with François I conceptualized and designed all the experiments found therein. I collected and analyzed all data presented and wrote the manuscript with guidance from François.

Chapter IV

I prepared and wrote the entirety of this chapter with the guidance of François.

Chapter I – Literature Review and Thesis Objectives

Introduction

Morphogenesis is the process whereby precisely shaped and patterned structures are produced from a previously unstructured form. It is fundamentally a mechanical process, requiring the generation and transmission of forces to sculpt the tissues of the embryo. Keller and colleagues (2003) elegantly outlined several questions that must be addressed in order to fully understand the mechanical side of embryonic development. This essay emphasized the importance of both understanding which cells are responsible for generating forces, but also the mechanical environment in which they act, as the outcome of the application of a force depends on the mechanical properties of the tissues subjected to it. It is now clear that the actin cytoskeleton is one of the main machines that produce force in the embryo, and that cell-cell adhesions – which physically couple cells together – allow these forces to be propagated, thus facilitating the scaling of forces from the cell to tissue scale. The research presented in this thesis aims to explore the roles of the actomyosin cytoskeleton, cell-cell adhesion, and their integration within the context of the *Xenopus laevis* gastrula. Though there is a wide variety of actin-based structures that are capable of generating forces, this work primarily focuses on the actin cortex, a key determinant of the mechanical properties of tissues.

The actin cortex

The cortex is a thin layer of dense, cross-linked actin filaments found just below the plasma membrane. Measurements of the cortex estimate that it has a thickness of 0.13-4 um, with an average mesh size of 100 nm (Chugh and Paluch, 2018). It lies ~20 nm below the plasma membrane, which it connects to mainly through ezrin-radixin-moesin (ERM) proteins. In fact, the cortex is the meeting place for many proteins with proteomic analysis identifying over 100 actin binding and regulatory proteins in association with the cortex (Biro et al., 2013). Arguably the most important of which being non-muscle myosin 2 (NMII) that contributes to the overall organization of actin filaments but also generates a critical mechanical property of the cortex through its contractile activity: cortical tension (Chugh and Paluch, 2018). The primary functions of cortical tension are in resisting internal hydrostatic pressure and in determining cell shape,

though its precise regulation contributes to many cellular processes: from rear retraction during cell migration (Cramer, 2013), the mitotic rounding of cells (Taubenberger et al., 2020), pulsed contractions of the junctional cortex to stimulate cell rearrangement in epithelial tissues (Pinheiro and Bellaïche, 2018), and influencing the equilibrium strength of cell-cell adhesions (Maître et al., 2012; Winklbauer, 2015). Another key property of the cortex is that it is a highly dynamic structure, completely turning over on the scale of seconds (Salbreux et al., 2012). This dynamicity allows cells to deform in response to environmental stresses, and if they persist, adjust their shape entirely. Before going further into the details of the cortex and the regulation of cortical tension, I will first review the principle molecular components: actin, myosin, and the primary regulators of actomyosin filaments the RhoGTPases.

Actin

Isolated in solution, actin exists in its monomeric form, G-actin. This is largely due to the fact that spontaneous nucleation of actin filaments is unfavourable owing to the instability of actin dimers and monomers (Pollard, 2016). Additionally, binding of additional proteins can block nucleation: thymosin β4 binds and completely sequesters G-actin (Safer et al., 1991), while binding of profilin blocks nucleation while still allowing the elongation of growing filaments (Pollard, 2016). However, with the help of actin nucleators monomeric G-actin readily organizes into the well-known F-actin form. Actin filaments are double helical polymers whose subunits are all oriented in the same direction, giving rise to filament polarity (Pollard, 2016). The barbed end is associated with growth while the less dynamic pointed end is where disassembly of the filament takes place. These polymers are extremely dynamic, forming and turning over on a time frame of tens of seconds due to the balance of several inputs (Pollard, 2016).

The first step in the formation of an actin filament is nucleation, which is mediated by two well characterized classes nucleators that mediate dramatically different actin network organizations: the formins and the Arp2/3 complex. The formins are a family of proteins that homodimerize to promote the nucleation of actin and the polymerization of linear actin filaments (Breitsprecher and Goode, 2013). Formin-mediated nucleation is inefficient when G-actin is

bound to profilin, though this interaction enhances the rate of elongation of the filament (Breitsprecher and Goode, 2013). Importantly, formins remain bound to the barbed end of the filament as elongation proceeds and prevents the aptly named capping protein from capping the filament and preventing further elongation (Breitsprecher and Goode, 2013). If capping protein does not associate with an actin filament it can in theory continue to elongate as long as enough free G-actin is available (Suarez and Kovar, 2016). Ena/VASP is also capable of elongating linear actin filaments nucleated by formin, and similar to formin, remains bound to the barbed end while doing so, protecting the filament from capping protein in the process (Pollard, 2016). The actin-related proteins 2 and 3 (Arp2/3) complex with five other protein subunits nucleate and organize actin into branched networks (Swaney and Li, 2016). Actin branching occurs when the Arp2/3 complex binds an existing actin filament at 70° to the mother filament, with Arp2/3 themselves acting as the new barbed end where further elongation by G-actin can occur (Swaney and Li, 2016). The extent of actin branching can be regulated by high proportions of profilin bound G-actin as profilin prevents Arp2/3 mediated nucleation (Rotty et al., 2015). Further, since Arp2/3 remains at the branching point, it cannot prevent binding of capping protein and subsequent cessation of elongation.

Notably, neither the formins nor the Arp2/3 complex are natively active but instead exist in autoinhibited states. Interestingly, both classes of actin nucleators can be activated downstream of different RhoGTPases (important molecular switches that are described later): formin activation is generally downstream of RhoA (Kühn and Geyer, 2014) while the Arp2/3 complex can be activated indirectly by Cdc42 or Rac1. Autoinhibition of Arp2/3 can be relieved by the action of either WASp or WAVE, who are also natively inactive. Activation of WASp occurs downstream of Cdc42 (Alekhina et al., 2017) while WAVE (after complexing with other proteins to form the WAVE regulatory complex) can bind Rac1 thus relieving its autoinhibition (Chen et al., 2010).

As the total amount of actin is thought to be constant in a cell, filaments must be continually disassembled in order to maintain a pool of G-actin for nucleation of new filaments or elongation of old. GDP-bound actin naturally dissociates from the pointed end of filaments, but this disassembly can be enhanced through the action of the actin binding protein, cofilin

(Kanellos and Frame, 2016). Cofilin preferentially binds GDP-actin over GTP-actin, which is enriched in the older portions of actin filaments. After binding, cofilin severs the filament producing a new barbed and pointed end (Kanellos and Frame, 2016). Though the new barbed end may be elongated, many are capped allowing them to depolymerize through dissociation of GDP-actin from the pointed end (Pollard, 2016). Other proteins can increase the rate of association of cofilin with actin, or the rate of severing, thus increasing rates of filament disassembly.

Since the pool of available G-actin is limited, it has recently been proposed that different actin networks – linear or branched – may compete for the available monomer (Suarez and Kovar, 2016). This is a critical point in actin biology as different network organizations are associated with different cellular structures and functions. Studies have demonstrated that preventing Arp2/3 complex activity leads to an enrichment of actin in formin-mediated actin filaments (Burke et al., 2014), while the inverse is observed with overexpression of Arp2/3 (Gao and Bretscher, 2008). Further, formin overexpression decreases the amount of Arp2/3 mediated structures (Gao and Bretscher, 2008). Several mechanisms for how this competition may be used naturally within the cell have been proposed (Suarez and Kovar, 2016). Increasing levels of profilin would favour the formation of linear actin networks, as profilin prevents Arp2/3 nucleation but accelerates formin mediated elongation of filaments. Similarly, increasing the amount of capping protein would shift the balance to formin mediated structures as formin can block filament association with capping protein while the Arp2/3 complex cannot. Lastly, inhibition of myosin contractility (an important component of the actin cytoskeleton, discussed further below) destabilizes contractile linear actin filaments thus increasing the availability of G-actin for Arp2/3 complex associated structures (Lomakin et al., 2015).

Finally, the overall organization of the actin network is influenced by cross-linking proteins that can simultaneously bind several actin filaments and stabilize higher order structures (Skau and Waterman, 2015). This requires the presence of at least two actin binding domains (ABDs), the most common of which being the calponin-homolgy (CH) domain. This class of proteins adds a further level of regulation to the organization of actin-based structures, and several will be mentioned in later sections.

Myosin

Myosins are a superfamily of actin-associated motor proteins that convert chemical energy – through the hydrolysis of ATP – into mechanical force (Hartman and Spudich, 2012). In the absence of any bound nucleotide, myosin binds tightly to actin, but upon binding of ATP and its subsequent hydrolysis due to the natural ATPase activity of the myosin head, affinity for actin is drastically increased. This cycle of ATP hydrolysis produces force through the 'swinging' of the myosin neck domain which is referred to as the powerstroke. In its ATP bound form, the myosin neck is primed for the powerstroke, upon actin binding and release of the cleaved Pi after ATP hydrolysis the neck domain forcefully changes conformation displacing the bound actin filament and generating force (Houdusse and Sweeney, 2016). Notably, movement of myosin along the actin filament is polarized, as the powerstroke moves myosin towards the barbed end of the filament. Consequently, the degree of alignment of the actin network will determine how efficiently forces can be generated by myosin contractions (Ennomani et al., 2016). After the powerstroke, ADP is released and myosin releases actin, after which ATP can rebind and the cycle restarts (Houdusse and Sweeney, 2016). A key descriptive parameter of myosin is the duty ratio, that is, how long the myosin head remains bound to actin before the cycle restarts; a high duty ratio is associated with prolonged contractions (Vicente-Manzanares et al., 2009).

The non-muscle myosin IIs (NMIIs) are particularly relevant for this work. The basic unit of NMIIs is three pairs of proteins (Vicente-Manzanares et al., 2009). The heavy chain (NMHC) is composed of the head domain that binds actin and has ATPase activity, the neck domain that acts as a lever for the powerstroke as well as being the binding site for the other proteins of the complex, a long rod domain that is important for both dimerization as well as association with other NMII dimers, and the short-non helical tail which can affect localization of NMII (Vicente-Manzanares et al., 2009). The regulatory light chain (RLC) bind to the NMHC neck region and regulates NMII activity though two phosphorylation sites that, upon phosphorylation, prevents the autoinhibitory folded state while also increasing the ATPase activity of the head domain (Vicente-Manzanares et al., 2009). Finally, the essential light chain (ELC) also binds to the neck region of NMHC and stabilizes the structure of the complex (Vicente-Manzanares et al., 2009). These hexameric complexes can then associate with the rod domains of other complexes in a

head-to-tail orientation, forming bipolar filaments of 10-20 individual myosins (Brito and Sousa, 2020). These filaments are thought to also stabilize actin filaments in addition to their contractile activity (Brito and Sousa, 2020).

The RLC of NMII can be regulated by a number of different kinases. The best characterized being myosin light chain kinase (MLCK) which is activated by calmodulin and directly phosphorylates the RLC (Vicente-Manzanares et al., 2009), and Rho-associated kinase (ROCK), which in addition to phosphorylating the RLC, also inhibits the activity of MYPT1, a phosphatase that targets the RLC (Vicente-Manzanares et al., 2009). Protein kinase C (PKC) negatively regulates NMII activity through phosphorylations of the RLC that prevent association of MLCK and preventing phosphorylation (Brito and Sousa, 2020).

In vertebrates, there are three major isoforms of NMII that are determined by the specific isoform of the NMHC found in the complex: NMIIA, NMIIB, and NMIIC. The isoforms show differences in filament assembly, ATPase activities, and duty ratios as well as tissue specific expression patterns and even intracellular distributions (Brito and Sousa, 2020). Thus, it is unsurprising that the different isoforms have divergent cellular functions. However, it has been proposed that NMII functions that are mediated by its actin crosslinking functions can be compensated for by other isoforms, while functions that depend on its contractile properties are more difficult for other isoforms to replace (Wang et al., 2011). NMIIA is thought to be the main force transducer in the cell, as its knockdown decreases the traction force exerted by cells and reduces the amount of stress fibers and size of focal adhesions (Heuzé et al., 2019; Weißenbruch et al., 2021). Further, there is evidence that the different NMII isoforms are differentially regulated, with activation of NMIIA being downstream of ROCK and MLCK, whereas NMIIB activation was downstream of the GTPase Rap1 (Smutny et al., 2010). While it was initially thought that each NMII isoform arranged into homotypic filaments (Vicente-Manzanares et al., 2009), this view has since been challenged by the discovery of heterotypic NMII filaments composed of multiple NMII isoforms (Beach et al., 2014; Shutova et al., 2014), adding further nuance to the distinct and overlapping roles of the different isoforms.

RhoGTPases

The RhoGTPases are a family of 20 proteins that act as molecular switches, being key intermediates in transducing signals into a wide array of cellular outcomes. The best characterized of the RhoGTPases, RhoA, Rac1, and Cdc42, are also the most conserved across eukaryotes (Boureux et al., 2007), playing critical roles in cell migration (Ridley, 2015), cell-matrix adhesion (Lawson and Burridge, 2014), cell-cell adhesion (McCormack et al., 2013; Ratheesh et al., 2013), and organization of the actin cytoskeleton (Sit and Manser, 2011). RhoGTPases function through a dynamic cycling between an active GTP bound and an inactive GDP bound state and are directly regulated by three classes of proteins (Etienne-Manneville and Hall, 2002). Guanine nucleotide exchange factors (GEFs) activate RhoGTPases by promoting the exchange of GDP for GTP. GTPase-activating proteins (GAPs) increase the GTPase activity hastening the rate of GTP hydrolysis into GDP, inactivating the RhoGTPase. Additionally, the activity and localization of RhoGTPases, GEFs, and GAPs can be altered by post-translational modifications (PTMs) (Hodge and Ridley, 2016). A critical PTM common to almost all RhoGTPases is the addition of lipid groups that facilitate interaction with the plasma membrane (Hodge and Ridley, 2016). The final class of regulators are the guanine nucleotide dissociation inhibitors (GDIs) that inactivate RhoGTPases by binding their lipid interacting regions thus preventing them from associating with the plasma membrane and sequestering them in the cytosol. Due to their diverse impact on cellular processes and their position downstream of many signalling inputs, precise spatiotemporal regulation of RhoGTPases is required and can be accomplished through the collective action of GAPs, GEFs, and GDIs (Denk-Lobnig and Martin, 2019). To provide the relevant context for the discussion of the actin cortex I will focus here specifically on RhoA and its downstream effector ROCK, though Rac1 and Cdc42 will make appearances in later sections.

As mentioned above, ROCK is a key activator of NMII contractility through both the phosphorylation of MRLC and the inhibition of MYPT1. ROCK has three domains, an N-terminal kinase domain, a central region that contains the Rho binding domain (RBD), and the autoinhibitory C-terminal domain that can interact with the N-terminal domain and block its kinase activity (Julian and Olson, 2014). Binding of activated RhoA is suspected to alleviate this

interaction and activate the kinase domain of ROCK (Julian and Olson, 2014). Deletion of the C-terminal domain leads to constitutive activation of ROCK (Amano et al., 1999).

There are two isoforms of ROCK in vertebrates, ROCK1 and ROCK2, that share this overall structure, but whose precise functions diverge. Both ROCK1 and ROCK2 are widely expressed during development, though in later stages ROCK2 may be restricted to the muscle, brain, heart, lung, and placenta (Hartmann et al., 2015). ROCK1/2 seem to be redundant in regulating actomyosin contraction through MYPT1 inhibition (Kümper et al., 2016), though they have opposing effects on the organization of stress fibers and focal adhesions (Lock et al., 2012; Yoneda et al., 2005). The atypical RhoGTPases Rnd1/2/3 antagonize the Rho/ROCK pathway through the recruitment of p190 RhoGAP (Wennerberg et al., 2003). It has been demonstrated that ROCK1 but not ROCK2 can localize to cell-cell junctions in epithelial cells through an interaction with NMIIA where it then phosphorylates Rnd3, preventing the accumulation of p190B RhoGAP and inactivation of RhoA (Priya et al., 2015; Priya et al., 2017). Interestingly, ROCK1 and ROCK2 have isoform-specific activation pathways independent of RhoA through cleavage of the C-terminal domain: ROCK1 by caspase 3 and ROCK2 by granzyme B (Julian and Olson, 2014).

Regulation of cortical tension

The prevailing view of cortical tension was that it was mediated almost entirely by NMII contractility, with estimates based on NMII contractile forces suggesting that it can generate the force required to account for experimentally measured values of cortical tension (Salbreux et al., 2012). Cortical contractility though NMII is downstream of RhoA/ROCK signalling (Kelkar et al., 2020), which is clearly demonstrated in the mitotic rounding of cells (Taubenberger et al., 2020). Additionally, turnover of the cortex is thought to influence its contractility. If turnover is too low myosin contractility can fracture actin filaments, decreasing tension. If turnover is too high, tension is dissipated (Clarke and Martin, 2021).

Recently, the connectivity of the actomyosin network has been shown to be a critical factor in determining cortical tension. Generally, if connectivity is too low stresses cannot be

transmitted through the network efficiently, but if it is too high the network becomes too stiff to be deformed, suggesting that there is an intermediate point where cortical tension is optimized. Thus far three different sources of network connectivity have been studied, with intermediate levels of each parameter being optimal for propagation of tension: Levels of actin filament cross-linking mediated by either α-actinin (Bendix et al., 2008; Ennomani et al., 2016) or plastin (Ding et al., 2017), filament length regulated by cofilin, capping protein, or the formin DIAPH1 (Chugh et al., 2017), and the degree of branching through the action of Arp2/3 (Ennomani et al., 2016). Unsurprisingly, well ordered bundles (e.g. stress fibers) with optimal alignment of filaments with respect to their polarity were better optimized for tension propagation than a disordered network (e.g. the cortex), and both were better than disordered bundles (Ennomani et al., 2016).

Cortical tension can have large impacts on tissue morphogenesis, as the mechanical properties of a tissue depend on the properties of their constituent cells. Therefore, in addition to its key role in generating forces, it can also influence the mechanical context in which morphogenetic forces act, which is a key determinant for the outcome of morphogenetic processes (Keller et al., 2003). For example, embryonic tissues dramatically stiffen throughout development in a ROCK dependent manner (Zhou et al., 2009), which was later shown to permit tissue elongation when tissue explants were placed in stiffer environments, demonstrating that tissues can accommodate variations in their mechanical environment to ensure robust morphogenesis (Zhou et al., 2015). Tissue elongation in response to the stresses produced during dorsal closure in *Drosophila* and epiboly in zebrafish was dependent on a downregulation of tissue stiffness (West et al., 2017). Further, the outcome of apical constriction of the bottle cells in *Xenopus* is influenced by its mechanical environment. In isolated explants the contraction is isotropic leading to an even shrinking of the apical domain, but in the embryo the constricting cells are posed between two tissues with different mechanical properties causing the apical constriction to be biased mediolaterally (Keller et al., 2003).

Cell-matrix adhesion and migration

Another important function of the actin cytoskeleton that merits discussion to contextualize this work is its integration with cell-matrix adhesions to facilitate attachment and migration on the extracellular matrix (ECM). The actin structures involved are lamellipodia, filopodia, and stress fibers; these structures can be though of as derivatives of the cortex, as they contain similar molecular components and are also regulated by RhoGTPases. Importantly, after a cell contacts the ECM, RhoA and NMII cortical contractility must be downregulated to facilitate spreading and eventual migration of cells (Arthur and Burridge, 2001; Ren et al., 1999; Wakatsuki et al., 2003). Cell migration can be broken down into four steps: the extension of membrane protrusions at the leading edge (associated with Cdc42/Rac1 activity), the formation of matrix adhesions, detachment and disassembly of said adhesions, and finally, retraction of the rear of the cell (associated with RhoA activity). I will now give a brief overview of the actin structures involved in these processes and the integrin adhesion receptors that together promote cell-matrix adhesion and migration.

Integrins are adhesion receptors responsible for adhesion of cells to the ECM substrates (e.g. fibronectin). Through the recruitment of adaptor proteins (e.g. vinculin, paxillin, talin) to their cytoplasmic domain, they link the ECM to the actomyosin cytoskeleton. There are 24 distinct integrins chains, 18 α and 6 β chains, who must heterodimerize using one α and on β chain. Different combinations have different substrate specificities and may regulate RhoGTPase signalling differently; the most common combinations being $\alpha_5\beta_1$ and $\alpha_V\beta_3$, both of which bind to fibronectin (Chastney et al., 2021). Clustering of integrins and their adaptor proteins leads to maturation of the adhesion in a tension dependent manner (Burridge and Guilluy, 2016). The maturation of integrin mediated adhesions proceeds through a continuum, with each step increasing the size and stability of the adhesion while also recruiting new proteins: nascent adhesions are found immediately behind the leading edge, focal complexes slightly further back, and the elongated focal adhesions are located from just behind the lamelliopodia all the way to the rear of the cell (Parsons et al., 2010). This maturation is regulated by RhoGTPases requiring the crosstalk between multiple signalling pathways and the precise activity of many GEFs and

GAPs (Lawson and Burridge, 2014). Briefly, early stages are associated with Rac1 activation and RhoA inhibition, while at later stages RhoA is activated and Rac1 repressed. Importantly, due to their links with specific actin structures, they facilitate the transmission of traction force on the substrate and are important for mesenchymal cell migration.

At the leading edge of a migrating mesenchymal cell, there are two specialized actin structures, lamellipodia and filopodia. Lamellipodia are dynamic protrusions composed of branched actin networks mediated by Arp2/3 downstream of either Rac1 or Cdc42 activity (Krause and Gautreau, 2014). Polymerizing filaments are pushed against the extremity of the protrusions. Nascent adhesions act as a molecular clutch, stabilizing the polymerizing filaments preventing them from flowing rearward and allowing them to push the cell forward (Case and Waterman, 2015). This in turn generates a traction force on the substrate. Filopodia are thin finger-like protrusions that are embedded in lamellipodia and composed of bundled actin filaments. They are formed through the activity of formins, bundled with fascin, and are typically associated with Cdc42 activity (Skau and Waterman, 2015). Their principal function is to probe the ECM to find permissive attachment sites (Skau and Waterman, 2015).

Stress fibers are another class of cytoskeletal components that are critical for generating the traction forces required for cell migration (Burridge and Guilluy, 2016). Several types of stress fibers are found in migratory animal cells. The dorsal stress fibers run perpendicular to the cell edge and are linked directly to focal adhesions on one end and either the dorsal cortex or transverse arcs (Tojkander et al., 2012). Though they have no myosin themselves and are thus not contractile, through their coupling to other contractile actin machinery they can exert traction force through focal adhesions onto the substrate (Burridge and Guilluy, 2016). Transverse arcs run parallel to the cell edge and are not connected to focal adhesions, but indirectly act on the substrate through dorsal stress fibers (Tojkander et al., 2012). Finally, ventral stress fibers are found in the rear of the cell and are anchored on either end by focal adhesions and are thought to regulate contractility in the rear of the cell (Skau and Waterman, 2015).

Cadherin mediated cell-cell adhesion

For cells to organize into tissues, they must be able to adhere together after making an initial contact. Cell-cell adhesions must also be able to be dynamically disassembled and remodelled to facilitate many morphogenetic processes, a property that cancer can also take advantage of. The cell-cell adhesion protein found in nearly every animal was discovered by Takeichi and Kemler, eventually being termed cadherin for **ca**lcium **d**ependent ad**he**sion p**r**ote**in** (Nelson, 2020).

Since the initial discovery and characterization of what is now known as E-cadherin, many more cadherins have been identified with the human genome containing 114 cadherin genes (Hulpiau et al., 2016). Cadherins are transmembrane glycoproteins with a typical architecture (with some exceptions): an extracellular ectodomain with variable organization, a single transmembrane domain, and a widely divergent cytoplasmic domain. The defining feature of a cadherin is the presence of at least two of the well-conserved extracellular cadherin (EC) repeats, a 110 amino acid domain composed of seven β-strands together forming two β-sheets (the first sheet containing strands ACFG and the second BED). The interdomain linker binds three Ca2+ ions which provide rigidity to the structure and are typically required for cadherins adhesive function.

As it tends to happen with the ongoing piecemeal discovery of related genes and proteins, the naming and classification of cadherins can at times be confusing. For example, atypical cadherins was initially used to refer to type II classic cadherins (Nollet et al., 2000), but is now apparently used as a catch all term for anything that isn't a classic cadherin. While comparison of cytoplasmic domains can be useful for functional groupings (e.g. type I and III classic cadherins), comparisons of EC repeat sequences provide a more robust phylogenetic classification. Initial EC repeat analyses were based on comparing the EC1 repeat (Nollet et al., 2000), but more recent studies have focused on comparing blocks of 4-7 EC repeats (Hulpiau et al., 2016; Sotomayor et al., 2014). Using a combination of these approaches, the cadherin superfamily can be split into two main branches. First, the Cadherin Major Branch (CMB) which is further subdivided into the C1 branch, where we find the vertebrate specific type I and II classic cadherins as well as the

desmosomal cadherins (Kowalczyk and Green, 2013), and the C2 branch comprised of type III and IV classic cadherins and the planar cell polarity (PCP) proteins, the CELSRs (flamingo in *Drosophila*) (Berger-Müller and Suzuki, 2011; Butler and Wallingford, 2017). Second, the Cadherin related Major Branch (CrMB) that includes the protocadherins (Pcdhs) (clustered and non-clustered) (Hayashi and Takeichi, 2015; Honig and Shapiro, 2020), and Cadherin Related Proteins (Cdhrs) where the 'giant' cadherins are found. The best characterized cadherins found here are the PCP receptors FAT and dachsous (Butler and Wallingford, 2017; Strutt and Strutt, 2021), and the CDHR15/CDHR23 (also known as PCDH15/CDH23) that form the tip-link filament in the hair cells of the inner ear and are important for auditory perception (Hulpiau et al., 2016; Jaiganesh et al., 2018).

In this section, I will focus primarily on type I classic cadherins, whose ectodomains consist of five EC repeats and interact with the catenins with their cytoplasmic domain, together forming the cadherin-catenin complex which can interact with the actomyosin cytoskeleton. I will first discuss how the structural basis of how the extracellular ectodomain of type I classic cadherins mediates adhesion, before detailing the roles of p120-, β-, and α-catenin and their various interactors. Next, I discuss how cadherins cluster allowing them to function from the molecular scale to the cellular and tissue scale, and the outcomes of such organization and how cadherin can influence tissue level processes. I finish by discussing the different ways that cadherin contributes to cell-cell adhesion, and how each role may be required at different stages during the lifetime of a cell-cell contact. Here it is important to note that while the cytoplasmic domain interactions are generalizable to type I-IV classic cadherins, the extracellular ectodomain interactions and their specific impacts on cadherin adhesion and clustering described here may only apply to type I and II classic cadherins, as well as the desmosomal cadherins. Currently, the adhesive interface of type III and IV classic cadherins used in invertebrate systems are unknown. Unless otherwise stated, when I use the term 'cadherin' I am referring specifically to type I classic cadherins.

The structural and biophysical basis of cell-cell adhesion

The first structures of the cadherin ectodomain were published around 25 years ago (Nagar et al., 1996; Shapiro et al., 1995), and ongoing structural and biophysical studies continue to reveal the details of how cadherins mediate cell-cell adhesion. Initial structural studies identified two potential interfaces responsible for trans interactions between cadherins on opposing cell membranes. The first study, using the purified EC1 repeat of N-cadherin, reported what would later be termed the strand-swap dimer (S-dimer) which involved the Trp2 (found within the A strand) residues of opposing EC1 repeats docking into the hyrdrophobic pockets of their binding partners (Shapiro et al., 1995). The second study worked with the EC1 and EC2 repeats of E-cadherin and discovered that a unique interface formed between the EC1 and the interdomain calcium-binding motif of its binding partner, later referred to as the X-dimer as the configuration resembles an X (Nagar et al., 1996). This difference was at one point thought to be due to a difference in the adhesive interface between E- and N-cadherin. However, this idea was revisited after the structure of the solitary C1 branch cadherin, T-cadherin, was determined (Ciatto et al., 2010). T-cadherin is peculiar as - though closely related to classical cadherins and capable of mediating cell-cell adhesion (Vestal and Ranscht, 1992) - it lacks both transmembrane and cytoplasmic domains, as well as the conserved Trp2 on the A strand. The elucidation of its structure revealed that adhesion is accomplished through the X-dimer (Ciatto et al., 2010). A follow up study using classic type I and II classic cadherin mutants incapable of forming S-dimers (W2A mutants) instead formed X-dimers (Harrison et al., 2010). Mutants incapable of forming X-dimers (K14E mutants) were still able to form S-dimers of equal affinity, albeit much slower, leading to the conclusion that the X-dimer formed as an intermediate to both the formation and dissociation of the S-dimer (Brasch et al., 2012; Harrison et al., 2011; Hong et al., 2011; Sivasankar et al., 2009). Further, X-dimers interact strictly through surface residues so no refolding is necessary, and while in this configuration the strands that swap are directly apposed to one another which is thought to facilitate S-dimer formation (Harrison et al., 2010).

An important point in S-dimer formation is that the non-swapped monomer must be less stable than the swapped dimer. An intriguing in silico study addressed this by comparing EC1 (S-dimer capable) and EC2-5 (S-dimer incapable) repeats of type I classic cadherins. Overall, the

domains are very similar, but they identified several key differences seemingly important for S-dimer formation. Namely, a shortened A strand thought to increase strain and destabilize the monomer, the Trp2 residue previously mentioned, and several stabilizing residues (Posy et al., 2008). Interestingly, only classic type I, II, and desmosomal cadherins contain these determinants suggesting that other cadherins must mediate adhesion through a different interface (Posy et al., 2008). Published structures of type II classic cadherins (Brasch et al., 2018; Patel et al., 2006) and desmosomal cadherins (Harrison et al., 2016) confirm they form S-dimers (though the adhesive interface of type II classic cadherins is much larger than type I and involves swapping two tryptophan residues). Thus far, all other published structures of cadherins from other branches have different adhesive interfaces (Goodman et al., 2016; Nicoludis et al., 2015; Rubinstein et al., 2015; Sotomayor et al., 2012).

Recent biophysical studies have added more nuance to the formation and function of cadherin trans interactions. Using atomic force microscopy (AFM) to take single molecule force measurements of the cadherin trans interaction while under tensile stress revealed that cadherin ectodomain could form three types of adhesive bonds, the aforementioned S- and X-dimers, and a third previously unidentified 'ideal' bond (Rakshit et al., 2012). Each bond has distinct physical characteristics. The S-dimer is a slip bond, meaning that the lifetime of the bond decreases with increasing load, while the X-dimer forms a catch bond that – up to a certain threshold – is stabilized under a tensile load (Rakshit et al., 2012). Further investigation revealed that when the X-dimer is under a tensile load the ectodomains rearrange and new hydrogen bonds form between the EC1-EC2 repeats (Manibog et al., 2014). It was then established that even though the S-dimer is far more stable than the X-dimer in the absence of force, trans dimers actively interconvert between the two conformations (Manibog et al., 2016). This result coupled with the fact that in the single molecule force measurement experiments, only mutants incapable of forming X-dimers formed slip bonds, while wild type cadherins formed catch bonds (Rakshit et al., 2012), makes it tempting to speculate that the X-dimer may play a larger role than just that of a kinetic intermediate during the formation and dissociation of the S-dimer.

The third, previously unidentified, interaction forms an ideal bond which means that its lifetime is insensitive to the tensile load (Rakshit et al., 2012). This novel interaction was shown

to be an intermediate state between the transition from an X- to S-dimer with a very low lifetime that would be preferentially ruptured – compared to either the X- or S-dimer - when subject to a tensile force. Additionally, the formation of ideal bonds likely only occurs in isolated trans dimers, as cis interactions preclude their formation (Manibog et al., 2016).

In addition to the trans interactions, a secondary interface facilitating cis interaction between cadherins was initially proposed in the first crystal structure of the entire ectodomain of C-cadherin (Boggon et al., 2002). This interface was validated after the structures of the full ectodomains of E- and N-cadherin were elucidated showing conclusively that the EC1 repeat could interact with the neighbouring EC2/EC3 repeats of a cadherin on the same cell (Harrison et al., 2011). After mutating the residues responsible for the cis interaction (V81D and L175D), structural and functional experiments showed that the cis interaction was indeed abolished and these mutants could not form stable cell-cell junctions (Harrison et al., 2011). These results indicated that even though cis interactions are very weak, they play a crucial role in establishing adhesion. This was consistent with earlier theoretical and single molecule studies that suggested that lateral interactions increase the probability that trans interactions form (Zhang et al., 2009) and that adhesion is a cooperative process between both cis and trans interactions (Wu et al., 2010).

Finally, there is evidence that the cytoplasmic domain of cadherin may also impact the adhesive properties of the ectodomain through inside-out mechanisms. Studies showed that the phosphorylation state of p120 catenin can alter E-cadherin binding affinities (Petrova et al., 2012; Shashikanth et al., 2015), and that the loss of α-catenin decreases the binding strength and lifetime of single E-cadherin dimers measured using AFM (Bajpai et al., 2008; Bajpai et al., 2009). These studies suggest that in addition to the many other roles played by the cytoplasmic domain and its binding partners they may also allosterically regulate adhesion of the ectodomain.

Binding Specificity

After the discovery of E-cadherin an additional four type I classic cadherins were found. The prevailing notion of cadherin mediated adhesion at that time was that it was selective, in other

words, E-cadherin strictly binds E-cadherin, N-cadherin binds N-cadherin, etc. Several lines of evidence supported this conclusion. Developing tissues have distinct expression patterns of cadherins (Takeichi Masatoshi, 1988) that dynamically change, often concomitantly with morphogenetic events that lead to separation of developmental structures. For example, cells of the developing neural tube stop expressing E-cadherin and start expressing N-cadherin at the onset of neurulation (Hatta and Takeichi, 1986; Thiery et al., 1984). Further, after dissociation and mixing of cells from tissues expressing different cadherins the cells did not remain mixed but segregated upon reaggregation (Nose and Takeichi, 1986; Takeichi et al., 1981). Finally, immunostaining of cadherin revealed no or very weak signals at heterotypic contacts between different tissues (Hirano et al., 1987). These observations were formalized in the Selective Adhesion Hyptothesis, which supposed that cadherin binding specificities could explain tissue segregation and boundary formation between different types of tissues (Takeichi, 1990; Takeichi Masatoshi, 1988).

However, later experiments challenged this view. The initial study that began to cast doubt showed that tissue segregation could be accomplished by simply varying the amount of expression of the same cadherin between two cell populations (Steinberg and Takeichi, 1994); even slight differences in expression levels were enough to segregate cells (Duguay et al., 2003; Foty and Steinberg, 2005). This was then extended to cells expressing different cadherins while carefully controlling expression levels of each. In these experiments, cells expressing either E- or P-cadherin only segregated when they differed in expression level; if expression levels were the same the different populations completely intermixed (Duguay et al., 2003). The authors proposed that earlier studies observed segregation based on apparent cadherin specificities because they either did not control for levels of cadherin expression, or they unknowingly used aggregation conditions that were too stringent for the formation of heterotypic bonds. Using less stringent reaggregation conditions, they observed mixing of cells expressing many different combinations of cadherins that were previously reported to segregate (Duguay et al., 2003). Later biophysical binding data supported this notion. Analytical ultracentrifugation (AUC) and surface plasmon resonance (SPR) measurements demonstrated that type I cadherins have appreciable heterophilic binding affinities with certain combinations having higher heterophilic binding

affinities than homophilic (Katsamba et al., 2009; Vendome et al., 2014). For example, N-cadherin has a much higher homophilic binding affinity than E-cadherin, but their heterophilic binding affinity is intermediate between both, though closer to E- than N-cadherin (Katsamba et al., 2009). This agreed with an earlier study that noted that cells expressing either E-, N-, or C-cadherin were able to adhere to E- or C-cadherin substrates with similar strengths, suggesting heterophilic binding was possible (Niessen and Gumbiner, 2002). In fact, several studies had already observed enrichment of different cadherins at heterotypic cell-cell contacts (Omelchenko et al., 2001; Shan et al., 2000; Volk et al., 1987).

It is interesting to note that N-cadherin has a higher binding affinity than that of E-cadherin (Katsamba et al., 2009; Vendome et al., 2014), since that is the opposite of what one may intuitively predict based on their expression patterns: N-cadherin is commonly expressed in migratory tissues, while the inverse is true for E-cadherin. In fact, 'cadherin switching', that is, changing expression from E- to N-cadherin, is a common hallmark of the epithelial to mesenchymal transition (EMT), an important developmental process where typically non-migratory epithelial cells are converted into migratory mesenchymal cells (Francou and Anderson, 2020). How then can one rationalize such a clear link between the expression of the apparently more adhesive N-cadherin and weakly adhesive migratory cells? One possibility is that binding affinity may not be an accurate representation of adhesive strength, as other methods to measure adhesion suggested that E-cadherin was indeed more resistant to applied forces than N-cadherin (Chu et al., 2004; Panorchan et al., 2006). Regardless, experiments in the *Xenopus* neural crest can provide further insight. This system is a classic example of EMT, where before adopting a migratory mesenchymal phenotype and delaminating from the neural tube (ostensibly requiring a decrease in adhesion), the neural crest cells (NCCs) switch from expression of E- to N-cadherin. Cadherin chimeras and point mutations demonstrated that the cytoplasmic tail of E-cadherin, and specifically its association with p120-catenin, can prevent delamination and migration of the NCCs away from the neural tube (Scarpa et al., 2015). Up to this point I have only discussed cadherin function with respect to the binding affinity and physical association of the cadherin ectodomain, in the following sections I will focus on the cytoplasmic domain and its principal binding partners, the catenins.

The cytoplasmic domain of cadherin

The cytoplasmic domain of cadherin is conserved across the metazoans (Hulpiau and Van Roy, 2011) and is the most highly conserved region within classic cadherins (Nollet et al., 2000). Deletion of the cytoplasmic domain prevents accumulation of cadherin at cell-cell contacts, blocks cell-cell adhesion, and abrogates cadherins ability to associate with the cytoskeleton (Nagafuchi and Takeichi, 1988). In stark contrast to the extracellular ectodomain, the cytoplasmic domain is intrinsically unstructured in the absence of its binding partners, the catenins (Huber et al., 2001), through which the cadherin-catenin complex (CCC) derives most of its cytoplasmic activity. p120 catenin binds directly to the juxtamembrane domain (JMD) of cadherin (Daniel and Reynolds, 1995; Yap et al., 1998), β-catenin the catenin binding domain (Hülsken et al., 1994; Stappert and Kemler, 1994), and while α-catenin does not directly bind to cadherin it simultaneously associates with β-catenin and actin (Aberle et al., 1994; Huber et al., 1997; Rimm et al., 1995). β-catenin associates with cadherin immediately after synthesis in the golgi while α-catenin joins the complex as it arrives at the plasma membrane (Hinck et al., 1994; Ozawa and Kemler, 1992), which is also likely the case for p120 catenin. Orthologs of each catenin can be found in the basal metazoan species (Gul et al., 2017), indicative of their influence on classic cadherin function. Indeed, each catenin has unique roles to play during cell-cell adhesion which are discussed below.

p120 catenin and the juxtamembrane domain

p120 catenin (hereafter p120) was initially identified in a screen for Src substrates (Reynolds et al., 1989), and then later found to contain armadillo (ARM) repeats similar to β-catenin (Reynolds et al., 1992). This observation led Reynolds and colleagues to test if p120 could interact with cadherin as β-catenin does, which was indeed the case (Reynolds, 2007; Reynolds et al., 1994). It was later demonstrated that p120 associates with the JMD of the cadherin tail via a central ARM repeat domain (Daniel and Reynolds, 1995). Interestingly, this interaction appears to be regulated by phosphorylation of both the JMD and p120; p120 phosphorylation by Src or Fyn/Fer kinases increase its affinity for the JMD (Piedra et al., 2003; Roura et al., 1999), while

phosphorylation of the JMD prevents association of p120 by increasing its affinity for other interactors (Fujita et al., 2002).

The principal function of p120 appears to be in influencing the amount and half-life of cadherin present at the plasma membrane (Davis et al., 2003; Ireton et al., 2002; Xiao et al., 2003). Binding of p120 to the JMD prevents clathrin dependent endocytosis and subsequent degradation or recycling of the cadherin complex (Le et al., 1999; Xiao et al., 2005), as the presence of p120 masks a dileucine motif located in the JMD that likely binds endocytic machinery (Miyashita and Ozawa, 2007). More recently, a second endocytic signal (DEE) within the JMD was identified that is conserved in both type I and type II classic cadherins (Nanes et al., 2012). A second route to cadherin complex internalization and degradation involves binding of the E3 ligase Hakai to the JMD and subsequent ubiquitination of the JMD which sterically hinders association of p120 and tags cadherin for degradation (Fujita et al., 2002; Hartsock and Nelson, 2012). Detailed structural analysis demonstrated that the JMD has subdomains that facilitate either strong 'static' or weak 'dynamic' interactions with p120 (Ishiyama et al., 2010). The static interface - which corresponds to a 15 residue stretch previously identified as the 'JMD core' (Thoreson et al., 2000) - includes tyrosine residues that mediate association with Hakai as well as the DEE endocytic signal, while the dynamic interface includes both the dileucine motif and the lysine that is ubiquitinated by Hakai (Hartsock and Nelson, 2012; Ishiyama et al., 2010). Notably, binding of Hakai is dependent on the phosphorylation of two tyrosine residues that are only present in E-cadherin (Fujita et al., 2002), suggesting that clathrin dependent endocytosis via the dileucine or DEE motif is likely the common mechanism for internalization of classic cadherins. It has been proposed that the dynamic interface allows cycles of binding and release of the dileucine motif, providing opportunities for the endocytic machinery to competitively bind to cadherin to initiate internalization (Ishiyama et al., 2010), while complete dissociation of p120 would be required for the endocytic machinery to access the DEE motif (Nanes et al., 2012). This would suggest that the JMD of different cadherins may have several alternative endocytic signals that can trigger internalization.

p120 also plays a central role in the coordination of the RhoGTPases RhoA and Rac, whose precise activities are crucial for regulation of the actin cytoskeleton and cell-cell adhesion

(Ratheesh et al., 2013). Generally, p120 stimulates Rac activity while suppressing RhoA activity (Elia et al., 2006; Noren et al., 2000); several pathways that may influence this relationship. First, p120 can act as a RhoGDI by directly binding inactive GDP-bound RhoA and preventing its activation (Anastasiadis et al., 2000; Magie et al., 2002). Though, this activity is strictly mediated by the cytosolic pool of p120, as the RhoA and cadherin binding sites overlap (Ireton et al., 2002; Yanagisawa et al., 2008). Next, p120 can bind the RacGEF Vav2, thus stimulating Rac activity (Noren et al., 2000). Initially it was suggested that this interaction is also mediated by the cytosolic pool of p120 catenin, but a later study demonstrated that Vav2 was recruited to sites of cell-cell adhesion, though the dependency on p120 was not assayed (Fukuyama et al., 2006). Finally, the RhoA inactivating p190RhoGAP translocates to cell-cell adhesions upon Rac activation where it binds directly to p120, decreasing junctional RhoA activity (Wildenberg et al., 2006). Although it is tempting to speculate that p190RhoGAP recruitment is downstream of p120 activation of Rac by Vav2, this has not been directly demonstrated, and expression of GEFs and GAPs is likely cell type dependent (Ratheesh et al., 2013). Further, p120 interactors and downstream GAP/GEF activity are also dependent on subcellular localization of the cadherin complex (i.e. apical vs basolateral; (Kourtidis et al., 2015), and different p120 isoforms produced by alternative splicing have different effects on Rho activity (Yanagisawa et al., 2008). All these factors must be taken into account when considering the relationship between RhoGTPases and p120. Interestingly, p120 also binds to ROCK1, a downstream effector of RhoA activity (Smith et al., 2012), suggesting that p120 may also help positively regulate RhoA contrasting its typical association with inhibition of RhoA.

β-catenin and the catenin binding domain

Due to the highly conserved nature of cadherins cytoplasmic tail, Kemler and colleauges sought to search for potential interactors, leading them to discover three distinct proteins that immunoprecipitated with cadherin that they termed α-, β-, and γ-catenin (later shown to be the same protein as plakoglobin) (Ozawa et al., 1989). As a side note, these earliest studies likely missed p120 in these screens as it comigrates with α- and β-catenin in many cell types masking

its presence (Reynolds, 2007). β-catenin binds to the terminal end of cadherins cytoplasmic tail (Ozawa et al., 1990) to a highly phosphorylated stretch of 30 amino acids known as the CBD (Stappert and Kemler, 1994) using a central ARM repeat domain (Hülsken et al., 1994). Analogous to the p120/JMD interaction, the β-catenin/CBD interaction can also be regulated by phosphorylation, however the pattern is inversed. Phosphorylation of several serine residues in the CBD drastically increases its affinity for β-catenin and stabilizes the interaction (Choi et al., 2006; Lickert et al., 2000), while preventing this phosphorylation decreases binding of β-catenin and causes a loss of cell-cell adhesion reminiscent of deletion of the entire CBD (McEwen et al., 2014; Stappert and Kemler, 1994). On the other hand, phosphorylation of specific tyrosine residues of β-catenin decreases its affinity for the CBD (Rosato et al., 1998; Roura et al., 1999). Intriguingly, p120 may also be involved in regulating the phosphorylation state of β-catenin through binding to Fer kinase (Kim and Wong, 1995). Fer phosphorylates the tyrosine phosphatase PTP1B enabling it to interact with cadherin and dephosphorylate β-catenin, thereby increasing its affinity for the CBD (Xu et al., 2004).

The earliest notions of catenin function were that β-catenin simultaneously binds both the CBD and α-catenin, which then binds to actin, as deletion of the CBD blocked adhesion and prevented association of cadherin with the cytoskeleton (Aberle et al., 1994; Ozawa et al., 1989; Ozawa et al., 1990). Despite some uncertainties - detailed below - this initial supposition has held true. β-catenin binds α-catenin using its N-terminal domain (Aberle et al., 1994; Hülsken et al., 1994). The β-catenin/α-catenin interaction may also be mediated by p120 through Fer, as Fer phosphorylates a tyrosine residue within the α-catenin binding domain of β-catenin, disrupting the interaction (Piedra et al., 2003).

Outside of its role at the plasma membrane, β-catenin also has a well-established role in nuclear signalling as the primary signal transducer of the canonical Wnt pathway. To summarize, in the absence of a Wnt signal, cytosolic β-catenin is degraded by a destruction complex (which includes Axin, APC, and the kinases CK1 and GSK3); if the canonical Wnt pathway is active the destruction complex is inhibited and the cytosolic pool of β-catenin is stabilized, allowing it to be transported into the nucleus where it can relieve TCF/LEF transcriptional repression (Valenta et al., 2012). An important question then is if and how the cadherin-bound and signalling pools of

β-catenin interact. The answer remains somewhat nebulous, though it is clear that cadherin competes with β-catenin's other interactors for binding, potentially sequestering it from its other activities (reviewed in (McCrea et al., 2015). Not to be outdone, p120 and α-catenin have recently received more attention as potential transcriptional regulators (McCrea and Gottardi, 2016). Cytosolic pools of α-catenin appear to act as negative regulators of β-catenin's signalling activity (Choi et al., 2013; Daugherty et al., 2014), while p120 activates transcription though an analogous Wnt sensitive pathway (Hong et al., 2010); p120 binds the transcriptional repressor Kaiso (Daniel and Reynolds, 1999), and in doing so prevents it from interacting with its target genes leading to their activation (Park et al., 2005).

α-catenin, vinculin, and the actin cytoskeleton

In contrast to p120 and β-catenin, α-catenin does not contain any ARM repeats. Though, it is related to vinculin (Herrenknecht et al., 1991), another actin binding protein that is associated with cell-cell and cell-matrix adhesions that binds both α-catenin and actin (Bays and DeMali, 2017). α-catenin has three domains: the N-terminal domain binds β-catenin (Huber et al., 1997), the modulation (M) domain binds vinculin (Watabe-Uchida et al., 1998), and the C-terminal domain binds actin (Rimm et al., 1995). As mentioned, the common sentiment in the field after the discovery of the catenins was that α-catenin bound simultaneously to β-catenin and actin, thus linking the cadherin-catenin complex to the cytoskeleton (Ozawa et al., 1990). However, after 15 years of relative peace this paradigm was questioned after experiments with purified proteins failed to reconstitute this complex in vitro: complexes of cadherin, β-catenin, and α-catenin were incapable of binding actin (Yamada et al., 2005). This confusion was left unresolved for 10 years until it was demonstrated that the cadherin/β-catenin/α-catenin complex stably binds actin while under tension, but only weakly associates with it while applied forces are low, revealing that the α-catenin/actin link is a catch bond (Buckley et al., 2014). This behaviour stems from a force-dependent allosteric regulation of the actin binding domain of α-catenin that controls the cadherin-catenin complexes dynamic interaction with the cytoskeleton (Ishiyama et al., 2018).

Though vinculin is not considered a core member of the cadherin-catenin complex, it is a key component in its ability to respond to mechanical stimuli. Vinculin is recruited to the cadherin-catenin complex in response to force leading to stiffening of the junction, ostensibly through increased anchoring of the cadherin-catenin complex to actin (Le Duc et al., 2010). Vinculin recruitment depends on force dependent unfolding of α-catenin to reveal a cryptic binding site in the M domain, and subsequent binding of vinculin stabilizes α-catenin in its unfolded form (Yao et al., 2014; Yonemura et al., 2010). Similar to the α-catenin/actin link, the vinculin/actin bond is also more stable under tension (Huang et al., 2017). Strikingly, α-catenin unfolds when submitted to forces of ~5 pN (Yao et al., 2014), and both the α-catenin/actin and vinculin/actin bonds begin to stabilize at ~8 pN of applied tension (Buckley et al., 2014; Huang et al., 2017), which are within the range of the estimated constitutive tension exerted on the cadherin tail (1-2 pN; Borghi et al., 2012) and the force exerted by the contraction of myosin (3-4 pN; Finer et al., 1994). Like α-catenin, vinculin is an autoinhibited protein, and despite several mechanism being proposed for its activation - ranging from force-dependent unfolding or binding of other interactors (Bays and DeMali, 2017) - most of the studies were performed in the context of focal adhesions. Recent work revealed that activation of vinculin and recruitment to the cadherin-catenin complex requires a combination of tension and a phosphorylation of vinculin that is unique to cell-cell adhesions (Bays et al., 2014; Bertocchi et al., 2012).

In the intervening years when the direct interaction of β-catenin/α-catenin/actin was being questioned, focus shifted to studying the cytosolic pool of α-catenin and its ability to homodimerize (Koslov et al., 1997). Indeed, a small portion of cytosolic α-catenin homodimerizes preventing association with β-catenin while increasing its affinity for actin (Drees et al., 2005). These homodimers inhibit the activity of the actin branching complex Arp2/3 and the actin severing protein cofilin by causing conformational changes in actin, therefore favouring the assembly of stable, unbranched actin filaments (Benjamin et al., 2010; Drees et al., 2005; Hansen et al., 2013). Another study that forcibly induced the homodimerization of α-catenin noted that α-catenin homodimers were subsequently recruited to the cortex where they promoted formation of filopodia, decreases in actin density, and favoured cell-cell adhesion, though there did not appear to be any effect on Arp2/3 (Wood et al., 2017). Though the precise function of α-

catenin homodimers may be unclear, α-catenin has always been considered to be the master regulator of the CCCs interactions with the cytoskeleton, even outside of its own binding to actin. α-catenin binds several other actin binding proteins including afadin (Pokutta et al., 2002), α-actinin (Knudsen et al., 1995), ZO1 (Itoh et al., 1997), and EPLIN (Abe and Takeichi, 2008), as well as associating with formin-1, an actin nucleator that creates unbranched actin networks (Kobielak et al., 2004).

Finally, it is important to note that there are three subtypes of α-catenin in mammals, αE-, αN-, and αT-catenin. aE-catenin is ubiquitously expressed and is the focus of the majority of studies on α-catenin, while αN-catenin and αT-catenin are expressed in the brain and heart, respectively (Chiarella et al., 2018). This is important to note as they do have divergent functions, for example, αT-catenin constitutively binds actin and β-catenin independent of force (Wickline et al., 2016), and αN-catenin does not recruit vinculin as efficiently as αE-catenin (Ishiyama et al., 2013). Further, it seems that only αE-catenin forms homodimers (Takeichi, 2018). Intriguingly, homodimerization of αE-catenin may be species specific, while it has been demonstrated in mouse and *drosophila*, it does not occur in *c. elegans* or zebrafish (Takeichi, 2018).

Mechanisms of cadherin clustering

Thus far I have considered the CCC function at the molecular level, but it is capable of exerting its effects at the cellular and tissue level. A critical property of the complex that facilitates its scaling from the molecular to the cellular is its propensity to organize into larger structures known as adherens junctions (AJs). While the morphology of adherens junctions is extremely diverse, varying between cell type or even subcellular localization (Efimova and Svitkina, 2018; Takeichi, 2014), their formation relies on the ability of individual cadherins to organize into clusters. Studies using super-resolution microscopy provided a first detailed look at the organization of cadherin clusters, revealing that the larger clusters visible by standard light microscopy techniques (now referred to as microclusters) are composed of densely packed nanoclusters that have an average size of around five cadherins, though much larger clusters consisting of ~100 cadherins can form (Truong Quang et al., 2013; Wu et al., 2015). These clusters

have extremely dense cores interspersed by less dense regions (Indra et al., 2018; Truong Quang et al., 2013; Wu et al., 2015).

Though cluster formation has been directly linked to adhesive strength for nearly 25 years (Brieher et al., 1996; Yap et al., 1998), the precise details that mediate this process are still a focus of intense research. For instance, despite initial studies suggesting that lateral dimerization increases trans affinity (Brieher et al., 1996), later theoretical and simulation studies proposed that trans dimers must form from cadherin monomers before cis interactions (Wu et al., 2010; Wu et al., 2011), but recent studies have again suggested that lateral dimers are the basic adhesive unit used for cluster formation and cis interactions can stimulate oligomerization (Singh et al., 2017; Thompson et al., 2019; Thompson et al., 2020; Vu et al., 2021). Further, it is increasingly clear that clustering results from the integration of several inputs: interactions of the ectodomain, association with the actin cytoskeleton, as well as p120 binding to the cytoplasmic tail.

One of the first models for cadherin clustering was based on structural data of the cadherin ectodomain. Crystal structures of E-, N-, and C-cadherin revealed a lattice organization with cadherins forming cis and trans interactions oriented in different directions allowing the lattice to form in two dimensions and reach a characteristic density, referred to as crystal lattice density (Boggon et al., 2002; Brasch et al., 2012; Harrison et al., 2011). Simulations of just the ectodomain suggested that trans and cis interactions must work in concert - with trans forming first - to allow growth of the cluster, as cis interactions alone can only organize cadherin in one dimension and trans interactions of the ectodomain alone have no capacity to organize at a larger scale (Wu et al., 2010; Wu et al., 2011). Electron and super-resolution microscopy provided the first experimental evidence for cooperativity: while cis mutants were still able to form clusters, their density was drastically decreased and they no longer reached crystal lattice density at their core in contrast to wild-type cadherin clusters (Strale et al., 2015; Wu et al., 2015). Additionally, cadherin mutants lacking the cytoplasmic tail still formed clusters with cores at crystal lattice density suggesting that the ectodomain itself can drive clustering (Wu et al., 2015).

Interactions of the ectodomain alone cannot entirely explain the clustering phenomenon. Non-adhesive clusters still formed when the residues that mediate cis and trans interactions were mutated, albeit with reduced density (Wu et al., 2015). In fact, the only way to achieve a completely homogenous, cluster-free distribution of cadherin was to mutate cis and trans interactions on a tailless mutant (Wu et al., 2015). Together with the fact that simulations also needed to add a 'diffusion trap' parameter to maximize clustering (Wu et al., 2010), it is clear that the cytoplasmic domain may also play a role in cadherin clustering. Indeed, deletion of the cytoplasmic tail or the CBD, depolymerization of actin, and inhibiting myosin contractility have all been shown to increase the size of cadherin clusters suggesting that association with actin may limit the size of clusters (Chandran et al., 2021; Wu et al., 2015). Though the average density of the clusters was decreased after uncoupling from actin, there were still patches with crystal lattice density (Wu et al., 2015). Interestingly, the inverse relationship has also been found, with deletion of α-catenin or actin depolymerization leading to smaller clusters. There the authors suggested that actin prevents the fission of clusters allowing larger clusters to form (Truong Quang et al., 2013). Whatever the case, it seems that association with the actomyosin cytoskeleton can control the size of the clusters, while the interactions of the ectodomain may decide the density.

A second impact of association with the cytoskeleton appears to be stabilization of clusters, as clusters uncoupled from the cytoskeleton diffuse faster on the membrane (Chandran et al., 2021; Erami et al., 2015; Hong et al., 2013). This could explain why cluster size is increased when this interaction is perturbed as higher motility may lead to clusters encountering each other and fusing more frequently (Chandran et al., 2021; Wu et al., 2015). This decrease in cluster motility (Chandran et al., 2021) coupled with observations that clusters are delimited by actin (Wu et al., 2015) raise the possibility that cytoskeletal associations provide the diffusion trap mechanism that simulations suggested was required for cluster formation (Wu et al., 2010).

Finally, though association of p120 with the JMD was originally thought to induce clustering (Yap et al., 1998), this potential function did not receive much attention after p120s impact on cadherin internalization was discovered. The first crystal structure of p120 in association with the JMD suggested a potential head to tail interaction of p120 that could

facilitate clustering (Ishiyama et al., 2010), but it wasn't until recently that this possibility was fully revisited after studies revealed that cadherin exists as a constitutive dimer and the cytoplasmic domain was the strongest driver of dimerization (Singh et al., 2017). Leckband and colleagues then demonstrated that uncoupling p120 from the cytoplasmic tail prevented dimerization leading to decreased trans binding affinity and cell adhesion (Vu et al., 2021). However, this may not tell the full story as the original dimerization study noted that the cytoplasmic tail could still induce dimerization in the absence of any cytoplasmic components i.e. p120 (Singh et al., 2017).

Considering all these points, we can propose a simple model for how cadherin clusters may form. The minimum adhesive unit of cadherin may be several actin delimited cadherin dimers, formed through association of dimerized p120 of neighbouring cadherins (Vu et al., 2021), in a loosely packed non-adhesive cluster (Chandran et al., 2021; Wu et al., 2015). Though it is important to note here that the presence of non-adhesive clusters has recently been questioned and may not exist in every cell type (Indra et al., 2018). Upon contact of two cells, trans interactions are able to efficiently form as their affinity is increased by lateral association via p120 (Vu et al., 2021), which is subsequently followed by formation of cis interactions, which stabilize cadherins at the junction (Erami et al., 2015; Strale et al., 2015), and allow clusters to expand in a second dimension (Wu et al., 2010). As these clusters mature, they may form tighter associations with the actin cytoskeleton increasing their stability and density, while maintaining their size below a certain threshold (Chandran et al., 2021; Wu et al., 2015). Maximizing trans and cis interactions would allow the cores of certain clusters to reach crystal lattice densities while surrounding and intervening regions have lower density clusters (Harrison et al., 2011; Strale et al., 2015; Wu et al., 2015).

New data from the Troyanovsky group has questioned the clustering paradigm that has so far focused on the crystal lattice model. In a proteomic screen for clustering dependent CCC associated proteins (CAPs), they found that wild type and trans mutants had a nearly identical interactome (Troyanovsky et al., 2021). This result combined with the observation that when arranging 3D structures of the CCC at crystal lattice density there was no space for anything beyond the catenins in the cytoplasmic space implied that there may be several populations of

cadherin clusters (terming the standard crystal lattice clusters E-clusters, and clusters that bind CAPs C-clusters). They went on to show with two CAPs that they do indeed form spatially distinct clusters not only from E-clusters, but also each other, suggesting that there are distinct C-clusters based on which specific CAPs bind the cytoplasmic tail (Troyanovsky et al., 2021). This raises the exciting possibility that C-clusters may be able to organize specialized structures on either side of a cell-cell contact that could synchronize signalling events or actin remodelling.

Once a cluster is formed, how long does it persist at the junction? FRAP experiments revealed that nearly 30% of cadherin is adhesive and immobile while a further 15% is mobile (Erami et al., 2015). This is consistent with a model where the dense core of a cluster is immobile while mobile cadherin is recruited or exchanges with cadherins in the less dense intervening regions surrounding the core. This view has since been challenged through imaging of single cadherins within clusters. These new data support a model where the denser nanoclusters are continuously disassembled and newly released cadherins are immediately recruited into new clusters (Indra et al., 2018). This dynamicity was shown to depend on remodelling of the actin cytoskeleton, as stabilizing actin also slowed internal cadherin cluster dynamics (Indra et al., 2018). Additionally, a later study demonstrated the reverse relationship is also true, and that stabilizing cadherin clusters can also stabilize actin dynamics (Indra et al., 2020).

Outcomes of cadherin clustering at the molecular level

While it is clear that cadherin clustering is critical for cell-cell adhesion, the direct functional implications of clustering are still being investigated. Several potential outcomes are quite intuitive but still lack direct evidence. Denser cadherin organizations can distribute applied tensions onto more molecules, potentially preventing rupture. If a single trans interaction is ruptured, rebinding will probably be more likely if it is already engaged in cis interactions and its motion is restrained, as appears to be the case for the CDHR15/CDHR23 dimer found in the tip-link filament of hair cells in the inner ear (Mulhall et al., 2021). Another key question is whether or not clustering can directly influence the strength of the trans interaction beyond what has been measured for isolated cadherin dimers engaged in trans interactions.

Two recent studies have provided some insight. As already mentioned, p120 mediated lateral interactions directly increase the binding affinity of the trans bond (Vu et al., 2021), while cis interactions increase trans binding affinity and vice versa, presumably through allosteric stabilization (Thompson et al., 2021). However, binding affinity is not necessarily predictive of how much force a cadherin bond can withstand so may not be a good measure of adhesive strength (Thiery et al., 2012), so a clear demonstration that clustering enhances resistance to rupture force is still required. Such an approach was recently applied to the β-catenin/α-catenin/actin linkage using laser tweezers to apply forces directly on the interaction between the β-catenin/α-catenin dimer and actin (Arbore et al., 2020). The authors demonstrated that a single α-catenin/β-catenin heterodimer forms a slip bond with actin, while groups of 5-10 α-catenin/β-catenin heterodimers allowed α-catenin to unfold and form a catch bond with actin (Arbore et al., 2020), which would then ostensibly recruit vinculin and increase anchoring to the cytoskeleton. To date, this is the clearest evidence that clustering may increase mechanical resistance of the CCC to an applied force.

Impacts of cadherin adhesion at the tissue level

Once a cell-cell contact is established, it must be able to withstand any applied forces to maintain tissue integrity. The most intuitive way to do this is to reinforce the cadherin-catenin complex and its coupling to the actomyosin cytoskeleton. I have discussed several mechanosensitive mechanisms found at the CCC that may contribute to reinforcement, namely the force stabilized X-dimer thought to favour formation of trans interactions under tension (Rakshit et al., 2012), the catch bond between actin and α-catenin (Buckley et al., 2014), and the force dependent unfolding of α-catenin that reveals a cryptic vinculin binding site (Yao et al., 2014; Yonemura et al., 2010), whose interaction also is a catch bond (Huang et al., 2017). In addition to these molecular mechanisms, it is increasingly clear that cadherin itself is enriched at cell-cell contacts as a direct response to increased tension (Engl et al., 2014; Gao et al., 2018; Ladoux et al., 2010; Liu et al., 2010). Several approaches to measure the resistance of cell-cell adhesions to rupture from an applied force have shown that adhesive strength scales with

cadherin levels (Chu et al., 2004; Yap et al., 1997). This stabilization could simply be due to the increased numbers of cadherins to bear the load, or the additional strengthening that clustering may bestow as discussed above, as higher cadherin levels correspond to a higher degree of clustering (Truong Quang et al., 2013).

Another way to maintain tissue integrity is cell intercalation. By adding more cells along the axis of the applied stress, the stress can be dissipated and reinforcement of the adhesion may not be necessary (Charras and Yap, 2018). In this scenario, the CCC plays a permissive role, precisely remodelling to allow dynamic cellular rearrangements while maintaining overall cohesion of the tissue. The mechanisms that regulate the CCC during these events are still poorly understood. To date, research efforts have primarily focused on endocytosis as it is established that endocytosis controls surface levels of cadherin (Davis et al., 2003; Ireton et al., 2002; Xiao et al., 2003) and it has been proposed that endocytosis can specifically target and internalize large cadherin clusters (Truong Quang et al., 2013). Two related models have been elucidated. The first showed that as neighbouring fibroblast cells migrate cadherin clusters flow towards the cell rear where they are endocytosed due to phosphorylation and unbinding of p120 after which they are recycled to the front of the cell to form new adhesive clusters (Peglion et al., 2014). The second study demonstrated in the *Drosophila* wing epithelium that p120 unbinds cadherin in response to increased tension, leading to an increase of cadherin internalization and lower levels of cadherin at cell-cell contacts that facilitated cell rearrangements (Iyer et al., 2019).

An alternative method to disassemble and remodel cadherin clusters may be related to the orientation of the applied forces. Lecuit and colleagues revealed that in embryonic *Drosophila* epithelia contractions of the apico-medial cortex apply a tensile stress that stimulated cadherin recruitment, while contraction of the junctional cortex applies a shear force that decreases the level of cadherin at the cell-cell contact, raising the possibility that cadherin is more prone to rupture when a shear force is applied (Kale et al., 2018). Both single molecule and cell detachment studies thus far have measured cadherin bond resistance to tensile forces (Chu et al., 2004; Rakshit et al., 2012), so it would be interesting to see how sensitive the cadherin bond is to shear forces at the molecular level. Importantly, these mechanisms to remodel the CCC could be generalized to also facilitate cell-cell rearrangements when the driving force isn't stress

dissipation, for example, intercellular migration of cells in response to chemotactic cues as found in the posterior mesoderm of the Xenopus gastrula (Damm and Winklbauer, 2011).

Beyond maintaining tissue integrity, the cadherin catenin complex coordinates with the actomyosin cytoskeleton to transmit forces across tissues (Vasquez and Martin, 2016), which is critical for many morphogenetic processes. Indeed, generation of tissue-scale forces corresponds with the formation of AJs (Harris et al., 2014), and knockdown of α- or β-catenin impaired transmission of forces in an epithelial sheet (Bazellières et al., 2015). Furthermore, it was recently demonstrated that altering actin dynamics in one cell alters the cytoskeletal dynamics of its neighbours in the same way, and the change was seemingly coordinated by AJs (Indra et al., 2020). These data together raising the possibility that AJs may coordinate the transmission of force, but also the physical properties that influence how the tissue responds to such a force.

The three functions of the CCC in cell adhesion

So far I have discussed cadherin mediated adhesion in terms of either binding affinity/energy or its ability to resist rupture while under tension, though in the last decade a third property critical for cadherin adhesion has emerged. While it has always been appreciated that cadherin and the actomyosin cytoskeleton have an intimate and complicated relationship, it has become clear that cortical tension - in part determined by actin density and myosin activity (Chugh and Paluch, 2018) - plays a direct role in determining adhesive strength at a cell-cell contact. Two different approaches, one measuring the work generated by the healing of toroid cell aggregates and the other estimating adhesive forces by directly separating individual cell-cell contacts, revealed that the binding energy of cadherin is not sufficient to explain the amount of adhesion at the cell-cell contact, and cortical tension is in fact a key adhesive parameter (Maître et al., 2012; Youssef et al., 2011). Consistently, actin levels and myosin activity are often downregulated at cell-cell contacts (Engl et al., 2014; Maître et al., 2012; Toret et al., 2014; Yamada and Nelson, 2007), and the magnitude of these effects appear dependent on cadherin levels at the cell-cell contact (David et al., 2014). This ability to regulate cortical tension at the contact has been termed cadherin signalling (Maître and Heisenberg, 2013), and is likely due to

the CCCs ability to interact with several actin and myosin regulators (see discussion above regarding p120 and α-catenin). In an elegant essay, Winklbauer proposed that at the cell level, the level of adhesion at equilibrium is equivalent to the difference between cortical tension at the free edge (hereafter referred to as cortical tension) and that at the contact (or contact tension), which at the tissue level can be directly measured by the tissue surface tension (Winklbauer, 2015). This would suggest that cells with higher cortical tensions have a higher potential adhesive strength as long as the mechanisms to lower contact tension can 'keep up' with the increasing cortical tension. Estimating adhesion via tissue surface tension measurements for several different tissues in the Xenopus gastrula demonstrated that contact tension was consistently reduced to about one quarter of cortical tension resulting in higher adhesion in the stiffer tissues (David et al., 2014).

This then leads to the question of among the three ways the literature has measured adhesion, which is the proper representation? Each of these properties is in fact one part that contributes to the function of adhesion as a whole (Arslan et al., 2021), though it is likely that their relative importance varies throughout the lifetime of a cell-cell contact. For instance, the binding affinity will be critical in the initial stages of adhesion, as Steinberg demonstrated that higher affinity homotypic cadherin bonds form faster and need less contact time to establish adhesion compared to a pair of lower affinity heterotypic bonds (Duguay et al., 2003; Vendome et al., 2014). If the initial contact between cells is transient due to formation and retractions of protrusions, the cadherin bonds ability to resist tension becomes immediately relevant to resist rupture upon retraction, but if contact is made within a relatively immotile tissue with little contractility this will be less important. Cadherin signalling to decrease contact tension is likely the key factor in expanding the contact (the rate determined by a combination of binding affinity and signalling) and determining the maximal adhesive strength the contact will attain as it equilibrates, and may also play a role in how force is transduced at the contact when a stress is applied. This could occur through as of yet unknown effects of cadherin signalling on the precise molecular organization of the cortex at the contact. Finally, when there is stress at the contact the most important parameter will be the cadherin bonds ability to resist rupture. Generally, binding affinity will dominate the initial stages of contact formation, cadherin signalling the

growth of the contact until it equilibrates, and bond resistance to tension the maintenance of the contact while under stress.

Experimental model: the *Xenopus laevis* gastrula

In this work, I use the *Xenopus laevis* gastrula as a model to probe the roles of cell-cell adhesion and cortical tension during morphogenetic processes. Here I will summarize the major developmental landmarks before highlighting the benefits *Xenopus* offers as a model.

Early development of *Xenopus laevis*

The *Xenopus* oocyte is clearly defined by a heavily pigmented animal pole and a vegetal pole enriched with yolk platelets. The animal-vegetal (AV) and dorsal-ventral (DV) axis are pre-patterned after fertilization thanks to maternally localized mRNAs and proteins (Heasman, 2006). Briefly, Zic2 and Xgrh11 are found in the animal pole while VegT and TGFβ family members are concentrated vegetally to establish the AV axis (Heasman, 2006). After fertilization, cortical rotation moves the vegetally localized Wnt11 to the future dorsal side of the embryo opposite the point of sperm entry. There, it heterodimerizes with the ubiquitously distributed Wnt5a to induce the dorsal axis (Cha et al., 2008; Fagotto, 2014). After zygotic transcription commences, the three germ layers of the embryo are specified through the localized activation of four principal signalling pathways (Heasman, 2006). To present a simplified view: endoderm is characterized by high TGFβ signalling, ectoderm by BMP signalling, while mesoderm forms through a combination of TGFβ and FGF signalling and is dorsalized by Wnt activity (Heasman, 2006; Smith, 2009). Within the mesoderm, cells exposed to higher levels of TGFβ will form the prechordal mesoderm, marked by expression of goosecoid, while lower levels of TGFβ induce expression of Brachyury and formation of the chordamesoderm (Smith, 2009).

After specification of the three germ layers, extensive tissue-level rearrangements are initiated that lead to the complete internalization of the endoderm, the spreading of the ectoderm over the exterior of the embryo, and the placement of the mesoderm between the two. Before gastrulation, the ectoderm is found in the animal pole as a multiplayers epithelial

sheet surrounding the blastocoel forming the blastocoel roof (BCR), the endoderm occupies the vegetal pole, and the mesoderm at the interface between the two at the marginal zone. At the onset of gastrulation, the endoderm begins an ingression-like migration flowing up and out and helping bring the mesoderm at the marginal zone in contact with the BCR. The dorsal mesoderm involutes, turning over the blastopore lip, and migrates inside the embryo using the BCR as a substrate. As involution proceeds the mesoderm is thinned through radial cell intercalations in the prechordal mesoderm, and then later extensive medio-lateral intercalations drive convergence and extension of the tissue. Involution extends laterally and ventrally as the blastopore slowly closes. Meanwhile, the multilayered ectoderm thins through epiboly as it spreads to cover the exterior of the embryo (Keller et al., 2003).

This reorganization of the embryo establishes the basic body plan of the embryo and is driven primarily by cell-cell rearrangements (Huang and Winklbauer, 2018). Many common models used to study morphogenetic processes are driven by remodelling of epithelial tissues whose cells are rearranged through the stereotypical T1 transition driven by periodic contractions of the junctional actomyosin cytoskeleton (Lemke and Nelson, 2021; Pinheiro and Bellaïche, 2018). However, the *Xenopus* gastrula does not rely on the standard tactics found within epithelial models to stimulate cell rearrangements. Instead, it utilizes differential cell motility through two modes of cell migration; amoeboid-like in the endoderm and mesenchymal in the mesoderm (Huang and Winklbauer, 2018; Wen and Winklbauer, 2017). This is reflected in the fact that the cells of the highly dynamic mesodermal tissue retain their motility when they are isolated and plated on FN (Wacker et al., 1998). On the other hand, isolated ectoderm cells are not migratory consistent with the less dynamic properties of the tissue during gastrulation. This makes the *Xenopus* gastrula an exciting model to attempt to study under-characterized types of morphogenesis.

Xenopus laevis **as a model**

The biggest advantage of *Xenopus laevis* is the ability to work at multiple scales, from the whole embryo, to explanted tissues, to dissociated single cells, a feature I exploit throughout this work. Importantly, many morphogenetic processes are tissue autonomous and are preserved in

explanted tissues, for example: mesoderm involution and intercalation (Evren et al., 2014), vegetal rotation (Wen and Winklbauer, 2017), and blastopore closure (Shook et al., 2018). Further, single cells isolated from tissues maintain the differences in morphology and motility that is observed between their parent tissues (Wacker et al., 1998). Single cells and tissues are amenable to measurements of their mechanical properties (Canty et al., 2017; David et al., 2014), and a vast range of established explant systems can be used to explore tissue properties. Injection of mRNAs to augment expression of genes or to introduce fluorescently tagged constructs is well established; morpholino (MO) mediated sequestering of mRNAs provides a simple tool for specific and reliable suppression of target mRNA expression (Rossi et al., 2015). Additionally, mRNAs and MOs can be targeted to specific tissues through injection of specific blastomeres during cleavage. Finally, exogenous activation of TGFβ and Wnt signalling in the ectoderm can induce mesoderm specification, which is used in Chapter III (Green et al., 1992; Wardle and Smith, 2004).

Thesis Objectives

The principal objective for this thesis was to examine the different roles that cortical tension and cell-cell adhesion play within a model of mesenchymal morphogenesis.

Chapter II objective

The main objective of this chapter was to first attempt to identify what causes the basic differences in motility between ectoderm and mesodermal cells, which was performed primarily by my co-author on the published article, Leily Kashkooli. After identification and characterization of two mesoderm specific negative regulators of RhoA, we sought to characterize the single cell phenotypes from overexpression in the ectoderm or inhibition in the mesoderm. I then extended this characterization to the tissue level, examining both the collective migratory properties as well as the mechanical properties of the tissue, finding data perfectly consistent with the single cell characterization.

Chapter III objective

Models of mesenchymal morphogenesis, like the *Xenopus* mesoderm, rely on cell migration to remodel their cell-cell contacts. After identifying developmentally required regulators of mesoderm migration in Chapter II, in Chapter III I sought to understand how cell-cell contacts are dynamically regulated to permit cell rearrangements in response to tension applied by differential cell migration. I identify a remodelling paradigm that depends on peeling of the cadherin trans bond to displace cadherin from the contact before a final stage required cytoplasmic rupture of the CCCs link to the cytoskeleton. I also note that modulating cortical tension influences how the cell-cell contact is remodelled.

Chapter IV objective

The objective of this final chapter is to provide a more in-depth, narrative discussion of the results found in Chapters II and III. I will also discuss some interesting remaining questions not only related to the results of Chapter II and III, but also the cadherin field in general which I considered while preparing Chapter I.

References

Abe, K. and Takeichi, M. (2008). EPLIN mediates linkage of the cadherin-catenin complex to F-actin and stabilizes the circumferential actin belt. *Proceedings of the National Academy of Sciences of the United States of America* **105**, 13–19.

Aberle, H., Butz, S., Stappert, J., Weissig, H., Kemler, R. and Hoschuetzky, H. (1994). Assembly of the cadherin-catenin complex in vitro with recombinant proteins. *Journal of Cell Science* **107**, 3655–3663.

Alekhina, O., Burstein, E. and Billadeau, D. D. (2017). Cellular functions of WASP family proteins at a glance. *Journal of Cell Science* **130**, 2235–2241.

Amano, M., Chihara, K., Nakamura, N., Kaneko, T., Matsuura, Y. and Kaibuchi, K. (1999). The COOH terminus of Rho-kinase negatively regulates Rho-kinase activity. *Journal of Biological Chemistry* **274**, 32418–32424.

Anastasiadis, P. Z., Moon, S. Y., Thoreson, M. A., Mariner, D. J., Crawford, H. C., Zheng, Y. and Reynolds, A. B. (2000). Inhibition of RhoA by p120 catenin. *Nature Cell Biology* **2**, 637–644.

Arbore, C., Sergides, M., Gardini, L., Pavone, F. and Capitanio, M. (2020). a-catenin switches between a slip and a cooperative catch bond with F-actin to regulate cell junction fluidity. *bioRxiv*.

Arslan, F. N., Eckert, J., Schmidt, T. and Heisenberg, C. P. (2021). Holding it together: when cadherin meets cadherin. *Biophysical Journal* 1–11.

Arthur, W. T. and Burridge, K. (2001). RhoA inactivation by p190RhoGAP regulates cell spreading and migration by promoting membrane protrusion and polarity. *Molecular Biology of the Cell* **12**, 2711–2720.

Bajpai, S., Correia, J., Feng, Y., Figueiredo, J., Sun, S. X., Longmore, G. D., Suriano, G. and Wirtz, D. (2008). α-Catenin mediates initial E-cadherin-dependent cell- cell recognition and subsequent bond strengthening. *Proceedings of the National Academy of Sciences of the United States of America* **105**, 18331–18336.

Bajpai, S., Feng, Y., Krishnamurthy, R., Longmore, G. D. and Wirtz, D. (2009). Loss of α-catenin decreases the strength of single E-cadherin bonds between human cancer cells. *Journal of Biological Chemistry* **284**, 18252–18259.

Bays, J. L. and DeMali, K. A. (2017). Vinculin in cell–cell and cell–matrix adhesions. *Cellular and Molecular Life Sciences* **74**, 2999–3009.

Bays, J. L., Peng, X., Tolbert, C. E., Guilluy, C., Angell, A. E., Pan, Y., Superfine, R., Burridge, K. and DeMali, K. A. (2014). Vinculin phosphorylation differentially regulates

mechanotransduction at cell-cell and cell-matrix adhesions. *Journal of Cell Biology* **205**, 251–263.

Bazellières, E., Conte, V., Elosegui-Artola, A., Serra-Picamal, X., Bintanel-Morcillo, M., Roca-Cusachs, P., Muñoz, J. J., Sales-Pardo, M., Guimerà, R. and Trepat, X. (2015). Control of cell-cell forces and collective cell dynamics by the intercellular adhesome. *Nature Cell Biology* **17**, 409–420.

Beach, J. R., Shao, L., Remmert, K., Li, D., Betzig, E. and Hammer, J. A. (2014). Nonmuscle myosin II isoforms coassemble in living cells. *Current Biology* **24**, 1160–1166.

Bendix, P. M., Koenderink, G. H., Cuvelier, D., Dogic, Z., Koeleman, B. N., Brieher, W. M., Field, C. M., Mahadevan, L. and Weitz, D. A. (2008). A quantitative analysis of contractility in active cytoskeletal protein networks. *Biophysical Journal* **94**, 3126–3136.

Benjamin, J. M., Kwiatkowski, A. V., Yang, C., Korobova, F., Pokutta, S., Svitkina, T., Weis, W. I. and Nelson, W. J. (2010). αE-catenin regulates actin dynamics independently of cadherin-mediated cell-cell adhesion. *Journal of Cell Biology* **189**, 339–352.

Berger-Müller, S. and Suzuki, T. (2011). Seven-pass transmembrane cadherins: roles and emerging mechanisms in axonal and dendritic patterning. *Molecular neurobiology* **44**, 313–320.

Bertocchi, C., Vaman Rao, M. and Zaidel-Bar, R. (2012). Regulation of Adherens Junction Dynamics by Phosphorylation Switches. *Journal of Signal Transduction* **2012**, 1–14.

Biro, M., Romeo, Y., Kroschwald, S., Bovellan, M., Boden, A., Tcherkezian, J., Roux, P. P., Charras, G. and Paluch, E. K. (2013). Cell cortex composition and homeostasis resolved by integrating proteomics and quantitative imaging. *Cytoskeleton* **70**, 741–754.

Boggon, T. J., Murray, J., Chappuis-Flament, S., Wong, E., Gumbiner, B. M. and Shapiro, L. (2002). C-cadherin ectodomain structure and implications for cell adhesion mechanisms. *Science* **296**, 1308–1313.

Borghi, N., Sorokina, M., Shcherbakova, O. G., Weis, W. I., Pruitt, B. L., Nelson, W. J. and Dunn, A. R. (2012). Erratum: E-cadherin is under constitutive actomyosingenerated tension that is increased at cell-cell contacts upon externally applied stretch (Proceedings of the National Academy of Sciences of the United States of America (2012) 109, 31 (12568-12573) DOI. *Proceedings of the National Academy of Sciences of the United States of America* **109**, 19034.

Boureux, A., Vignal, E., Faure, S. and Fort, P. (2007). Evolution of the Rho family of Ras-like GTPases in eukaryotes. *Molecular Biology and Evolution* **24**, 203–216.

Brasch, J., Harrison, O. J., Honig, B. and Shapiro, L. (2012). Thinking outside the cell: How cadherins drive adhesion. *Trends in Cell Biology* **22**, 299–310.

Brasch, J., Katsamba, P. S., Harrison, O. J., Ahlsén, G., Troyanovsky, R. B., Indra, I., Kaczynska, A., Kaeser, B., Troyanovsky, S., Honig, B., et al. (2018). Homophilic and Heterophilic Interactions of Type II Cadherins Identify Specificity Groups Underlying Cell-Adhesive Behavior. *Cell Reports* **23**, 1840–1852.

Breitsprecher, D. and Goode, B. L. (2013). Formins at a glance. *Journal of Cell Science* **126**, 1–7.

Brieher, W. M., Yap, A. S. and Gumbiner, B. M. (1996). Lateral dimerization is required for the homophilic binding activity of C-cadherin. *Journal of Cell Biology* **135**, 487–496.

Brito, C. and Sousa, S. (2020). Non-Muscle Myosin 2A (NM2A): Structure, Regulation and Function. *Cells* **9**, 12–16.

Buckley, C. D., Tan, J., Anderson, K. L., Hanein, D., Volkmann, N., Weis, W. I., Nelson, W. J. and Dunn, A. R. (2014). The minimal cadherin-catenin complex binds to actin filaments under force. *Science* **346**,.

Burke, T. A., Christensen, J. R., Barone, E., Suarez, C., Sirotkin, V. and Kovar, D. R. (2014). Homeostatic actin cytoskeleton networks are regulated by assembly factor competition for monomers. *Current Biology* **24**, 579–585.

Burridge, K. and Guilluy, C. (2016). Focal adhesions, stress fibers and mechanical tension. *Experimental Cell Research* **343**, 14–20.

Butler, M. T. and Wallingford, J. B. (2017). Planar cell polarity in development and disease. *Nature Reviews Molecular Cell Biology* **18**, 375–388.

Canty, L., Zarour, E., Kashkooli, L., François, P. and Fagotto, F. (2017). Sorting at embryonic boundaries requires high heterotypic interfacial tension. *Nature communications* **8**, 157.

Case, L. B. and Waterman, C. M. (2015). Integration of actin dynamics and cell adhesion by a three-dimensional, mechanosensitive molecular clutch. *Nature Cell Biology* **17**, 955–963.

Cha, S. W., Tadjuidje, E., Tao, Q., Wylie, C. and Heasman, J. (2008). Wnt5a and Wnt11 interact in a maternal Dkk1-regulated fashion to activate both canonical and non-canonical signalling in Xenopus axis formation. *Development* **135**, 3719–3729.

Chandran, R., Kale, G., Philippe, J. M., Lecuit, T. and Mayor, S. (2021). Distinct actin-dependent nanoscale assemblies underlie the dynamic and hierarchical organization of E-cadherin. *Current Biology* **31**, 1726-1736.e4.

Charras, G. and Yap, A. S. (2018). Tensile Forces and Mechanotransduction at Cell–Cell Junctions. *Current Biology* **28**, R445–R457.

Chastney, M. R., Conway, J. R. W. and Ivaska, J. (2021). Integrin adhesion complexes. *Current Biology* **31**, R536–R542.

Chen, Z., Borek, D., Padrick, S. B., Gomez, T. S., Metlagel, Z., Ismail, A. M., Umetani, J., Billadeau, D. D., Otwinowski, Z. and Rosen, M. K. (2010). Structure and control of the actin regulatory WAVE complex. *Nature* **468**, 533–538.

Chiarella, S. E., Rabin, E. E., Ostilla, L. A., Flozak, A. S. and Gottardi, C. J. (2018). αT-catenin: A developmentally dispensable, disease-linked member of the α-catenin family. *Tissue Barriers* **6**, 1–12.

Choi, H. J., Huber, A. H. and Weis, W. I. (2006). Thermodynamics of β-catenin-ligand interactions: The roles of the N- and C-terminal tails in modulating binding affinity. *Journal of Biological Chemistry* **281**, 1027–1038.

Choi, S. H., Estarás, C., Moresco, J. J., Yates, J. R. and Jones, K. A. (2013). α-Catenin interacts with APC to regulate β-catenin proteolysis and transcriptional repression of Wnt target genes. *Genes and Development* **27**, 2473–2488.

Chu, Y. S., Thomas, W. A., Eder, O., Pincet, F., Perez, E., Thiery, J. P. and Dufour, S. (2004). Force measurements in E-cadherin-mediated cell doublets reveal rapid adhesion strengthened by actin cytoskeleton remodelling through Rac and Cdc42. *Journal of Cell Biology* **167**, 1183–1194.

Chugh, P. and Paluch, E. K. (2018). The actin cortex at a glance. *Journal of Cell Science* **131**, 1–9.

Chugh, P., Clark, A. G., Smith, M. B., Cassani, D. A. D., Dierkes, K., Ragab, A., Roux, P. P., Charras, G., Salbreux, G. and Paluch, E. K. (2017). Actin cortex architecture regulates cell surface tension. *Nature Cell Biology* **19**, 689–697.

Ciatto, C., Bahna, F., Zampieri, N., Vansteenhouse, H. C., Katsamba, P. S., Ahlsen, G., Harrison, O. J., Brasch, J., Jin, X., Posy, S., et al. (2010). T-cadherin structures reveal a novel adhesive binding mechanism. *Nature Structural and Molecular Biology* **17**, 339–347.

Clarke, D. N. and Martin, A. C. (2021). Actin-based force generation and cell adhesion in tissue morphogenesis. *Current Biology* **31**, R667–R680.

Cramer, L. P. (2013). Mechanism of cell rear retraction in migrating cells. *Current Opinion in Cell Biology* **25**, 591–599.

Damm, E. W. and Winklbauer, R. (2011). PDGF-A controls mesoderm cell orientation and radial intercalation during Xenopus gastrulation. *Development* **138**, 565–575.

Daniel, J. M. and Reynolds, A. B. (1995). The tyrosine kinase substrate p120cas binds directly to E-cadherin but not to the adenomatous polyposis coli protein or alpha-catenin. *Molecular and Cellular Biology* **15**, 4819–4824.

Daniel, J. M. and Reynolds, A. B. (1999). The Catenin p120 ctn Interacts with Kaiso, a Novel BTB/POZ Domain Zinc Finger Transcription Factor . *Molecular and Cellular Biology* **19**, 3614–3623.

Daugherty, R. L., Serebryannyy, L., Yemelyanov, A., Flozak, A. S., Yu, H. J., Kosak, S. T., De Lanerolle, P. and Gottardi, C. J. (2014). α-Catenin is an inhibitor of transcription. *Proceedings of the National Academy of Sciences of the United States of America* **111**, 5260–5265.

David, R., Luu, O., Damm, E. W., Wen, J. W. H., Nagel, M. and Winklbauer, R. (2014a). Tissue cohesion and the mechanics of cell rearrangement. *Development (Cambridge)* **141**, 3672–3682.

David, R., Luu, O., Damm, E. W., Wen, J. W. H., Nagel, M. and Winklbauer, R. (2014b). Tissue cohesion and the mechanics of cell rearrangement. *Development (Cambridge, England)* **141**, 3672–3682.

Davis, M. A., Ireton, R. C. and Reynolds, A. B. (2003). A core function for p120-catenin in cadherin turnover. *Journal of Cell Biology* **163**, 525–534.

Denk-Lobnig, M. and Martin, A. C. (2019). Modular regulation of Rho family GTPases in development. *Small GTPases* **10**, 122–129.

Ding, W. Y., Ong, H. T., Hara, Y., Wongsantichon, J., Toyama, Y., Robinson, R. C., Nédélec, F. and Zaidel-Bar, R. (2017). Plastin increases cortical connectivity to facilitate robust polarization and timely cytokinesis. *Journal of Cell Biology* **216**, 1371–1386.

Drees, F., Pokutta, S., Yamada, S., Nelson, W. J. and Weis, W. I. (2005). α-catenin is a molecular switch that binds E-cadherin-β-catenin and regulates actin-filament assembly. *Cell* **123**, 903–915.

Duguay, D., Foty, R. A. and Steinberg, M. S. (2003). Cadherin-mediated cell adhesion and tissue segregation: Qualitative and quantitative determinants. *Developmental Biology* **253**, 309–323.

Efimova, N. and Svitkina, T. M. (2018). Branched actin networks push against each other at adherens junctions to maintain cell-cell adhesion. *Journal of Cell Biology* **217**, 1827–1845.

Elia, L. P., Yamamoto, M., Zang, K. and Reichardt, L. F. (2006). p120 Catenin Regulates Dendritic Spine and Synapse Development through Rho-Family GTPases and Cadherins. *Neuron* **51**, 43–56.

Engl, W., Arasi, B., Yap, L. L., Thiery, J. P. and Viasnoff, V. (2014). Actin dynamics modulate mechanosensitive immobilization of E-cadherin at adherens junctions. *Nature Cell Biology* **16**, 584–591.

Ennomani, H., Letort, G., Guérin, C., Martiel, J. L., Cao, W., Nédélec, F., de La Cruz, E. M., Théry, M. and Blanchoin, L. (2016). Architecture and Connectivity Govern Actin Network Contractility. *Current Biology* **26**, 616–626.

Erami, Z., Timpson, P., Yao, W., Zaidel-Bar, R. and Anderson, K. I. (2015). There are four dynamically and functionally distinct populations of E-cadherin in cell junctions. *Biology Open* **4**, 1481–1489.

Etienne-Manneville, S. and Hall, A. (2002). Rho GTPases in cell biology. *Nature* **420**, 629–635.

Evren, S., Wen, J. W. H., Luu, O., Damm, E. W., Nagel, M. and Winklbauer, R. (2014). EphA4-dependent Brachyury expression is required for dorsal mesoderm involution in the Xenopus gastrula. *Development* **141**, 3649–3661.

Fagotto, F. (2014). Wnt Signalling during Early Xenopus Development. *Xenopus Development* **9781118492**, 130–162.

Finer, J. T., Simmons, R. M. and Spudich, J. A. (1994). Single myosin molecule mechanics: Piconewton forces and nanometre steps. *Nature* **368**, 113–119.

Foty, R. A. and Steinberg, M. S. (2005). The differential adhesion hypothesis: A direct evaluation. *Developmental Biology* **278**, 255–263.

Francou, A. and Anderson, K. V. (2020). The Epithelial-to-Mesenchymal Transition in Development and Cancer. *Annual Review of Cancer Biology* **4**, 197–220.

Fujita, Y., Krause, G., Scheffner, M., Zechner, D., Leddy, H. E. M., Behrens, J., Sommer, T. and Birchmeier, W. (2002). Hakai, a c-Cbl-like protein, ubiquitinates and induces endocytosis of the E-cadherin complex. *Nature Cell Biology* **4**, 222–231.

Fukuyama, T., Ogita, H., Kawakatsu, T., Inagaki, M. and Takai, Y. (2006). Activation of Rac by cadherin through the c-Src-Rap1-phosphatidylinositol 3-kinase-Vav2 pathway. *Oncogene* **25**, 8–19.

Gao, L. and Bretscher, A. (2008). Analysis of unregulated formin activity reveals how yeast can balance F-actin assembly between different microfilament-based organizations. *Molecular biology of the cell* **19**, 1474–1484.

Gao, X., Acharya, B. R., Engl, W. C. O., De Mets, R., Thiery, J. P., Yap, A. S. and Viasnoff, V. (2018). Probing compression versus stretch activated recruitment of cortical actin and apical junction proteins using mechanical stimulations of suspended doublets. *APL Bioengineering* **2**,.

Goodman, K. M., Rubinstein, R., Thu, C. A., Mannepalli, S., Bahna, F., Ahlsén, G., Rittenhouse, C., Maniatis, T., Honig, B. and Shapiro, L. (2016). γ-Protocadherin structural diversity and functional implications. *eLife* **5**, 1–25.

Green, J. B. A., New, H. v and Smith, J. C. (1992). *Responses of Embryonic Xenopus Cells to Activin and FGF Are Separated by Multiple Dose Thresholds and Correspond to Distinct Axes of the Mesoderm*.

Gul, I. S., Hulpiau, P., Saeys, Y. and van Roy, F. (2017). Evolution and diversity of cadherins and catenins. *Experimental Cell Research* **358**, 3–9.

Hansen, S. D., Kwiatkowski, A. V., Ouyang, C. Y., Liud, H. J., Pokutta, S., Watkins, S. C., Volkmann, N., Hanein, D., Weis, W. I., Mullins, R. D., et al. (2013). Ae-Catenin Actin-Binding Domain Alters Actin Filament Conformation and Regulates Binding of Nucleation and Disassembly Factors. *Molecular Biology of the Cell* **24**, 3710–3720.

Harris, A. R., Daeden, A. and Charras, G. T. (2014). Formation of adherens junctions leads to the emergence of a tissue-level tension in epithelial monolayers. *Journal of Cell Science* **127**, 2507–2517.

Harrison, O. J., Bahna, F., Katsamba, P. S., Jin, X., Brasch, J., Vendome, J., Ahlsen, G., Carroll, K. J., Price, S. R., Honig, B., et al. (2010). Two-step adhesive binding by classical cadherins. *Nature Structural and Molecular Biology* **17**, 348–357.

Harrison, O. J., Jin, X., Hong, S., Bahna, F., Ahlsen, G., Brasch, J., Wu, Y., Vendome, J., Felsovalyi, K., Hampton, C. M., et al. (2011). The extracellular architecture of adherens junctions revealed by crystal structures of type i cadherins. *Structure* **19**, 244–256.

Harrison, O. J., Brasch, J., Lasso, G., Katsamba, P. S., Ahlsen, G., Honig, B. and Shapiro, L. (2016). Structural basis of adhesive binding by desmocollins and desmogleins. *Proceedings of the National Academy of Sciences of the United States of America* **113**, 7160–7165.

Hartman, M. A. and Spudich, J. A. (2012). The myosin superfamily at a glance. *Journal of Cell Science* **125**, 1627–1632.

Hartmann, S., Ridley, A. J. and Lutz, S. (2015). The function of rho-associated kinases ROCK1 and ROCK2 in the pathogenesis of cardiovascular disease. *Frontiers in Pharmacology* **6**, 1–16.

Hartsock, A. and Nelson, W. J. (2012). Competitive regulation of E-cadherin juxtamembrane domain degradation by p120-catenin binding and Hakai-mediated ubiquitination. *PLoS ONE* **7**, 1–14.

Hatta, K. and Takeichi, M. (1986). Expression of N-cadherin adhesion molecules associated with early morphogenetic events in chick development. *Nature* **320**, 447–449.

Hayashi, S. and Takeichi, M. (2015). Emerging roles of protocadherins: From self-avoidance to enhancement of motility. *Journal of Cell Science* **128**, 1455–1464.

Heasman, J. (2006). Patterning the early Xenopus embryo. *Development* **133**, 1205–1217.

Herrenknecht, K., Ozawa, M., Eckerskorn, C., Lottspeich, F., Lenter, M. and Kemler, R. (1991). The uvomorulin-anchorage protein α catenin is a vinculin homologue. *Proceedings of the National Academy of Sciences of the United States of America* **88**, 9156–9160.

Heuzé, M. L., Sankara Narayana, G. H. N., D'Alessandro, J., Cellerin, V., Dang, T., Williams, D. S., van Hest, J. C. M., Marcq, P., Mège, R. M. and Ladoux, B. (2019). Myosin II isoforms play distinct roles in adherens junction biogenesis. *eLife* **8**, 1–30.

Hinck, L., Näthke, I. S., Papkoff, J. and Nelson, W. J. (1994). Dynamics of cadherin/catenin complex formation: Novel protein interactions and pathways of complex assembly. *Journal of Cell Biology* **125**, 1327–1340.

Hirano, S., Nose, A., Hatta, K., Kawakami, A. and Takeichi, M. (1987). Calcium-dependent Cell-Cell Adhesion Molecules (Cadherins): Subclass Specificities and Possible Involvement of Actin Bundles. **105**, 2501–2510.

Hodge, R. G. and Ridley, A. J. (2016). Regulating Rho GTPases and their regulators. *Nature Reviews Molecular Cell Biology* **17**, 496–510.

Hong, J. Y., Park, J. Il, Cho, K., Gu, D., Ji, H., Artandi, S. E. and McCrea, P. D. (2010). Shared molecular mechanisms regulate multiple catenin proteins: Canonical Wnt signals and components modulate p120-catenin isoform-1 and additional p120 subfamily members. *Journal of Cell Science* **123**, 4351–4365.

Hong, S., Troyanovsky, R. B. and Troyanovsky, S. M. (2011). Cadherin exits the junction by switching its adhesive bond. *Journal of Cell Biology* **192**, 1073–1083.

Hong, S., Troyanovsky, R. B. and Troyanovsky, S. M. (2013). Binding to F-actin guides cadherin cluster assembly, stability, and movement. *Journal of Cell Biology* **201**, 131–143.

Honig, B. and Shapiro, L. (2020). Adhesion Protein Structure, Molecular Affinities, and Principles of Cell-Cell Recognition. *Cell* **181**, 520–535.

Houdusse, A. and Sweeney, H. L. (2016). How Myosin Generates Force on Actin Filaments. *Trends in Biochemical Sciences* **41**, 989–997.

Huang, Y. and Winklbauer, R. (2018). Cell migration in the Xenopus gastrula. *Wiley interdisciplinary reviews. Developmental biology* **7**, e325.

Huang, D. L., Bax, N. A., Buckley, C. D., Weis, W. I. and Dunn, A. R. (2017). Vinculin forms a directionally asymmetric catch bond with F-actin. *Science* **357**, 703–706.

Huber, O., Krohn, M. and Kemler, R. (1997). A specific domain in α-catenin mediates binding to β-catenin or plakoglobin. *Journal of Cell Science* **110**, 1759–1765.

Huber, A. H., Stewart, D. B., Laurents, D. V., Nelson, W. J. and Weis, W. I. (2001). The cadherin cytoplasmic domain is unstructured in the absence of β-catenin. A possible mechanism for regulating cadherin turnover. *Journal of Biological Chemistry* **276**, 12301–12309.

Hulpiau, P. and Van Roy, F. (2011). New insights into the evolution of metazoan cadherins. *Molecular Biology and Evolution* **28**, 647–657.

Hulpiau, P., Gul, I. S. and van Roy, F. (2016). Evolution of Cadherins and Associated Catenins. In *The Cadherin Superfamily: Key Regulators of Animal Development and Physiology* (ed. Suzuki, S. T.) and Hirano, S.), pp. 13–37.

Hülsken, J., Birchmeier, W. and Behrens, J. (1994). E-cadherin and APC compete for the interaction with β-catenin and the cytoskeleton. *Journal of Cell Biology* **127**, 2061–2069.

Indra, I., Choi, J., Chen, C. S., Troyanovsky, R. B., Shapiro, L., Honig, B. and Troyanovsky, S. M. (2018). Spatial and temporal organization of cadherin in punctate adherens junctions. *Proceedings of the National Academy of Sciences of the United States of America* **115**, E4406–E4415.

Indra, I., Troyanovsky, R. B., Shapiro, L., Honig, B. and Troyanovsky, S. M. (2020). Sensing Actin Dynamics through Adherens Junctions. *Cell Reports* **30**, 2820-2833.e3.

Ireton, R. C., Davis, M. A., Van Hengel, J., Mariner, D. J., Barnes, K., Thoreson, M. A., Anastasiadis, P. Z., Matrisian, L., Bundy, L. M., Sealy, L., et al. (2002). A novel role for p120 catenin in E-cadherin function. *Journal of Cell Biology* **159**, 465–476.

Ishiyama, N., Lee, S. H., Liu, S., Li, G. Y., Smith, M. J., Reichardt, L. F. and Ikura, M. (2010). Dynamic and Static Interactions between p120 Catenin and E-Cadherin Regulate the Stability of Cell-Cell Adhesion. *Cell* **141**, 117–128.

Ishiyama, N., Tanaka, N., Abe, K., Yang, Y. J., Abbas, Y. M., Umitsu, M., Nagar, B., Bueler, S. A., Rubinstein, J. L., Takeichi, M., et al. (2013). An autoinhibited structure of α-catenin and its implications for vinculin recruitment to adherens junctions. *Journal of Biological Chemistry* **288**, 15913–15925.

Ishiyama, N., Sarpal, R., Wood, M. N., Barrick, S. K., Nishikawa, T., Hayashi, H., Kobb, A. B., Flozak, A. S., Yemelyanov, A., Fernandez-Gonzalez, R., et al. (2018). Force-dependent allostery of the α-catenin actin-binding domain controls adherens junction dynamics and functions. *Nature Communications* **9**, 1–17.

Itoh, M., Nagafuchi, A., Moroi, S. and Tsukita, S. (1997). Involvement of ZO-1 in cadherin-based cell adhesion through its direct binding to α catenin and actin filaments. *Journal of Cell Biology* **138**, 181–192.

Iyer, K. V., Piscitello-Gómez, R., Paijmans, J., Jülicher, F. and Eaton, S. (2019). Epithelial Viscoelasticity Is Regulated by Mechanosensitive E-cadherin Turnover. *Current Biology* **29**, 578-591.e5.

Jaiganesh, A., Narui, Y., Araya-Secchi, R. and Sotomayor, M. (2018). Beyond cell–cell adhesion: Sensational cadherins for hearing and balance. *Cold Spring Harbor Perspectives in Biology* **10**, 1–26.

Julian, L. and Olson, M. F. (2014). Rho-associated coiled-coil containing kinases (ROCK), structure, regulation, and functions. *Small GTPases* **5**,.

Kale, G. R., Yang, X., Philippe, J. M., Mani, M., Lenne, P. F. and Lecuit, T. (2018). Distinct contributions of tensile and shear stress on E-cadherin levels during morphogenesis. *Nature Communications* **9**,.

Kanellos, G. and Frame, M. C. (2016). Cellular functions of the ADF/cofilin family at a glance. *Journal of Cell Science* **129**, 3211–3218.

Katsamba, P., Carroll, K., Ahlsen, G., Bahna, F., Vendome, J., Posy, S., Rajebhosale, M., Price, S., Jessell, T. M., Ben-Shaul, A., et al. (2009). Linking molecular affinity and cellular specificity in cadherin-mediated adhesion. *Proceedings of the National Academy of Sciences of the United States of America* **106**, 11594–11599.

Kelkar, M., Bohec, P. and Charras, G. (2020). Mechanics of the cellular actin cortex: From signalling to shape change. *Current Opinion in Cell Biology* **66**, 69–78.

Keller, R., Davidson, L. A. and Shook, D. R. (2003). How we are shaped: the biomechanics of gastrulation. *Differentiation; research in biological diversity* **71**, 171–205.

Kim, L. and Wong, T. W. (1995). The cytoplasmic tyrosine kinase FER is associated with the catenin-like substrate pp120 and is activated by growth factors. *Molecular and Cellular Biology* **15**, 4553–4561.

Knudsen, K. A., Soler, A. P., Johnson, K. R. and Wheelock, M. J. (1995). Interaction of α-actinin with the cadherin/catenin cell-cell adhesion complex via α-catenin. *Journal of Cell Biology* **130**, 67–77.

Kobielak, A., Pasolli, H. A. and Fuchs, E. (2004). Mammalian formin-1 participates in adherens junctions and polymerization of linear actin cables. *Nature Cell Biology* **6**, 21–30.

Koslov, E. R., Maupin, P., Pradhan, D., Morrow, J. S. and Rimm, D. L. (1997). A-Catenin Can Form Asymmetric Homodimeric Complexes and/or Heterodimeric Complexes With B-Catenin. *Journal of Biological Chemistry* **272**, 27301–27306.

Kourtidis, A., Ngok, S. P., Pulimeno, P., Feathers, R. W., Carpio, L. R., Baker, T. R., Carr, J. M., Yan, I. K., Borges, S., Perez, E. A., et al. (2015). Distinct E-cadherin-based complexes regulate

cell behaviour through miRNA processing or Src and p120 catenin activity. *Nature Cell Biology* **17**, 1145–1157.

Kowalczyk, A. P. and Green, K. J. (2013). *Structure, function, and regulation of desmosomes*. 1st ed. Elsevier Inc.

Krause, M. and Gautreau, A. (2014). Steering cell migration: Lamellipodium dynamics and the regulation of directional persistence. *Nature Reviews Molecular Cell Biology* **15**, 577–590.

Kühn, S. and Geyer, M. (2014). Formins as effector proteins of rho GTPases. *Small GTPases* **5**, 1–16.

Kümper, S., Mardakheh, F. K., McCarthy, A., Yeo, M., Stamp, G. W., Paul, A., Worboys, J., Sadok, A., Jørgensen, C., Guichard, S., et al. (2016). Rho-associated kinase (ROCK) function is essential for cell cycle progression, senescence and tumorigenesis. *eLife* **5**, 1–24.

Ladoux, B., Anon, E., Lambert, M., Rabodzey, A., Hersen, P., Buguin, A., Silberzan, P. and Mège, R. M. (2010). Strength dependence of cadherin-mediated adhesions. *Biophysical Journal* **98**, 534–542.

Lawson, C. D. and Burridge, K. (2014). The on-off relationship of Rho and Rac during integrin-mediated adhesion and cell migration. *Small GTPases* **5**,.

Le, T. L., Yap, A. S. and Stow, J. L. (1999). Recycling of E-cadherin: A potential mechanism for regulating cadherin dynamics. *Journal of Cell Biology* **146**, 219–232.

Le Duc, Q., Shi, Q., Blonk, I., Sonnenberg, A., Wang, N., Leckband, D. and De Rooij, J. (2010). Vinculin potentiates E-cadherin mechanosensing and is recruited to actin-anchored sites within adherens junctions in a myosin II-dependent manner. *Journal of Cell Biology* **189**, 1107–1115.

Lemke, S. B. and Nelson, C. M. (2021). Dynamic changes in epithelial cell packing during tissue morphogenesis. *Current Biology* **31**, R1098–R1110.

Lickert, H., Bauer, A., Kemler, R. and Stappert, J. (2000). Casein kinase II phosphorylation of E-cadherin increases E-cadherin/β- catenin interaction and strengthens cell-cell adhesion. *Journal of Biological Chemistry* **275**, 5090–5095.

Liu, Z., Tan, J. L., Cohen, D. M., Yang, M. T., Sniadecki, N. J., Ruiz, S. A., Nelson, C. M. and Chen, C. S. (2010). Mechanical tugging force regulates the size of cell-cell junctions. *Proceedings of the National Academy of Sciences of the United States of America* **107**, 9944–9949.

Lock, F. E., Ryan, K. R., Poulter, N. S., Parsons, M. and Hotchin, N. A. (2012). Differential regulation of adhesion complex turnover by ROCK1 and ROCK2. *PLoS ONE* **7**,.

Lomakin, A. J., Lee, K. C., Han, S. J., Bui, D. A., Davidson, M., Mogilner, A. and Danuser, G. (2015). Competition for actin between two distinct F-actin networks defines a bistable switch for cell polarization. *Nature Cell Biology* **17**, 1435–1445.

Magie, C. R., Pinto-Santini, D. and Parkhurst, S. M. (2002). Adherens junction components in Drosophila. *Development* **129**, 3771–3782.

Maître, J. L. and Heisenberg, C. P. (2013). Three functions of cadherins in cell adhesion. *Current Biology* **23**, 626–633.

Maître, J. L., Berthoumieux, H., Krens, S. F. G., Salbreux, G., Jülicher, F., Paluch, E. and Heisenberg, C. P. (2012). Adhesion functions in cell sorting by mechanically coupling the cortices of adhering cells. *Science* **338**, 253–256.

Manibog, K., Li, H., Rakshit, S. and Sivasankar, S. (2014). Resolving the molecular mechanism of cadherin catch bond formation. *Nature Communications* **5**, 1–11.

Manibog, K., Sankar, K., Kim, S. A., Zhang, Y., Jernigan, R. L. and Sivasankar, S. (2016). Molecular determinants of cadherin ideal bond formation: Conformation-dependent unbinding on a multidimensional landscape. *Proceedings of the National Academy of Sciences of the United States of America* **113**, E5711–E5720.

McCormack, J., Welsh, N. J. and Braga, V. M. M. (2013). Cycling around cell-cell adhesion with rho GTPase regulators. *Journal of Cell Science* **126**, 379–391.

McCrea, P. D. and Gottardi, C. J. (2016). Beyond β-catenin: Prospects for a larger catenin network in the nucleus. *Nature Reviews Molecular Cell Biology* **17**, 55–64.

McCrea, P. D., Maher, M. T. and Gottardi, C. J. (2015). *Nuclear signalling from cadherin adhesion complexes*. 1st ed. Elsevier Inc.

McEwen, A. E., Maher, M. T., Mo, R. and Gottardi, C. J. (2014). E-cadherin phosphorylation occurs during its biosynthesis to promote its cell surface stability and adhesion. *Molecular Biology of the Cell* **25**, 2365–2374.

Miyashita, Y. and Ozawa, M. (2007). Increased internalization of p120-uncoupled E-cadherin and a requirement for a dileucine motif in the cytoplasmic domain for endocytosis of the protein. *Journal of Biological Chemistry* **282**, 11540–11548.

Mulhall, E. M., Ward, A., Yang, D., Koussa, M. A., Corey, D. P. and Wong, W. P. (2021). Single-molecule force spectroscopy reveals the dynamic strength of the hair-cell tip-link connection. *Nature Communications* **12**, 1–15.

Nagafuchi, A. and Takeichi, M. (1988). Cell binding function of E-cadherin is regulated by the cytoplasmic domain. *The EMBO journal* **7**, 3679–3684.

Nagar, B., Overduin, M., Ikura, M. and Rini, J. M. (1996). Structural basis of calcium-induced E-cadherin rigidification and dimerization. *Nature* **380**, 360–364.

Nanes, B. A., Chiasson-MacKenzie, C., Lowery, A. M., Ishiyama, N., Faundez, V., Ikura, M., Vincent, P. A. and Kowalczyk, A. P. (2012). P120-Catenin Binding Masks an Endocytic Signal Conserved in Classical Cadherins. *Journal of Cell Biology* **199**, 365–380.

Nelson, W. J. (2020). The Glue that Binds Us: The Hunt for the Molecular Basis for Multicellularity. *Cell* **181**, 495–497.

Nicoludis, J. M., Lau, S. Y., Schärfe, C. P. I., Marks, D. S., Weihofen, W. A. and Gaudet, R. (2015). Structure and Sequence Analyses of Clustered Protocadherins Reveal Antiparallel Interactions that Mediate Homophilic Specificity. *Structure* **23**, 2087–2098.

Niessen, C. M. and Gumbiner, B. M. (2002). Cadherin-mediated cell sorting not determined by binding or adhesion specificity. *Journal of Cell Biology* **156**, 389–399.

Nollet, F., Kools, P. and Van Roy, F. (2000). Phylogenetic analysis of the cadherin superfamily allows identification of six major subfamilies besides several solitary members. *Journal of Molecular Biology* **299**, 551–572.

Noren, N. K., Liu, B. P., Burridge, K. and Kreft, B. (2000). p120 Catenin regulates the actin cytoskeleton via RHO family GTPases. *Journal of Cell Biology* **150**, 567–579.

Nose, A. and Takeichi, M. (1986). A novel cadherin cell adhesion molecule: Its expression patterns associated with implantation and organogenesis of mouse embryos. *Journal of Cell Biology* **103**, 2649–2658.

Omelchenko, T., Fetisova, E., Ivanova, O., Bonder, E. M., Feder, H., Vasiliev, J. M. and Gelfand, I. M. (2001). Contact interactions between epitheliocytes and fibroblasts: Formation of heterotypic cadherin-containing adhesion sites is accompanied by local cytoskeletal reorganization. *Proceedings of the National Academy of Sciences of the United States of America* **98**, 8632–8637.

Ozawa, M. and Kemler, R. (1992). Molecular organization of the uvomorulin-catenin complex. *Journal of Cell Biology* **116**, 989–996.

Ozawa, M., Barbault, H. and Kemler, R. (1989). The cytoplasmic domain of the cell adhesion molecule uvomorulin assoicates with three independent proteins structurally related in different species. *EMBO Journal* **8**, 1711–1717.

Ozawa, M., Ringwald, M. and Kemler, R. (1990). Uvomorulin-catenin complex formation is regulated by a specific domain in the cytoplasmic region of the cell adhesion molecule. *Proceedings of the National Academy of Sciences of the United States of America* **87**, 4246–4250.

Panorchan, P., Thompson, M. S., Davis, K. J., Tseng, Y., Konstantopoulos, K. and Wirtz, D. (2006). Single-molecule analysis of cadherin-mediated cell-cell adhesion. *Journal of Cell Science* **119**, 66–74.

Park, J. Il, Kim, S. W., Lyons, J. P., Ji, H., Nguyen, T. T., Cho, K., Barton, M. C., Deroo, T., Vleminckx, K. and McCrea, P. D. (2005). Kaiso/p120-Catenin and TCF/β-Catenin complexes coordinately regulate canonical Wnt gene targets. *Developmental Cell* **8**, 843–854.

Parsons, J. T., Horwitz, A. R. and Schwartz, M. A. (2010). Cell adhesion: Integrating cytoskeletal dynamics and cellular tension. *Nature Reviews Molecular Cell Biology* **11**, 633–643.

Patel, S. D., Ciatto, C., Chen, C. P., Bahna, F., Rajebhosale, M., Arkus, N., Schieren, I., Jessell, T. M., Honig, B., Price, S. R., et al. (2006). Type II Cadherin Ectodomain Structures: Implications for Classical Cadherin Specificity. *Cell* **124**, 1255–1268.

Peglion, F., Llense, F. and Etienne-Manneville, S. (2014). Adherens junction treadmilling during collective migration. *Nature Cell Biology* **16**, 639–651.

Petrova, Y. I., Spano, M. J. M. and Gumbiner, B. M. (2012). Conformational epitopes at cadherin calcium-binding sites and p120-catenin phosphorylation regulate cell adhesion. *Molecular Biology of the Cell* **23**, 2092–2108.

Piedra, J., Miravet, S., Castaño, J., Pálmer, H. G., Heisterkamp, N., García de Herreros, A. and Duñach, M. (2003). p120 Catenin-Associated Fer and Fyn Tyrosine Kinases Regulate β-Catenin Tyr-142 Phosphorylation and β-Catenin-α-Catenin Interaction. *Molecular and Cellular Biology* **23**, 2287–2297.

Pinheiro, D. and Bellaïche, Y. (2018). Mechanical Force-Driven Adherens Junction Remodelling and Epithelial Dynamics. *Developmental Cell* **47**, 3–19.

Pokutta, S., Drees, F., Takai, Y., James Nelson, W. and Weis, W. I. (2002). Biochemical and structural definition of the 1-afadin- and actin-binding sites of α-catenin. *Journal of Biological Chemistry* **277**, 18868–18874.

Pollard, T. D. (2016). Actin and actin-binding proteins. *Cold Spring Harbor Perspectives in Biology* **8**,.

Posy, S., Shapiro, L. and Honig, B. (2008). Sequence and Structural Determinants of Strand Swapping in Cadherin Domains: Do All Cadherins Bind Through the Same Adhesive Interface? *Journal of Molecular Biology* **378**, 954–968.

Priya, R., Gomez, G. A., Budnar, S., Verma, S., Cox, H. L., Hamilton, N. A. and Yap, A. S. (2015). Feedback regulation through myosin II confers robustness on RhoA signalling at E-cadherin junctions. *Nature Cell Biology* **17**, 1282–1293.

Priya, R., Liang, X., Teo, J. L., Duszyc, K., Yap, A. S. and Gomez, G. A. (2017). ROCK1 but not ROCK2 contributes to RhoA signalling and NMIIA-mediated contractility at the epithelial zonula adherens. *Molecular Biology of the Cell* **28**, 12–20.

Rakshit, S., Zhang, Y., Manibog, K., Shafraz, O. and Sivasankar, S. (2012). Ideal, catch, and slip bonds in cadherin adhesion. *Proceedings of the National Academy of Sciences of the United States of America* **109**, 18815–18820.

Ratheesh, A., Priya, R. and Yap, A. S. (2013). *Coordinating Rho and Rac: The regulation of Rho GTPase signalling and cadherin junctions*. 1st ed. Elsevier Inc.

Ren, X., Kiosses, W. B. and Schwartz, M. A. (1999). Regulation of the small GTP-binding protein Rho.pdf. *The EMBO Journal* **18**, 578–585.

Reynolds, A. B. (2007). p120-catenin: Past and present. *Biochimica et Biophysica Acta - Molecular Cell Research* **1773**, 2–7.

Reynolds, A. B., Roesel, D. J., Kanner, S. B. and Parsons, J. T. (1989). Transformation-specific tyrosine phosphorylation of a novel cellular protein in chicken cells expressing oncogenic variants of the avian cellular src gene. *Molecular and Cellular Biology* **9**, 629–638.

Reynolds, A. B., Herbert, L., Cleveland, J. L., Berg, S. T. and Gaut, J. R. (1992). p120, a novel substrate of protein tyrosine kinase receptors and of p60v-src, is related to cadherin-binding factors beta-catenin, plakoglobin and armadillo. *Oncogene* **7**, 2439—2445.

Reynolds, A. B., Daniel, J., McCrea, P. D., Wheelock, M. J., Wu, J. and Zhang, Z. (1994). Identification of a new catenin: the tyrosine kinase substrate p120cas associates with E-cadherin complexes. *Molecular and Cellular Biology* **14**, 8333–8342.

Ridley, A. J. (2015). Rho GTPase signalling in cell migration. *Current Opinion in Cell Biology* **36**, 103–112.

Rimm, D. L., Koslov, E. R., Kebriaei, P., Cianci, C. D. and Morrow, J. S. (1995). α1(E)-catenin is an actin-binding and -bundling protein mediating the attachment of F-actin to the membrane adhesion complex. *Proceedings of the National Academy of Sciences of the United States of America* **92**, 8813–8817.

Rosato, R., Veltmaat, J. M., Groffen, J. and Heisterkamp, N. (1998). Involvement of the Tyrosine Kinase Fer in Cell Adhesion. *Molecular and Cellular Biology* **18**, 5762–5770.

Rossi, A., Kontarakis, Z., Gerri, C., Nolte, H., Hölper, S., Krüger, M. and Stainier, D. Y. R. (2015). Genetic compensation induced by deleterious mutations but not gene knockdowns. *Nature* **524**, 230–233.

Rotty, J. D., Wu, C., Haynes, E. M., Suarez, C., Winkelman, J. D., Johnson, H. E., Haugh, J. M., Kovar, D. R. and Bear, J. E. (2015). Profilin-1 Serves as a gatekeeper for actin assembly by Arp2/3-Dependent and - Independent pathways. *Developmental Cell* **32**, 54–67.

Roura, S., Miravet, S., Piedra, J., García De Herreros, A. and Duñachl, M. (1999). Regulation of E-cadherin/catenin association by tyrosine phosphorylation. *Journal of Biological Chemistry* **274**, 36734–36740.

Rubinstein, R., Thu, C. A., Goodman, K. M., Wolcott, H. N., Bahna, F., Mannepalli, S., Ahlsen, G., Chevee, M., Halim, A., Clausen, H., et al. (2015). Molecular Logic of Neuronal Self-Recognition through Protocadherin Domain Interactions. *Cell* **163**, 629–642.

Safer, D., Elzinga, M. and Nachmias, V. T. (1991). Thymosin β4 and Fx, an actin-sequestering peptide, are indistinguishable. *Journal of Biological Chemistry* **266**, 4029–4032.

Salbreux, G., Charras, G. and Paluch, E. (2012). Actin cortex mechanics and cellular morphogenesis. *Trends in Cell Biology* **22**, 536–545.

Scarpa, E., Szabó, A., Bibonne, A., Theveneau, E., Parsons, M. and Mayor, R. (2015). Cadherin Switch during EMT in Neural Crest Cells Leads to Contact Inhibition of Locomotion via Repolarization of Forces. *Developmental Cell* **34**, 421–434.

Shan, W., Tanaka, H., Phillips, G. R., Arndt, K., Yoshida, M., Colman, D. R. and Shapiro, L. (2000). Functional cis-Heterodimers of N- and R-Cadherins. **148**, 579–590.

Shapiro, L., Fannon, A. M., Kwong, P. D., Thompson, A., Lehmann, M. S., Grübel, G., Legrand, J. F., Als-Nielson, J., Colma, D. R. and Hendricksonn, W. A. (1995). Hydrophobe Interaktions-Chromatographie Structural basis of cell-cell adhesion by cadherins. *Merck Spectrum* **2**, 24–25.

Shashikanth, N., Petrova, Y. I., Park, S., Chekan, J., Maiden, S., Spano, M., Ha, T., Gumbiner, B. M. and Leckband, D. E. (2015). Allosteric regulation of E-cadherin adhesion. *Journal of Biological Chemistry* **290**, 21749–21761.

Shook, D. R., Kasprowicz, E. M., Davidson, L. A. and Keller, R. (2018). Large, long range tensile forces drive convergence during Xenopus blastopore closure and body axis elongation. *eLife* **7**,.

Shutova, M. S., Spessott, W. A., Giraudo, C. G. and Svitkina, T. (2014). Endogenous species of mammalian nonmuscle myosin IIA and IIB include activated monomers and heteropolymers. *Current Biology* **24**, 1958–1968.

Singh, D. R., Ahmed, F., Sarabipour, S. and Hristova, K. (2017). Intracellular Domain Contacts Contribute to Ecadherin Constitutive Dimerization in the Plasma Membrane. *Journal of Molecular Biology* **429**, 2231–2245.

Sit, S. T. and Manser, E. (2011). Rho GTPases and their role in organizing the actin cytoskeleton. *Journal of Cell Science* **124**, 679–683.

Sivasankar, S., Zhang, Y., Nelson, W. J. and Chu, S. (2009). Characterizing the Initial Encounter Complex in Cadherin Adhesion. *Structure* **17**, 1075–1081.

Skau, C. T. and Waterman, C. M. (2015). Specification of Architecture and Function of Actin Structures by Actin Nucleation Factors. *Annual Review of Biophysics* **44**, 285–310.

Smith, J. C. (2009). Early Xenopus Embryo. *Spring* 1–13.

Smith, A. L., Dohn, M. R., Brown, M. V. and Reynolds, A. B. (2012). Association of Rho-associated protein kinase 1 with E-cadherin complexes is mediated by p120-catenin. *Molecular Biology of the Cell* **23**, 99–110.

Smutny, M., Cox, H. L., Leerberg, J. M., Kovacs, E. M., Conti, M. A., Ferguson, C., Hamilton, N. A., Parton, R. G., Adelstein, R. S. and Yap, A. S. (2010). Myosin II isoforms identify distinct functional modules that support integrity of the epithelial zonula adherens. *Nature Cell Biology* **12**, 696–702.

Sotomayor, M., Weihofen, W. A., Weihofen, W. A. and Corey, D. P. (2012). Structure of a force-conveying cadherin bond essential for inner-ear mechanotransduction. *Nature* **492**, 128–132.

Sotomayor, M., Gaudet, R. and Corey, D. P. (2014). Sorting out a promiscuous superfamily: Towards cadherin connectomics. *Trends in Cell Biology* **24**, 524–536.

Stappert, J. and Kemler, R. (1994). A short core region of e-cadherin is essential for catenin binding and is highly phosphorylated. *Cell Communication and Adhesion* **2**, 319–327.

Steinberg, M. S. and Takeichi, M. (1994). Experimental specification of cell sorting, tissue spreading, and specific spatial patterning by quantitative differences in cadherin expression. *Proceedings of the National Academy of Sciences of the United States of America* **91**, 206–209.

Strale, P. O., Duchesne, L., Peyret, G., Montel, L., Nguyen, T., Png, E., Tampé, R., Troyanovsky, S., Hénon, S., Ladoux, B., et al. (2015). The formation of ordered nanoclusters controls cadherin anchoring to actin and cell-cell contact fluidity. *Journal of Cell Biology* **210**, 333–346.

Strutt, H. and Strutt, D. (2021). How do the Fat-Dachsous and core planar polarity pathways act together and independently to coordinate polarized cell behaviours? *Open Biology* **11**,.

Suarez, C. and Kovar, D. R. (2016). Internetwork competition for monomers governs actin cytoskeleton organization. *Nature Reviews Molecular Cell Biology* **17**, 799–810.

Swaney, K. F. and Li, R. (2016). Function and regulation of the Arp2/3 complex during cell migration in diverse environments. *Current Opinion in Cell Biology* **42**, 63–72.

Takeichi, M. (1990). Cadherins: A molecular family important in selective cell-cell adhesion. *Annual Review of Biochemistry* **59**, 237–252.

Takeichi, M. (2014). Dynamic contacts: Rearranging adherens junctions to drive epithelial remodelling. *Nature Reviews Molecular Cell Biology* **15**, 397–410.

Takeichi, M. (2018). Multiple functions of α-catenin beyond cell adhesion regulation. *Current Opinion in Cell Biology* **54**, 24–29.

Takeichi, M., Atsumi, T., Yoshida, C., Uno, K. and Okada, T. S. (1981). Selective adhesion of embryonal carcinoma cells and differentiated cells by Ca2+-dependent sites. *Developmental Biology* **87**, 340–350.

Takeichi Masatoshi (1988). The cadherins: Cell-cell adhesion molecules controlling animal morphogenesis. *Development* **102**, 639–655.

Taubenberger, A. v., Baum, B. and Matthews, H. K. (2020). The Mechanics of Mitotic Cell Rounding. *Frontiers in Cell and Developmental Biology* **8**, 1–16.

Thiery, J. P., Delouvée, A., Gallin, W. J., Cunningham, B. A. and Edelman, G. M. (1984). Ontogenetic expression of cell adhesion molecules: L-CAM is found in epithelia derived from the three primary germ layers. *Developmental Biology* **102**, 61–78.

Thiery, J. P., Engl, W., Viasnoff, V. and Dufour, S. (2012). Biochemical and biophysical origins of cadherin selectivity and adhesion strength. *Current Opinion in Cell Biology* **24**, 614–619.

Thompson, C. J., Vu, V. H., Leckband, D. E. and Schwartz, D. K. (2019). Cadherin Extracellular Domain Clustering in the Absence of Trans-Interactions. *Journal of Physical Chemistry Letters* **10**, 4528–4534.

Thompson, C. J., Su, Z., Vu, V. H., Wu, Y., Leckband, D. E. and Schwartz, D. K. (2020). Cadherin clusters stabilized by a combination of specific and nonspecific cis-interactions. *eLife* **9**, 1–28.

Thompson, C. J., Vu, V. H., Leckband, D. E. and Schwartz, D. K. (2021). Cadherin cis and trans interactions are mutually cooperative. *Proceedings of the National Academy of Sciences of the United States of America* **118**, 1–10.

Thoreson, M. A., Anastasiadis, P. Z., Daniel, J. M., Ireton, R. C., Wheelock, M. J., Johnson, K. R., Hummingbird, D. K. and Reynolds, A. B. (2000). Selective uncoupling of p120(ctn) from E-cadherin disrupts strong adhesion. *Journal of Cell Biology* **148**, 189–201.

Tojkander, S., Gateva, G. and Lappalainen, P. (2012). Actin stress fibers - Assembly, dynamics and biological roles. *Journal of Cell Science* **125**, 1855–1864.

Toret, C. P., Collins, C. and Nelson, W. J. (2014). An Elmo-Dock complex locally controls rho gtpases and actin remodelling during cadherin-mediated adhesion. *Journal of Cell Biology* **207**, 577–587.

Troyanovsky, R. B., Sergeeva, A. P., Indra, I., Chen, C., Kato, R., Shapiro, L., Honig, B., and Troyanovsky, S. M. (2021). Sorting of cadherin – catenin-associated proteins into individual clusters. 1–11. *Proc Natl Acad Sci* **188**, e2105550118.

Truong Quang, B. A., Mani, M., Markova, O., Lecuit, T. and Lenne, P. F. (2013). Principles of E-cadherin supramolecular organization in vivo. *Current Biology* **23**, 2197–2207.

Valenta, T., Hausmann, G. and Basler, K. (2012). The many faces and functions of Î 2-catenin. *EMBO Journal* **31**, 2714–2736.

Vasquez, C. G. and Martin, A. C. (2016). Force transmission in epithelial tissues. *Developmental Dynamics* **245**, 361–371.

Vendome, J., Felsovalyi, K., Song, H., Yang, Z., Jin, X., Brasch, J., Harrison, O. J., Ahlsen, G., Bahna, F., Kaczynska, A., et al. (2014). Structural and energetic determinants of adhesive binding specificity in type i cadherins. *Proceedings of the National Academy of Sciences of the United States of America* **111**, E4175–E4184.

Vestal, D. J. and Ranscht, B. (1992). Glycosyl phosphatidylinositol-anchored T-cadherin mediates calcium-dependent, homophilic cell adhesion. *Journal of Cell Biology* **119**, 451–461.

Vicente-Manzanares, M., Ma, X., Adelstein, R. S. and Horwitz, A. R. (2009). Non-muscle myosin II takes centre stage in cell adhesion and migration. *Nature Reviews Molecular Cell Biology* **10**, 778–790.

Volk, T., Cohen, O. and Geiger, B. (1987). Formation of heterotypic adherens-type junctions between L-CAM-containing liver cells and A-CAM-containing lens cells. *Cell* **50**, 987–994.

Vu, V., Light, T., Sullivan, B., Greiner, D., Hristova, K. and Leckband, D. (2021). P120 catenin potentiates constitutive E-cadherin dimerization at the plasma membrane and regulates trans binding. *Current Biology* 1–11.

Wacker, S., Brodbeck, A., Lemaire, P., Niehrs, C. and Winklbauer, R. (1998). Patterns and control of cell motility in the Xenopus gastrula. *Development (Cambridge, England)* **125**, 1931–1942.

Wakatsuki, T., Wysolmerski, R. B. and Elson, E. L. (2003). Mechanics of cell spreading: Role of myosin II. *Journal of Cell Science* **116**, 1617–1625.

Wang, A., Ma, X., Conti, M. A. and Adelstein, R. S. (2011). Distinct and redundant roles of the non-muscle myosin II isoforms and functional domains. *Biochemical Society Transactions* **39**, 1131–1135.

Wardle, F. C. and Smith, J. C. (2004). Refinement of gene expression patterns in the early Xenopus embryo. *Development* **131**, 4687–4696.

Watabe-Uchida, M., Uchida, N., Imamura, Y., Nagafuchi, A., Fujimoto, K., Uemura, T., Vermeulen, S., Van Roy, F., Adamson, E. D. and Takeichi, M. (1998). α-Catenin-vinculin interaction functions to organize the apical junctional complex in epithelial cells. *Journal of Cell Biology* **142**, 847–857.

Weißenbruch, K., Grewe, J., Hippler, M., Fladung, M., Tremmel, M., Stricker, K., Schwarz, U. S. and Bastmeyer, M. (2021). Distinct roles of nonmuscle myosin ii isoforms for establishing tension and elasticity during cell morphodynamics. *eLife* **10**, 1–35.

Wen, J. W. and Winklbauer, R. (2017). Ingression-type cell migration drives vegetal endoderm internalisation in the Xenopus gastrula. *eLife* **6**,.

Wennerberg, K., Forget, M.-A., Ellerbroek, S. M., Arthur, W. T., Burridge, K., Settleman, J., Der, C. J. and Hansen, S. H. (2003). Rnd proteins function as RhoA antagonists by activating p190 RhoGAP. *Current biology : CB* **13**, 1106–1115.

West, J. J., Zulueta-Coarasa, T., Maier, J. A., Lee, D. M., Bruce, A. E. E., Fernandez-Gonzalez, R. and Harris, T. J. C. (2017). An Actomyosin-Arf-GEF Negative Feedback Loop for Tissue Elongation under Stress. *Current Biology* **27**, 2260-2270.e5.

Wickline, E. D., Dale, I. W., Merkel, C. D., Heier, J. A., Stolz, D. B. and Kwiatkowski, A. V. (2016). αT-catenin is a constitutive actin-binding α-catenin that directly couples the cadherin·catenin complex to actin filaments. *Journal of Biological Chemistry* **291**, 15687–15699.

Wildenberg, G. A., Dohn, M. R., Carnahan, R. H., Davis, M. A., Lobdell, N. A., Settleman, J. and Reynolds, A. B. (2006). p120-Catenin and p190RhoGAP Regulate Cell-Cell Adhesion by Coordinating Antagonism between Rac and Rho. *Cell* **127**, 1027–1039.

Winklbauer, R. (2015). Cell adhesion strength from cortical tension - An integration of concepts. *Journal of Cell Science* **128**, 3687–3693.

Wood, M. N., Ishiyama, N., Singaram, I., Chung, C. M., Flozak, A. S., Yemelyanov, A., Ikura, M., Cho, W. and Gottardi, C. J. (2017). α-Catenin homodimers are recruited to phosphoinositide-activated membranes to promote adhesion. *Journal of Cell Biology* **216**, 3767–3783.

Wu, Y., Jin, X., Harrison, O., Shapiro, L., Honig, B. H. and Ben-Shaul, A. (2010). Cooperativity between trans and cis interactions in cadherin-mediated junction formation. *Proceedings of the National Academy of Sciences of the United States of America* **107**, 17592–17597.

Wu, Y., Vendome, J., Shapiro, L., Ben-Shaul, A. and Honig, B. (2011). Transforming binding affinities from three dimensions to two with application to cadherin clustering. *Nature* **475**, 510–513.

Wu, Y., Kanchanawong, P. and Zaidel-Bar, R. (2015). Actin-Delimited Adhesion-Independent Clustering of E-Cadherin Forms the Nanoscale Building Blocks of Adherens Junctions. *Developmental Cell* **32**, 139–154.

Xiao, K., Allison, D. F., Buckley, K. M., Kottke, M. D., Vincent, P. A., Faundez, V. and Kowalczyk, A. P. (2003). Cellular levels of p120 catenin function as a set point for cadherin expression levels in microvascular endothelial cells. *Journal of Cell Biology* **163**, 535–545.

Xiao, K., Garner, J., Buckley, K. M., Vincent, P. A., Chiasson, C. M., Dejana, E., Faundez, V. and Kowalczyk, A. P. (2005). p120-Catenin regulates clathrin-dependent endocytosis of VE-cadherin. *Molecular biology of the cell* **16**, 5141–5151.

Xu, G., Craig, A. W. B., Greer, P., Miller, M., Anastasiadis, P. Z., Lilien, J. and Balsamo, J. (2004). Continuous association of cadherin with β-catenin requires the non-receptor tyrosine-kinase Fer. *Journal of Cell Science* **117**, 3207–3219.

Yamada, S. and Nelson, W. J. (2007). Localized zones of Rho and Rac activities drive initiation and expansion of epithelial cell-cell adhesion. *Journal of Cell Biology* **178**, 517–527.

Yamada, S., Pokutta, S., Drees, F., Weis, W. I. and Nelson, W. J. (2005). Deconstructing the cadherin-catenin-actin complex. *Cell* **123**, 889–901.

Yanagisawa, M., Huveldt, D., Kreinest, P., Lohse, C. M., Cheville, J. C., Parker, A. S., Copland, J. A. and Anastasiadis, P. Z. (2008). A p120 catenin isoform switch affects rho activity, induces tumor cell invasion, and predicts metastatic disease. *Journal of Biological Chemistry* **283**, 18344–18354.

Yao, M., Qiu, W., Liu, R., Efremov, A. K., Cong, P., Seddiki, R., Payre, M., Lim, C. T., Ladoux, B., Mège, R. M., et al. (2014). Force-dependent conformational switch of α -catenin controls vinculin binding. *Nature Communications* **5**,.

Yap, A. S., Brieher, W. M., Pruschy, M. and Gumbiner, B. M. (1997). Lateral clustering of the adhesive ectodomain: A fundamental determinant of cadherin function. *Current Biology* **7**, 308–315.

Yap, A. S., Niessen, C. M. and Gumbiner, B. M. (1998). The juxtamembrane region of the cadherin cytoplasmic tail supports lateral clustering, adhesive strengthening, and interaction with p120(ctn). *Journal of Cell Biology* **141**, 779–789.

Yoneda, A., Multhaupt, H. A. B. and Couchman, J. R. (2005). The Rho kinases I and II regulate different aspects of myosin II activity. *Journal of Cell Biology* **170**, 443–453.

Yonemura, S., Wada, Y., Watanabe, T., Nagafuchi, A. and Shibata, M. (2010). α-Catenin as a tension transducer that induces adherens junction development. *Nature Cell Biology* **12**, 533–542.

Youssef, J., Nurse, A. K., Freund, L. B. and Morgan, J. R. (2011). Quantification of the forces driving self-assembly of three-dimensional microtissues. *Proceedings of the National Academy of Sciences of the United States of America* **108**, 6993–6998.

Zhang, Y., Sivasankar, S., Nelson, W. J. and Chu, S. (2009). Resolving cadherin interactions and binding cooperativity at the single-molecule level. *Proceedings of the National Academy of Sciences of the United States of America* **106**, 109–114.

Zhou, J., Kim, H. Y. and Davidson, L. A. (2009). Actomyosin stiffens the vertebrate embryo during crucial stages of elongation and neural tube closure. *Development* **136**, 677–688.

Zhou, J., Pal, S., Maiti, S. and Davidson, L. A. (2015). Force production and mechanical accommodation during convergent extension. *Development (Cambridge)* **142**, 692–701.

Bridge to Chapter II – In Chapter I, I reviewed the literature surrounding cortical tension and it's influence on the mechanics of single cells and tissues, and how cells downregulate myosin contractility prior to spreading. I also introduced our model, the *Xenopus gastrula*, whose morphogenesis is driven by cell-cell rearrangements stimulated by differential cell migration. In Chapter II, we compare the migratory capabilities of the ectoderm (non-motile) and mesoderm (highly motile), attempt to identify how these differences are regulated, and how this regulation impacts properties at the cell, tissue, and embryo scale. This chapter is a reproduction of a published article of which I am the co-first author (for a breakdown of my contributions see Contributions on page 5):

Kashkooli, L.*, Rozema, D.*, Espejo-Ramirez, L., Lasko, P. and Fagotto, F. (2021). Ectoderm to mesoderm transition by down-regulation of actomyosin contractility. *PLOS Biology* **19**(1): e3001060. https://doi.org/10.1371/journal.pbio.3001060

*Denotes equal contribution

Chapter II – Ectoderm to mesoderm transition by down-regulation of actomyosin contractility

Abstract

Collective migration of cohesive tissues is a fundamental process in morphogenesis and is particularly well illustrated during gastrulation by the rapid and massive internalization of the mesoderm, which contrasts with the much more modest movements of the ectoderm. In the Xenopus embryo, the differences in morphogenetic capabilities of ectoderm and mesoderm can be connected to the intrinsic motility of individual cells, very low for ectoderm, high for mesoderm. Surprisingly, we find that these seemingly deep differences can be accounted for simply by differences in Rho-kinases (Rock)-dependent actomyosin contractility. We show that Rock inhibition is sufficient to rapidly unleash motility in the ectoderm and confer it with mesoderm-like properties. In the mesoderm, this motility is dependent on two negative regulators of RhoA, the small GTPase Rnd1 and the RhoGAP Shirin/Dlc2/ArhGAP37. Both are absolutely essential for gastrulation. At the cellular and tissue level, the two regulators show overlapping yet distinct functions. They both contribute to decrease cortical tension and confer motility, but Shirin tends to increase tissue fluidity and stimulate dispersion, while Rnd1 tends to favor more compact collective migration. Thus, each is able to contribute to a specific property of the migratory behavior of the mesoderm. We propose that the “ectoderm to mesoderm transition” is a prototypic case of collective migration driven by a down-regulation of cellular tension, without the need for the complex changes traditionally associated with the epithelial-to-mesenchymal transition.

Introduction

The ability of tissues to dynamically rearrange is at the core of animal morphogenesis. In some systems, this is primarily accomplished by epithelial morphogenesis requiring cell shape changes or planar cell rearrangements. However, other systems rely instead on migration of cell masses. Gastrulation in Xenopus is a prototypical example of such type of morphogenesis (Huang and Winklbauer, 2018). Here massive, coordinated cell migration results in the animally positioned ectoderm engulfing the vegetal endoderm, with the equatorial mesoderm positioned between the two germ layers. One of the main actors of early gastrulation is the prechordal

mesoderm (PCM) which involutes and migrates collectively on the blastocoel roof (BCR) using the ectodermal cells and a thinly deposited fibronectin (FN) matrix as substrates (Huang and Winklbauer, 2018; Winklbauer and Keller, 1996). As it does so, there is ongoing intercellular migration within the tissue that leads to extensive radial intercalations, resulting in progressive thinning of the tissue until eventually all cells contact the BCR.

The PCM, which originates from the ectoderm through an inductive process, exhibits high migratory activity that contrast with the non-motile ectoderm from which it is derived. At a first glance, this behaviour appears related to the classical epithelial to mesenchymal transition (EMT) observed for cells escaping solid tumours. However, the mesoderm cells move inside the embryo as a compact mass. Furthermore, the early Xenopus embryo is already multi-layered, and the mesoderm derives from the deep ectoderm layer, which does not display apical-basal polarity at the time of gastrulation, removing one of the principle hurdles that must be overcome during a classical EMT. Therefore, in this simple system, one can directly witness a tissue acquiring a migratory behaviour without loss of cell-cell adhesion or changes in polarity. We propose that this process, which we name the “ectoderm to mesoderm transition”, or “mesoderm transition” for short, constitutes a basal mode, which can teach us a great deal about the core cellular mechanisms that control tissue dynamicity.

The Xenopus embryo offers the unique possibility to easily dissect specific tissues, prepare explants and/or dissociate them into single cells, allowing the study of intrinsic cell and tissue properties in the absence of confounding influences of other surrounding embryonic structures. Importantly, the morphogenetic events occurring during Xenopus gastrulation are recapitulated in isolated explants, and furthermore, even individual dissociated cells have characteristics that clearly relate to the properties of the corresponding tissues: Ectoderm cells show higher cortical stiffness, higher cell-cell adhesion, and are largely immotile, while the softer mesoderm cells spread and migrate when laid on a FN substrate, similar to the mesoderm at the BCR (Canty et al., 2017; Huang and Winklbauer, 2018; Wacker et al., 1998; Winklbauer, 2009). Note that there are two other mesodermal populations, the more anterior leading edge mesendoderm (LEM) and the posterior chordamesoderm (CM). The LEM migrates along the BCR in front of the PCM, while the CM undergoes the particular process of convergent extension at

later stages of development. However, in this study we focus on the PCM, which for the sake of simplicity is here referred to as mesoderm.

We have based this investigation of mesoderm transition on the hypothesis that the high cortical contractility of ectoderm cells may be prohibitive for motility, and that its decrease may be a key step in the mesoderm transition. We show that inhibition of the Rho-Rock pathway is sufficient to confer ectoderm cells with migratory properties, which is the most fundamental aspect of gastrulating cells. We identify two mesoderm-specific negative regulators of RhoA, Rnd1 and Shirin (also called Dlc2, Stard13 or AhrGAP37), as absolutely required for gastrulation and more specifically for proper mesoderm migration, as predicted from our initial hypothesis. Our analysis of the impact of these regulators at the cell and tissue level supports a model where Rnd1 and Shirin cooperate toward a general downregulation of actomyosin contractility, allowing cells to become motile, but also have opposing activities, with Shirin negatively impacting cell-cell adhesion leading to dispersive migration while Rnd1 is capable of maintaining it for efficient collective migration. These differing roles likely balance each other to produce the right physical properties for effective mesoderm involution and intercalation.

Results

Distinct characteristics of ectoderm and mesoderm at the cell level

We first studied ectoderm and mesoderm cells *in vitro* in order to firmly characterize their basic intrinsic properties. Dissociated cells from early gastrula tissues were plated on fibronectin (FN) and imaged by live confocal microscopy. FN is the major extracellular matrix component in the gastrula, where it forms a sparse network (Nakatsuji et al., 1985; Winklbauer and Nagel, 1991). Accordingly, we used low levels of FN for all our assays. Ectoderm and mesoderm cells have radically different morphologies and behaviour: Ectoderm cells typically remain round and produce large blebs (Figure 2.1A,F) (Charras and Paluch, 2008), and they do not migrate (Figure 2.1G) (Wacker et al., 1998). Note that the small apparent “speed” (Figure 2.1G) does not represent actual migration, but reflects wobbling, as cells are “shaken” by constant blebbing. On

the contrary, mesoderm cells spread, form multiple prominent protrusions (Figure 2.1B,F') and migrate at high speed (Figure 2.1G) (Wacker et al., 1998). Single mesoderm cell migration typically has low persistence, with one of the extended lamellipodia rapidly commuted to the cell's tail (Figure S2.1A) (Winklbauer and Keller, 1996). As a consequence, protrusive and retracting structures can be considered as oscillating states, unlike the strongly polarized extensions of many classical mesenchymal cell types.

The organization of matrix adhesions, marked by vinculin and paxillin, completely accounted for the differences in morphology and behaviour, as mesoderm cells displayed typical vinculin and paxillin-positive focal adhesions (FAs) (Figure 2.1B'). These FAs were rapidly remodelled during migration (Figure 2.1F'). Ectoderm cells showed a completely different organization, harboring a highly stereotypical ring-shaped vinculin and paxillin-rich structure (Figure 2.1A',F). These rings were immobile (Figure 2.1F). Note that mesoderm cells displayed a spectrum of protrusions, from large lamellipodia to thin extensions, which all showed vinculin and paxillin enriched structures (Figure 2.1D',F'). For simplicity, we will refer here to all the vinculin-rich structures detected on the ventral cell surface as FAs. Note also that in all subsequent experiments, we only tracked vinculin. Its absence did not preclude the occurrence of vinculin-negative FAs, but vinculin recruitment is an established parameter reflecting the tension exerted on adhesive structures (Han and de Rooij, 2016; Kale et al., 2018). We quantified the fraction of vinculin-Cherry detected on the ventral surface that concentrated at FAs in ectoderm and mesoderm cells. We verified that this fraction is independent of expression levels (Figure S2.1B). The peculiar ectodermal adhesive rings concentrated high amounts of vinculin (Figure 2.1E), suggesting that these cells were interacting rather strongly with the substrate. We thus compared adhesion to FN by a rotation assay (Figure 2.1H). Ectoderm cells adhered almost as efficiently as mesoderm cells. This important observation indicated that the known inability of ectoderm cells to spread and migrate on FN was not due, as one may have hypothesized, to lack of efficient cell-matrix adhesion, but rather to an intrinsic property to organize a different type of adhesive structure. We used the same adhesion assay to compare cadherin-based adhesion, replacing FN with recombinant C-cadherin extracellular domain as the adhesive substrate. Ectoderm cells showed significantly higher cadherin adhesion than mesoderm cells (Figure 2.1H),

consistent with previous measurements (Brieher and Gumbiner, 1994; Canty et al., 2017). However, the difference was relatively mild, an observation that became relevant later in this study.

The analysis of small groups of cells showed that the properties of single dissociated cells were directly reflected at the supra-cellular level, each cell type adopting a distinct, highly stereotypic organization (Figure 2.1C,D): Ectoderm cells formed compact groups; they still emitted blebs, but exclusively along the edge of the group (Figure 2.1C). Cells did form some protrusions that crawled under adjacent cells, but typically in an inwards orientation (Figure 2.1C, yellow concave arrows). The cell group shared a multicellular vinculin/paxillin ring constituted by the juxtaposition of partial rings formed by the individual cells (Figure 2.1C', arrowheads). On the contrary, mesoderm cells formed widely spread groups with numerous lamellipodia. Both peripheral and internal lamellipodia were oriented outwards (Figure 2.1D,D', white and yellow concave arrows). FAs were aligned along the outward direction of the expanding protrusions (arrowheads).

This characterization highlighted deep intrinsic differences between ectoderm and mesoderm cells, which resulted in very different morphologies and in distinct adhesive structures. These correlated well with their migratory capabilities, while differences in matrix and cell-cell adhesion were not as striking. Lastly, the properties observed for isolated cells readily translated into diametrically opposed collective organizations, compacted for ectoderm, expanded for mesoderm.

Inhibition of Rock induces mesoderm-like spreading and migration of ectoderm cells

Ectoderm cells have intrinsically higher myosin-dependent cortical tension than mesoderm (Canty et al., 2017). This high tension is reflected in cells plated on FN through their blebbing and by a stronger accumulation of cortical myosin light chain (MLC) (Figure S2.2A-C). We therefore hypothesized that differences in actomyosin contractility could be responsible for the distinct properties of ectoderm and mesoderm with respect to their spreading and migratory capabilities. Rho-kinases (Rock) are important myosin activators. In both ectoderm and

mesoderm cells, Rock1 and Rock2 are concentrated along the free cell cortex (Figure S2.2D-K, arrowheads), but present only at low levels at sites of cell-matrix and cell-cell adhesion (Figure S2.2D-K, arrows), consistent with a major role in controlling cortical tension.

We tested the effect of a short-term acute Rock inactivation on ectoderm cellular behaviour using two specific chemical Rock inhibitors, Y27632 and H1152. The effect of these inhibitors on single ectoderm cells plated on FN was spectacular: Cells almost instantaneously stopped blebbing, and within minutes started to spread, emit lamellipodia, and migrate (Figure 2.2A-B). These changes were quantified by monitoring the increase in cell surface area (Figure S2.3A,B), the modification of cell morphology (Figure 2.2D), and by tracking migration (Figure 2.2E). In all these aspects, Rock inhibition appeared sufficient to induce a dramatic transformation of ectoderm cells into mesoderm-like cells, although the speed of migration remained significantly lower than that of mesoderm. Similarly, Rock inhibition caused groups of ectoderm cells (Figure 2.2C and Figure S2.3C) to adopt the typical expanding configuration of mesoderm groups (compare to Figure 2.1D). The matrix adhesive structures were completely reorganized during this transition: the vinculin ring was disassembled, often starting asymmetrically, coinciding with extension of a protrusion and formation of classical FAs (Figure S2.3C for a small group, also seen in Figure 2.2A-C). This observation further emphasized the congruence between single cell and collective behaviours. Importantly, the rapidity of the changes caused by the inhibitors (Figure S2.3A,B) clearly reflected a direct effect and excluded the involvement of transcriptional processes and changes in cell fate.

We also evaluated the effect of Rock inhibition on adhesion (Figure S2.3D,E). Rock inhibitors significantly increased adhesion of both ectoderm and mesoderm on FN. They also increased adhesion on cadherin for mesoderm, without a detectable change for ectoderm. In stark contrast, the MLCK inhibitor ML7 potently inhibited adhesion of both tissues, on both FN and cadherin substrates. We concluded that both cell-matrix and cell-cell adhesions require MLCK activity, but not Rock activity. The latter, on the contrary, appears to act antagonistically to adhesion, which is precisely the expected impact of tension of the cell cortex, where Rock1/2 localize (Figure S2.2D-K). Together, these experiments support our initial hypothesis, pointing towards cortical Rock activity as a gatekeeper that prevents ectoderm from migrating. This model

would predict that mesoderm cells should have acquired mechanisms to downregulate cortical contractility in order to spread and migrate.

Two Rho antagonists, Rnd1 and Shirin, are essential for mesoderm migratory and adhesive properties during gastrulation

The most parsimonious scenario that could account for the decreased myosin activity, lower cortical tension and high motility of mesoderm was that this tissue expresses negative regulators of the Rho-Rock pathway. We searched through the *Xenopus laevis* developmental gene expression database (Xenbase, http://www.xenbase.org, (Session et al., 2016) for putative regulators expressed at the onset of gastrulation, and determined by qPCR their relative transcript levels in ectoderm and mesoderm. Two candidates, Rnd1 and Shirin, stood out as being significantly enriched in the mesoderm (Figure 2.3A). Rnd1 is a small GTPase that antagonizes RhoA through activation of ArhGAP35/p190B-RhoGAP, and is implicated in the control of cell-cell adhesion (Wünnenberg-Stapleton et al., 1999). Shirin/Dlc2/Stard13/ArhGAP37 is a RhoGAP, that has been associated with various functions, such as migration, adhesion and cell division (Braun and Olayioye, 2015). The potential role of these two regulators in the migratory properties of the mesoderm had not yet been addressed.

Injection of specific morpholino antisense oligonucleotides (MOs) targeted against Rnd1 or Shirin mRNAs yielded severe gastrulation phenotypes, with virtually full penetrance (Figure 2.3B-F). In both cases, the dorsal blastopore lip was strongly reduced or missing altogether (Figure 2.3C-F). The internal morphology was similarly deeply affected, revealing a block of mesoderm involution (Figure 2.3C'-F'). Importantly, this dramatic defect contrasted with the normal thinning of the ectodermal blastocoel roof, which indicated that epiboly, another key morphogenetic movement during gastrulation, proceeded normally. We went on to investigate the Rnd1 and Shirin loss-of-function phenotypes at the tissue and cellular level. We started with the analysis of single dissociated cells. Rnd1MO and ShiMO had drastic effects: Most injected mesoderm cells failed to spread on FN and often showed blebbing (Figure 2.4A-C, quantification in Figure 2.4D). Their migration was significantly decreased compared to control mesoderm, the

effect being strongest for ShirinMO (Figure 2.4E). Specificity of the Rnd1 and Shirin MOs was demonstrated by rescue of spreading and migration upon expression of YFP-Rnd1/YFP-Shirin (Figure S2.4A-D). Moreover, spreading and migration were also rescued by Rock inhibition, demonstrating that indeed Rnd1 and Shirin act upstream of Rock (Figure S2.4A-D). Simultaneous depletion of Rnd1 and Shirin led to even stronger phenotype (Figure 2.4D,E), with an almost complete loss of migration (Figure 2.4E). We also found that adhesion on FN and cadherin were both significantly impaired (Figure 2.4G,H).

Beyond these common effects, we observed differences between Rnd1MO and ShiMO cellular phenotypes. Rnd1MO cells almost completely lacked detectable vinculin-positive FAs (Figure 2.4B,F), while vinculin distribution in ShiMO cells was heterogeneous (Figure 2.4F): Some ShiMO cells still harboured classical FAs, others had none, and others started to assemble peripheral concentric FAs strikingly reminiscent of the rings observed in ectoderm cells (Figure 2.4C). A closer look at migration brought further interesting insights. So far, we had compiled the average migration speed of all cells, independently of their morphology (Figure 2.4E). In order to better understand the cause of the decreased migration, we analyzed the speed of each category of cells (Figure S2.4E). While the overwhelming majority of wild type mesoderm cells had a spread morphology, other types could be found at low frequency, which allowed us to confirm that the morphology correlated with migration: Spread cells showed the highest speed, while round cells (with or without blebs) showed the lowest. Nevertheless, round and blebbing mesoderm cells were still faster than ectoderm cells (1µm/min versus less than 0.3µm/min), indicating that, even for this typical “immobile” morphology, mesoderm cells remained capable of some migration. RndMO mesoderm cells showed an identical profile to control mesoderm throughout all categories (Figure S2.4E). We could conclude that the lower average speed of RndMO cells directly reflected their switch from spread to round morphology (Figure 2.4D). The profile was different for ShiMO: We calculated that the migration speed was significantly decreased by knockdown of Shirin for all morphological categories (Figure S2.4E), implying that ShiMO, in addition to causing a shift in morphology, had also a separate impact on motility. These data argued for a differential role of the two regulators.

In summary, the specific activation of Rnd1 and Shirin expression in mesoderm cells appears absolutely required for mesoderm involution, controlling cell spreading, motility and adhesion, accounting for the predicted pro-migratory effect of downregulation of the Rho-Rock pathway. However, the loss-of-function phenotypes clearly differed in several aspects, indicating that Rnd1 and Shirin had distinct activities.

Expression of Rnd1 and Shirin confer ectoderm with mesoderm-like migratory properties

Next, we tested the effect of overexpressing Rnd1 or Shirin in ectoderm cells, with the rationale that they may reproduce the transition toward a mesoderm-like phenotype observed upon Rock inhibition. Indeed, both Rnd1 and Shirin induced remarkable changes in ectoderm cells: The frequency of blebs was strongly decreased, and a significant number of cells spread on FN, elongated, and extended protrusions (Figure 2.5B-E,G), and became motile (Figure 2.5H,I). Thus, either of these components was indeed capable to drive ectoderm cells into a migratory mode.

However, we also observed clear differences in the effect of the two regulators: Shirin was extremely potent at inducing cell spreading and formation of protrusions (Figure 2.5D,E,G), while Rnd1-expressing cells remained more circular and formed more modest protrusions (Figure 2.5B,C,G, see Figure S2.5A for a detailed quantitative morphometric analysis). On the other hand, Rnd1 had a higher pro-migratory activity (Figure 2.5I and S2.5B). Note that cells tended to round up again for high levels expression (S5A Fig). The effect was marginal for Rnd1 (Figure 2.5C), but strong for Shirin (Figure 2.5E, S5A''' Fig), which, at the same time, induced extension of multiple tentacular protrusions (Figure 2.5E, S2.5A Fig). This effect presumably resulted from excessive loss of contractility (see below), and may explain stalling of migration (last frames of Figure 2.5H"). In terms of vinculin localization, most Rnd1 and Shirin expressing cells lacked ring structures, and some FA-like structures could be observed in cells expressing moderate levels of either regulator (Figure 2.5B,D, arrows). Neither Rnd1 nor Shirin expression led to detectable changes in adhesion on FN (Figure 2.5J), but Shirin significantly decreased cadherin adhesion (Figure 2.5K). In conclusion, these experiments showed that both Rnd1 and Shirin could induce

spreading and migration, but each expressed this property in a slightly different manner, further supporting overlapping yet diverging activities.

Impact of Rnd1 and Shirin expression on ectoderm organization and myosin activation

We also analyzed the effect of ectopic Rnd1 and Shirin on ectoderm tissue *in situ*, by performing immunofluorescence on cryosections of whole embryos (Figure 2.6 and S2.6). We focused on two key components, i.e. levels of phosphorylated MLC (pMLC) at the cell cortex, and cadherin-based adhesive contacts, marked by β-catenin. Membrane and cortex largely overlapped at the resolution used in these experiments, and β-catenin labelling could be used to segment what we generically call the "cell periphery", from which we quantified the relative signals of both markers. The ectoderm and the involuted prechordal mesoderm of wild type embryos were used as reference (Figure 2.6A-B). Consistent with previous reports (Canty et al., 2017; Rohani et al., 2014), levels of β-catenin and pMLC levels were significantly lower in the mesoderm (75% and 50%, respectively). Expression of Rnd1 or Shirin caused a significant decrease in cortical pMLC levels (Figure 2.6C,E''',F'''), consistent with their role as negative regulators of the Rho-myosin pathway. The negative effect of Rnd1 and Shirin on pMLC cortical levels was also observed in dissected ectoderm explants, which provide large homogenous fields of cells, particularly favorable for quantitative immunofluorescence (S6F-I Fig). It is important to highlight the fact that in whole embryos and tissues, the peripheral or "cortical" pMLC signal results from contributions of the cytoskeleton associated with cell-cell contacts, cell-matrix contacts (FN secreted by the ectoderm), and "free" edges. These multiple inputs cannot be dissected apart in this complex setting.

We also verified that Rnd1 and Shirin acted via Rock by Western blot analysis of phosphorylation of the regulatory subunit of myosin light chain phosphatase (MYPT), a direct target of Rock1/2, in ectoderm explants. Expression of Rnd1 and Shirin significantly decreased levels of phosphorylated MYPT (Figure S2.6H).

Membrane β-catenin was also affected by expression of the two regulators. We observed a mild decrease for Rnd1 (Figure 2.6C,E"), but much stronger downregulation for Shirin (Figure

2.6C,F"). Sparse punctate accumulations were observed, again more frequently for Shirin (arrowheads, Figure 2.6E",F" and S2.6A'). The same uneven distribution was observed in ectoderm explants (Figure S2.6H',I'). The strong effect of Shirin on β-catenin levels and distribution is fully consistent with the observed inhibition of cadherin-based adhesion by Shirin (Figure 2.5K).

The two regulators also strongly affected tissue organization (Figure S2.6B-E): In this region of wild type embryos, cells of the deep ectoderm layer tend to orient roughly perpendicular to the inner surface (the blastocoel roof). This orientation was largely lost in Rnd1-expressing embryos (Figure S2.6C,E). Shirin expression led to a complete reorganization of the tissue. Cells became fusiform, aligning parallel to the ectoderm surface, forming a multilayered "mesenchymal-like" tissue (Figure 2.6F and S2.6A,D,E), occasionally with large intercellular spaces (Figure S2.6A). In conclusion, these data demonstrated that Rnd1 and Shirin indeed negatively regulated cortical myosin activity, as well as cadherin-based adhesive structures and tissue organization, with the two latter features being most strongly affected by Shirin.

Overlapping but distinct subcellular localization of Rnd1 and Shirin

In order to gain additional insights in Rnd1 and Shirin properties in these embryonic cells, we set to examine their subcellular localization. In the absence of adequate antibodies, we used the distribution of YFP fusion constructs as a proxy (Figure 2.7). In the Xenopus embryo, titration of injected mRNA allows the expression of low levels of these fluorescent constructs, and to verify that subcellular patterns are reproducible even at the lowest detectable levels. For Shirin, because of the potent activity of RhoGAPs, even when expressed at low levels, we used a GAP-deficient R488A mutant (mShi) in order to visualize the subcellular distribution with minimal impact on the cell phenotype.

Rnd1 was homogenously distributed along the cell cortex, both on the ventral side (Figure 2.7A') and at free cell edges (Figure 2.7A"), but significantly accumulated at cell-cell contacts (Figure 2.7A"). We measured a more than two-fold enrichment at contacts, which is comparable to cadherin accumulation (Figure 2.7C). mShi also localized to the cell cortex, but, unlike Rnd1, it

did not accumulate at cell-cell contacts (Figure 2.7B",C). Instead, it formed prominent clusters on the ventral side of protrusions (Figure 2.7B,B',D,D'). We compared this ventral pattern with the localization of FAs, marked by vinculin-Cherry. A large proportion of mShi clusters perfectly colocalized with vinculin-positive FAs (Figure 2.7D, quantification in Figure 2.7H). We also examined the localization of wild type Shirin (wtShi), which, when expressed at low levels, did not induce overt changes in the morphology of mesoderm cells. wtShi localization was very similar to mShi, i.e. cortical with prominent accumulation of clusters in the protrusions (Figure 2.7E). However, wtShi had a strong impact on vinculin-positive FAs, which were largely excluded from the Shirin-rich regions and confined to the edge of the protrusions (Figure 2.7E). wtShi clusters showed limited overlap with to FAs (Figure 2.7E, white and yellow concave arrowheads, quantification in Figure 2.7H). We also examined the protrusions induced by Shirin ectopic expression in ectoderm cells. The organization of these protrusions was similar to that of mesoderm protrusions, with accumulation of clustered Shirin and confinement of vinculin to the periphery (Figure 2.7F). Consistently, calculated colocalization was relatively low (Figure 2.7H). Interestingly, in ectoderm cells that had only undergone an incomplete transition to a mesoderm-like phenotype (Figure 2.7G), Shirin lined the inner side of the remnants of the vinculin ring (white and orange arrowheads). One could conclude that Shirin is not only preferentially localized to protrusions, but more specifically targeted to FAs. While inactive Shirin accumulates at these structures, expression of wild type Shirin appears to "clear" vinculin from protrusions, consistent with its reported function in FA disassembly (Braun and Olayioye, 2015). However, the presence of numerous FAs in non-manipulated mesoderm cells indicates that the normal function of endogenous Shirin is to moderate rather than to remove FAs altogether.

Most strikingly, the sites of Rnd1 and Shirin enrichment, respectively at cell-cell contacts and in ventral protrusions, coincided with the two prominent regions where Rock1/2 were at their lowest level (Figure S2.2). Together with the functional data, these observations suggested that both regulators contributed to the downregulation of Rock-dependent cortical tension along free cell edges, while their complementary specific enrichments fulfill distinct functions: The ventral pool of Shirin would promote lamellipodium extension and keep tension at FAs under

control at the cell-matrix interface, while Rnd1 would downregulate tension at cell-cell contacts and help maintain cell-cell adhesion.

Rnd1 and Shirin modulate cell surface tension and adhesiveness

To dissect the effect of Rnd1 and Shirin on cortical contractility and adhesiveness, we analyzed isolated cell doublets. In this simple system, the geometry of contact vertices directly reflects the balance of the forces exerted along the three interfaces, i.e. the cortical tensions along free edges (Ct_A and Ct_B) and the contact tension T_{AB} (Figure 2.8A) (Canty et al., 2017; David et al., 2014; Winklbauer, 2015). T_{AB} is the sum of the two cortical tensions along the contact interface (Ct_A' and Ct_B', which are lower than Ct_A and Ct_B) and of the negative contribution due to cell-cell adhesion (see S2.1 Appendix). Heterotypic doublets made of a wild type ectoderm cell and a cell expressing Rnd1 or Shirin tended to be asymmetric, reflecting differences in their cortical tension (Figure 2.8B-I). The asymmetry was particularly strong for Shirin: The heterotypic interface was systematically concave, with the Shirin-expressing cell engulfing the wild type cell to various degrees (Figure 2.8H,I). We calculated that Ct was decreased about two-fold in Shirin-expressing cells (Figure 2.8J). Rnd1 caused a more modest but significant reduction of about 10%. As comparison, we had previously shown that mesoderm cortical tension was about 2 to 3-fold lower than ectoderm (Canty et al., 2017). Doublet geometry also allowed us to compare the relative contact tension (relT), which was significantly decreased by both Rnd1 and Shirin (Figure 2.8K). Since cell-cell adhesion is largely dictated by the reduction of cortical tension along the contacts (Maître et al., 2012; Parent et al., 2017; Winklbauer, 2015), this reduction can be used to express a relative "adhesiveness", α, an absolute value that stands from 0 (no adhesion) to 1 (maximal adhesion) (Parent et al., 2017) (see S2.1 Appendix). Interestingly, α significantly decreased upon Shirin expression, but not Rnd1 expression (Figure 2.8L). In summary, these measurements confirmed that both Rnd1 and Shirin repressed cortical tension, although to different extents. The stronger effect of Shirin explained why Shirin-expressing cells spread at higher frequency and more extensively (Figure 2.5, S2.5A). These cell doublet experiments also provided key information about the differential impact of Rnd1 and Shirin on cell-cell adhesion.

For Rnd1, the modest decrease in Ct was compensated by the parallel decrease in contact tension T, and adhesiveness was maintained. The balance between T and Ct was less favorable to adhesion in the case of Shirin, resulting in decreased adhesiveness. These biophysical measurements of adhesiveness were fully consistent with our adhesion assay, which showed that cadherin adhesion was significantly weakened by Shirin, but not by Rnd1 (Figure 2.5K), as well as with the stronger effect of Shirin on β-catenin, pMLC and tissue organization observed in whole embryos (Figure 2.6).

Rho/Rock regulation affects collective migration of ectoderm and mesoderm tissue explants.

We extended our analysis to tissue-scale dynamics by investigating collective cell migration. For this purpose, we dissected tissue explants, let them heal for about 45 minutes until they formed a compact sphere, and then tested them for their ability to spread on FN for about 3 hours (Figure 2.9 and S2.8). The behaviour of the explants was quantitatively analyzed based on three parameters. 1) We first measured global explant spreading, expressed as relative total area expansion over time. 2) We further quantified the degree of dispersion during spreading using Delaunay triangulation of the nuclei. We determined the average triangle area between each trio of nuclei and calculated the relative ratio between the last point of the assay (170 min) and the beginning of spreading (30 min). Constant average area over time (ratio close to 1.0) meant that the tissue remained compact during spreading. A ratio greater than 1.0 was indicative of dispersion, a lower ratio suggested that the cells were further compacting. 3) We also measured the rate of intercalation by calculating the number of nuclei that were added to the basal cell layer (closest to the substrate).

In this assay, wild-type ectoderm explants did not spread on the substrate (Figure 2.9A). Wild-type mesoderm explants quickly began to expand (Figure 2.9E). Strikingly, however, their expansion was repeatedly interrupted by rapid, large scale contractions (Figure 2.9E; red arrowheads, trace in supplementary Figure S2.7B). Mesoderm explants reached an apparent “steady-state” mode of alternating spreading and contraction, with an average maximal expansion 2 to 2.5 fold their initial size (Figure 2.9G,G’). These irregular phases of retraction

explain the broad distribution of dispersion and intercalation data for this tissue (Figure 2.9M,N). This behavior suggested that mesoderm spreading was limited by internal tension. Consistently, treatment of mesoderm with Y27632 completely abolished the retraction phases, leading to a smooth and broader expansion (Figure 2.9F,G,G'), which involved intense intercalation (Figure 2.9N) but tended to be slightly dispersive (Figure 2.9M). Y27632 treatment also induced spreading of ectoderm explants (Figure 2.9B,G,G'). Interestingly, Y27632-treated ectoderm remained highly cohesive while capable of active intercalation (Figure 2.9M,N). Note that, at later time points (> 2hrs), a small proportion of wild type ectoderm explants also started to spread (Figure 2.9G,G', S2.7A), consistent with rare cases of spreading and migration of single ectoderm cells (Figure 2.2J). The behaviour of ectoderm and mesoderm tissues and the response to Rock inhibition were highly reminiscent of the behaviour of single cells (Figure 2.2), emphasizing the connection between the cell autonomous characteristics and the tissue properties.

Expression of either Rnd1 or Shirin induced extensive spreading of the ectoderm explants (Figure 2.9C,D,H,H'). However, each regulator caused a distinct mode of spreading. Rnd1-expressing explants, after a delay, rapidly spread and efficiently intercalated (Figure 2.9C,H,N). Migration remained thoroughly cohesive, and in fact cells further compacted over time (Figure 2.9K,M). On the contrary, explants expressing Shirin became looser as they spread and partly disintegrated with numerous single cells migrating individually (Figure 2.9D). Consistently, Delaunay triangulation confirmed cell dispersion, while intercalation was comparatively lower than for Rnd1 (Figure 2.9L,M,N). This mode of migration was consistent with the negative effect of Shirin on cell-cell adhesiveness (Figure 2.5K, Figure 2.6C, Figure 2.8L).

The trends observed in ectopically expressing ectoderm were partially mirrored by the behaviour of depleted mesoderm explants. Note that in these MO experiments, Delaunay triangulation appeared different, both due to the intrinsically larger size of mesoderm cells, but also because in the Rnd and Shirin morphant conditions, the mesoderm explants were both looser and less adherent to FN (see inhibition of adhesion of single cells to both cadherin and FN, Figure 2.4G,H). As a result, at the early time points, there were very few nuclei in the morphant explants at the basal cell layer, leading to large initial triangle areas (Figure S2.7K) and likely an

underestimation of dispersion and overestimation of intercalation. Nonetheless, clear conclusions could be made from the comparison of these conditions.

Shirin MO strongly decreased spreading (Figure S2.8D,E,E'). Interestingly, intercalation was left intact (Figure S2.8M), and the tissue was strongly compacted (Figure S2.8I,L). Characteristic phases of spreading and contraction were still observed but the average maximal expansion was much less than that of control mesoderm (Figure S2.8D,E,E'; red arrowheads). This phenotype can be explained considering that spreading was decreased due to Shirin depletion, while intercalation continued under the main influence of Rnd1. As for Rnd1MO, it caused two distinct phenotypes, depending on the embryo batch: About one third of the Rnd1MO mesoderm explants failed to spread. A majority of explants, however, spread quite extensively in an unusual way (Figure S2.8C,E,E'): After a slow initial phase, rapid expansion and intercalation coincided with loss of cohesion among cells as they dispersed on the matrix (Figure S2.8H,L). This behaviour is clearly reminiscent of cell dissemination observed in Shirin-expressing ectoderm (Figure 2.9D,L,M), suggesting that, in the absence of Rnd1, mesoderm behaviour was dictated by the dispersive activity of Shirin.

Effect of Rock inhibition and Rho regulators on tissue physical properties

To study global effects on physical properties of these tissues, we performed stress-relaxation experiments using the micropipette aspiration technique (MPA). While the actual properties of tissues are quite complex, they can be modelled as viscoelastic materials, where the "elastic" component corresponds to short-term tissue behavior (determined by cortical tension and cell viscoelasticity), while the viscous component reflects the ability of the cells to actively rearrange within the tissue. In an MPA experiment, the initial fast deformation phase is dominated by the short-term properties, and the slower subsequent phase by the long-term properties ("viscosity"). When the pressure is reset to zero, the aspirated portion of the explant will retract due to tissue surface tension (TST), which tends to restore the original spherical shape (Guevorkian and Maître, 2017; Guevorkian et al., 2010). Stiffness and viscosity of the tissue offer resistance to the retraction, determining again a fast and a slow response. This model enables

estimation of both tissue viscosity and TST based on the slopes of the slow viscous phases of aspiration and retraction (see Materials and Methods) (Guevorkian and Maître, 2017; Guevorkian et al., 2010). In addition, we have also quantified the initial fast deformation, as an indicator of the short-term "stiffness" of the tissue.

We observed clear differences in the behaviour of ectoderm and mesoderm explants (Figure 2.10A,B). During the initial fast phase, mesoderm explants were aspirated significantly deeper in the pipette (Figure 2.10A',B',D). Viscosity calculated from the slow phases was also significantly lower for the mesoderm (Figure 2.10E), while TST was only slightly weaker (Figure 2.10F), in agreement with previous estimates (David et al., 2014). Thus, mesoderm appears to be softer and more fluid than ectoderm, but maintains nevertheless a relatively high global tension. Different manipulations of the ectoderm gave distinct phenotypes (examples in Figure 2.10C, quantification in Figure 2.10D-I): Y27632 treatment strongly decreased both viscosity and TST of ectoderm, but did not impact on the initial fast aspiration phase. Shirin expression strongly impacted on all parameters, indicating that the tissue had become softer, more fluid, and less cohesive. On the other hand, TST was the sole parameter significantly decreased by Rnd1, stiffness and viscosity remained largely unaffected. These results are in agreement with the cell doublet measurements and with the explant spreading data. Altogether, our data show that while mesoderm properties can be approximated as the result of a global decrease in Rock-dependent contractility, they are best accounted for by distinct actions of Rnd1 and Shirin. The former mostly operates on TST by moderating cortical tension while preserving cell-cell adhesion, while the latter stimulates tissue fluidity and dispersion by dampening both cortical tension and adhesiveness.

Discussion

Ectoderm and mesoderm cells show diametrically opposed organizations in terms of cytoskeletal organization and adhesive structures, which explains their distinct migratory capabilities at both the single cell and tissue level. Yet we could surprisingly easily convert ectoderm into a migratory, mesoderm-like tissue, by simply tuning down contractility via the

Rho-Rock pathway. In fact, even non-manipulated ectoderm is capable, at low frequency, of spontaneous spreading and migration (Figure 2.2J and S2.7). An important conclusion is that the ectoderm is not irreversibly locked into a non-migratory configuration, but is actively maintained in a low dynamic state by its high contractility. Reciprocally, by targeting the mesoderm-specific Rho negative regulators Rnd1 and Shirin, we could make mesoderm cells at least partly revert to a low-migratory, blebbing, ectoderm-like state. Quite remarkably, this reversion could go so far as to reproduce the characteristic concentric organization of adhesive structures (Figure 2.3D). These observations suggest that the seemingly deep morphological and behavioural dissimilarities between the two cell types derive from relatively simple molecular differences.

The transition from a static to migratory state is reminiscent of the maturation of pre-migratory precursors into migratory neural crest cells that occurs a few hours later (Scarpa et al., 2015). In the neural crest model, the process is driven by a switch from E-cadherin to N-cadherin expression, leading to a shift from inwards to outwards protrusive activity, analogous to what we observe in gastrula tissues (Figure 2.1C,D) (Scarpa et al., 2015). In this study, however, we find that the mesoderm transition seems to rely on a direct modulation of the cytoskeleton by expression of two negative regulators of RhoA. Most importantly, neural crest cells typically migrate in a relatively loose configuration, while the mesoderm remains coherent. Our various assays highlight the fascinating property of the mesoderm cells to be at the same time highly motile, which is observed both in isolation and in the tissue, and capable to be highly cohesive (Figure 2.9). This is amply confirmed by the fact that global tensile and viscous properties of this tissue are only marginally lower that those of the ectoderm (Figure 2.10), as previously reported by Winklbauer and colleagues (David et al., 2014; Luu et al., 2011). Thus, this transition only involves a moderate shift in viscoelastic properties and clearly is not the result of a powerful fluidization. The necessity for the mesoderm to remain cohesive and tensile is obvious, as it must be able to generate and withstand the significant forces that are involved in gastrulation movements (Keller et al., 2003).

The apparent simplicity of this transition to high tissue motility, simply controlled by the regulation of cellular tension, contrast to the more complicated shift in parameters associated with EMT. It stands to reason that at this early stage of development the ‘barrier to entry’ of a

migratory state is much smaller than that in more differentiated tissues. The same principle most likely applies to mesoderm involution in fish. Furthermore, we would like to propose that a similar downregulation of contractility is a likely general mechanism to generate motility, which we expect to be also utilized in the EMT-like modes of gastrulation found in amniotes or in Drosophila.

Note that the viscosity and TST values obtained with the aspiration technique differ significantly from those reported by Winklbauer and colleagues (David et al., 2014; Luu et al., 2011). This difference likely reflects the different techniques used, and the different situations that were addressed: Previous work determined the properties of tissue explants through their global deformation under the sole influence of gravity, while we challenged the capacity of the tissues to resist local stress. Differences in "apparent" physical values have to be expected, considering that the cytoskeleton and cell adhesion are likely to behave differently under different stress conditions, and that cells are capable of active reactions that can rapidly and deeply modify these structures and consequently tissue rheology. Therefore, these estimates must be considered as relative values, valid under specific experimental conditions. They are nevertheless highly informative about the properties of tissues and the influence of molecular manipulations. Along the same lines, the spreading assay (Figure 2.9) tests yet another situation, as spreading is controlled by the balance between the internal properties of the tissue (such as cell-cell adhesion, cortical tension, intercellular motility), and the capacity of cells to spread, adhere and migrate on extracellular matrix. We believe these various assays provide complementary approaches to unravel the mechanisms underlying morphogenetic processes.

This study implicates the Rnd1 - Shirin pair as a key regulator of the ectoderm to mesoderm transition. Rnd1 and Shirin MO embryonic phenotypes are extremely strong and penetrant, demonstrating an absolute requirement of these molecules for mesoderm movements. At the tissue and cell level, Rnd1 and Shirin fulfill common as well as distinct complementary functions. They both promote mesoderm motility, as demonstrated by the decreased single cell migration in Rnd1 MO and Shirin MO mesoderm, which is perfectly mirrored by induction of single cell migration and of explant spreading in the gain-of-function experiments. This effect is in both cases related to their inhibitory activity toward the Rho-Rock pathway,

resulting in significant reduction of cortical tension. Their activities, however, differ both quantitatively and qualitatively: In general, Shirin appears to be a more potent regulator, as observed for a variety of parameters examined in this study. Examples include stronger downregulation of cortical tension, induction of cell spreading, decrease in β-catenin at cell contacts, and, to a lesser degree, in pMLC at the cortex. A likely explanation is that Shirin is a GAP, which has a direct catalytic activity on RhoA, while Rnd1 action is indirect. This apparent higher activity does not necessarily make Shirin "better" at all tasks. A good example is single cell migration, for which Shirin is less efficient than Rnd1. This is not surprising, as adhesion and migration rely on a fine balance of myosin activity that depends not only on levels of activity, but also on additional parameters such as subcellular localization. These considerations also explain why global Rock inhibition, which efficiently stimulates spreading and migration in the ectoderm, falls short of reaching the migration capacity of mesoderm cells.

The two regulators also show clear qualitative differences in their action. Rnd1 appears specifically in charge of maintaining cell-cell contacts, while Shirin controls protrusive activity and FAs, and negatively impacts cell-cell adhesion (though this may be an indirect effect of its powerful impact on the regulation of cortical tension). The complementarity of these two regulators in controlling collective migration was evident in the tissue spreading assay. In the hybrid phenotype of Rnd1 MO, the initial slower spreading was consistent with the contribution of Rnd1 in decreasing contractility and promoting motility. The subsequent emergence of a strong dispersive behaviour revealed the underlying Shirin activity, which is otherwise counterbalanced by Rnd1 in the wild type mesoderm. Consistently, ectopic expression of Shirin in the ectoderm caused a dispersive mode of spreading. Conversely, the prominent capacity of Rnd1 to stimulate intercalation, while imposing strong tissue coherence, was highlighted under conditions of Shirin depletion in the mesoderm and ectopic expression of Rnd1 in the ectoderm. Although these two regulators need to be further characterized, their doppelgänger nature is consistent with the overlapping yet partly complementary subcellular localizations. Thus, their global cortical pools are probably responsible for decreased cell cortical tension, spreading and migration, while their sites of accumulation at protrusions for Shirin and at cell contacts for Rnd1 are consistent with their opposite effects on adhesiveness and tissue cohesion. The dual function

of these regulators may also explain some less intuitive phenotypes, in particular the decreased cadherin adhesion for Shirin MO mesoderm cells, which most likely results from an imbalance in cellular tensions under these artificial conditions. Note that we also expect the input of additional components on the contractile and adhesive properties of these tissues, which remain to be identified.

The pro-migratory activity of both Rnd1 and Shirin uncovered here may seem unexpected, since Rnd1 and the Dlc1,2,3 family, to which Shirin belongs, are traditionally viewed as inhibitors of migration and as suppressors of invasion (Braun and Olayioye, 2015; Haga and Ridley, 2016). Rnd1 was also reported as an anti-adhesive in Xenopus (Ogata et al., 2007; Wünnenberg-Stapleton et al., 1999). We also observed defects in adhesion and migration, but only in the case of cells expressing these regulators at high levels (Figure 2.5C,E, S2.5). This is to be expected considering the multiple effects of RhoA-dependent contractility and the intricacy of its regulation. The simplest interpretation is that overexpression of RhoA inhibitors brings contractility below the basal level minimally required for adhesion and migration. Such considerations can readily explain why these molecules are found to have opposite effects depending on the cell type and the context (Braun and Olayioye, 2015; Haga and Ridley, 2016). The ability of Rnd1 to stimulate both migration and cohesion is reminiscent of the properties of EpCAM, a cell membrane protein that also acts as an indirect inhibitor of myosin contractility, although through a completely different pathway (Maghzal et al., 2010; Maghzal et al., 2013). These types of regulators must share the ability to simultaneously repress global cortical tension, accounting for their pro-migratory activity and tension at cell-cell contacts, maintaining the proper force balance that insures tissue cohesiveness (David et al., 2014; Winklbauer, 2015).

It is important to point out that some of the phenotypes observed at the tissue level could not be fully explained by the single cell experiments. For instance, Shirin expression induced extensive migration of ectoderm explants (Figure 2.9), but only modest migration of single cells (Figure 2.5). We similarly recognize that the *in vitro* analysis of isolated tissues may not reflect all the properties of these tissues in the *in vivo* context. Obviously, their morphogenesis *in vivo* is influenced by multiple factors, such as the geometry of the embryo, the forces exerted by the surrounding tissues, and the signals that they emit (e.g. the impact of ectodermal PDGF on

mesoderm intercalation (Damm and Winklbauer, 2011). One thus must be cautious when extrapolating properties observed from a lower to an upper level of organization. Yet, studies on the Xenopus gastrula have amply demonstrated that explanted tissues retain many of their characteristic morphogenetic properties. Certain morphogenetic movements do appear to be at least partially tissue autonomous, including mesoderm involution and intercalation (Evren et al., 2014), vegetal rotation (Wen and Winklbauer, 2017), or blastopore closure (Shook et al., 2018). Furthermore, key cellular properties observed in the embryo and in isolated tissues are also retained in isolated cells. Directly relevant for this study, the differences in cell morphology and motility observed between subregions of the mesoderm (and endoderm) are preserved in isolated cells (Wacker et al., 1998). Even kinetics, which are expected to be most sensitive to changes in cellular and matrix environment, surprisingly remain within the physiological scale. Indeed, mesoderm cells migrate at a speed of ~1µm/min during explant spreading (estimates based on experiments of Figure 2.9), which is not only close to the speed of single cell migration (Figure 2.1), but also to the estimated speed in the embryo (~ 2µm/min, R. Winklbauer, personal communication). Our results at the all three levels of organization provide a very coherent picture of the mechanism at the base of motility of the mesoderm, in particular in showing common and distinct activities of Rnd1 and Shirin.

Obviously additional regulatory mechanisms are expected to fine tune the tissue properties in order to achieve the perfectly coordinated ballet of gastrulation movements. For instance, Rnd1 interactors were reported to modulate its function in the mesoderm (Chen and Chen, 2009; Ogata et al., 2007). We must stress, however, that both Shirin and Rnd1 are sufficient on their own to induce the distinct modes of migration described in this study, as shown unambiguously by the effect of their ectopic expression on single ectoderm cells and tissue explants. The cooperation of Rnd1 and Shirin/Dlc2 in enabling mesoderm involution provides an example of how different cytoskeletal regulators may be used to tune tissue behaviour. It will be important to see if the same molecules, or similar pairs of rivals contribute to other processes involving collective migration.

Materials and methods

Embryo preparation and injection

All plasmids are based on the pCS2+MTYFP vector (Fagotto et al., 2013). Plasmids and morpholino oligonucleotides (Genetools LLC) are listed in S2.1 and S2.2 Tables in the supplemental information section. mRNAs were synthesized according to manufacturer instructions (mMessage mMachine kit, Ambion). MOs and mRNAs were injected animally in the two blastomeres of 2-cell stage embryos for ectoderm targeting, or equatorially in the two dorsal blastomeres of 4-cell stage embryos for mesoderm targeting, at amounts listed in S2.1 and S2.2 Tables.

Chemicals

Y27632, H1125 and ML7 were from Millipore and Enzo Life Sciences. Stock solutions of inhibitors were prepared in DMSO. They were used at a 1/1000 or higher dilution. Equivalent dilutions of DMSO were added to control conditions and had no detectable effect on cell and tissue properties.

Microdissections and cell dissociation

All dissected explants and cells were taken either from the inner layer of the ectodermal animal cap or from the anterior mesoderm at stage 10.5, except for the MO experiments, in which case the mesoderm was dissected from the dorsal lip at stage 10+, i.e. before involution. Dissections were performed in 1x MBSH (88mM NaCl, 1mM KCl, 2.4mM $NaHCO_3$, 0.82mM $MgSO_4$, 0.33mM $Ca(NO_3)_2$, 0.33mM $CaCl_2$, 10mM Hepes and 10 µg/ml Streptomycin and Penicillin, pH 7.4. Single cells were dissociated in alkaline buffer (88mM NaCl, 1mM KCl and 10mM $NaHCO_3$, pH = 9.5) (Rohani et al., 2014). All subsequent assays were performed in 0.5x MBSH buffer, at room temperature (23^{o}C).

Western blots

Animal caps were dissected at stage 9 and allowed to heal on non-adhesive agarose coated dishes until control embryos reached stage 10.25, after which protein was extracted. Rabbit anti-

pMYPT1 Thr696 (Cell Signalling Technology) was used at 1:1000 and anti-GAPDH FL-335 (Santa Cruz Biotech) was used at 1:4000. A peroxidase conjugated donkey anti-rabbit secondary (Jackson Immuno Research) was used at a 1:4000 dilution.

Immunofluorescence

Whole embryos were fixed at stage 10.5 in 2% paraformaldehyde, 100mM NaCal, 100mM HEPES-NaOH pH 7.4 for 60min, then permeabilized with 1% Triton X100 for 30min, embedded in fish gelatine as previously described (Fagotto and Brown, 2008; Schohl and Fagotto, 2002). Ectoderm explants were dissecting at stage 9 (late blastula), and left to heal until control embryos at reached stage 10+, then fixed and processed as whole embryos. Cryosections were prepared and immunostained as described (Fagotto and Brown, 2008; Schohl and Fagotto, 2002), except that Eriochrome counterstaining of the yolk was omitted in order to permit triple staining. Sections from multiple conditions, including a control condition, were collected on the same slide, in order to minimize immunostaining variability. Antibodies used were rabbit anti-β-catenin H102 (Santa Cruz Biotech.)(1:200 dilution), mouse anti-phospho-myosin light chain 2 (Ser19)(Cell Signalling)(1:200 dilution), and chicken anti-GFP (Sigma-Aldrich)(1:1000 dilution). Secondary antibodies were coupled to Alexa488, 546 and 647 (Thermofisher). Nuclei were counterstained with Hoechst. Images were acquired on a SP5-SMD laser scanning confocal microscope (Leica) with an oil immersion 20x objective (HC Plan Apo IMM 0.7NA).

Live confocal microscopy

Glass bottom dishes (CellVis) were coated for 45min with 10µg/ml bovine fibronectin (Sigma-Aldrich) followed by blocking with 5mg/ml bovine serum albumin. Dissociated cells from embryos expressing various fluorescent fusion proteins were plated on the dish and imaged using a spinning disc confocal microscope (Dragonfly, Andor), mounted with two EMCCD cameras (iXon888 Life Andor) for simultaneous dual color imaging, with a 60x objective (Apo lambda, 1.4 NA) and the Fusion acquisition software (Andor). Images were deconvoluted using Fusion software (Andor) and further analyzed using ImageJ.

Image analysis and quantification

All image quantification of confocal images was performed using ImageJ software.

Vinculin-Cherry enrichment was measured on maximal projections of 2 to 3 0.25µm-thick z stacks encompassing the ventral cell surface. A mask was produced to extract the brighter signal of "clustered" vinculin-Cherry corresponding to focal adhesions. The total fluorescence intensity within this mask was divided by the total fluorescence intensity to the whole ventral surface of the cell, after background subtraction.

Quantification of colocalization between Shirin-YFP and Vinculin-Che at the ventral surface was performed using the JaCoP plugin of Image J.

Relative cortical and contact enrichments of MLC-Cherry, Cadherin-dTomato, Rnd1-YFP and Shirin-YFP were obtained by measuring the average fluorescence intensity of line scans manually drawn along free cell edges or along cell-cell contacts, as well as the intensity in the cytoplasm immediately adjacent to the cell periphery. After background subtraction, the "cortical" enrichment was calculated as cell edge (or cell contact)/cytoplasm.

Relative cell membrane/cortical enrichment of β-catenin and pMLC from immunofluorescence images were measured as follows: The β-catenin signal was used to produce a mask, which involved Gaussian filtering, two rounds background subtraction (global and local), thresholding to obtain a binary image, which was then skeletonized, and finally dilated to a thickness of 3 pixels (~1.5µm). The mask was used to extract the signal from both β-catenin and pMLC original images, and measure the average intensity, to which the cytoplasmic background, obtained through a complementary mask, was subtracted. For embryo immunostaining, three fields of deep ectoderm cells were taken from each side (dorsal and ventral) of the embryo, on at least two different sections. For ectoderm explants, two large fields, together covering the majority of the section area, were imaged for each explant.

Cell morphology, categories

The morphology analysis was performed from bright field time lapse movies. The morphology of each single cell from a whole field was assessed at each time point of the migration assay, and categorized as follows (examples in Figure 2.2J): Round and blebbing (s), round not blebbing (r), polarized, i.e. elongated but still round-shaped or only partially spread (p), or spread (s). A fifth category included a special phenotype (polarized blebbing, pb), where cells were partially elongated, but had blebs and typically remained anchored to the substrate by one side of the cell. The distribution of morphologies presented in Figures 2D,4D,5G was expressed as the percentage of cells in these five categories observed at time 25'. The speed for each morphological category (Figure S2.4) was calculated by extracting the average values for each segment of a track (within frames 10 and 40) during which the cell had adopted a particular morphology.

Cell morphology, morphometry

The analysis was performed on stacks of live spinning confocal images. Two binary images were obtained, one from the ventral cell surface (closest to the glass), one from the maximal z projection. Blebs were omitted from the segmentation. Absolute surface areas and circularity were obtained from the "measure object" function of ImageJ.

Migration assay

Dissociated cells were plated on fibronectin-coated glass bottom dishes and left to adhere for 45-60min, then imaged every 2.5min for 100-170min using a bright field inverted Olympus IX83 microscope (10X UPFLN 0.3NA PH1 objective) and a scMOS ZYLA 4.2 MP camera. Chemical inhibitors were added after four frames (10min) after the beginning of the time lapse. Addition of the inhibitor was set as time zero. The path of individual cells that did not establish contacts with neighbouring cells were manually tracked using ImageJ software. Average speed corresponds to the average of the speeds calculated between each consecutive time point, within the window frames 10 to 40 (25 to 100min).

Adhesion assay

We used a modified assay based on Niessen et al (Niessen and Gumbiner, 2002). 35mm round dishes with a 20mm diameter glass bottom (CellVis) were freshly coated as follows: 1mm diameter circles positioned near the edge of the coverglass, at 8.5mm from the center, were coated with either 10µg/ml fibronectin (Sigma-Aldrich), or with 100µg/ml Protein A followed by 15 µg/µl recombinant C-cadherin extracellular domain fused to human IgG Fc domain, produced and prepared as previously described (Niessen and Gumbiner, 2002). Blocking buffer was as in (Niessen and Gumbiner, 2002). Dissociated cells were laid in the coated circles, left to adhere for 45min, and images with an inverted microscope mounted with a 5x objective were collected to determine the initial number of adherent cells. The dishes were then subjected to rotation (10 min at 180rpm for FN, 25min at 200rpm for cadherin), and the fields were imaged a second time to determine the number of cells that had remained attached.

Calculation of relative tensions for cell doublets is presented in the S2.1 appendix.

Tissue spreading assay

About 200-300µm diameter explants were prepared by cutting pieces of dissected ectoderm or mesoderm tissues, which were left to heal and round up for 45min on a non-adhesive agarose coated dish. In cases of treatment with Y27632, the explants were incubated for an additional 45 minutes after healing. The explants were then transferred to fibronectin-coated glass bottom dishes and imaged for 170 min every 2.5 minutes with a 10x objective as described for cell migration. Areas of explants were calculated at each timepoint using CellProfiler (Kamentsky et al., 2011). To measure cell dispersion during spreading, the XY coordinates of each nucleus was determined using CellProfiler. The coordinates were then used to perform Delaunay triangulation, followed by calculation of the area of each triangle using Matlab.

Micropipette Aspiration Assay

MPA was used to measure the viscosity and surface tension of explants as previously described (Guevorkian and Maître, 2017; Guevorkian et al., 2010). Custom made pipettes with diameters of either 100 or 125 µm with a 15° bend (Sutter Instruments) were passivated with BSA before

being used to apply an aspiration pressure of 250 or 220 Pa (depending on the size of the pipette). The aspiration lasted 4-5 minutes, sufficient for the aspiration of the explant to reach a constant velocity; the pressure was then set to zero and the explant was allowed to relax. The pressure was modulated using a Microfludic Flow Control System and the Maesflow software (Fluigent), and the pipettes were controlled using a PatchStar Micromanipulator and the LinLab2 software (Scientifica). The size of the deformation was automatically calculated using a custom ImageJ macro and used to calculate the rates of aspiration ($v_{Asp} = dL_{Asp}/dt$) and retraction ($v_{Ret} = dL_{Ret}/dt$) of the deformation, which were in turn used to calculate tissue viscosity and surface tension (Guevorkian and Maître, 2017). Briefly, viscosity $\eta=R_p\Delta P/3\pi(v_{Asp}+ v_{Ret})$ where R_p is the radius of the pipette and ΔP is the applied pressure. Surface tension $\gamma=P_c/2*(1/R_p-1/R_0)$, where R_0 is the radius of curvature of the explant, and P_c is the pressure that when applied the length of the deformation is equal to R_p. It can also be calculated from $P_c=\Delta P\ v_{Ret}/ (v_{Asp}+ v_{Ret})$. Images were acquired every 1 second using a brightfield Zeiss Axiovert 135TV microscope (5x Plan-Neofluar 0.15NA PH1) with a Retiga 2000R camera (QImaging).

Acknowledgements

F.F. dedicates this study to Ray Keller, intrepid adventurer of morphogenesis and inspiring master. We thank Drs. C. Niessen and B. Gumbiner for generous gift of the C-cadherin-Fc-expressing CHO cell line, Dr. K. Cho, F. Spagnoli, A. Brivanlou, N. Kinoshita, and S. Yonemura for plasmids. We are deeply grateful to Drs. Karine Guevorkian and David Gonzales-Rodriquez for invaluable help with setting and interpreting MPA experiments. We thank the Montpellier Rio Imaging platform for technical support.

References

Braun, A. C. and Olayioye, M. A. (2015). Rho regulation: DLC proteins in space and time. *Cellular signalling* **27**, 1643–1651.

Brieher, W. M. and Gumbiner, B. M. (1994). Regulation of C-cadherin function during activin induced morphogenesis of Xenopus animal caps. *The Journal of cell biology* **126**, 519–527.

Canty, L., Zarour, E., Kashkooli, L., François, P. and Fagotto, F. (2017). Sorting at embryonic boundaries requires high heterotypic interfacial tension. *Nature communications* **8**, 157.

Charras, G. and Paluch, E. (2008). Blebs lead the way: how to migrate without lamellipodia. *Nature reviews. Molecular cell biology* **9**, 730–736.

Chen, C.-L. and Chen, H.-C. (2009). Functional suppression of E-cadherin by protein kinase Cdelta. *Journal of cell science* **122**, 513–523.

Damm, E. W. and Winklbauer, R. (2011). PDGF-A controls mesoderm cell orientation and radial intercalation during Xenopus gastrulation. *Development (Cambridge, England)* **138**, 565–575.

David, R., Luu, O., Damm, E. W., Wen, J. W. H., Nagel, M. and Winklbauer, R. (2014). Tissue cohesion and the mechanics of cell rearrangement. *Development (Cambridge, England)* **141**, 3672–3682.

Evren, S., Wen, J. W. H., Luu, O., Damm, E. W., Nagel, M. and Winklbauer, R. (2014). EphA4-dependent Brachyury expression is required for dorsal mesoderm involution in the Xenopus gastrula. *Development* **141**, 3649–3661.

Fagotto, F. and Brown, C. M. (2008). Detection of nuclear beta-catenin in Xenopus embryos. *Methods in molecular biology (Clifton, N.J.)* **469**, 363–380.

Fagotto, F., Rohani, N., Touret, A.-S. and Li, R. (2013). A molecular base for cell sorting at embryonic boundaries: contact inhibition of cadherin adhesion by ephrin/ Eph-dependent contractility. *Developmental cell* **27**, 72–87.

Guevorkian, K. and Maître, J.-L. (2017). Micropipette aspiration: A unique tool for exploring cell and tissue mechanics in vivo. *Methods in cell biology* **139**, 187–201.

Guevorkian, K., Colbert, M.-J., Durth, M., Dufour, S. and Brochard-Wyart, F. (2010). Aspiration of biological viscoelastic drops. *Physical review letters* **104**, 218101.

Haga, R. B. and Ridley, A. J. (2016). Rho GTPases: Regulation and roles in cancer cell biology. *Small GTPases* **7**, 207–221.

Han, M. K. L. and de Rooij, J. (2016). Converging and Unique Mechanisms of Mechanotransduction at Adhesion Sites. *Trends in cell biology* **26**, 612–623.

Huang, Y. and Winklbauer, R. (2018). Cell migration in the Xenopus gastrula. *Wiley interdisciplinary reviews. Developmental biology* **7**, e325.

Kale, G. R., Yang, X., Philippe, J.-M., Mani, M., Lenne, P.-F. and Lecuit, T. (2018). Distinct contributions of tensile and shear stress on E-cadherin levels during morphogenesis. *Nature communications* **9**, 5021.

Kamentsky, L., Jones, T. R., Fraser, A., Bray, M.-A., Logan, D. J., Madden, K. L., Ljosa, V., Rueden, C., Eliceiri, K. W. and Carpenter, A. E. (2011). Improved structure, function and compatibility for CellProfiler: modular high-throughput image analysis software. *Bioinformatics (Oxford, England)* **27**, 1179–1180.

Keller, R., Davidson, L. A. and Shook, D. R. (2003). How we are shaped: the biomechanics of gastrulation. *Differentiation; research in biological diversity* **71**, 171–205.

Luu, O., David, R., Ninomiya, H. and Winklbauer, R. (2011). Large-scale mechanical properties of Xenopus embryonic epithelium. *Proceedings of the National Academy of Sciences of the United States of America* **108**, 4000–4005.

Maghzal, N., Vogt, E., Reintsch, W., Fraser, J. S. and Fagotto, F. (2010). The tumor-associated EpCAM regulates morphogenetic movements through intracellular signalling. *The Journal of cell biology* **191**, 645–659.

Maghzal, N., Kayali, H. A., Rohani, N., Kajava, A. v and Fagotto, F. (2013). EpCAM controls actomyosin contractility and cell adhesion by direct inhibition of PKC. *Developmental cell* **27**, 263–277.

Maître, J.-L., Berthoumieux, H., Krens, S. F. G., Salbreux, G., Jülicher, F., Paluch, E. and Heisenberg, C.-P. (2012). Adhesion functions in cell sorting by mechanically coupling the cortices of adhering cells. *Science (New York, N.Y.)* **338**, 253–256.

Nakatsuji, N., Smolira, M. A. and Wylie, C. C. (1985). Fibronectin visualized by scanning electron microscopy immunocytochemistry on the substratum for cell migration in Xenopus laevis gastrulae. *Developmental biology* **107**, 264–268.

Niessen, C. M. and Gumbiner, B. M. (2002). Cadherin-mediated cell sorting not determined by binding or adhesion specificity. *The Journal of cell biology* **156**, 389–399.

Ogata, S., Morokuma, J., Hayata, T., Kolle, G., Niehrs, C., Ueno, N. and Cho, K. W. Y. (2007). TGF-beta signalling-mediated morphogenesis: modulation of cell adhesion via cadherin endocytosis. *Genes & development* **21**, 1817–1831.

Parent, S. E., Barua, D. and Winklbauer, R. (2017). Mechanics of Fluid-Filled Interstitial Gaps. I. Modeling Gaps in a Compact Tissue. *Biophysical journal* **113**, 913–922.

Rohani, N., Parmeggiani, A., Winklbauer, R. and Fagotto, F. (2014). Variable combinations of specific ephrin ligand/Eph receptor pairs control embryonic tissue separation. *PLoS biology* **12**, e1001955.

Scarpa, E., Szabó, A., Bibonne, A., Theveneau, E., Parsons, M. and Mayor, R. (2015). Cadherin Switch during EMT in Neural Crest Cells Leads to Contact Inhibition of Locomotion via Repolarization of Forces. *Developmental cell* **34**, 421–434.

Schohl, A. and Fagotto, F. (2002). Beta-catenin, MAPK and Smad signalling during early Xenopus development. *Development (Cambridge, England)* **129**, 37–52.

Session, A. M., Uno, Y., Kwon, T., Chapman, J. A., Toyoda, A., Takahashi, S., Fukui, A., Hikosaka, A., Suzuki, A., Kondo, M., et al. (2016). Genome evolution in the allotetraploid frog Xenopus laevis. *Nature* **538**, 336–343.

Shook, D. R., Kasprowicz, E. M., Davidson, L. A. and Keller, R. (2018). Large, long range tensile forces drive convergence during Xenopus blastopore closure and body axis elongation. *eLife* **7**,.

Wacker, S., Brodbeck, A., Lemaire, P., Niehrs, C. and Winklbauer, R. (1998). Patterns and control of cell motility in the Xenopus gastrula. *Development (Cambridge, England)* **125**, 1931–1942.

Wen, J. W. and Winklbauer, R. (2017). Ingression-type cell migration drives vegetal endoderm internalisation in the Xenopus gastrula. *eLife* **6**,.

Winklbauer, R. (2009). Cell adhesion in amphibian gastrulation. *International review of cell and molecular biology* **278**, 215–275.

Winklbauer, R. (2015). Cell adhesion strength from cortical tension - an integration of concepts. *Journal of cell science* **128**, 3687–3693.

Winklbauer, R. and Keller, R. E. (1996). Fibronectin, mesoderm migration, and gastrulation in Xenopus. *Developmental biology* **177**, 413–426.

Winklbauer, R. and Nagel, M. (1991). Directional mesoderm cell migration in the Xenopus gastrula. *Developmental biology* **148**, 573–589.

Wünnenberg-Stapleton, K., Blitz, I. L., Hashimoto, C. and Cho, K. W. (1999). Involvement of the small GTPases XRhoA and XRnd1 in cell adhesion and head formation in early Xenopus development. *Development (Cambridge, England)* **126**, 5339–5351.

Figures

Figure 2.1

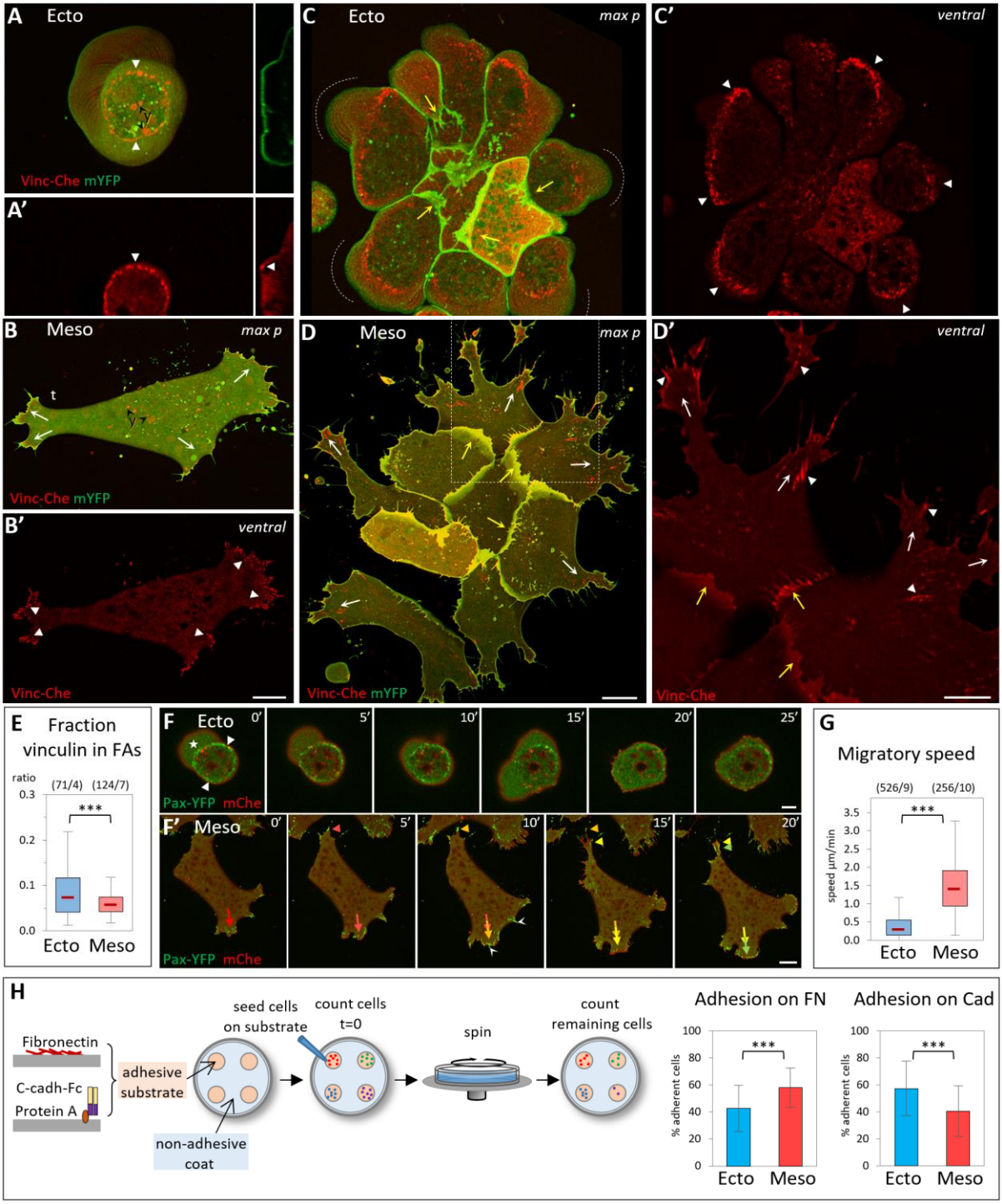

Figure 2.2

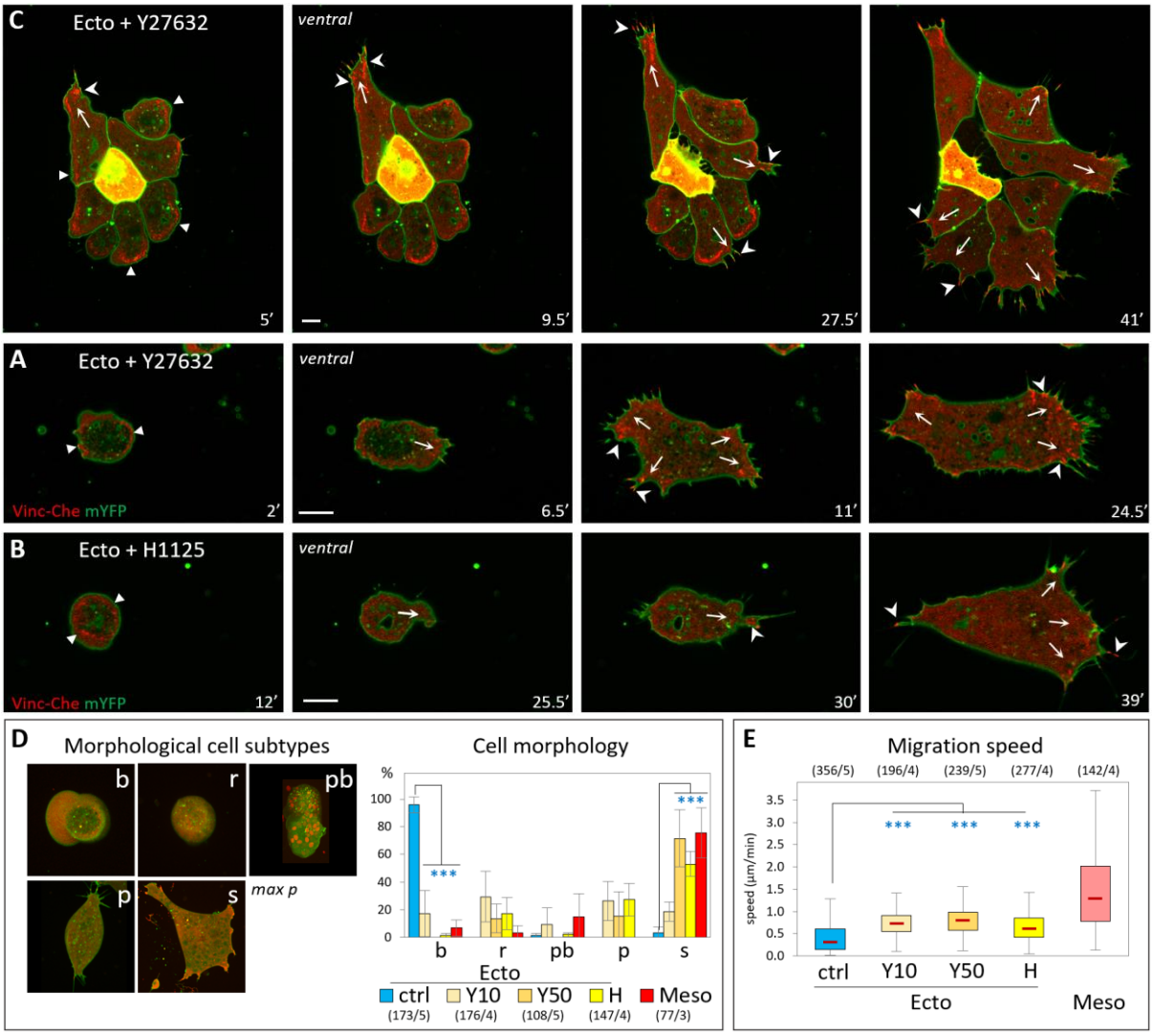
C
Ecto + Y27632
ventral
5′
9.5′
27.5′
41′
A
Ecto + Y27632
Vinc-Che mYFP
2′
6.5′
11′
24.5′
B
Ecto + H1125
Vinc-Che mYFP
12′
25.5′
30′
39′
D
Morphological cell subtypes
b
r
pb
p
s
max p
Cell morphology
%
100
80
60
40
20
0
***
b
r
pb
p
s
Ecto
ctrl
Y10
Y50
H
Meso
(173/5)
(176/4)
(108/5)
(147/4)
(77/3)
E
Migration speed
(356/5)
(196/4)
(239/5)
(277/4)
(142/4)
speed (µm/min)
3.5
3.0
2.5
2.0
1.5
1.0
0.5
0.0
***
***
***
ctrl
Y10
Y50
H
Ecto
Meso

Figure 2.3

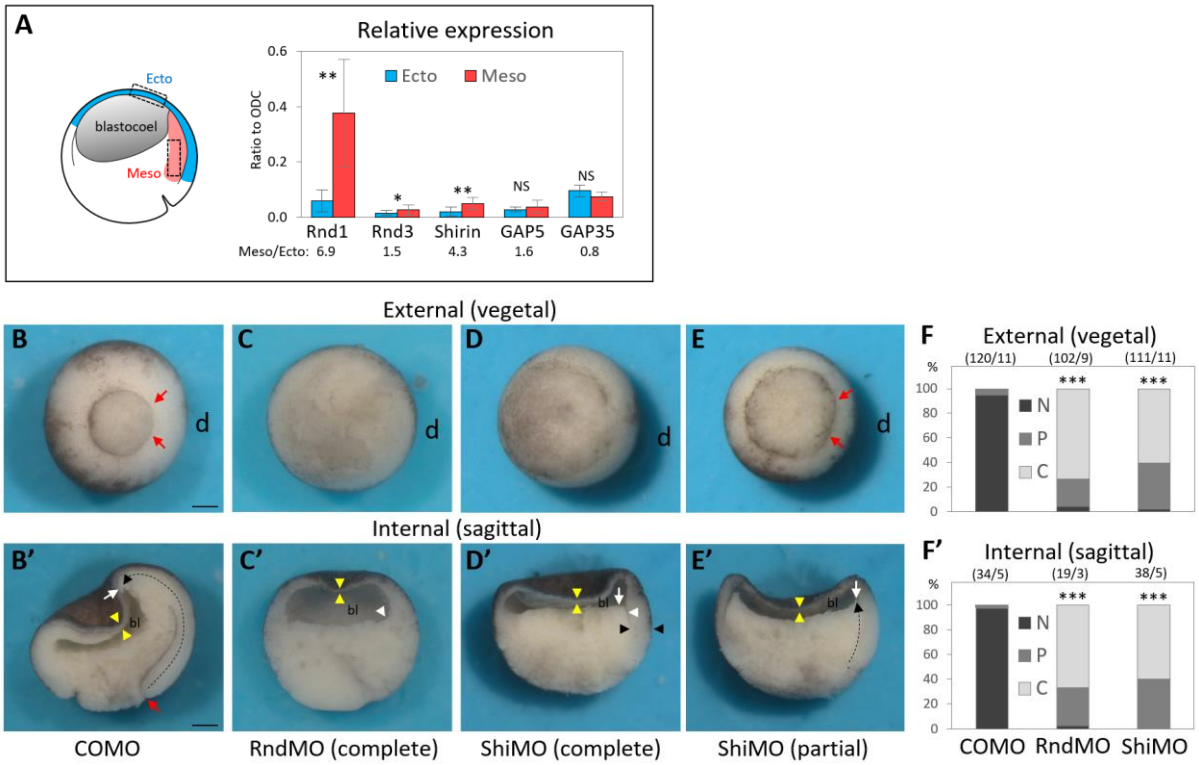
A
Relative expression
Ecto
blastocoel
Meso
Ecto
Meso
Ratio to ODC
0.6
0.4
0.2
0.0
**
*
**
NS
NS
Rnd1
Rnd3
Shirin
GAP5
GAP35
Meso/Ecto: 6.9
1.5
4.3
1.6
0.8
External (vegetal)
B
C
D
E
d
Internal (sagittal)
B'
C'
D'
E'
bl
COMO
RndMO (complete)
ShiMO (complete)
ShiMO (partial)
F
External (vegetal)
(120/11)
(102/9)
(111/11)
%
100
80
60
40
20
0
***
N
P
C
F'
Internal (sagittal)
(34/5)
(19/3)
38/5)
COMO
RndMO
ShiMO

Figure 2.4

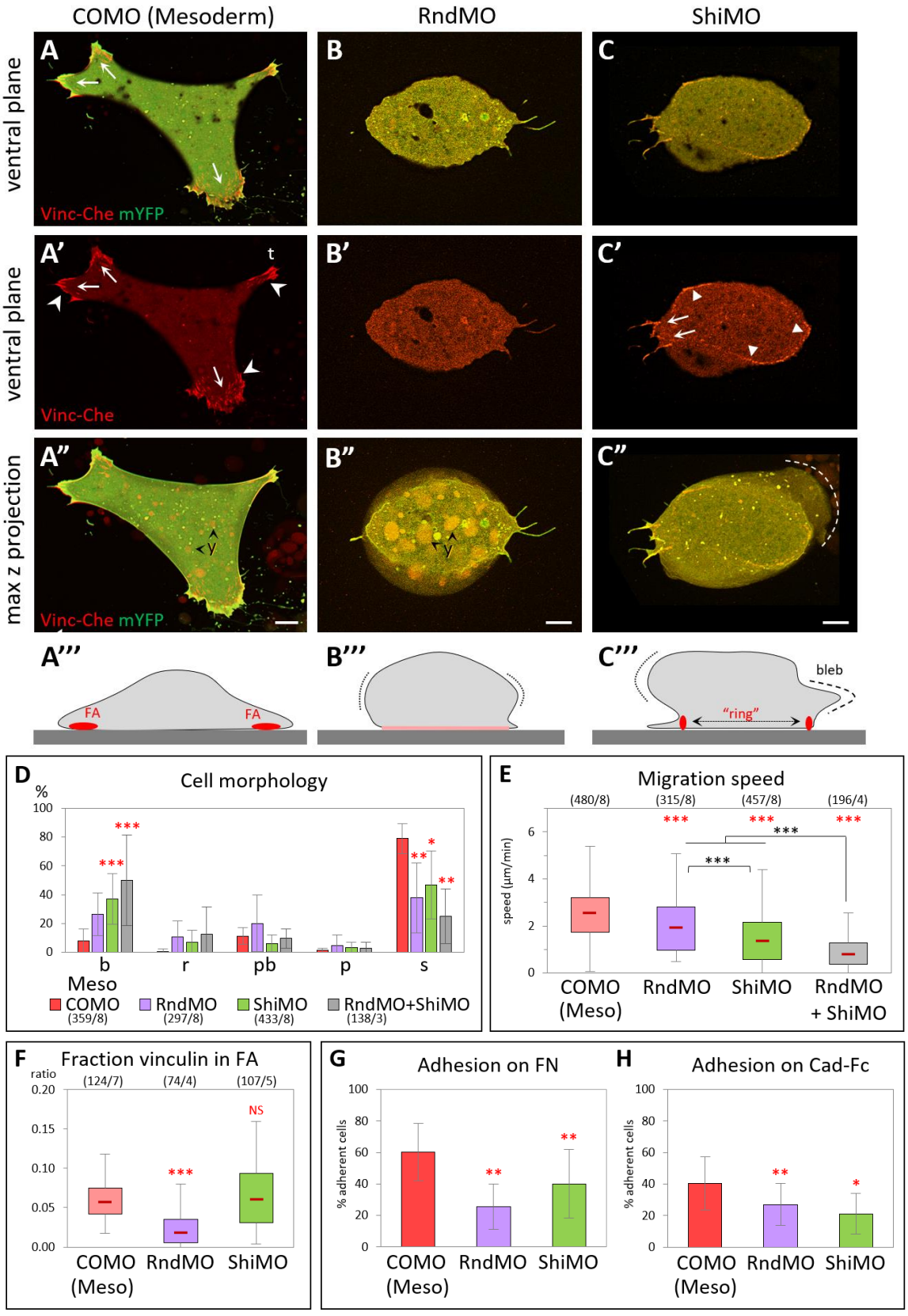
COMO (Mesoderm)
RndMO
ShiMO
ventral plane
max z projection
A
B
C
A'
B'
C'
A''
B''
C''
Vinc-Che mYFP
Vinc-Che
t
A'''
B'''
C'''
FA
bleb
"ring"
D
Cell morphology
%
b
r
pb
p
s
Meso
COMO (359/8)
RndMO (297/8)
ShiMO (433/8)
RndMO+ShiMO (138/3)
E
Migration speed
(480/8)
(315/8)
(457/8)
(196/4)
speed (µm/min)
COMO (Meso)
RndMO
ShiMO
RndMO + ShiMO
F
Fraction vinculin in FA
ratio
(124/7)
(74/4)
(107/5)
NS
G
Adhesion on FN
% adherent cells
H
Adhesion on Cad-Fc

Figure 2.5

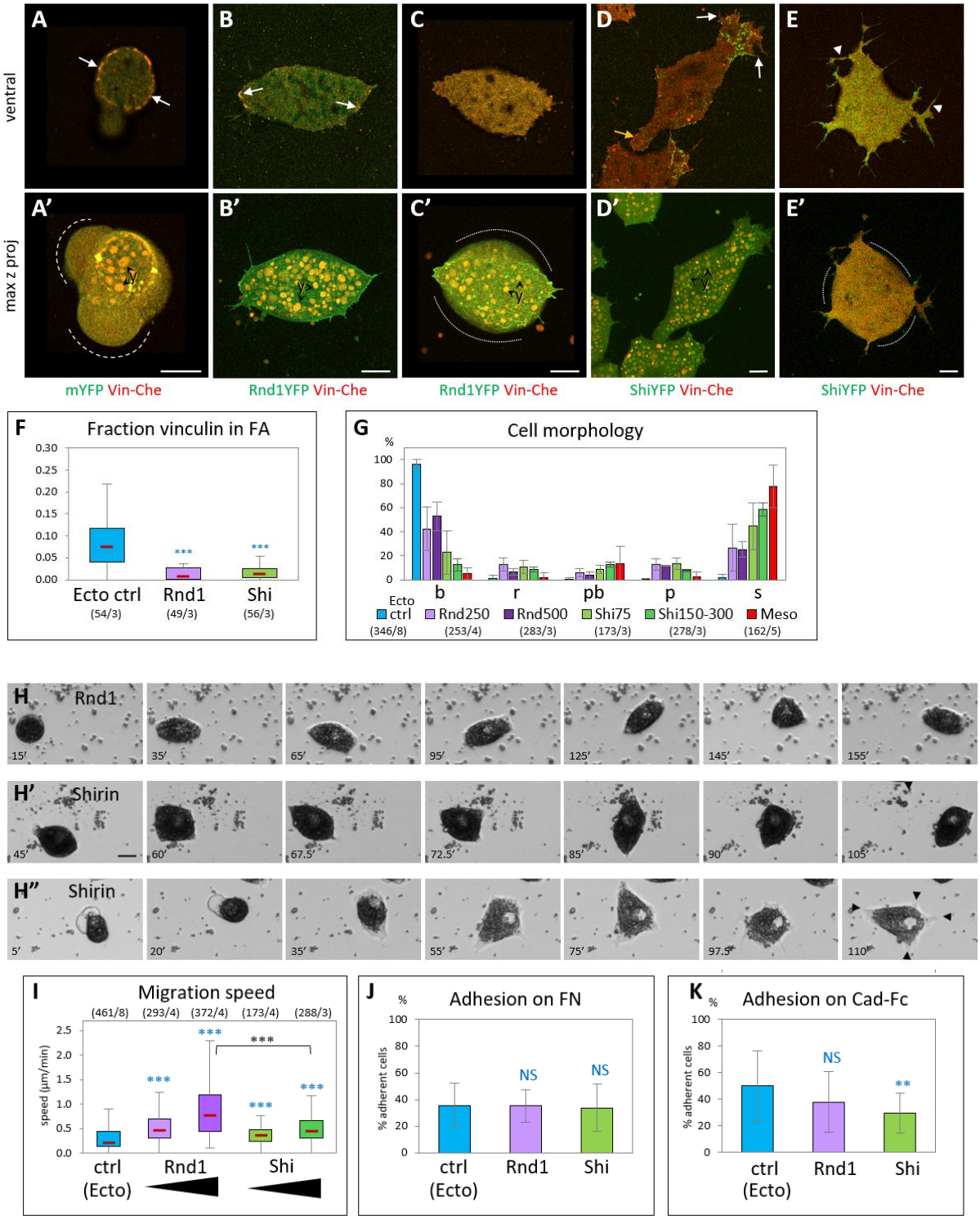
A
B
C
D
E
ventral
A'
B'
C'
D'
E'
max z proj
mYFP Vin-Che
Rnd1YFP Vin-Che
Rnd1YFP Vin-Che
ShiYFP Vin-Che
ShiYFP Vin-Che
F
Fraction vinculin in FA
0.30
0.25
0.20
0.15
0.10
0.05
0.00
***
***
Ecto ctrl
(54/3)
Rnd1
(49/3)
Shi
(56/3)
G
Cell morphology
%
100
80
60
40
20
0
b
r
pb
p
s
Ecto ctrl
(346/8)
Rnd250
(253/4)
Rnd500
(283/3)
Shi75
(173/3)
Shi150-300
(278/3)
Meso
(162/5)
H
Rnd1
15′
35′
65′
95′
125′
145′
155′
H'
Shirin
45′
60′
67.5′
72.5′
85′
90′
105′
H"
Shirin
5′
20′
35′
55′
75′
97.5′
110′
I
Migration speed
(461/8)
(293/4)
(372/4)
(173/4)
(288/3)
speed (µm/min)
2.5
2.0
1.5
1.0
0.5
0.0
***
***
***
***
***
ctrl
(Ecto)
Rnd1
Shi
J
%
Adhesion on FN
100
80
60
40
20
0
% adherent cells
NS
NS
ctrl
(Ecto)
Rnd1
Shi
K
%
Adhesion on Cad-Fc
100
80
60
40
20
0
% adherent cells
NS
**
ctrl
(Ecto)
Rnd1
Shi

Figure 2.6

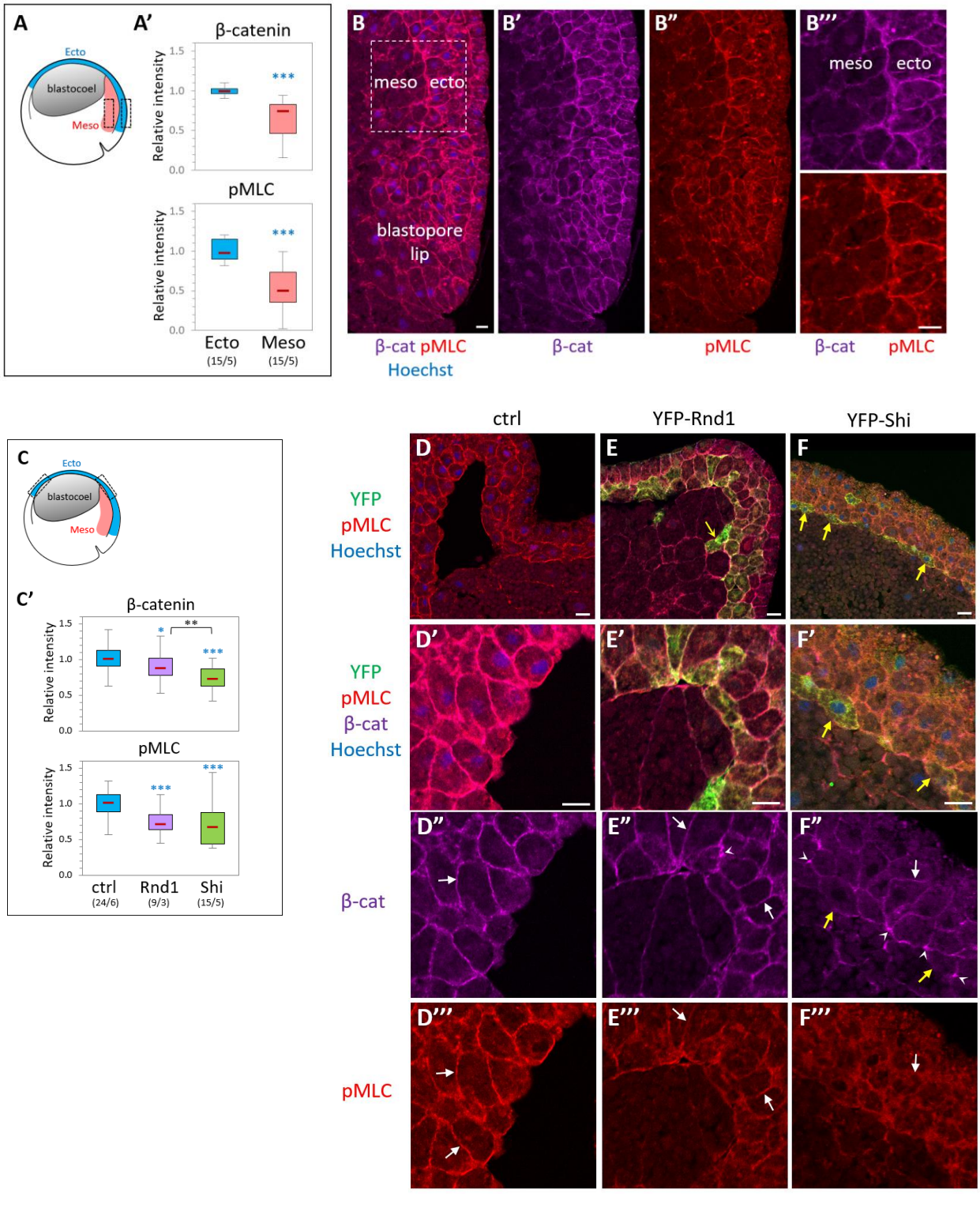
A
A'
Ecto
blastocoel
Meso
β-catenin
Relative intensity
1.5
1.0
0.5
0.0
***
pMLC
Ecto
(15/5)
Meso
(15/5)
B
meso ecto
blastopore lip
B'
B''
B'''
β-cat pMLC
Hoechst
β-cat
pMLC
β-cat
pMLC
C
C'
*
**
ctrl
(24/6)
Rnd1
(9/3)
Shi
(15/5)
ctrl
YFP-Rnd1
YFP-Shi
YFP
pMLC
Hoechst
D
E
F
D'
E'
F'
YFP
pMLC
β-cat
Hoechst
β-cat
D''
E''
F''
pMLC
D'''
E'''
F'''

Figure 2.7

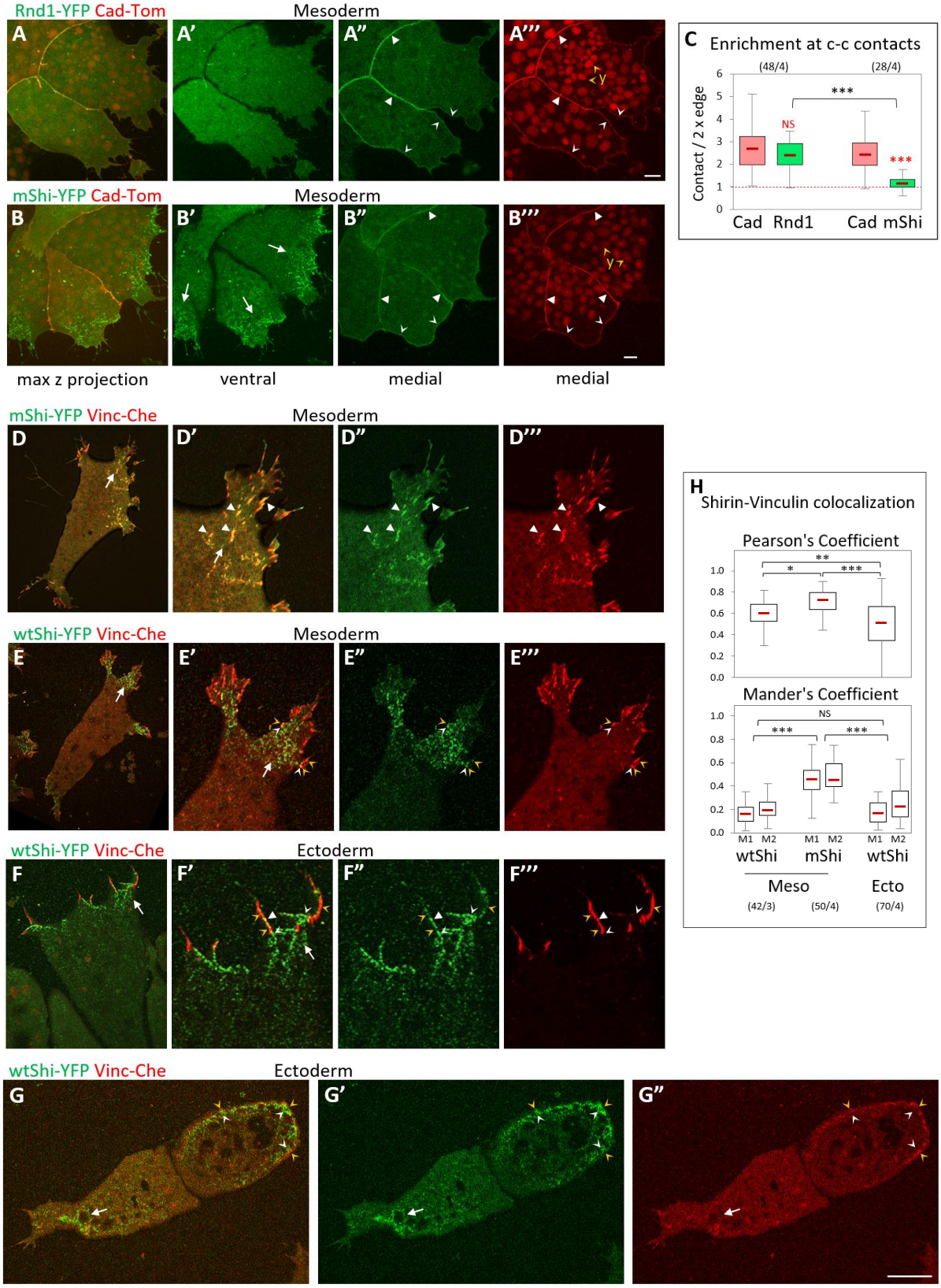
Rnd1-YFP Cad-Tom
Mesoderm
A
A'
A''
A'''
mShi-YFP Cad-Tom
Mesoderm
B
B'
B''
B'''
max z projection
ventral
medial
medial
C
Enrichment at c-c contacts
(48/4)
(28/4)
***
NS
***
Contact / 2 x edge
Cad
Rnd1
Cad
mShi
mShi-YFP Vinc-Che
Mesoderm
D
D'
D''
D'''
wtShi-YFP Vinc-Che
Mesoderm
E
E'
E''
E'''
wtShi-YFP Vinc-Che
Ectoderm
F
F'
F''
F'''
H
Shirin-Vinculin colocalization
Pearson's Coefficient
Mander's Coefficient
NS
wtShi
mShi
wtShi
Meso
Ecto
(42/3)
(50/4)
(70/4)
wtShi-YFP Vinc-Che
Ectoderm
G
G'
G''

Figure 2.8

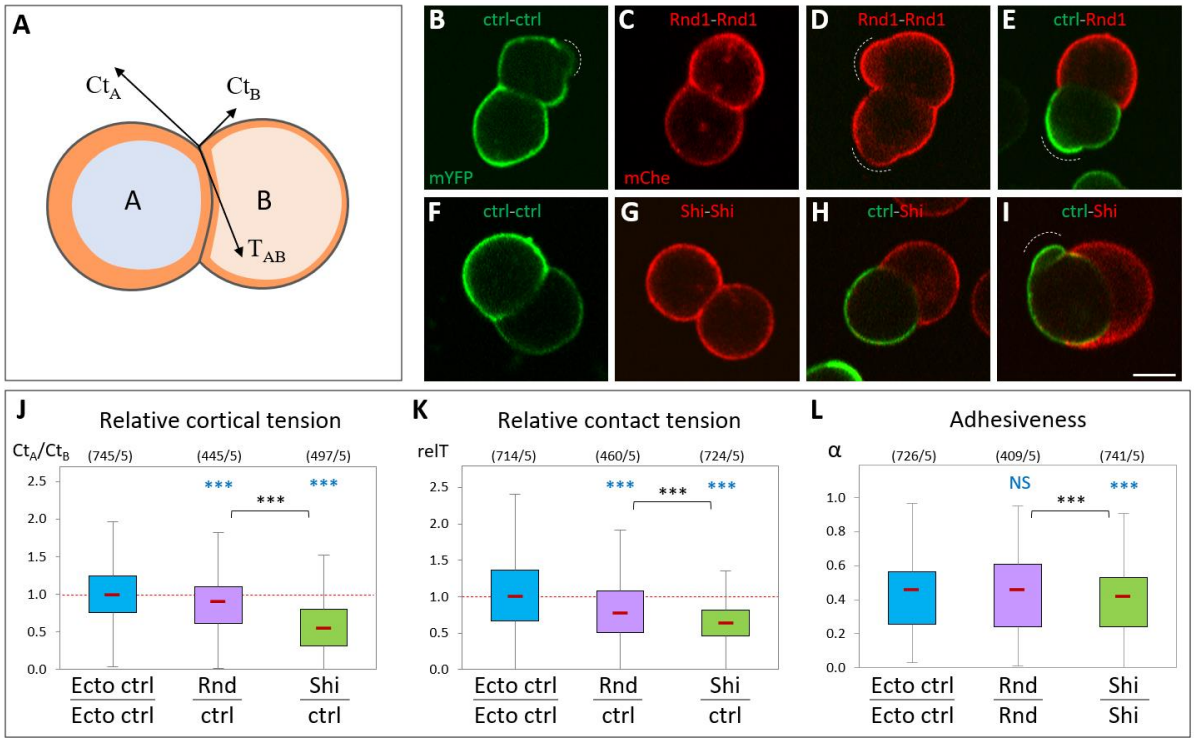
A
Ct_A
Ct_B
A
B
T_{AB}
B ctrl-ctrl
mYFP
C Rnd1-Rnd1
mChe
D Rnd1-Rnd1
E ctrl-Rnd1
F ctrl-ctrl
G Shi-Shi
H ctrl-Shi
I ctrl-Shi
J
Relative cortical tension
Ct_A/Ct_B
(745/5)
(445/5)
(497/5)
***
***
***
2.5
2.0
1.5
1.0
0.5
0.0
Ecto ctrl / Ecto ctrl
Rnd / ctrl
Shi / ctrl
K
Relative contact tension
relT
(714/5)
(460/5)
(724/5)
***
***
***
2.5
2.0
1.5
1.0
0.5
0.0
Ecto ctrl / Ecto ctrl
Rnd / ctrl
Shi / ctrl
L
Adhesiveness
α
(726/5)
(409/5)
(741/5)
NS
***
***
1.0
0.8
0.6
0.4
0.2
0.0
Ecto ctrl / Ecto ctrl
Rnd / Rnd
Shi / Shi

Figure 2.9

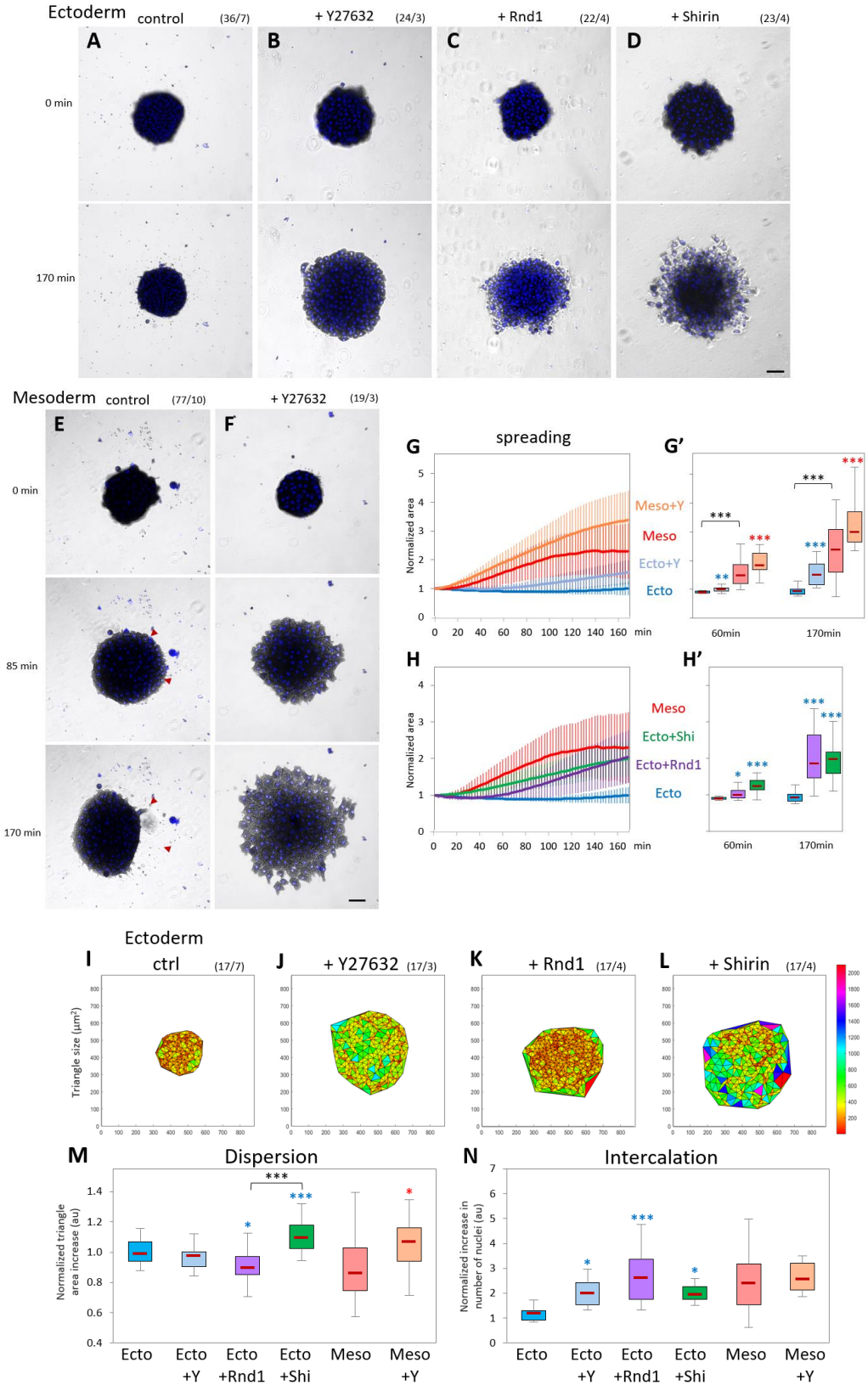
Ectoderm
control (36/7)
+ Y27632 (24/3)
+ Rnd1 (22/4)
+ Shirin (23/4)
A
B
C
D
0 min
170 min
Mesoderm
control (77/10)
+ Y27632 (19/3)
E
F
0 min
85 min
170 min
G
spreading
G'
Meso+Y
Meso
Ecto+Y
Ecto
Normalized area
0 20 40 60 80 100 120 140 160 min
60min
170min
H
H'
Meso
Ecto+Shi
Ecto+Rnd1
Ecto
Ectoderm
I
ctrl (17/7)
J
+ Y27632 (17/3)
K
+ Rnd1 (17/4)
L
+ Shirin (17/4)
Triangle size (µm²)
M
Dispersion
Normalized triangle area increase (au)
Ecto
Ecto +Y
Ecto +Rnd1
Ecto +Shi
Meso
Meso +Y
N
Intercalation
Normalized increase in number of nuclei (au)

Figure 2.10

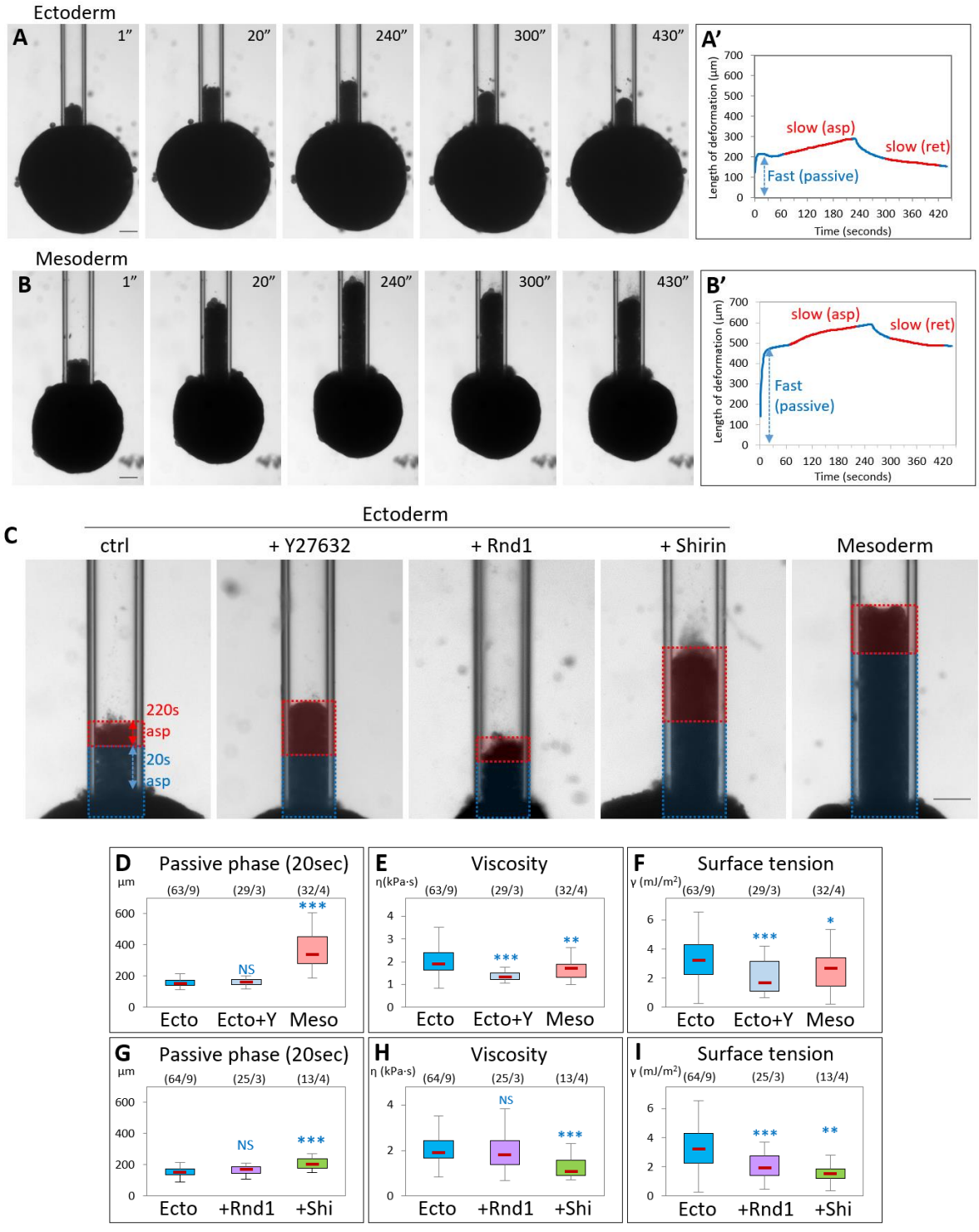
Ectoderm
A
1″
20″
240″
300″
430″
A′
Length of deformation (µm)
slow (asp)
slow (ret)
Fast (passive)
Time (seconds)
Mesoderm
B
B′
Fast
(passive)
C
Ectoderm
ctrl
+ Y27632
+ Rnd1
+ Shirin
Mesoderm
220s
asp
20s
asp
D
Passive phase (20sec)
µm
(63/9)
(29/3)
(32/4)
NS
Ecto
Ecto+Y
Meso
E
Viscosity
η(kPa·s)
F
Surface tension
γ (mJ/m²)
G
(64/9)
(25/3)
(13/4)
+Rnd1
+Shi
H
η (kPa·s)
I

Figure legends

Figure 2.1 – Distinct properties of ectoderm and mesoderm at the cellular level

A-E) Organization of cell-matrix adhesive structures. Dissociated Xenopus ectoderm (A,C) and mesoderm (B,D) cells expressing vinculin-Cherry (Vin-Che) and membrane-targeted YFP (mYFP) were plated on fibronectin (FN), either as single cells (A,B) or as small groups (C,D) and imaged live by spinning disc confocal microscopy. y: autofluorescence of yolk platelets. Ventral: ventral z plane close to the glass. max p: Maximal z projection.

A) Ectoderm cells do not spread on FN, but adhere to it through a characteristic adhesive ring (A,A', filled arrowheads). They typically form blebs that are continuously pushed around the cell (dashed line with arrow). Right inserts: Orthogonal view (orth) showing the cross-section of the membrane and of the vinculin ring (filled arrowheads). The dashed line underlines the bottom of the bleb.

B) Mesoderm cells spread on FN, and extend multiple lamellipodia. They transiently polarize during their migration, with one protrusion becoming the tail (t), see also time lapse Figure S2.1. They form vinculin-positive focal adhesions (FAs, filled arrowheads), generally oriented in the direction of the protrusions (arrows).

C) Ectoderm cells form compact groups, with few protrusions in the center, and numerous blebs at the periphery (dashed lines). External cells emit protrusions under the more central cells (yellow arrows). Individual cells build partial adhesive structures (filled arrowheads), which together form an supra-cellular ring.

D) Mesoderm cells form looser groups, each cell emitting multiple lamellipodia, most of them extending outwards (white and yellow arrows indicate peripheral and internal lamellipodia, respectively), with numerous focal adhesions oriented radially (arrowheads). Panel D' is an enlargement of the boxed portion of panel D). Scale bars: A,C,D 10µm; B 20µm; D' 5µm.

E) Quantification of vinculin accumulation at FAs of isolated cells, expressed as Vinc-Che fluorescence concentrated in clusters divided by the total fluorescence along the ventral cortex. A colour code is used throughout the figures, including blue for control ectoderm and red for control mesoderm. The box plots show the interquartile range (box limits), median (centre line

and corresponding value), and min and max values without outliers (whiskers). Statistical comparison using two-sided Student's *t*-test. For all experiments presented in this study, p values are indicated as follows: *P < 0.05, **P < 0.01, ***P < 0.001, NS not significant. The same colour code is also used to indicate statistical comparison between one condition and control ectoderm (blue) or control mesoderm (red). Other comparisons are indicated by black asterisks and brackets. The numbers in parentheses correspond to the number of cells/ number of experiments.

F) Single cell motility. Frames of spinning disc confocal time lapse movies. Cells expressed paxillin fused to YFP (Pax-YFP) and membrane Cherry. F) Ectoderm cells are immobile, anchored by their stationary adhesive ring (arrowheads) and bleb (star). Scale bars: F 5µm; F' 20µm. F') Mesoderm cells actively migrate, rapidly remodelling protrusions and FAs (red-yellow-green colour-coded arrows and arrowheads indicate successive positions respectively of one extending lamellipodium and the retracting tail). White arrowheads: FAs at thin protrusions.

G) Quantification of single cell migration.

H) Adhesion assay. Dissociated cells were plated on the adherent substrate, either FN or recombinant cadherin-Fc fusion protein, then subjected to rotation. Adhesion is expressed as the percentage of cells remaining adherent after rotation (see Materials and Methods). The column plots show averages and standard deviation of 15 experiments, total ~5000 cells/conditions. Statistical comparison on the % adherent cells/experiment, pairwise two-sided Student's *t*-test.

Figure 2.2 – Inhibition of Rock confers ectoderm cells with mesoderm-like properties

A-C) Induction of cell spreading and migration by Rock inhibition.

A-D) Confocal imaging of initiation of spreading and migration for single cells (A,B) and a small group of cells (C). Rock inhibitors, Y27632 (50µM) and H1125 (1µM) were added at time = 0'. Note that the onset of the transition is not synchronous. Arrows: Nascent protrusions; Filled arrowheads: ring-like adhesion; Concave arrowheads: FAs. Scale bars: 10µm.

D) Shift in cell morphology. Cells were classified in morphological subtypes: Round and blebbing (b), round without blebs (r), polarized (p) and spread (s). In wild type conditions, round cells are typically immotile, while polarized and spread cells migrate. A fifth category, named polarized

with bleb (pb), includes cells with irregular morphology and blebs. The diagram shows the distribution of wild type mesoderm and ectoderm cells, as well as of ectoderm cells treated for 50min with 10µM or 50µM Y27632 (Y10, Y50) or 1µM H1125 (H). For b and s categories, conditions were compared to control ectoderm by one-way ANOVA followed by Tukey's HSD post hoc test.

E) Migration speed of Rock-inhibited cells. Quantification as in Figure 2.1. Comparison to ectoderm control by one-way ANOVA followed by Tukey's HSD post hoc test.

Figure 2.3 – Rnd1 and Shirin are essential for gastrulation. A) Rnd1 and Shirin expressions are enriched in the mesoderm. RT-qPCR from dissected tissue. mRNA levels in ectoderm and mesoderm, normalized to homogenously expressed ODC. 3 to 6 experiments, pairwise one-sided Student's *t*-test. **B-E) Whole embryo loss-of-function phenotypes**: 4-cell stage embryos were injected in the dorsal side (d) with a control (COMO), Rnd1 (RndMO) or Shirin (ShiMO) morpholinos. Embryos were fixed and imaged at stage 11. B-D) Examples of typical control mesoderm, and RndMO and ShiMO phenotypes. E) Example of a "partial" phenotype (here ShiMO). B-E) External views from the vegetal pole. Red arrows point to the position of the dorsal blastopore lip of a control embryo, absent in RndMO (C) and ShiMO (D) embryos. E) In the partial phenotype, the lip is present but the blastopore has remained widely open compared to control. In many embryos the ventral blastopore is also affected, due to the diffusion of the morpholinos to the ventral blastomeres before complete separation after the 2nd cleavage. B'-E') Sagittally bisected embryos. In a control embryo (B'), the extent of involution (dashed black arrow) can be seen by the position of the tip of the mesendoderm (white arrow) that has moved far away from the blastopore lip (red arrow). C') RndMO embryo lacking any sign of involution. The white arrowhead points to the dorsal edge of the blastocoel cavity (bl), resembling that of a pregastrula embryo. D') Characteristic ShiMO phenotype, with flat blastocoel floor (white arrow) and thicker non-involuted dorsal marginal zone (black arrowheads), both indicative of failed involution. E') Partial involution (white arrow). Yellow arrowheads: thin blastocoel roof, indicative of ectoderm epiboly in all conditions. Scale bars: 200µm. F and F') Score of the penetrance of the gastrulation

external and internal phenotype: N, normal embryo; P, partial inhibition, C, complete inhibition. Comparison by one-way ANOVA followed by Tukey's HSD post hoc test.

Figure 2.4 – Rnd1 and Shirin are essential for mesoderm spreading and migration

A-E) Loss-of-function cellular phenotypes.

A-C) Examples of control morpholino (COMO), RndMO and ShiMO mesoderm cells, expressing Vin-Che and mYFP, plated on FN. A-C) Ventral z planes, merged channels; A'-C') vinculin alone; A"-C") Maximal z projections. A'''-C''') Schematic diagrams summarizing the general cell morphology and adhesive structures. Protrusions are indicated by arrows, FAs by concave arrowheads, vinculin ring by filled arrowheads. Dotted lines highlight the max lateral extension of the cell mass. A) Control spread mesoderm with large protrusions and numerous FAs. t, tail. B) Typical RndMO cell displaying a bulging body (B''', dotted lines) and a small ventral surface with diffuse vinculin (B''', pink line). C) Example of a bulky ShiMO cell with intermediate adhesive structures, including small FAs at short protrusions (arrows) and ectoderm-like partial ring encompassing most of the ventral surface (arrowheads). A bleb is visible in the max projection (C", dashed line). Y, yolk platelets. Scale bars 10µm.

D) RndMO and ShiMO cells show a significant shift in morphology from spread to round and blebbing cell. Comparison for either of the two categories with corresponding COMO (red asterisks), one-way ANOVA followed by Tukey's HSD post hoc test.

E) Both RndMO and ShiMO inhibit cell migration. Grey asterisks: Comparison with double injection RndMO + ShiMO, which significantly enhanced the migration phenotype. One-way ANOVA followed by Tukey's HSD post hoc test.

F) Quantification of vinculin accumulation. Comparison to COMO using pairwise two-sided Student's *t*-test. RndMO cells have little to no detectable vinculin-rich structures. ShiMO cells show high variability (see main text).

G,H) Inhibition of cell adhesion on FN and on cadherin substrates. 5 experiments, total 375-740 cells/conditions for FN, >1000 cells for cadherin. Statistical comparison on the % adherent cells/experiment, pairwise two-sided Student's *t*-test.

Figure 2.5 – Ectopic expression of Rnd1 or Shirin confers ectoderm with mesoderm-like morphological and migratory properties

A-G) Effect on cell morphology and vinculin distribution.

A-E) Examples of ectoderm cells co-expressing Vinc-Che and either mYFP (A, control ectoderm), Rnd1-YFP (B,C) or Shirin-YFP (Shi-YFP, D,E). A) Typical control ectoderm cell, with its distinctive vinculin ring (arrows) and blebs (dashed lines). B) Rnd1-expressing cells elongate, expand their ventral surface in contact with the substrate, but form only few vinculin-positive FA-like structures (arrows). C) High Rnd1 expression: The ventral surface is expanded, but lacks vinculin FAs. Cells are bulkier (contours highlighted by dotted lines), although blebs are absent. D) Shirin-expressing cells spread and form prominent lamellipodia with FAs (white arrows). The yellow arrow points the retracting tail. (E) High Shirin expression: Cells emit long and disorganized protrusions in all directions, but lack detectable FAs, and the cell body tends to round up (dotted lines). Y, yolk platelets. Scale bars: 10µm.

F) Quantification of vinculin accumulation. Consistent with the loss of the ring and the paucity of FAs, most of vinculin is homogeneously distributed on the ventral surface.

G) Distribution of morphological subtypes. Both Rnd1 and Shirin cause a strong shift toward spread cells. See Figure S2.5A for additional morphometric data.

H-I) Effect on cell migration and adhesion

H) Frames from time lapse movies. Examples of Rnd1 and Shirin-expressing ectoderm cells spreading and migrating. The cell in H" spreads extensively, ending with multiple protrusions (black arrowheads) and low motility. Scale bar: 20µm.

I) Quantification of cell migration, as in Figure 2.2. Different levels of Rnd1 and Shirin expression were tested (250 and 500pg mRNA for Rnd1, 75 and 150-300pg for Shirin). Rnd-expressing cells show higher migration than wild type or Shi-expressing cells. Statistical comparisons: One-way ANOVA followed by Tukey's HSD post hoc test.

J,K) Quantification of cell adhesion on FN and on cadherin. 4-5 experiments, >1000 cells per condition. Statistical comparison on the % adherent cells/experiment, pairwise one-sided Student's *t*-test.

Figure 2.6 – Effect of ectopic expression of Rnd1 and Shirin on cell adhesive structures and cortical myosin. β-catenin, used as general marker for cadherin-based cell adhesions, and pMLC were localized by immunofluorescence on cryosections of whole embryos at early gastrula stage. The fluorescence along the cell periphery, defined by the β-catenin signal, was quantified and expressed relative to the median intensity of control ectoderm. A,B) Comparison of β-catenin and pMLC levels in the dorsal ectoderm and dorsal prechordal mesoderm of normal embryos. A) Diagram of the embryo with boxes indicating the regions used for quantification. A') Quantification. Numbers into brackets: Number of embryos/number of experiments. Statistical comparison to ectoderm using two-sided Student's *t*-test. B) Example of dorsal region, immunolabelled for β-catenin (magenta) and pMLC (red). Nuclei were counterstained with Hoechst. B''') Enlarged view of the region used for quantification. C-G) Effect of Rnd1 and Shirin ectopic expression in the ectoderm. C) Diagram indicating the regions of the ectoderm used for quantification. For consistency, all analyses were performed on the upper lateral region (both dorsal and ventral, indicated by dashed boxes in the diagram, because it constitutes a robust landmark where the inner ectoderm layer has a stereotyped organization. C') Quantification. Statistical comparison using two sided, pairwise Student's *t*-test. D-G) Examples of control (D), YFP-Rnd1-expressing (E), and YFP-Shirin-expressing (F) ectoderm, immunolabelled for the YFP-tag (green), β-catenin (far red, coloured in magenta) and pMLC (red). Top panels present general views, the other panels show enlarged portions of the inner ectoderm layer used for quantification. Note that the strong bending of the ectoderm layer is due to the partial collapse of the blastocoel cavity during fixation. White arrows point to plasma membranes marked by β-catenin (D',E',F') and to the corresponding pMLC signal (D",E",F"). Little to no pMLC enrichment is observed in Shirin-expressing cells (F"). Arrowheads in E' and F' point to concentrations of β-catenin, particularly frequent in Shirin-expressing ectoderm, and which contrast with the low membrane signal (arrow). Yellow arrow in E: Rnd1-expressing ectoderm cells that have penetrated into the mesoderm layer. Yellow arrows in F: Ectoderm cells expressing particularly high levels of YFP-Shirin.

Figure 2.7 – Differential subcellular distribution of Rnd1 and Shirin

A-B) General distribution of Rnd1 and Shirin in mesoderm cells. A,B) Live confocal microscope images of groups of mesoderm cells co-expressing cadherin-dTomato (Cad-Tom) and either Rnd1-YFP or GAP-deficient mutant ShirinR488A-YFP (mShi-YFP). Both Rnd1 and mShi localized to the cell cortex (concave arrowheads). On the ventral side, mShi was concentrated at protrusions (B', arrows, see D-H), while Rnd1 was always homogenously distributed (example in A'). Rnd1, but not mShi, is concentrated at cell-cell contacts (filled arrowheads). Y, yolk platelets.

C) Quantification of Rnd1 and Shirin at cell-cell contacts, expressed as ratio of the signal intensity at cell-cell contacts divided by twice the signal along free cell edges. Rnd1 is enriched more than two fold at contacts, similar to cadherin. mShi is distributed homogenously along the cell periphery. Comparison Rnd1/mShi to cadherin (red), or mShi to Rnd1 (black) using two-sided Student's *t*-test.

D-H) Shirin localization at the ventral surface. D,E) Ventral surface of mesoderm cells co-expressing either mShi (D) or wild type Shirin (wtShi, E) together with Vinc-Che. D,E) General view; D'-D''', E'-E''') enlargements of protrusions. mShi extensively colocalises with vinculin at FAs (white arrowheads). E) wtShi clusters are present throughout the ventral side of protrusions (arrow). Vinculin-positive FAs are largely confined to the periphery, only partially overlapping with wtShi clusters (orange arrowheads for vinculin, white concave arrowheads for wtShi). F,G) Ectopic wtShi in ectoderm cells. F) Detail of a protrusion of a fully spread cell. Similar to mesoderm, the centre of the protrusion is occupied by clusters of wtShi and devoid of FAs (arrow). Small FAs are located at the periphery, close to Shirin clusters (orange and white concave arrowheads), but rarely colocalizing (white filled arrowhead). G) Incompletely spread wtShi-expressing ectoderm cells. The left cell has lost its vinculin ring, and a wtShi-enriched protrusion is forming (arrow). The right cell still shows a weak ring lined in the inside by wtShi clusters (orange and white concave arrowheads). Scale bars: 10µm. H) Quantification of Shirin and Vinculin co-localization, expressed by the general Pearson,s coefficient, as well as by Mander's coefficients, which indicates the portion of Shirin that overlap with Vinculin (M1) and the converse portion of Vinculin that overlap with Shirin (M2). Statistical comparison using one-way ANOVA followed by Tukey's HSD post hoc test.

Figure 2.8 – Ectopic expression of Rnd1 or Shirin modulates ectoderm cortical tension and adhesiveness.

A) Diagram of an asymmetrical cell doublet, representing the balance between cortical tensions at free edges Ct_A, Ct_B and contact tension T_{AB}. The orange layer symbolises the actomyosin cortex. The curved cell–cell interface reflects unequal Ct_A and Ct_B tensions.

B-I) Examples of homotypic and heterotypic doublets, imaged by live confocal microscopy. Doublets were made by combining dissociated control ectoderm expressing mYFP (ctrl) and either Rnd1 or Shirin-expressing cells markerd with mCherry. Wild type and Rnd1-expressing cells often displayed blebs (dashed lines). Curved interfaces indicative of tensile differences were observed for all combinations, including for homotypic doublets (e.g. panel F), but were most systematically found for heterotypic ctrl-Shirin doublets (H,I). Scale bar: 20µm.

J-L) Relative tension measurements based on the geometry at cell vertices (see S1 Appendix). J) Relative cortical tension between Rnd1 or Shirin-expressing cells and control ectoderm cells calculated from the ratio Ct_A/Ct_B of heterotypic doublets. The ratio for control homotypic doublets is provided for comparison. See S1 appendix for complete measurements. Vertices flanked by a bleb (D and I) were omitted from calculations. K) Relative strength of contact tension T_{AB} at homotypic contacts, compared to control ectoderm-ectoderm T, the median of which was set arbitrarily at 1. See S1 appendix for more details. L) Relative adhesiveness α, calculated for homotypic doublets. Numbers in brackets: vertices/experiments. Statistical comparison using one-way ANOVA followed by Tukey's HSD post hoc test.

Figure 2.9 – Rho/Rock regulation affects collective migration of ectoderm and mesoderm tissue explants.

Tissue explants were laid on FN and their spreading was imaged for 170 minutes.

A-D) Control ectoderm, ectoderm treated with 50µM Y27632, and ectoderm expressing Rnd1 or Shirin. Numbers in brackets are number of explants and number of experiments. Scale bar: 100µm.

E,F) Control mesoderm and mesoderm treated with Y27632. Red arrowheads in E indicate areas of large-scale retractions (compare 85 and 170min). Scale bar: 100µm.

G,H) Quantification of explant spreading. After segmentation, the area was calculated for the time course and normalized to the first time point. Traces show average time course curves with SD for the various experimental conditions. G',H') Corresponding relative spreading after 60min and 170min, chosen to represent an intermediate and advanced stage of the spreading process .Statistical analysis, one-way ANOVA followed by Tukey's HSD post hoc test.

I-M) Delaunay triangulation of nuclei and quantification of cell dispersion. I-L) Representative maps of triangulated nuclei after 170 minutes of imaging. X and Y labels mark the coordinates in µm, the colour coded scale bar indicates the area of the triangles in μm^2. M) Quantification of the relative change in triangle size over time calculated by dividing the average triangle area at 170 minutes by that at 30 minutes. The 30 minutes time point was chosen as it corresponds to the stage when explant had adhered to the substrate and started to spread. N) Quantification of intercalation calculated by dividing number of nuclei at the ventral surface at 170 minutes by the number at 30 minutes. Statistical comparisons: One-way ANOVA followed by Tukey's HSD post hoc test.

Figure 2.10 – ROCK inhibition and Rho regulators modulate tissue stiffness, viscosity and surface tension.

Micropipette aspiration was used to measure physical properties of tissue explants. Explants were aspirated into the pipette at constant pressure, then pressure was reset to zero to let the explant retract.

A,B) Examples of aspiration and retraction of control ectoderm and mesoderm explants. Aspiration pressure was 250 Pa. Pressure was released after 240 sec. Scale bars: 100µm.A',B') Corresponding aspiration and release profiles. The blue double arrows indicate the extent of deformation of the tissue during the first 20 seconds, defined as the fast "passive" phase. The two slow, linear phases of aspiration and release, highlighted in red, were used to calculate viscosity and tissue surface tension. Scale bars: 100µm.

C) Examples of aspiration of control ectoderm, ectoderm treated with Y27632, or expressing Rnd1 or Shirin, and control mesoderm. Pressure was 250Pa. Images display the frame corresponding to the deformation 220 seconds after the initiation of aspiration. The colored

overlays indicate the distances of deformation during the first fast phase (20s, blue) and during the subsequent slow phase (220 s, red). Scale bar: 100µm.

D-I) Calculated parameters: D,G) Length of deformation 20 seconds after initiation of aspiration, encompassing the initial passive phase. E,H) Tissue viscosity calculated from the rates of aspiration and retraction (see Material and Methods). (F,I) Tissue surface tension. Numbers in brackets are number of explants and number of experiments. Statistical comparisons: One-way ANOVA followed by Tukey's HSD post hoc test.

Supporting information

S2.1 Table

List of mRNA used in this study with injected amounts

Plasmid	mRNA injected per blastomere at 2 cell stage (pg)
mCherry (membrane-targeted YFP)	50-250
mYFP (membrane-targeted YFP)	50-250
C-cadherin-dTomato	1000
Vinculin-Cherry	125-250
Paxillin-YFP	250
Myosin light chain (MLC)-Cherry	500
Non-muscle myosin heavy chain 2A (NMHC2A)-YFP	1000
Non-muscle myosin heavy chain 2B (NMHC2B)-YFP	1000
Rnd1-YFP	125-500
Shirin-YFP	75-300
ShirinR488A-YFP	75

S2.2 Table.

List of morpholinos with injected amounts

Target	Sequence	Amount/injected blastomore
C-cadherin	CCACCGTCCCGAACGAAGCCTCAT	40ng
Rnd1a Rnd1b	AGTACGGTGGGACAAATCCAACAAC ACAAGTCCTAATTAAAAGCTCCACG	20ng+ 20ng
ShirinS2a ShirinS2b	CTGGCCTCCCATTTTCCCAGAAGGT GCCTCCCATTTTCCCAGAGACACGA	20ng+ 20ng

Supplemental Figures

Figure S2.1

A

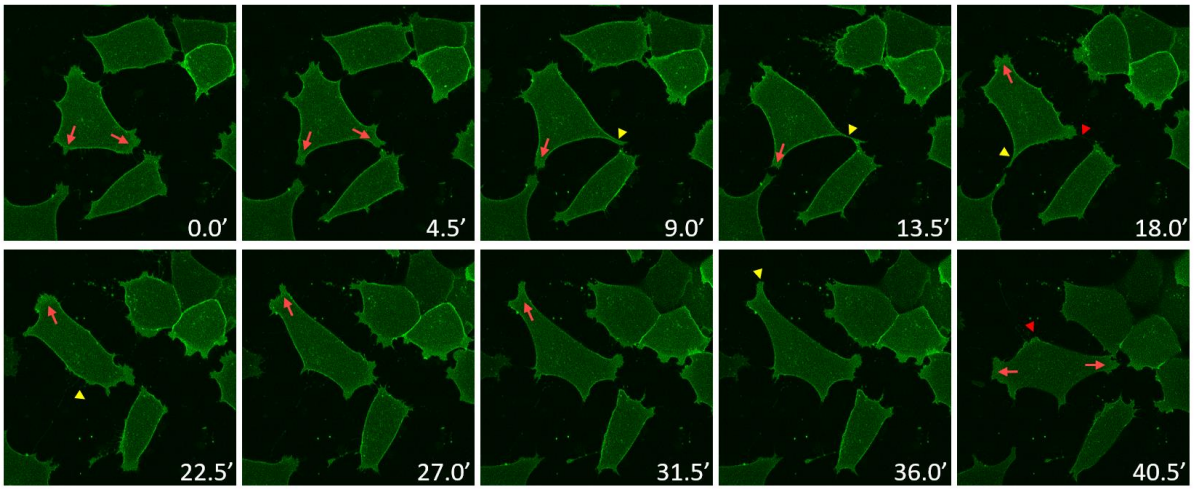

B

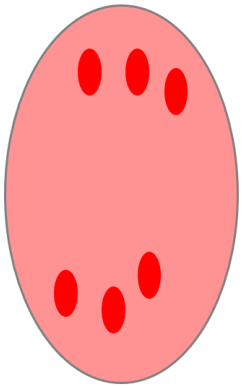

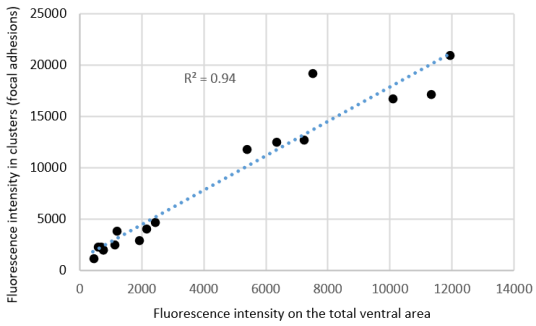

Figure S2.2

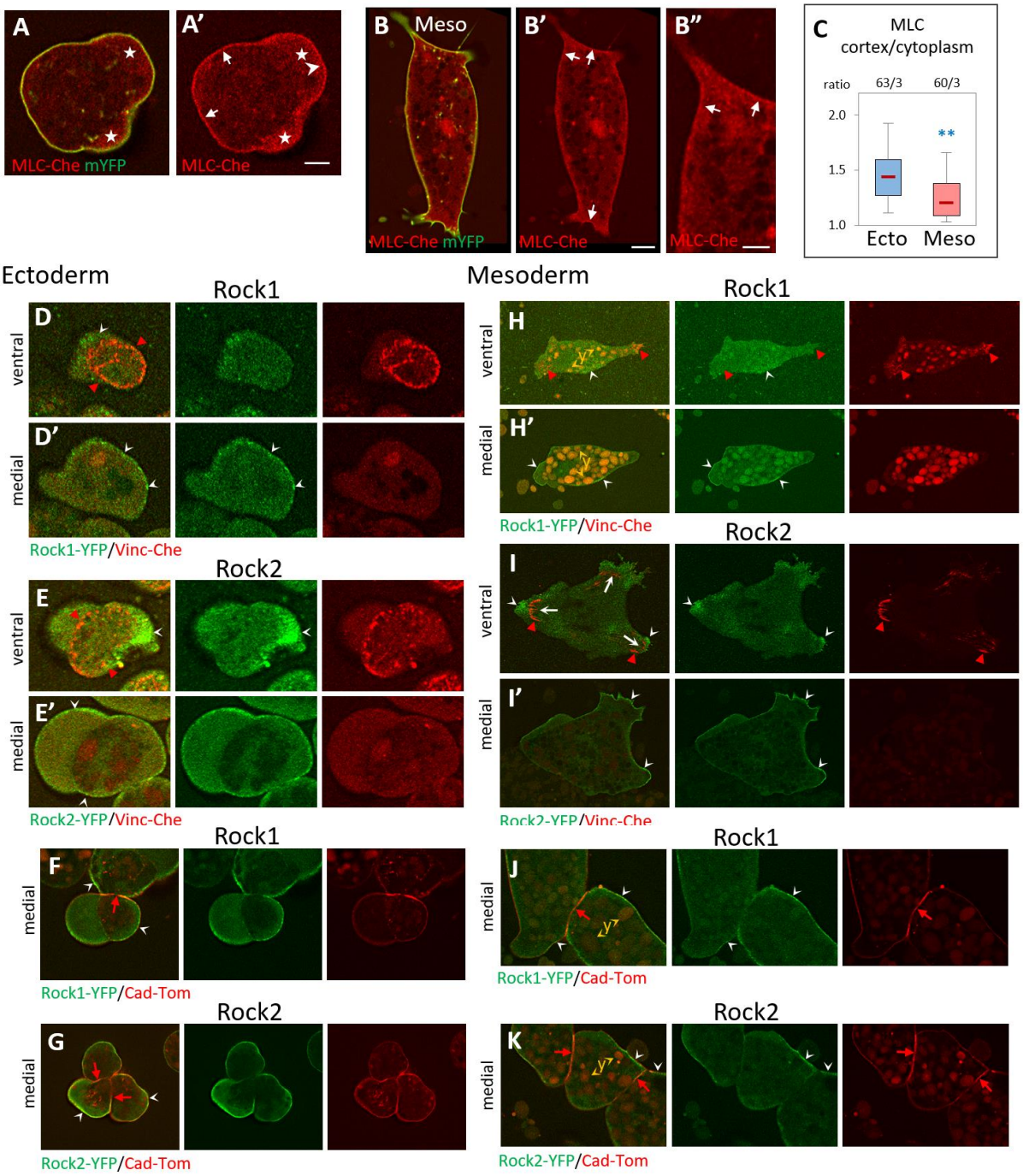
A
MLC-Che mYFP
A'
MLC-Che
B
Meso
MLC-Che mYFP
B'
MLC-Che
B"
MLC-Che
C
MLC
cortex/cytoplasm
ratio
63/3
60/3
2.0
1.5
1.0
**
Ecto
Meso
Ectoderm
Rock1
ventral
D
medial
D'
Rock1-YFP/Vinc-Che
Rock2
ventral
E
medial
E'
Rock2-YFP/Vinc-Che
Rock1
medial
F
Rock1-YFP/Cad-Tom
Rock2
medial
G
Rock2-YFP/Cad-Tom
Mesoderm
Rock1
ventral
H
medial
H'
Rock1-YFP/Vinc-Che
Rock2
ventral
I
medial
I'
Rock2-YFP/Vinc-Che
Rock1
medial
J
Rock1-YFP/Cad-Tom
Rock2
medial
K
Rock2-YFP/Cad-Tom

Figure S2.3

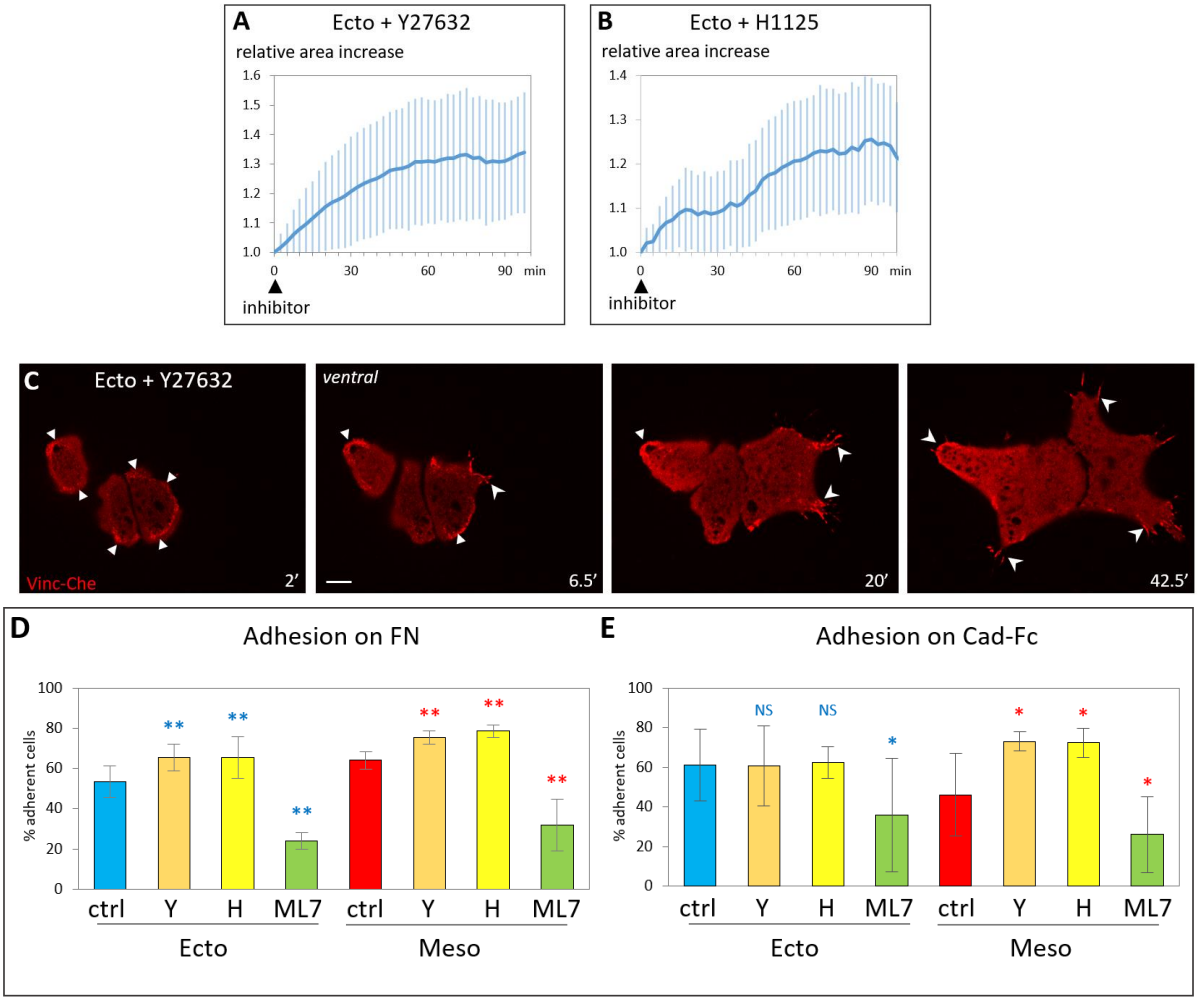
A
Ecto + Y27632
relative area increase
1.6
1.5
1.4
1.3
1.2
1.1
1.0
0
30
60
90 min
inhibitor
B
Ecto + H1125
relative area increase
1.4
1.3
1.2
1.1
1.0
0
30
60
90 min
inhibitor
C
Ecto + Y27632
Vinc-Che
2'
ventral
6.5'
20'
42.5'
D
Adhesion on FN
% adherent cells
100
80
60
40
20
0
**
**
**
**
**
**
ctrl
Y
H
ML7
ctrl
Y
H
ML7
Ecto
Meso
E
Adhesion on Cad-Fc
% adherent cells
100
80
60
40
20
0
NS
NS
*
*
*
*
ctrl
Y
H
ML7
ctrl
Y
H
ML7
Ecto
Meso

Figure S2.4

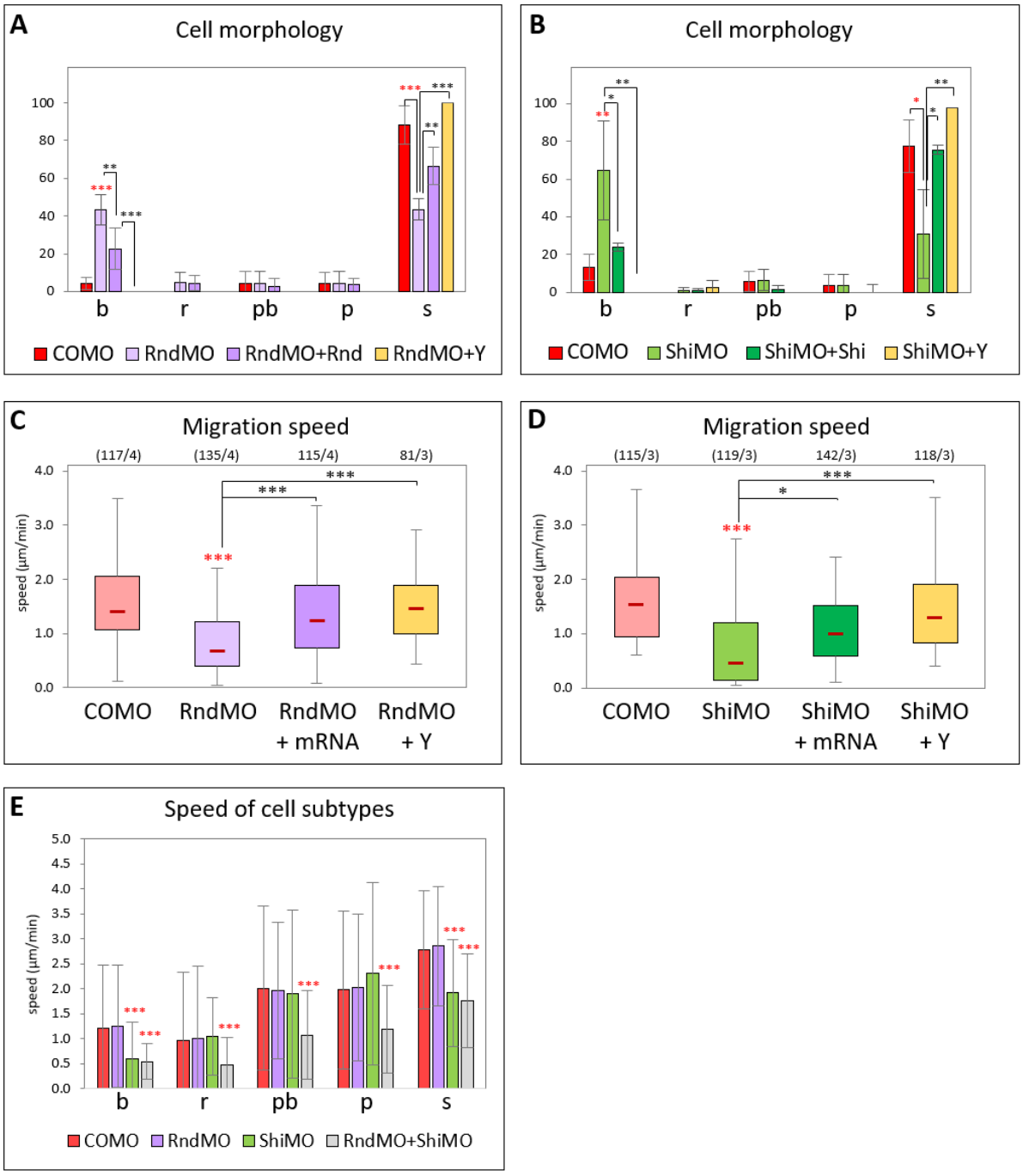
A
Cell morphology
b
r
pb
p
s
COMO
RndMO
RndMO+Rnd
RndMO+Y
B
Cell morphology
b
r
pb
p
s
COMO
ShiMO
ShiMO+Shi
ShiMO+Y
C
Migration speed
(117/4)
(135/4)
115/4)
81/3)
speed (µm/min)
COMO
RndMO
RndMO + mRNA
RndMO + Y
D
Migration speed
(115/3)
(119/3)
142/3)
118/3)
speed (µm/min)
COMO
ShiMO
ShiMO + mRNA
ShiMO + Y
E
Speed of cell subtypes
speed (µm/min)
b
r
pb
p
s
COMO
RndMO
ShiMO
RndMO+ShiMO

Figure S2.5

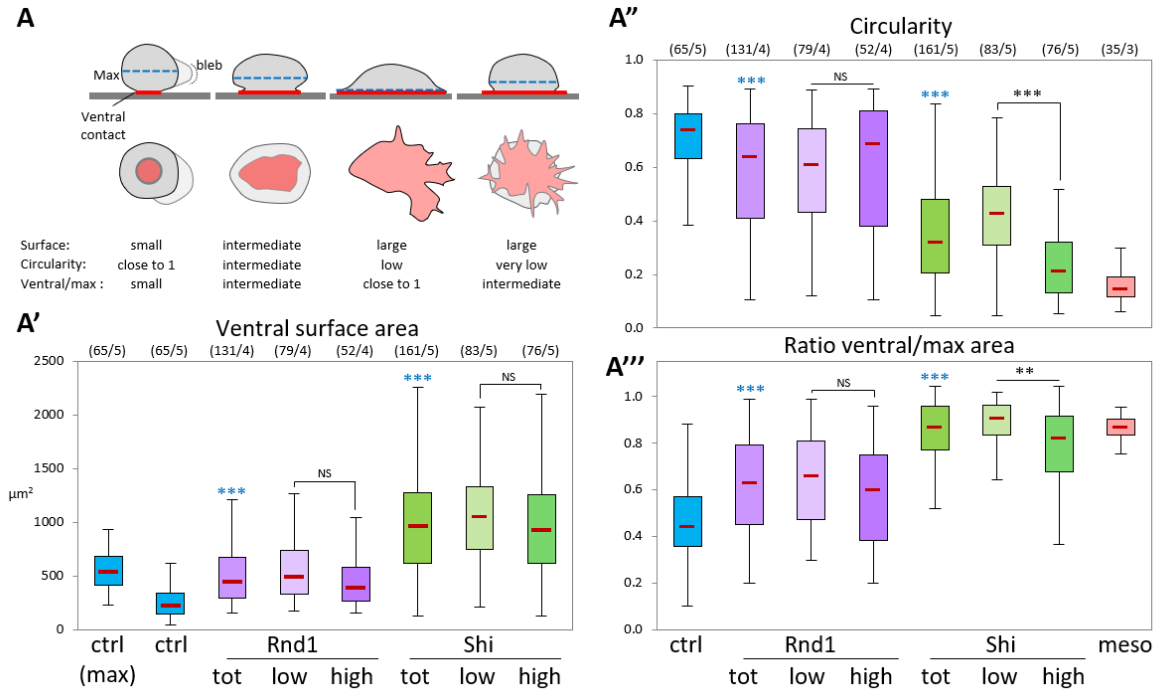
A
Max
bleb
Ventral contact
Surface: small intermediate large large
Circularity: close to 1 intermediate low very low
Ventral/max : small intermediate close to 1 intermediate
A'
Ventral surface area
(65/5) (65/5) (131/4) (79/4) (52/4) (161/5) (83/5) (76/5)
µm²
ctrl ctrl Rnd1 Shi
(max) tot low high tot low high
A''
Circularity
(65/5) (131/4) (79/4) (52/4) (161/5) (83/5) (76/5) (35/3)
A'''
Ratio ventral/max area
ctrl Rnd1 Shi meso
tot low high tot low high

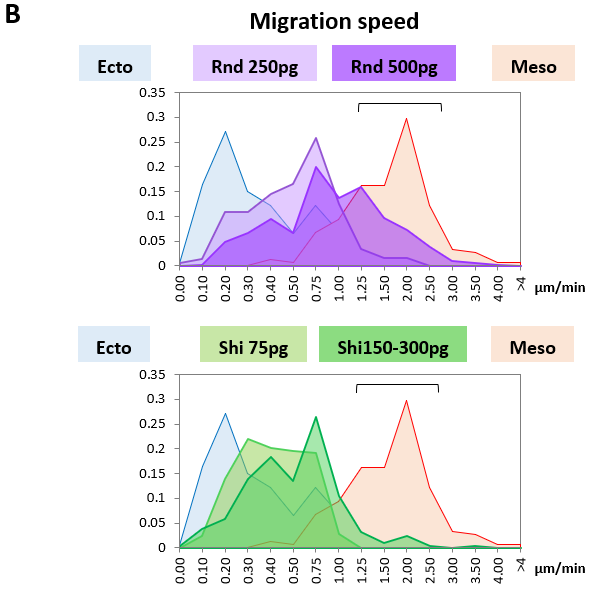
B
Migration speed
Ecto
Rnd 250pg
Rnd 500pg
Meso
µm/min
Ecto
Shi 75pg
Shi150-300pg
Meso
µm/min

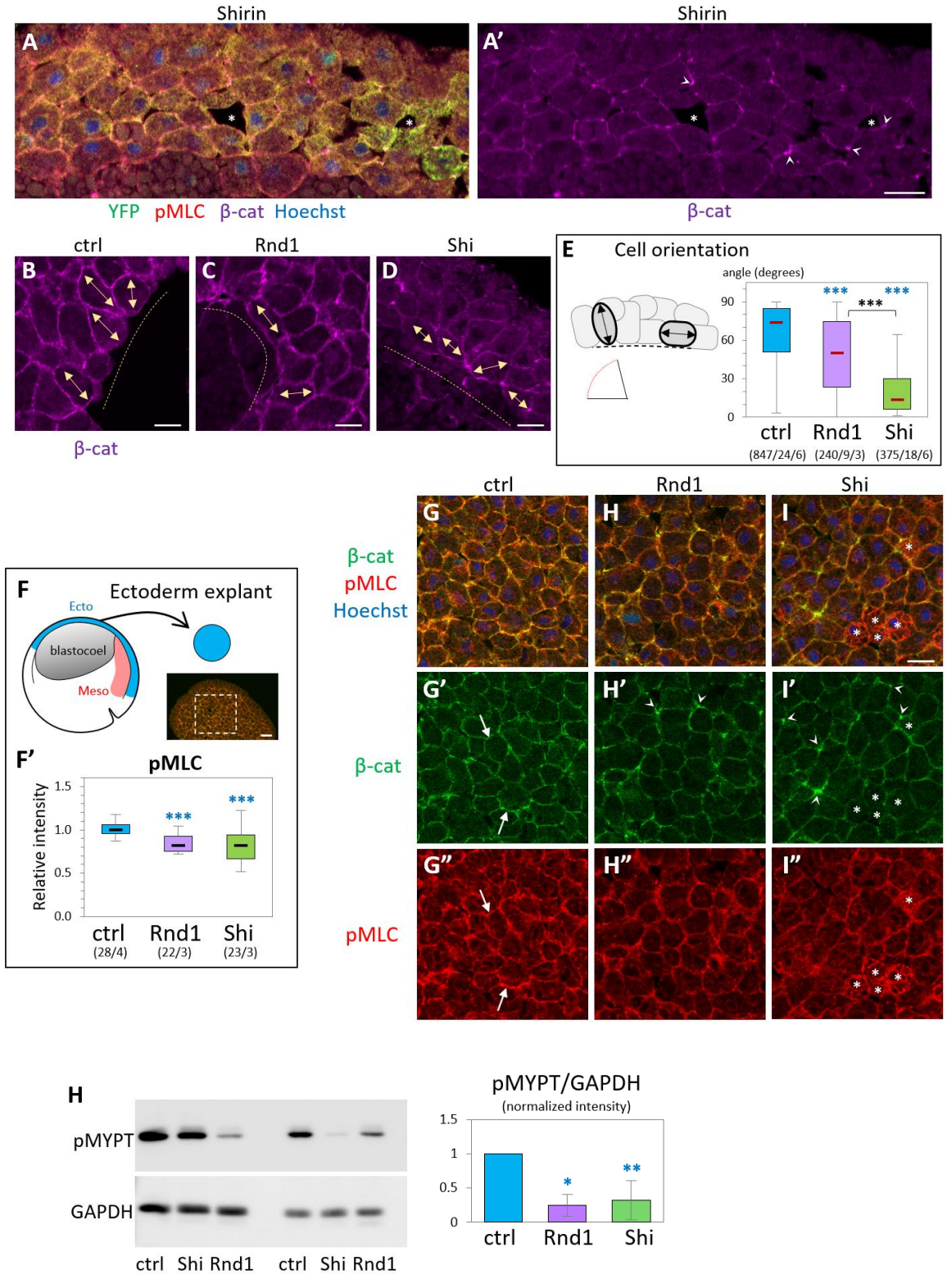
Shirin
A
A'
Shirin
YFP pMLC β-cat Hoechst
β-cat
ctrl
Rnd1
Shi
B
C
D
β-cat
E
Cell orientation
angle (degrees)
90
60
30
0
***
***
***
ctrl
Rnd1
Shi
(847/24/6)
(240/9/3)
(375/18/6)
F
Ectoderm explant
Ecto
blastocoel
Meso
F'
pMLC
Relative intensity
1.5
1.0
0.5
0.0
***
***
ctrl
Rnd1
Shi
(28/4)
(22/3)
(23/3)
ctrl
Rnd1
Shi
β-cat
pMLC
Hoechst
G
H
I
G'
H'
I'
β-cat
G"
H"
I"
pMLC
H
pMYPT
GAPDH
ctrl Shi Rnd1 ctrl Shi Rnd1
pMYPT/GAPDH
(normalized intensity)
1.5
1
0.5
0
*
**
ctrl
Rnd1
Shi

Figure S2.7

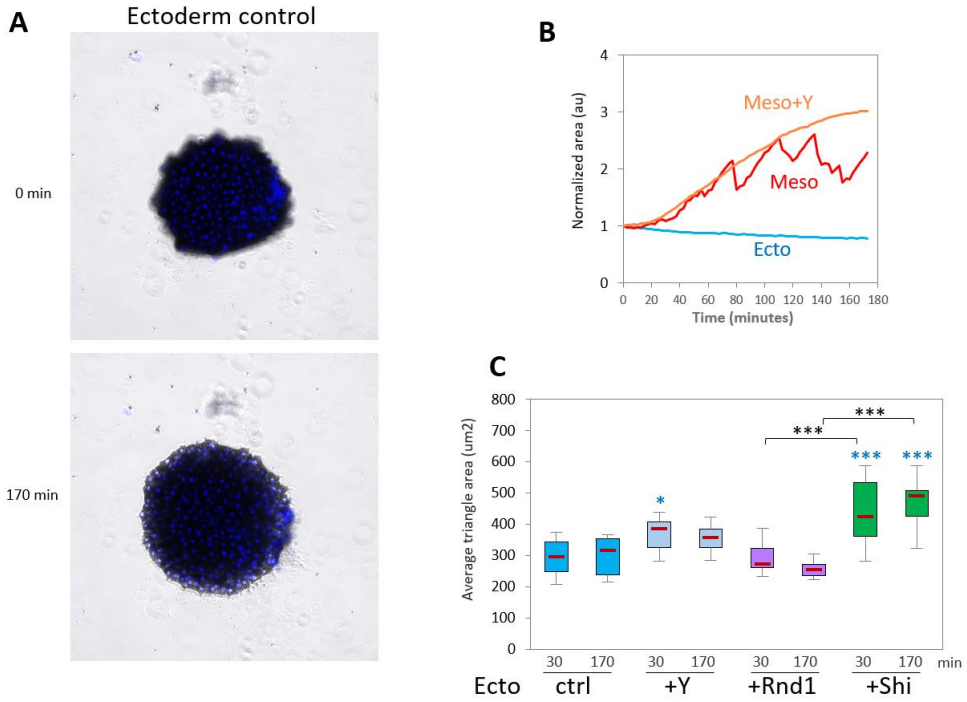
A
Ectoderm control
0 min
170 min
B
Meso+Y
Meso
Ecto
Normalized area (au)
Time (minutes)
C
Average triangle area (um2)
***
***
***
***
*
30
170
min
Ecto
ctrl
+Y
+Rnd1
+Shi

Figure S2.8

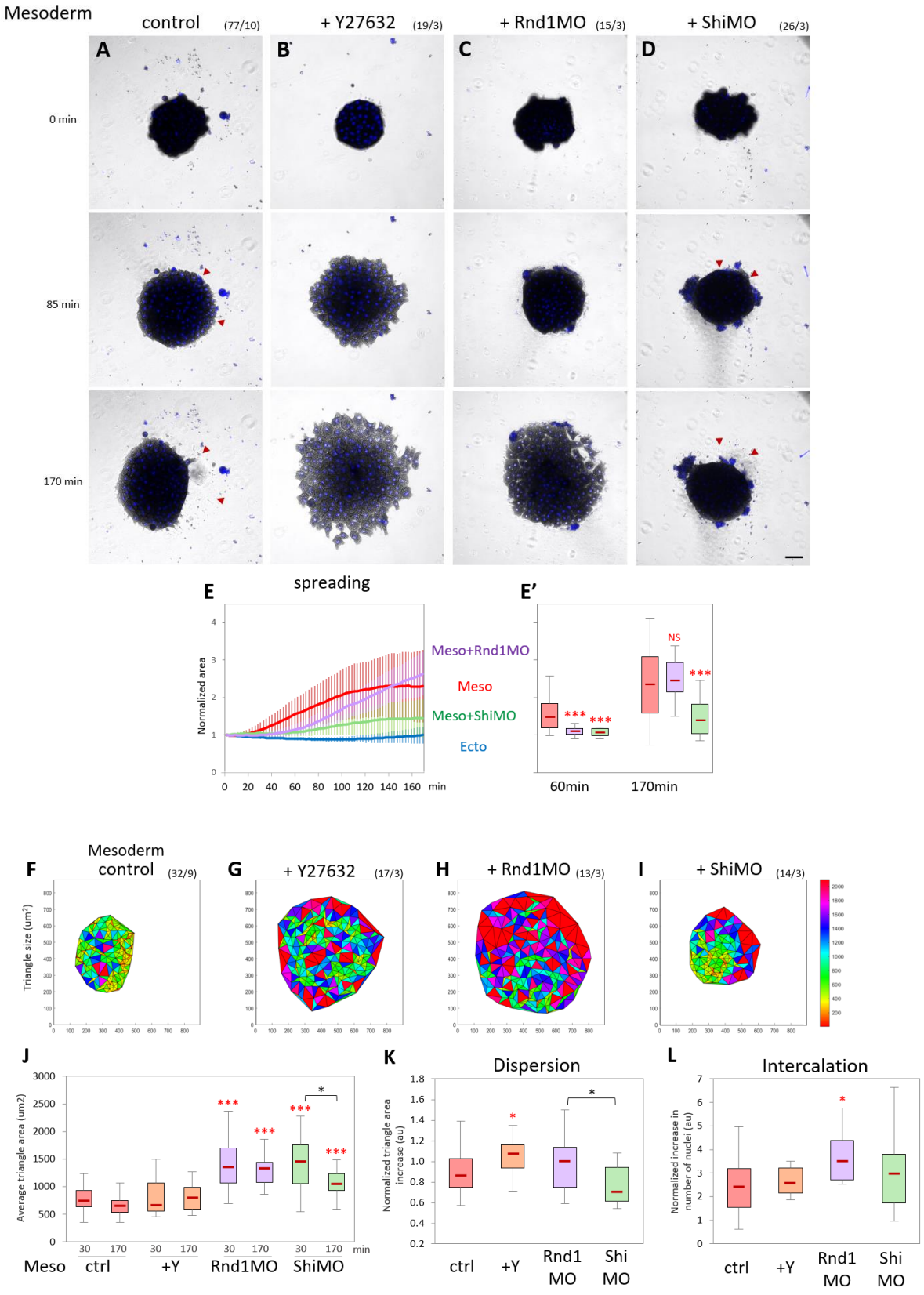
Mesoderm
control (77/10)
+ Y27632 (19/3)
+ Rnd1MO (15/3)
+ ShiMO (26/3)
A
B
C
D
0 min
85 min
170 min
E
spreading
Normalized area
Meso+Rnd1MO
Meso
Meso+ShiMO
Ecto
min
E'
NS
***
60min
170min
F
Mesoderm
control (32/9)
G
+ Y27632 (17/3)
H
+ Rnd1MO (13/3)
I
+ ShiMO (14/3)
Triangle size (um²)
J
Average triangle area (um2)
Meso
ctrl
+Y
Rnd1MO
ShiMO
K
Dispersion
Normalized triangle area increase (au)
ctrl
+Y
Rnd1 MO
Shi MO
L
Intercalation
Normalized increase in number of nuclei (au)

Supplemental Figure Legends

Figure S2.1 – (Related to Figure 2.1) **A) Mode of mesoderm locomotion.** Consecutive frames from time lapse of mYFP labelled mesoderm cells migrating on FN. The behaviour of the central cell is highlighted: The cell emits one or multiple protrusions (red arrows). One of the protrusions becomes a tail (yellow arrowhead) as the cell stretches toward another direction, and eventually retracts (red arrowheads). **B) Quantification of accumulation of Vinculin-Cherry in focal adhesions: Linearity between fluorescence levels in focal adhesion and total intensity** (Related to Figure 2.1A-D) Because Vinculin-Cherry expression levels vary from cell to cell, quantification was performed for individual cells by measuring fluorescence in bright clusters (corresponding to focal adhesions) and in the total ventral cell surface (pink on the diagram). The plot shows the average intensity of the ventral surface versus the average intensity in focal adhesions for control mesoderm cells in one experiment, each dot corresponding to a single cell. It shows that accumulation at focal adhesions is proportional to total expression levels over a wide range. Linearity was similarly verified for each experiment.

Figure S2.2 – Localization of MLC and Rock (Related to Figure 2.2) **A-C) Differential MLC accumulation at the cell cortex.** Ectoderm and mesoderm cells expressing MLC-Cherry (MLC-Che) and mYFP. A) Ectoderm cells show strong accumulation around the cell body (arrows) and part of the blebs (arrowhead). B) Mesoderm cells show irregular cortical MLC, mostly at the concave regions near or between protrusion. C) Quantification of cortical MLC, expressed as the ratio of cortical /cytoplasmic fluorescence intensities. Blebs and protrusions were excluded from the measurements. Statistical comparison using two-sided Student's *t*-test. Scale bars: A' 5µm, B' 10µm, B" 5µm. **D-K) Subcellular localization of Rock1-YFP and Rock2-YFP in ectoderm and mesoderm cells.** Selected single planes from live confocal microscopy, either near the glass (ventral), or about 5-10µm above (medial). Concave white arrowheads point at examples of Rock1/2 accumulation. D,E,H,I) Localization relative to the cell cortex and to vinculin-Cherry labelled cell-matrix adhesive structures (red arrowheads). F,G,J,K) Localization relative to cell-cell contacts, marked by cadherin-dTomato (red arrows). D,E) In the ectoderm, Rock1 and 2 have both a cortical localization. Levels are low on the ventral side inside the adhesive ring, but

stronger outside of the ring, particularly for Rock2. F,G) Levels are very low at cell-cell contacts. H,I) In the ventral face of mesoderm cells, Rock1 tend to be enriched in the central part, Rock2 at the periphery of the protrusions. Both are low at FAs. They both accumulate at the cortex along cell free edges (medial planes). J,K) Levels are low at cell-cell contacts. Y: autofluorescence of yolk platelets, abundant in mesoderm cells.

Figure S2.3 – (Related to Figure 2.2) **A,B) Area expansion** for single cells after treatment with Rock inhibitors Y27632 (50µM) and H1125 (1µM)**.** Average and SD of 107 cells (A) and 34 cells (B). **C) Changes in vinculin distribution.** Images from a time lapse movie of a small group of three cells expressing Vinculin-Cherry, treated at time = 0 with Y27632. Filled arrowheads: ring-like adhesion; Concave arrowheads: FAs. Scale bars: 10µm. **D,E) Opposite effects of Rock and MLCK inhibition on cell adhesion.** Ectoderm and mesoderm adhesion to FN or cadherin was measured after treatment with Rock inhibitors Y27632 (Y, 50µM), H1125 (H, 1µM), or the MLCK inhibitor ML7. 5 experiments, total 1000-2000 cells/conditions. Statistical comparison to control ectoderm or mesoderm, comparing the % adherent cells/experiment, pairwise two-sided Student's *t*-test.

Figure S2.4 – (Related to Figure 2.4) **A-D) Rescue of Rnd1MO and ShiMO spreading and migration phenotypes.** 4-cell stage embryos were injected in the dorsal side with COMO, RndMO, RndMO + YFP-Rnd1 mRNA (rescue), ShiMO, or ShiMO + YFP-Shirin mRNA (rescue). Dissociated mesoderm cells were plated on FN and time lapse movies were recorded. The fourth condition represents RndMO or ShiMO cells treated with 50µM Y27632 Rock inhibitor (Y). Statistical comparions: One-way ANOVA followed by Tukey's HSD post hoc test. Red asterisks: Comparison to COMO. **E) Migration speed for different cell morphology categories**. Analysis of data from Figure 2.4I. Red asterisks: Comparison to COMO. one-way ANOVA followed by Tukey's HSD post hoc test.

Figure S2.5 – (Related to Figure 2.5) **(A) Morphometry of Rnd1 and Shirin induced spreading of ectoderm cells**. The diagrams illustrate typical cell shapes. Corresponding images can be found in main Figure 2.5A-E. These shapes were analysed based on the following parameters: A') Area

of the ventral contact surface (red in the schemes in A). A") Circularity of the ventral surface, which depends both on the roundness and regularity/convolution of the shape. A"') Ratio between the ventral area and the maximal cell area, calculated from maximal z projections. Blebs were excluded from measurements. Rnd1 and Shirin-expressing cells were here subdivided in two categorises, low and high-expression, based on the YFP fluorescence intensity. Note that these two categories overlap but are not equivalent Rnd1 expression levels had no significant impact on any parameter. Shirin expression had no effect on contact surface area, but high levels stimulated formation of convoluted protrusions (lower circularity) but decreased ventral/max area, reflecting the fact that many of them rounded up (4^{th} cell shape in panel A, see main Figure 2.5E). **B) Distribution of speed for ectoderm cells expressing Rnd1 or Shirin**, compared to wild type ectoderm and mesoderm. Brackets: Range of high speed, comparable to mesoderm, achieved mainly by Rnd1-expressing cells.

Figure S2.6 – (Related to Figure 2.6) **Effect of Rnd1 and Shirin ectopic expression**. **A) Loosening of ectoderm tissue upon expression of Shirin.** Immunostained section of a YFP-Shirin expressing embryo showing a loosely organized ectoderm, characterized by the presence of large intercellular spaces (asterisks) and heterogenous β-catenin signal, weak signal along membranes except for strong local concentrations (arrowheads). Scale bar, 10µm. **B-E) Cell orientation**. B-D) The main axis of deep ectoderm cells (double arrows) tend to orient roughly perpendicular to the inner surface of the tissue (dashed line). Rnd1-expressing cells show variable orientation. Shirin-expressing cells align parallel to the surface. Scale bars, 10µm. E) Quantification of the angle between the cell axis and the tissue interface. Numbers into brackets correspond to number of cells/embryos/experiments. **F-I) Analysis of β-catenin (green) and pMLC (red) in ectoderm explants**. F) Diagram, section of an control ectoderm explant (scale bar, 50µm) and quantification. Statistical comparison using one-way ANOVA followed by Tukey's HSD post hoc test. G-I) Examples of ectoderm explants. G) β-catenin and pMLC signal along cell edges is highest in control (arrows). H,I) Explants expressing Rnd1 or Shirin. β-catenin tends to accumulate at cell vertices (concave arrowheads). pMLC levels are lower except for some cells (I, asterisks) that have rounded up, and display high pMLC throughout the cell. Little to no β-catenin is seen between the round cells. Scale bars, 20µm. **H) Effect of Rnd1 and Shirin expression on**

phosphorylation of MYPT. Dissected ectoderm tissues were analysed by Western Blot. GAPDH was used as loading control, and the pMYPT signal was expressed as relative ratio, normalized to ectoderm control set to 1.0. Three independent experiments, statistical analysis using one sample, two-sided *t*-test.

Figure S2.7 – (Related to Figure 2.9) **A) Example of ectoderm explant showing late partial spreading**, which is only observed beyond the 120min. **B) Examples of traces for single explants**, illustrating the irregular expansion of mesoderm explants interrupted by retractions. In contrast, expansion of Y27632- treated mesoderm is smooth. C) Quantification of average triangle size at the initiation of spreading (30 min) and the end of the time lapse (170 min).

Figure S2.8 – (Related to Figure 2.9) **Knockdown of Rnd1 or Shirin affect collective properties of mesoderm tissue explants**. Analysis of spreading, dispersion, and intercalation of mesodermal explants under various conditions was performed as for experiments presented in Figure 2.9. A-D) Control mesoderm, mesoderm treated with Y27632, and mesoderm from embryos injected with Rnd1 MO or Shirin MO. Red arrowheads in A and D indicate areas of large scale retractions (compare 85 and 170min). Scale bar: 100µm. E) Average time course curves with SD for the various experimental conditions. E') Corresponding relative spreading after 60min and 170min. F-K) Delaunay triangulation of nuclei in order to measure cell dispersion. F-I) Representative plots of triangulated nuclei after 170 minutes of imaging. X and Y labels mark the coordinates in µm, the colour coded scale bar indicates the area of the triangles in μm^2. J) Quantification of average triangle size at the initiation of spreading (30 min) and the end of the time lapse. K) Quantification of the relative change in triangle size over time calculated by dividing the average triangle area at 170 minutes by that at 30 minutes. L) Quantification of intercalation calculated by dividing number of nuclei at the ventral surface at 170 minutes by the number at 30 minutes. Statistical comparisons: One-way ANOVA followed by Tukey's HSD post hoc test.

Appendix S2.1

Calculation of relative tensions and adhesiveness for cell doublets

Estimates of relative tensions were based on the principle that the geometry of the cell membranes at cell vertices reflects the equilibrium between the tensile forces exerted by the cell cortices (Canty et al., 2017; David et al., 2014). For a doublet formed of cell A and cell B, the equilibrium involved the cortical tensions at the two free cell surfaces (Ct_A and Ct_B) and the contact tension at cell-cell interface (T_{AB}). T_{AB} is defined as the sum of the cortical tensions of each cell at the contact (Ct_A' and Ct_B') and of the negative contribution due to cell-cell adhesion (-ω).

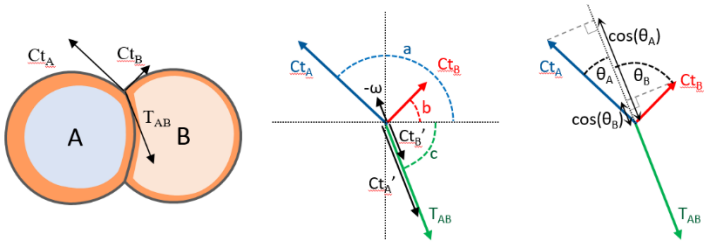

The force equilibrium was expressed by two equations:

(1) $$\sin(a) * Ct_A + \sin(b) * Ct_B + \sin(c) * T_{AB} = 0$$

(2) $$\cos(a) * Ct_A + \cos(b) * Ct_B + \cos(c) * T_{AB} = 0$$

Angles *a*, *b* and *c* corresponded to the orientation of each force vector.
Each of these angles was measured as the tangent to an arc fitted to three points of the cell membrane, including the cell vertex (Canty et al., 2017).

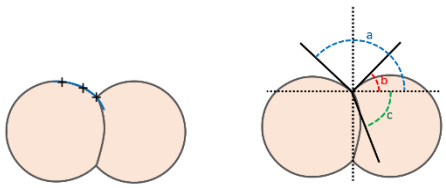

Based on equations (1) and (2), we could use the three angles to calculate the ratios between the two cortical tensions (Ct_A/Ct_B) and the ratio between contact tension and each of the cortical tensions (Canty et al., 2017) using the equation:

(3) $$T_{AB}/Ct_B = \left(\sin(b) - \frac{sin(a) * cos(b)}{cos(a)}\right) / \left(\frac{\sin(a) * \cos(c)}{\cos(a)} - \sin(c)\right)$$

and the ratio Ct_A/Ct_B between the two cortical tensions:

(4) $$\frac{Ct_A}{Ct_B} = \left(\frac{T_{AB}}{Ct_B}\right) / \left(\frac{T_{AB}}{Ct_A}\right)$$

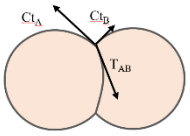

Ct_A/Ct_B is expected to be on average close to 1.0 for homotypic doublets. Ct_A/Ct_B of heterotypic provided a direct readout of the relative cortical tension of two cell types, here Rnd1 or Shirin-expressing cells compared to control ectoderm cells (Figure 2.8J, see below the complete results of all homotypic and heterotypic doublets). Note that Ct varies broadly even for cell of the same type/condition (e.g. homotypic control ectoderm, Figure 2.8J, see Canty et al., 2017).

To compare the tensions between different types of doublets, we calculated a relative contact tension *rel*T (T in the text and legends) expressed relative to the median value of control ectoderm contact tension set at 1. We also assumed that the average of the two cortical tensions (Ct_A+Ct_B)/2 was proportional to the median of the measured Cts. Thus, we defined a relative median cortical tension medCt for each condition, set to 1.0 for control ectoderm. *rel*T could then be calculated using the following equation:

(5) $$relT_{AB} = 2 * medT_A * \left(\frac{T_{AB}}{Ct_A}\right) / \left(1 + \frac{Ct_B}{Ct_A}\right) + 2 * medT_B * \left(\frac{T_{AB}}{Ct_B}\right) / \left(1 + \frac{Ct_A}{Ct_B}\right)$$

Adhesiveness α is an absolute number between 0 and 1, defined as the tension reduction at the contacts relative to free surface (Parent et al., 2017) and can be directly calculated via the

contact angles (Parent et al., 2017). We adapted this calculation to asymmetrical doublets, thus

(6) $$\alpha = 1 - \frac{T_{AB}}{Ct_A + Ct_B} = 1 - \left(\cos(\theta_A) + \cos(\theta_B)\right)/2$$

Note that adhesiveness does not depend on absolute Ct or T, but on the balance of both. Accordingly, as illustrated here below, two pairs of cells may have the same adhesiveness despite displaying very different cortical tensions.

Examples of configurations:

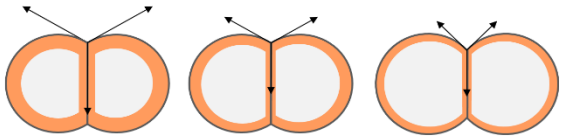

$Ct_{ctrl} > Ct_{Rnd1} > Ct_{Shi}$

$\alpha_{ctrl} \sim= \alpha_{Rnd1} > \alpha_{Shi}$

Complete results from doublet measurements:

Cortical tension, contact tension and adhesiveness of homotypic and heterotypic doublets of control ectoderm cells, and cells expressing Rnd1 or Shirin.

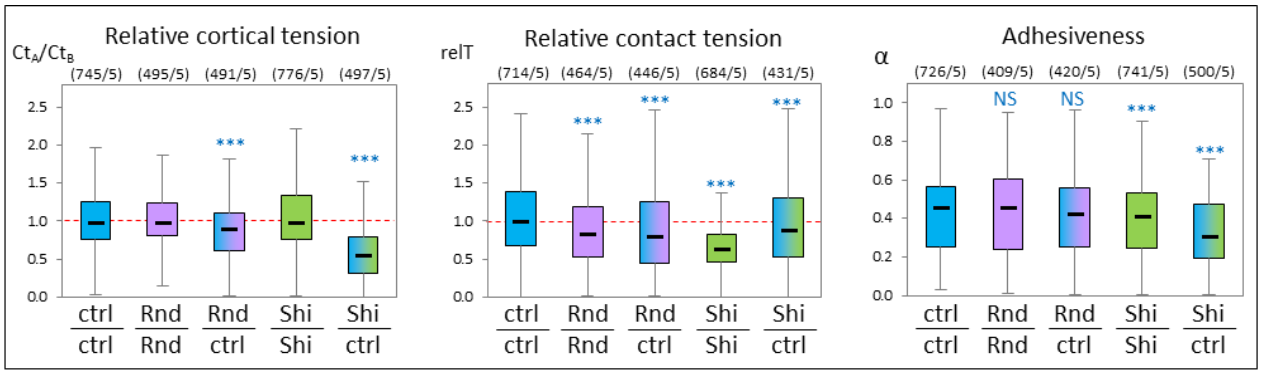

Bridge to Chapter III – In Chapter II we identified the mesoderm-specific expression of two negative regulators of RhoA, Shirin and Rnd1, expression of which lowered cortical tension of mesoderm cells. This lowered cortical tension enabled the migratory capabilities of mesoderm and influenced the mechanical properties of the tissue. Since cell-cell rearrangements within the mesoderm are driven by cell migration, I next sought to investigate how differential migration between two cells remodelled cadherin mediated cell-cell adhesions. This chapter is presented as a manuscript in preparation for submission to a journal.

Chapter III – Force dependent cell-cell contact remodelling in mesenchymal cells

Abstract

Gastrulation involves large rearrangements of tissues in the early embryo in order to set the basic body plan of the organism, often requiring that cells dynamically rearrange and exchange neighbours to facilitate these tissue-scale movements. This process must require the dynamic regulation of cell-cell adhesive complexes to mediate overall cohesion of the tissue while remaining permissive to neighbour exchange. While most previous studies investigating cell contact remodelling have focused on epithelial models, in this study we provide the first detailed look at how a mesenchymal cell type, the mesoderm of the *Xenopus laevis* gastrula, remodels and eventually disrupts its cadherin mediated cell-cell contacts. Using a dual pipette aspiration (DPA) setup to displace adhering cells away from each other and thus applying force on the cell contact, we find that cadherin is initially removed from the contact through disruption of the cadherin trans bond and subsequent lateral diffusion. In parallel to cadherin removal via peeling, a remnant of cadherin concentrates at the shrinking contact, and complete rupture of the adhesion requires breaking the cytoplasmic link between α-catenin/actin and the actin cytoskeleton. We also observed that myosin is recruited peripheral to the contact prior to detachment of the cells, and blocking this activity impairs contact detachment. Finally, by altering cortical tension of the cells, we can change how the contact remodels by altering the magnitude and orientation of how forces are applied on the contact during displacement, revealing another key relationship between cell-cell adhesion and the cortical cytoskeleton.

Introduction

Cell-cell rearrangements are critical for the morphogenesis of many tissues. The first major morphogenetic event is that of gastrulation where massive tissue-scale rearrangements are initiated, ending with the separation of the three germ layers: ectoderm coating the exterior, endoderm occupying the interior, and mesoderm placed in between. The gastrula of the *Xenopus laevis* embryo has a long history as a model for the study of gastrulation (Beetschen, 2001). Gastrulation in *Xenopus* is primarily mediated by rearrangements at the cellular level that – in the case of the mesendoderm and prechordal mesoderm – proceed through a mesenchymal

mode of migration where cells migrate using their neighbours as substrates (Huang and Winklbauer, 2018). This poses an interesting dilemma, as cell-cell adhesions must be able to facilitate the overall cohesion of the embryo while still permitting the cellular rearrangements that are required for gastrulation movements. At the core of this question stands the mechanism(s) responsible for disassembly of an existing adhesive contact.

Classic cadherins are transmembrane glycoproteins and are the principal cell-cell adhesive molecules found across the animal kingdom (Hulpiau and van Roy, 2009). In this study, we focus on the type I classic cadherin, C-cadherin, the main cadherin expressed at in the early *Xenopus* gastrula. Therefore, we will hereafter use 'cadherin' to refer to type I classic cadherins, although some of these concepts may be generalizable to all classic cadherins. Extracellularly, cadherins are able to form *trans* bonds with cadherins on opposing cell membranes (Harrison et al., 2011; Nagar et al., 1996; Shapiro et al., 1995), and *cis* bonds with cadherins on the same cell (Boggon et al., 2002; Harrison et al., 2011), both of which are important for developing mature adhesions (Harrison et al., 2011; Wu et al., 2015). The cytoplasmic tail has two highly conserved sites: the juxtamembrane domain (JMD) that binds to p120 catenin (Daniel and Reynolds, 1995; Yap et al., 1998), and the catenin binding domain (CBD) that binds β-catenin (Hülsken et al., 1994; McCrea and Gumbiner, 1991; Stappert and Kemler, 1994). Binding of p120 catenin masks endocytic motifs present in the JMD and thus negatively regulates endocytosis (Ishiyama et al., 2010; Miyashita and Ozawa, 2007; Nanes et al., 2012), while also regulating the RhoGTPases RhoA and Rac (Elia et al., 2006; Noren et al., 2000; Wildenberg et al., 2006). β-catenin binds α-catenin (Aberle et al., 1994; Huber et al., 1997), the final component of what is referred to as the cadherin-catenin complex (CCC), which in turn binds directly to the actin cytoskeleton (Buckley et al., 2014; Rimm et al., 1995), functionally linking the cytoskeletons of neighbouring cells. As an adhesion matures, cadherins organize into clusters, which is thought to strengthen adhesion (Brieher et al., 1996; Yap et al., 1998; Yap et al., 2015). Clustering is mediated extracellularly by both *trans* and *cis* interactions (Wu et al., 2010; Wu et al., 2011; Wu et al., 2015), with intracellular contributions through p120 catenin (Ishiyama et al., 2010; Vu et al., 2021; Yap et al., 1998) and interaction with the actin cytoskeleton (Truong Quang et al., 2013; Wu et al., 2015). Importantly, several of the interactions of the CCC are mechanosensitive (Buckley et al., 2014;

Huang et al., 2017; Rakshit et al., 2012; Yao et al., 2014; Yonemura et al., 2010), and cadherin is enriched at the contact as a direct response to increased tension (Engl et al., 2014; Gao et al., 2018; Ladoux et al., 2010; Liu et al., 2010). It is clear that the contact can be reinforced in response to force, however, force is also required in order to facilitate cell rearrangements (Pinheiro and Bellaïche, 2018), leading again to the dilemma that certain mechanisms must exist to remodel and disrupt cadherin adhesions.

The majority of studies examining contact remodelling have been done within the context of epithelial morphogenesis (Pinheiro and Bellaïche, 2018; Takeichi, 2014), while little is known about the process in mesenchymal-like tissues such as the gastrulating Xenopus mesoderm (Shih and Keller, 1992; Shindo and Wallingford, 2014). In epithelial models, it is established that endocytosis and recycling of cadherin – regulated through binding of p120 catenin to the JMD – influences the amount and dynamics of cadherin at the membrane (Davis et al., 2003; Ireton et al., 2002; Le et al., 1999; Xiao et al., 2003), and it has been suggested that it may entirely account for cadherin dynamics at mature cell contacts (de Beco et al., 2009). This relationship has been the focus of many studies regarding cadherin dynamics and contact remodelling during morphogenetic events. Briefly, in *Drosophila* epithelia it has been demonstrated that endocytosis induces junctional shrinkage to initiate cell rearrangements (Levayer et al., 2011), that it specifically targets large cadherin clusters (Truong Quang et al., 2013), and that p120 catenin is displaced from the contact in a tension sensitive manner leading to increased internalization of cadherin and remodelling of the contact (Iyer et al., 2019). In migrating astrocyte monolayers, a targeted recycling of cadherin from the cell rear to the front mediated by a polarized phosphorylation and subsequent unbinding of p120 catenin from cadherin is required for collective cell migration (Peglion et al., 2014). Though it has been proposed that endocytosis is directly responsible for disruption of the cadherin trans bond (de Beco et al., 2009; Troyanovsky et al., 2006), the issue remains unresolved, as removal of cadherin by endocytosis may be prevented when the cadherin is engaged in trans with other cadherins extracellularly and with the cytoskeleton cytoplasmically (Izumi et al., 2004; West and Harris, 2016). Alternatively, a different mechanism, termed ‘peeling’, has been proposed based on conceptual considerations (Garrivier et al., 2002). It is indeed predicted that a tension applied tangential to the cell

membrane acts primarily on the adhesive molecules at the periphery of the contact site. This would cause a gradual rupture of adhesion molecules, which would then free them to either be internalized or diffuse laterally on the free membrane. This model is consistent with recent evidence in *Drosophila* epithelia that forces applied perpendicular to the contact increase levels of cadherin at the contact, while forces applied parallel to the contact (shearing forces) decrease cadherin levels (Kale et al., 2018).

In this study we attempted to probe several basic aspects of force dependent contact remodelling and disruption. We used a combination of dissociated cells either freely migrating on fibronectin or manipulated with a dual pipette aspiration (DPA) setup to apply force on a contact to stimulate remodelling and eventual detachment of the cell contact while simultaneously imaging components of the CCC and cytoskeleton. Previous studies using the DPA assay typically used it to measure the 'separation force' of cell-cell contacts (Chu et al., 2004; Chu et al., 2006; Maître et al., 2012), which requires fast and large displacements to provoke instantaneous detachment of the contacts in order to avoid remodelling of the contact in response to the applied force (Biro and Maître, 2015). As we wished to directly observe this force sensitive remodelling on a physiological timescale, we used stepwise displacements punctuated by several minutes of imaging. We discover a stereotypical mode of cell-cell contact remodelling involving two parallel processes: a removal of cadherin through peeling and subsequent diffusion on the free membrane as well as a concomitant increase in cadherin density at the contact. While peeling involved dissociation of the cadherin trans bond, final detachment of the condense residual cadherin was resolved by abrupt rupture of the cytoplasmic link to the cytoskeleton, often involving the local recruitment of myosin. By altering cortical tension, we further uncover how the two mechanisms of peeling and condensation depend on both the magnitude and orientation of the forces applied on the cell-cell contact.

Results

Remodelling of the cell-cell contact prior to separation involves both condensation and removal of cadherin

In this study we primarily used dissociated cells from induced mesoderm (IM), which is produced by the ectopic activation of the Wnt and TGFβ signalling pathways in ectodermal cells through injection of a constitutively active activin receptor in the animal cap. Induction of ectoderm with activin leads to expression of mesodermal markers (Green et al., 1992; Wardle and Smith, 2004), spreading and migration of cells plated on FN (Smith et al., 1990), and recapitulation of gastrulation movements in explanted tissues (Symes and Smith, 1987). Additionally, we have previously demonstrated that IM has similar contractile and adhesive properties to endogenous mesoderm (Canty et al., 2017). Cells derived from IM tissues are more optically tractable than endogenous mesoderm due to their smaller size and reduced yolk content, making them an attractive model for this study. Our initial approach involved using dissociated IM cells plated on fibronectin (FN) imaged using confocal microscopy. We mixed cells from two populations, one expressing C-cadherin-GFP and the other expressing C-cadherin-tdTomato, and imaged isolated cell doublets (either homotypic or heterotypic). We focused on doublets that migrated in opposing directions, ostensibly applying a tension on the cell-cell contact, which led to its shrinking and eventual separation of the cells (Figure 3.1A). Subsequent 3D segmentation (Figure S3.1) allowed us to extract total signal and volume of cadherin at the cell-cell contact, which we then used to calculate the average density at each timepoint of the timelapse (Figure 3.1B,C).

This quantification allows to distinguish between possible scenarios: First, cadherin molecules could be progressively removed as the contact shrinks, either through rupture of the extracellular trans bond and lateral diffusion along the membrane (a process we refer to as “peeling”), or through endocytic internalization, as proposed for contact remodelling of epithelia (Iyer et al., 2019). Either mechanism would result in a decrease in both cadherin signal and volume, and if this removal is proportional to contact shrinkage, cadherin density at the contact may then remain constant. If, on the contrary, cadherins would not be removed from the

shrinking contact, they would concentrate, which will be reflected by increased density, decreased volume, and constant total signal. The question would then be to determine how the increasingly dense contact would eventually resolve.

The analysis of 26 cell-cell detachments revealed that 20% of them occurred without detectable cadherin accumulation, thus with all cadherin being progressively removed as the contact was shrinking. The remaining 80% showed a hybrid process, with both a progressive loss of cadherins as well as a condensation (Figure 3.1B,C). The graphs show that though there is some fluctuation of total signal and volume, the average density remains relatively stable over time (0-540s; Figure 3.1B,C). However, as the cells continue to migrate away from each other the contact starts to shrink, and cadherin is removed from the contact (Figure 3.1A YZ insets) with a concomitant condensation of the cadherin remaining at the shrinking contact (600s-960s; Figure 3.1A,B,C). The use of separate green and red cadherins allowed an important observation: although the magnitude of the changes in fluorescence differ between the cells expressing the different tagged cadherins, the overall pattern is the same, which was demonstrated by the very strong correlation when comparing the slopes of contact signal between C-cadherin-GFP and C-cadherin-tdTomato (Figure 3.1D). Due to this strong correlation, we will only present the data for C-cadherin-GFP cells when heterotypic cell-cell contacts were imaged. Another feature frequently observed during the final phase of detachment was the failure of the highly condensed remnant cadherin contact to resolve (Figure 3.1E). This resulted in the stretching of long membrane protrusions between the cells, which would eventually snap, leaving cadherin clusters containing cadherin from both cells on one or both cell membranes. Since the cadherin constructs were tagged on the cytoplasmic tail, this implies that the final rupture of the adhesion did not occur at the extracellular cadherin trans bond, but between one of the cytoplasmic interactions. This phenomenon indicated that under some conditions, cadherins failed to disengage from dense clusters.

These images showed that a large portion of cadherin was removed before the final detachment. If cadherin was internalized, we would expect to see the apparition of cadherin positive endosomes in the cytoplasmic compartment, which was not the case. We did not detect any sign of endocytosis, despite the fast imaging (one frame every 30 sec). Occasionally spots

corresponding to pre-existing clusters were seen diffusing on the membrane (blue arrowheads; Figure S3.1). It became clear to that cadherin removal could not occur via endocytosis in this system. We thus favored the alternative mechanism, i.e. cadherin trans bond disassembly and lateral diffusion. However, the complex and ultrafast dynamics of the plasma membrane in the migrating cells prevented direct visualization of this process in these settings. Though this analysis of cells plated on FN provided key insights for our initial hypothesis, there were additional limitations to this approach. The detachment of the cells relies on random migration. This inevitably leads to the application of inconsistent forces - in both magnitude, persistence, and orientation - on the cell-cell contact. Further, it is very difficult to image the full 'lifetime' of a cell-cell contact i.e. starting from a tension free equilibrium and moving towards increasing forces and contact remodelling. It is likely that the majority of doublets were imaged from a starting point where the remodelling had already commenced. These two issues complicate interpretation of the data. For instance, the ~20% of detachments that proceeded without any condensation of cadherin could be due to either imaging commencing after the condensation had already occurred, or potentially the migration of the cells applied a force on the contact at a specific orientation that did not favor condensation (Kale et al., 2018).

Separation of cells using dual-pipette aspiration reveals a consistent detachment paradigm

In order to address these issues, we opted for a more reductionist model, using a dual pipette aspiration (DPA) setup, where pipettes connected to a finely controlled negative pressure system were used to apply an aspiration pressure on cells allowing for the precise manipulation of cells (Biro and Maitre, 2015). After selecting two cells and bringing them into contact, they were allowed to establish their adhesion for ~5 minutes. This capacity to adhere extremely rapidly is characteristic of mesodermal cells (Rohani 2014). After the cell-cell contact was established we would grasp the cell doublet, image for several minutes at equilibrium, before displacing the cells incrementally away from each other until the contact was eventually ruptured. This approach has several benefits: each doublet starts at a similar level of adhesion,

the application of force on the contact is consistent and controlled, and during the initial stages of imaging the cell-cell contact is ostensibly under no tension.

The detachment behavior observed with DPA was overall quite similar to that of cell doublets migrating on FN, with some nuances. During the initial stages of displacement, there was a period of relative stability in terms of average density and cadherin signal and volume (0-180s; Figure 3.2A,B). For cells plated on FN this phase would correspond to the period where cells moved apart without yet signs of contact shrinkage (0-540s; Figure 3.1B,C). This was followed by a period of gradually decreasing signal and volume (180s-450s; Figure 3.2B), and a sudden increase in density, which in this example case occurred after 15 µm of displacement (360s; Figure 3.2B). By comparing the total cadherin signal at the contact and the average density between early and late stages of the remodelling process, we saw that in every case there is a decrease in contact signal and a parallel increase in average density (Figure 3.2C,D).

An unexpected benefit of cell-cell separation using the DPA system was that it became clear how cadherin was being removed from the cell-cell contact. Indeed, it was evident that as cadherin signal at the contact was decreasing, there was a large increase in signal at the free membrane (Figure 3.2E). The intensity of the membrane signal continued to increase throughout the later stages of the remodelling process (compare signal at white and yellow arrowheads from 90s-420s; Figure 3.2Eii,iii; Figure 3.2F). Line scans spanning the 5 µm of the membrane directly adjacent to the contact show two characteristic, highly reproducible features: A steep slope adjacent to the contact, as well and a progressive increase over time of the base level of the signal in the next few microns (Figure 3.2Ei,iv). Comparing the early and late stages of multiple cell-cell detachments showed that the cadherin signal at the membrane increases in every case (Figure 3.2G), as the signal at the contact decreases (Figure 3.2C). Notably, the majority of cadherin is displaced back to the free membrane of the cell from which it originated (i.e. C-cadherin-GFP signal increases on the C-cadherin-GFP expressing cell, not the C-cadherin-tdTomato expressing cell), although there are occasionally some small clusters that diffuse onto the other cell (red arrowheads; Figure 3.2Eii,iii).

As noted for cells on FN, we also observed that the final detachment would often leave membrane tethers from each cell temporarily maintaining the connection between the cells, and containing cadherin clusters positive for both colours of cadherin (white arrows; Figure 3.2H). Together these data clarify the observations from the doublets on FN and point towards a consistent mode of contact remodelling while under tension, involving a displacement of cadherin from the contact to the free membrane, while the cadherin remaining at the contact condenses before rupture of one of the cytoplasmic interactions of the CCC.

The cadherin-catenin complex behaves as one unit during contact remodelling

We next turned our attention to the principal cytoplasmic binding partners of cadherin, the catenins. Using the same approach with the DPA system we co-expressed C-cadherin-tdTomato with either p120 catenin-GFP or α-catenin-GFP. This allowed us to examine if other components of the CCC are removed from the contact prior to cadherin as has been suggested for p120 catenin in *Drosophila* epithelium (Iyer et al., 2019), and α-catenin in zebrafish progenitor cells (Maitre et al., 2012). If this was the case in our system, we would expect signal of either catenin to decrease before that of cadherin after displacement of the cells begins. Cadherin and p120 catenin co-localize at the cell-cell contact (Figure 3.3A; MIPs and YZ insets). Remodelling events observed for cadherin including decreasing signal at the contact and an increasing density (Figure 3.3A, D) were mirrored by p120 catenin (compare charts; Figure 3.3C, D). We found a strong temporal correlation between the slopes of cadherin and p120 catenin comparable to when the slopes of cadherin-GFP and cadherin-tdTomato were compared as a control (Figure 3.3I). Extending this analysis to α-catenin revealed similar results. The remodelling of cadherin was consistent with previous experiments (Figure 3.3E, H), and α-catenin followed a similar pattern (Figure 3.3G,I). Note that the clusters that appear behind the contact (white asterisks; Figure 3.3E) are in fact found on the free membrane on the lower planes of the image stack (see Figure S3.1; blue arrowheads).

After cells detached there were membrane tethers extending between the cells similar to what we previously observed, with clusters containing both cadherin and p120 catenin (Figure

3.3B) as well as cadherin and α-catenin (Figure 3.3F). This is consistent with the presence of dual coloured cadherin clusters after detachment (Figure 3.2H) indicating that the final rupture occurs cytoplasmically, potentially between α-catenin/actin or perhaps rupturing the actin cytoskeleton itself. These data suggest that the cadherin-catenin complex is remodelled as a whole, and that the catenins do not play specific roles to promote disassembly of the adhesion outside of the α-catenin/actin bond potentially being the weakest link at the final stage of contact detachment.

Recruitment of myosin facilitates detachment of cells after condensation of cadherin

We then began exploring the potential roles of the actomyosin cytoskeleton in regulating cell contact remodelling by co-injecting myosin heavy chain IIA YFP (MHCIIA-YFP) with C-cadherin-tdTomato and plating the cells on FN. Interestingly, there often appeared to be an enrichment of MHCIIA at the terminal phase of detachment following the condensation of cadherin at the contact (Figure 3.4A,B). MHCIIA was recruited immediately adjacent to the cell-cell contact, but did not localize directly with cadherin (YZ and XZ insets; Figure 3.4A), or the cell-matrix interface (XZ insets; Figure 3.4A). Overall, ~70% of imaged doublets recruited MHCIIA prior to the final detachment of the cells. Though we attempted to extend this analysis to doublets manipulated with DPA, the isolated dissociated cells appeared to be too sensitive to manipulation of MHCIIA and cells were too difficult to handle. To ensure that this recruitment is a physiological phenomenon, we imaged MHCIIA in endogenous mesoderm within open-faced Keller explants. Here as well we frequently see recruitment of MHCIIA to the rear of cells directly before they detach from their trailing neighbours (cells with white stars, arrowheads show MHCIIA recruitment; Figure 3.4C).

Due to the consistent recruitment of MHCIIA to the rear of cells prior to detachment we assayed whether or not myosin mediated contractility was required for this process. To this end, we used a contact lifetime assay (Roycroft et al., 2018), where we plated dissociated cells on FN and measured how long two cells remained adhered to one another after their initial encounter. After control cells encountered each other, they typically polarized and migrated away from each other leading to shrinking of the cell-cell contact (black arrowheads; Figure 3.5A) followed by a

brief phase where long membrane protrusions attached the cell before finally detaching reminiscent of the extended membrane protrusions observed prior to detachment when imaging cadherin (red arrowheads; Figure 3.5A). Though there was a wide distribution of contact lifetimes (Figure 3.5B), this process generally lasted 20-40 minutes (Figure 3.5C). However, MO knockdown of MHCIIA seemed to drastically prolong the persistence of the long membrane tethers (red arrowheads; Figure 3.5A'). This often completely prevented the detachment of the cells (130 min; Figure 3.5A'). Increasing the levels of injected MO increased the frequency of cells failing to detach (Figure 3.5B), leading to increased average lifetimes at higher MO levels (Figure 3.5C). Treatment of cells with Y27632 also increased the persistence of the membrane tethers (red arrowheads; Figure 3.5A''), preventing cells from detaching (Figure 3.5B) and increasing average contact lifetime to a degree similar to injection of 40 ng of MHCIIA MO. None of these treatments had any effect on the migration speed of single cells (Figure S3.2). Together these data imply that, though detachment of cells can occur without detectable recruitment of MHCIIA, ROCK induced activation of MHCIIA contractility contributes to the final phase of detachment.

Altering cortical tension impacts how cell contacts are remodelled

It is well established that cortical tension plays a central role in determining equilibrium adhesion strength (Maître and Heisenberg, 2013; Maître et al., 2012; Winklbauer, 2015). Due to this interplay we sought to explore if cortical tension influenced cell contact remodelling. Our first approach was to inject a utrophin-cherry construct that is known to bundle actin (Belin et al., 2014), and therefore likely increase cortical tension through increasing the organization and connectivity of the cortical network (Bendix et al., 2008; Ennomani et al., 2016). The aspiration pressures required to stably hold the utrophin injected cells were generally at least triple the pressure required to hold the control cells (~250 Pa versus ~80 Pa), which indicated that the cortex was much stiffer than that of the control cells. Upon displacing the utrophin expressing doublets the contact was only stable for a short time, then rapidly remodelled leading to an abrupt loss of cadherin at the contact (120s; Figure 3.6A,B). Large numbers of small cadherin clusters were often formed on one or both of the cell surfaces even prior to detachment (blue

arrowheads Y- and Z-projections; Figure 3.6A). These ruptured clusters were present in ~70% of cases, with only ~30% remodelling purely due to peeling, compared to every case for the control cells (Figure 3.6G). This was reminiscent of the clusters we occasionally observed during contact remodelling of control cells (Figure 3.2H), though the clusters here were much larger in both size and population. However, as we only had one colour of cadherin in these experiments, it was not clear if these clusters were formed due to cytoplasmic rupture or through another mechanism. Overall, utrophin-injected cells required much smaller displacements to stimulate detachment (Figure 3.6H) and there was little condensation of cadherin (Figure 3.6I).

As an additional way to modulate cortical tension, and to be sure that the clusters present after detachment in utrophin injected doublets were caused by cytoplasmic rupture, we expressed a constitutively active Rho (caRho) construct to stimulate ROCK mediated myosin contractility. We noted a similar effect to that of utrophin; higher aspiration pressures were needed to hold the cells, a smaller displacement was required before detachment of the cells occurred (Figure 3.6C,D,H), the peak density of cadherin reached before detachment was reduced (Figure 3.6D,I), and there were often several large clusters from one cell appearing on the other cell, preceding or after detachment, implying that the cytoplasmic interaction is ruptured (blue arrowheads; Figure 3.6C). In the example shown, cadherin is also removed from the contact via peeling, indicating that a mixture of both rupture and peeling can be used to remove cadherin from the contact (compare signal at yellow and white arrowheads; Figure 3.6C). The presence of clusters was less frequent in caRho injected cells compared to utrophin; utrophin-injected cells were more likely to remodel through rupture while the majority of caRho-injected cells remodelled through peeling (higher proportion of rupture and mixed; Figure 3.6G).

Taking the reverse approach, we expressed a dominant negative Rho (dnRho) construct. As expected, we noted the opposite effects compared to cells expressing utrophin or caRho: larger displacements were required to detach the cells, not only compared to utrophin and caRho but also to control cells (Figure 3.6E,F,H), and the peak density of cadherin attained before detachment was restored to levels similar to control cells (Figure 3.6F,I). The modality of remodelling was also similar to control cells, relying primarily on peeling (compare intensity at white and yellow arrowheads; Figure 3.6E,G).

The tension applied to the cell contact in these experiments is a product of the displacement and the cortical tension. The increased rate of removal of cadherin from the contact and the smaller displacements required for detachment in the utrophin and caRho injected cells could simply be due to the application of a larger tension. However, we also noted that in the stiffer cells, the angle of the vertex formed by the two cells at the contact was typically smaller than the angle in the control cells (Figure 3.6J; Figure S3.3A). Conversely, cells injected with dnRho had more oblique angles prior to detachment. Together this implied that altering cortical tension alters the deformability of the cells (Figure 3.6J; Figure S3.3A). Strikingly, when we plotted the peak cadherin density at the contact against the angle at the vertices immediately prior to detachment there was a strong correlation. Doublets that had acute angles prior to detachment often detached without any condensation of cadherin at the contact. On the other hand, doublets with oblique angles prior to detachment showed much higher levels of cadherin density (Figure 3.6K). These data demonstrate that in modulating the cortical tension of cells we also alter how the cell contact is remodelled; increased cortical tension leads to rapid removal of cadherin through either accelerated peeling or cytoplasmic rupture, and lower cortical tension favours cadherin condensation and eventual removal by peeling. By changing the cortical tension of a cell, we do not only change the magnitude of the tension applied on the contact, but also the orientation at which it is applied, which also likely impacts the modality of contact remodelling.

Discussion

In this study we used a combination of dissociated cells either freely migrating on FN or subjected to controlled manipulation using a DPA system to dissect the mechanisms used to remodel cadherin mediated cell-cell contacts in response to an applied tension. Using these approaches, we gained several new insights into tension sensitive cell contact remodelling in a model of compact mesenchymal tissue. While previous studies have emphasized either removal of cadherin through endocytosis or the rupture the cytoplasmic connection of the CCC, we have found conditions where breaking the cadherin trans bond through peeling is the primary route

used to remove cadherin from a remodelling cell-cell contact under tension. Removal through peeling consistently removes ~50% of cadherin from the contact prior to complete detachment of the cells, though the residual cadherin condenses at the shrinking contact. This results in the persistence of dense clusters that must detach through rupturing of the CCCs interaction with actin or the cytoskeleton itself. Neither peeling nor cytoplasmic rupture required differential remodelling of other components of the CCC, suggesting it is remodelled as a whole. The final stage of remodelling involves a recruitment of myosin adjacent to the contact and preventing this myosin mediated contraction inhibits detachment. Finally, by modulating the cortical tension the mode of detachment is altered. Increased cortical tension enhances the rate of remodelling apparently both by accelerating peeling and favouring rupture of the cytoskeletal link. Under these conditions the condensation of cadherin is prevented. Alternatively, decreasing cortical tension leads to inefficient remodelling, requiring excessive cell stretching, slowing peeling and favouring concentration of cadherin at the contact.

Our results suggest that neither p120- or α-catenin play major roles during the remodelling and detachment of cell contacts in the mesoderm of the *Xenopus* gastrula. Early stages of remodelling are mediated by peeling and involve the extracellular cadherin trans bond, condensation affects all components of the CCC equivalently (Figure 3.3E,I), while the final rupture of the contact occurs at the cytoskeleton. A prior study using a similar DPA setup but focusing on zebrafish progenitor cells also found that at the final step of detachment it was not the extracellular cadherin trans bond that ruptured (Maître et al., 2012). However, their data suggested that it was the β-catenin/α-catenin bond as α-catenin dissolved from the contact prior to detachment whereas in our study it persisted post detachment. This implies that the weakest link in the CCC at the final stage of contact remodelling is context dependent. This mode of detachment is reminiscent of one mode of focal adhesion remodelling where after the final rupture paxillin remains at the substrate, implying that the extracellular integrin adhesive bond is not ruptured but rather one of the cytoplasmic interactions (Selhuber-Unkel et al., 2010).

Many studies have emphasized the critical role that endocytosis plays during cell contact remodelling. However, none of our data supported any role for internalization of cadherin in remodelling of the cell contact. While increased cadherin internalization in *Drosophila* epithelium

induces contact remodelling (Levayer et al., 2011) and may even specifically target the largest – and brightest – cadherin clusters (Truong Quang et al., 2013), at no point was there any noticeable increase of cadherin clusters in the cytoplasmic compartment. Further, a recent study found that p120 catenin dissociates from cadherin in response to tension leading to internalization of cadherin (Iyer et al., 2019). However, in our assay direct application of tension on the cell contact did not provoke removal of p120 catenin from the contact prior to cadherin. On the other hand, it was clear that as cadherin signal decreased at the contact it gradually increased at the lateral membrane consistent with cadherin removal via peeling. While it has been suggested that endocytosis may be able to apply a tension that leads to disruption of the cadherin trans bond (de Beco et al., 2009; Troyanovsky et al., 2006), it seems that in mesenchymal *Xenopus* tissues the differential migration of cells, whether artificially using DPA or naturally occurring within the tissue (Evren et al., 2014), coupled with contraction of the actomyosin cytoskeleton adjacent to the cell contact (this work; Roycroft et al., 2018), provides an ample amount of force to remodel the cell contact and rupture the adhesive cadherin bond.

We have revealed that remodelling and detachment of cell-cell contacts requires two separate mechanisms. Our experiments using two different tagged cadherin constructs show that peeling of cadherin leads to an increase of cadherin signal on the lateral membrane almost exclusively composed of the specific cadherin construct that the cell expressed. This indicates that earlier stages of remodelling rely on peeling to rupture the trans bond in stark contrast to the final detachment of the cells which clearly occurs cytoplasmically, suggesting that the weakest link of the CCC differs at different stages of remodelling. This could stem from changes at the molecular or cellular level. Densely organized cadherin clusters will have more cadherin trans bonds to distribute applied forces, lowering the average load on each bond. Further, the strength of individual cadherin bonds may be increased due to clustering and higher density organizations: lateral dimerization increases the homophilic binding affinity of cadherin (Brieher et al., 1996), and higher densities may facilitate faster rebinding after dissociation of the trans bond as their movement is limited by cis interactions. This was recently shown to be the case for the PCDH15/CDH23 dimer that forms the tip-link filament in the hair cells of the inner ear (Mulhall et al., 2021). The second possibility, which we will discuss in more detail below, is that

deformation of the cells in response to increasing displacement will change the orientation of the force that is applied on the contact, moving from parallel to the contact at early stages to more perpendicular at later stages. Simulations have demonstrated that tangential forces with even 10° of a parallel component can be up to ~50 times more disruptive to an adhesive bond than a force applied perpendicular to the contact (Chang and Hammer, 1996), so the applied force at late stages of remodelling may not be able to efficiently rupture the cadherin trans bond. It could be possible that the force may be transmitted to the cytoplasmic domain at a consistent orientation despite the change in orientation at the extracellular domain, or that the cytoplasmic bond is equally resistant to parallel or perpendicular forces, causing it to be the new weakest link as the trans bond is stable when the force is applied perpendicular to the contact.

Recruitment of myosin adjacent to the contact immediately prior to detachment suggests that the cells may occasionally require an extra force in addition to forces supplied by displacement of the cells. Drawing an analogy to cell-matrix adhesion and migration is again informative as it is well established that cells migrating on an extracellular matrix can recruit myosin II to the rear of the cell to facilitate detachment from the substrate (Jay et al., 1995; Ridley et al., 2003), though other mechanisms can also be used (Cramer, 2013). However, myosin II based contractility appears to be the dominant detachment force when larger forces are required, while other mechanisms are used when conditions are less stringent (Cramer, 2013). It is tempting to speculate that myosin II is used in a similar way in our experiments, as it was consistently recruited after cadherin was already condensed at the contact and the forces required to detach are seemingly at their highest.

In the DPA assay, it was clear that cortical tension impacted the modality of cell contact remodelling. Doublets with high cortical tension rapidly detached with minimal displacement and condensation of cadherin was prevented, while doublets with low cortical tension required large displacements and cadherin density was comparatively much higher. In this assay, the doublets are displaced from each other, which causes a tension to be transmitted through the cortex onto the contact. The magnitude of this force is dependent on the size of the displacement and the cortical tension of the cells, in other words, a stiffer cell will apply a larger force on the contact than a softer cell moved with the same displacement. Therefore, it is possible that the differences

we observe in remodelling is due to a larger force being applied at a higher rate. However, it was also clear that the softer cells were more deformable than the stiffer cells, as the angles between the cells at the contact prior to detachment was much higher than the stiffer cells (Figure 3.6K, S3.3A). AFM has previously been used to show that Rho mediated contractility and actin organization are critical for resistance to deformation, as treatment with either Y27632 or cytochalasin D increased deformability and slowed recovery rate after deformation (Haase and Pelling, 2013). The strong correlation between the peak density of cadherin at the contact and angle prior to detachment indicate that cell deformability may impact contact remodelling as well. Modeling has suggested that when the applied force is perpendicular to the contact it is far less disruptive to adhesion than a tangential force with a parallel component (Chang and Hammer, 1996) which has been confirmed in *Drosophila* epithelia (Kale et al., 2018). Therefore, even if the magnitude of the force applied on the contact prior to detachment was the same in the high and low cortical tension doublets (with softer cells requiring more displacement), the low cortical tension cells would still need more force to detach due to the oblique angle between the cells as the applied force has a larger component applied perpendicular to the contact (Figure 3.7B',C'; Figure S3.3B). This inefficient detachment process proceeds slowly so that a large fraction of cadherin has ample time to condense. On the other hand, the stiffer less deformable doublets would maintain acute angles at the vertex causing the applied force to be exerted tangentially with a large parallel component (Figure S3.3C), favouring rapid peeling (Figure 3.7B',C'), and thus preventing condensation of cadherin as the contact shrinks.

In certain cases cytoplasmic rupture of clusters occurs prior to the final stage of detachment in stiff cells. We believe that this is a special case of remodelling where the increase in magnitude of the force is so large that the optimal orientation afforded by the resistance to deformation plays little role in accelerating contact detachment (Figure 3.7B''). The applied force is immediately above the threshold required for cytoplasmic rupture of all or most of the cadherin at the contact, so remodelling occurs through this route with or without peeling. The fact that a large portion of the stiff cells still remodel contacts just through peeling and not rupture while maintaining low peak cadherin density at the contact suggests that the orientation of the applied force is relevant in these cases, and the faster detachments isn't purely due to

increased magnitude (Figure 3.7B',C'), but it would still be useful to attempt to estimate the changes in applied force caused by modulating cortical tension. Though we observe peeling in stiffer cells and assume increased rates of peeling accelerates their detachment, direct comparison of peeling levels with control cells is not possible. This is largely due to the resistance to deformation causing a much larger membrane surface area peripheral to the contact compared to control and dnRho injected cells who have narrow extended membrane organizations, so the amount of peeling is emphasized.

Strikingly, when examining the relationship between peak density and angle prior to detachment, while the caRho and utrophin injected cells occupy one end of the spectrum and dnRho the other, the control cells exist across the entire continuum. This is consistent with previous measurements of mesoderm cortical tension that showed large variability from cell to cell (Canty et al., 2017; Kashkooli et al., 2021). One could imagine a stochastic distribution of the cortical tension of cells within the involuting mesoderm leading to contacts that are more susceptible to remodelling and detachment than others, which could help facilitate cell-cell rearrangements during tissue morphogenesis.

Finally, it is important to note that in our DPA setup we only are examining one type of contact remodelling, where the direction of migration is perpendicular to that of the contact. Within a tissue there is also cells crawling past each other laterally (migration parallel to the contact), and extensive radial cell intercalation initiated at the gaps between cells (Huang and Winklbauer, 2018), each of these movements likely differing in how they apply force on the contact and potentially causing different types of contact remodelling. For example, in cells sliding past each other the majority of the force generated will be applied parallel to the cell-cell contact, so these contacts are likely easily remodelled through peeling. We still imagine that the final detachment may require some cytoplasmic rupture as one cell takes a position ahead of the other. While informative, the results of this study only shed light on part of the elaborate movements required to facilitate morphogenesis of the involuting mesoderm.

Materials and Methods

Embryo preparation and injection

Plasmids and morpholino oligonucleotides (Genetools LLC) are listed in Tables S1 and S2 in the supplemental information section. mRNAs were synthesized according to manufacturer instructions (mMessage mMachine kit, Ambion). MOs and mRNAs were injected animally in the two blastomeres of 2-cell stage embryos for ectoderm targeting, or equatorially in the two dorsal blastomeres of 4-cell stage embryos for mesoderm targeting, at amounts listed in Tables S1 and S2.

Mesoderm Induction

Embryos were injected animally at the two cell stage with a mixture of mRNA including β-catenin (100 pg) and constitutively active Alk4 (1000 pg) as previously described (Canty et al., 2017).

Chemical inhibitors

Y27632 was from Millipore. Stock solutions of were prepared in DMSO. They were used at a 1/1000 or higher dilution. Equivalent dilutions of DMSO were added to control conditions and had no detectable effect on cell and tissue properties.

Microdissections and cell dissociation

All dissected explants and cells were taken either from the inner layer of the ectodermal animal cap after mesoderm induction or from the anterior mesoderm at stage 10+ at the onset of involution. Dissections were performed in 1x MBSH (88mM NaCl, 1mM KCl, 2.4mM $NaHCO_3$, 0.82mM $MgSO_4$, 0.33mM $Ca(NO_3)_2$, 0.33mM $CaCl_2$, 10mM Hepes and 10 µg/ml Streptomycin and Penicillin, pH 7.4. Single cells were dissociated in alkaline buffer (88mM NaCl, 1mM KCl and 10mM $NaHCO_3$, pH = 9.5) (Rohani et al., 2014). All subsequent assays were performed in 0.5x MBSH buffer, at room temperature (23^{o}C).

Live microscopy

For cell migration and open faced Keller explant assays, dissociated cells or explants were plated on glass bottom dishes (Cellvis) that had been coated in for 45 minutes with 10 µg/mL bovine FN

(Merck) followed by blocking with 5mg/mL bovine serum albumin (BSA). Cells and explants were then imaged on one of two spinning disk confocal microscopes: an Andor CSU-X1 with a iXon897 EMCCD camera controlled with Andor iQ3 software (Andor), or an Andor Dragonfly equipped with dual iXon888 EMCCD cameras and controlled by Fusion (Andor), both using a 40X 1.3 NA objective (Nikon).

Image analysis and quantification

All confocal images were deconvolved using either Huygens deconvolution software (SVI) or Fusion (Andor). Cadherin, p120-, and α-catenin signal was segmented using the 3D imagine software Imaris (Oxford Instruments) to extract the total signal and volume at the cell contact.

The signal of cadherin at the free membrane was determined using sum intensity projections of the seven Z planes surrounding the centre of the cell contact. Line scans were drawn from the cell-pipette interface of one cell to the other, and 5 µm on either side of the contact was considered for analysis.

Temporal correlation was determined by comparing the slopes of the total signals of p120 catenin-GFP, α-catenin-GFP, or C-cadherin-GFP to that of C-cadherin-tdTomato at each timepoint and calculating the correlation coefficient.

Dual pipette aspiration assay

Dissociated cells expressing fluorescent constructs were plated on a glass bottom custom-made chamber blocked for 45 minutes with BSA. The DPA assay was setup as described elsewhere (Biro and Maître, 2015), though instead of using large, fast displacements to rapidly detach cells and determine separation force, we incrementally displaced cell doublets 5 µm at a time while simultaneously imaging the double with confocal microscopy. We waited two to three minutes between each displacement to observe how the contact responded to increasing levels of force, and to imitate the speed at which cells migrate within the mesoderm or when freely migrating on FN (Kashkooli et al., 2021). Cells were manipulated with custom made pipettes with diameters from 13-17 µm with a 15° bend (Sutter Instruments) that were coated with BSA. Holding pressures of 80-400 Pa (condition dependent) were used to stably aspirate the cells for the course

of the displacement protocol. Pressure was controlled using a Microfluidic Flow Control System and the Maesflow software (Fluigent), and the pipettes were manipulated using PatchStar Micromanipulators and the LinLab2 software (Scientifica). A 25 µm Z-stack was acquired every 30 seconds until the cells detached using the Andor Dragonly microscope described above.

Contact lifetime assay

Dissociated cells were plated on FN coated glass bottom dishes and left to adhere for 30 minutes then imaged every 2.5 minutes for 150 minutes using a bright field inverted Olympus IX83 microscope equipped with a scMOS ZYLA 4.2 MP camera and a 10X 0.3 NA PH1 objective. Single cells that encountered another cell withing the first 40 minutes of observation were tracked and the duration of the cell-cell contact was measured. We counted any lifetime longer than 90 minutes as 90 minutes, as this was often near the point where cell viability decreased so any longer lifetimes could have been due to low cell viability. Inhibitors were added at the start of the timelapse, and equivalent concentrations of a DMSO vehicle control were added to the other conditions. When MHCIIA MO was injected the control cells were injected with an equivalent amount of control MO.

Migration assay

Dissociated cells were plated on fibronectin-coated glass bottom dishes and left to adhere for 45-60min, then imaged every 2.5min for 100-170min using a bright field inverted Olympus IX83 microscope (10X UPFLN 0.3NA PH1 objective) and a scMOS ZYLA 4.2 MP camera. Chemical inhibitors were added after four frames (10min) after the beginning of the time lapse. Addition of the inhibitor was set as time zero. The path of individual cells that did not establish contacts with neighbouring cells were manually tracked using ImageJ software. Average speed corresponds to the average of the speeds calculated between each consecutive time point.

References

Aberle, H., Butz, S., Stappert, J., Weissig, H., Kemler, R. and Hoschuetzky, H. (1994). Assembly of the cadherin-catenin complex in vitro with recombinant proteins. *Journal of Cell Science* **107**, 3655–3663.

Beetschen, J. C. (2001). Amphibian gastrulation: History and evolution of a 125 year-old concept. *International Journal of Developmental Biology* **45**, 771–795.

Belin, B. J., Goins, L. M. and Mullins, R. D. (2014). Comparative analysis of tools for live cell imaging of actin network architecture. *BioArchitecture* **4**, 189–202.

Bendix, P. M., Koenderink, G. H., Cuvelier, D., Dogic, Z., Koeleman, B. N., Brieher, W. M., Field, C. M., Mahadevan, L. and Weitz, D. A. (2008). A quantitative analysis of contractility in active cytoskeletal protein networks. *Biophysical Journal* **94**, 3126–3136.

Biro, M. and Maître, J. L. (2015). Dual pipette aspiration: A unique tool for studying intercellular adhesion. *Methods in Cell Biology* **125**, 255–267.

Boggon, T. J., Murray, J., Chappuis-Flament, S., Wong, E., Gumbiner, B. M. and Shapiro, L. (2002). C-cadherin ectodomain structure and implications for cell adhesion mechanisms. *Science* **296**, 1308–1313.

Brieher, W. M., Yap, A. S. and Gumbiner, B. M. (1996). Lateral dimerization is required for the homophilic binding activity of C-cadherin. *Journal of Cell Biology* **135**, 487–496.

Buckley, C. D., Tan, J., Anderson, K. L., Hanein, D., Volkmann, N., Weis, W. I., Nelson, W. J. and Dunn, A. R. (2014). The minimal cadherin-catenin complex binds to actin filaments under force. *Science* **346**,.

Canty, L., Zarour, E., Kashkooli, L., François, P. and Fagotto, F. (2017). Sorting at embryonic boundaries requires high heterotypic interfacial tension. *Nature Communications* **8**,.

Chang, K. C. and Hammer, D. A. (1996). Influence of direction and type of applied force on the detachment of macromolecularly-bound particles from surfaces. *Langmuir* **12**, 2271–2281.

Chu, Y. S., Thomas, W. A., Eder, O., Pincet, F., Perez, E., Thiery, J. P. and Dufour, S. (2004). Force measurements in E-cadherin-mediated cell doublets reveal rapid adhesion strengthened by actin cytoskeleton remodelling through Rac and Cdc42. *Journal of Cell Biology* **167**, 1183–1194.

Chu, Y. S., Eder, O., Thomas, W. A., Simcha, I., Pincet, F., Ben-Ze'ev, A., Perez, E., Thiery, J. P. and Dufour, S. (2006). Prototypical type I E-cadherin and type II cadherin-7 mediate very

distinct adhesiveness through their extracellular domains. *Journal of Biological Chemistry* **281**, 2901–2910.

Cramer, L. P. (2013). Mechanism of cell rear retraction in migrating cells. *Current Opinion in Cell Biology* **25**, 591–599.

Daniel, J. M. and Reynolds, A. B. (1995). The tyrosine kinase substrate p120cas binds directly to E-cadherin but not to the adenomatous polyposis coli protein or alpha-catenin. *Molecular and Cellular Biology* **15**, 4819–4824.

Davis, M. A., Ireton, R. C. and Reynolds, A. B. (2003). A core function for p120-catenin in cadherin turnover. *Journal of Cell Biology* **163**, 525–534.

de Beco, S., Gueudry, C., Amblard, F. and Coscoy, S. (2009). Endocytosis is required for E-cadherin redistribution at mature adherens junctions. *Proceedings of the National Academy of Sciences of the United States of America* **106**, 7010–7015.

Elia, L. P., Yamamoto, M., Zang, K. and Reichardt, L. F. (2006). p120 Catenin Regulates Dendritic Spine and Synapse Development through Rho-Family GTPases and Cadherins. *Neuron* **51**, 43–56.

Engl, W., Arasi, B., Yap, L. L., Thiery, J. P. and Viasnoff, V. (2014). Actin dynamics modulate mechanosensitive immobilization of E-cadherin at adherens junctions. *Nature Cell Biology* **16**, 584–591.

Ennomani, H., Letort, G., Guérin, C., Martiel, J. L., Cao, W., Nédélec, F., de La Cruz, E. M., Théry, M. and Blanchoin, L. (2016). Architecture and Connectivity Govern Actin Network Contractility. *Current Biology* **26**, 616–626.

Evren, S., Wen, J. W. H., Luu, O., Damm, E. W., Nagel, M. and Winklbauer, R. (2014). EphA4-dependent Brachyury expression is required for dorsal mesoderm involution in the Xenopus gastrula. *Development* **141**, 3649–3661.

Gao, X., Acharya, B. R., Engl, W. C. O., De Mets, R., Thiery, J. P., Yap, A. S. and Viasnoff, V. (2018). Probing compression versus stretch activated recruitment of cortical actin and apical junction proteins using mechanical stimulations of suspended doublets. *APL Bioengineering* **2**,.

Garrivier, D., Décavé, E., Bréchet, Y., Bruckert, F. and Fourcade, B. (2002). Peeling model for cell detachment. *European Physical Journal E* **8**, 79–97.

Green, J. B. A., New, H. v and Smith, J. C. (1992). *Responses of Embryonic Xenopus Cells to Activin and FGF Are Separated by Multiple Dose Thresholds and Correspond to Distinct Axes of the Mesoderm*.

Haase, K. and Pelling, A. E. (2013). Resiliency of the plasma membrane and actin cortex to large-scale deformation. *Cytoskeleton* **70**, 494–514.

Harrison, O. J., Jin, X., Hong, S., Bahna, F., Ahlsen, G., Brasch, J., Wu, Y., Vendome, J., Felsovalyi, K., Hampton, C. M., et al. (2011). The extracellular architecture of adherens junctions revealed by crystal structures of type i cadherins. *Structure* **19**, 244–256.

Huang, Y. and Winklbauer, R. (2018). Cell migration in the Xenopus gastrula. *Wiley Interdisciplinary Reviews: Developmental Biology* **7**,.

Huang, D. L., Bax, N. A., Buckley, C. D., Weis, W. I. and Dunn, A. R. (2017). Vinculin forms a directionally asymmetric catch bond with F-actin. *Science* **357**, 703–706.

Huber, O., Krohn, M. and Kemler, R. (1997). A specific domain in α-catenin mediates binding to β-catenin or plakoglobin. *Journal of Cell Science* **110**, 1759–1765.

Hulpiau, P. and van Roy, F. (2009). Molecular evolution of the cadherin superfamily. *International Journal of Biochemistry and Cell Biology* **41**, 349–369.

Hülsken, J., Birchmeier, W. and Behrens, J. (1994). E-cadherin and APC compete for the interaction with β-catenin and the cytoskeleton. *Journal of Cell Biology* **127**, 2061–2069.

Ireton, R. C., Davis, M. A., Van Hengel, J., Mariner, D. J., Barnes, K., Thoreson, M. A., Anastasiadis, P. Z., Matrisian, L., Bundy, L. M., Sealy, L., et al. (2002). A novel role for p120 catenin in E-cadherin function. *Journal of Cell Biology* **159**, 465–476.

Ishiyama, N., Lee, S. H., Liu, S., Li, G. Y., Smith, M. J., Reichardt, L. F. and Ikura, M. (2010). Dynamic and Static Interactions between p120 Catenin and E-Cadherin Regulate the Stability of Cell-Cell Adhesion. *Cell* **141**, 117–128.

Iyer, K. V., Piscitello-Gómez, R., Paijmans, J., Jülicher, F. and Eaton, S. (2019). Epithelial Viscoelasticity Is Regulated by Mechanosensitive E-cadherin Turnover. *Current Biology* **29**, 578-591.e5.

Izumi, G., Sakisaka, T., Baba, T., Tanaka, S., Morimoto, K. and Takai, Y. (2004). Endocytosis of E-cadherin regulated by Rac and Cdc42 small G proteins through IQGAP1 and actin filaments. *Journal of Cell Biology* **166**, 237–248.

Jay, P. Y., Pham, P. A., Wong, S. A. and Elson, E. L. (1995). A mechanical function of myosin II in cell motility. *Journal of Cell Science* **108**, 387–393.

Kale, G. R., Yang, X., Philippe, J. M., Mani, M., Lenne, P. F. and Lecuit, T. (2018). Distinct contributions of tensile and shear stress on E-cadherin levels during morphogenesis. *Nature Communications* **9**,.

Kashkooli, L., Rozema, D., Espejo-Ramirez, L., Lasko, P. and Fagotto, F. (2021). Ectoderm to mesoderm transition by down-regulation of actomyosin contractility. *PLOS Biology* **19**(1): e3001060.

Ladoux, B., Anon, E., Lambert, M., Rabodzey, A., Hersen, P., Buguin, A., Silberzan, P. and Mège, R. M. (2010). Strength dependence of cadherin-mediated adhesions. *Biophysical Journal* **98**, 534–542.

Le, T. L., Yap, A. S. and Stow, J. L. (1999). Recycling of E-cadherin: A potential mechanism for regulating cadherin dynamics. *Journal of Cell Biology* **146**, 219–232.

Levayer, R., Pelissier-Monier, A. and Lecuit, T. (2011). Spatial regulation of Dia and Myosin-II by RhoGEF2 controls initiation of E-cadherin endocytosis during epithelial morphogenesis. *Nature Cell Biology* **13**, 529–540.

Liu, Z., Tan, J. L., Cohen, D. M., Yang, M. T., Sniadecki, N. J., Ruiz, S. A., Nelson, C. M. and Chen, C. S. (2010). Mechanical tugging force regulates the size of cell-cell junctions. *Proceedings of the National Academy of Sciences of the United States of America* **107**, 9944–9949.

Maître, J. L. and Heisenberg, C. P. (2013). Three functions of cadherins in cell adhesion. *Current Biology* **23**, 626–633.

Maître, J. L., Berthoumieux, H., Krens, S. F. G., Salbreux, G., Jülicher, F., Paluch, E. and Heisenberg, C. P. (2012). Adhesion functions in cell sorting by mechanically coupling the cortices of adhering cells. *Science* **338**, 253–256.

McCrea, P. D. and Gumbiner, B. M. (1991). Purification of a 92-kDa cytoplasmic protein tightly associated with the cell-cell adhesion molecule E-cadherin (uvomorulin): Characterization and extractability of the protein complex from the cell cytostructure. *Journal of Biological Chemistry* **266**, 4514–4520.

Miyashita, Y. and Ozawa, M. (2007). Increased internalization of p120-uncoupled E-cadherin and a requirement for a dileucine motif in the cytoplasmic domain for endocytosis of the protein. *Journal of Biological Chemistry* **282**, 11540–11548.

Mulhall, E. M., Ward, A., Yang, D., Koussa, M. A., Corey, D. P. and Wong, W. P. (2021). Single-molecule force spectroscopy reveals the dynamic strength of the hair-cell tip-link connection. *Nature Communications* **12**, 1–15.

Nagar, B., Overduin, M., Ikura, M. and Rini, J. M. (1996). Structural basis of calcium-induced E-cadherin rigidification and dimerization. *Nature* **380**, 360–364.

Nanes, B. A., Chiasson-MacKenzie, C., Lowery, A. M., Ishiyama, N., Faundez, V., Ikura, M., Vincent, P. A. and Kowalczyk, A. P. (2012). P120-Catenin Binding Masks an Endocytic Signal Conserved in Classical Cadherins. *Journal of Cell Biology* **199**, 365–380.

Noren, N. K., Liu, B. P., Burridge, K. and Kreft, B. (2000). p120 Catenin regulates the actin cytoskeleton via RHO family GTPases. *Journal of Cell Biology* **150**, 567–579.

Peglion, F., Llense, F. and Etienne-Manneville, S. (2014). Adherens junction treadmilling during collective migration. *Nature Cell Biology* **16**, 639–651.

Pinheiro, D. and Bellaïche, Y. (2018). Mechanical Force-Driven Adherens Junction Remodelling and Epithelial Dynamics. *Developmental Cell* **47**, 3–19.

Rakshit, S., Zhang, Y., Manibog, K., Shafraz, O. and Sivasankar, S. (2012). Ideal, catch, and slip bonds in cadherin adhesion. *Proceedings of the National Academy of Sciences of the United States of America* **109**, 18815–18820.

Ridley, A. J., Schwartz, M. A., Burridge, K., Firtel, R. A., Ginsberg, M. H., Borisy, G., Parsons, J. T. and Horwitz, A. R. (2003). Cell migration: integrating signals from front to back. *Science (New York, N.Y.)* **302**, 1704–1709.

Rimm, D. L., Koslov, E. R., Kebriaei, P., Cianci, C. D. and Morrow, J. S. (1995). α1(E)-catenin is an actin-binding and -bundling protein mediating the attachment of F-actin to the membrane adhesion complex. *Proceedings of the National Academy of Sciences of the United States of America* **92**, 8813–8817.

Rohani, N., Parmeggiani, A., Winklbauer, R. and Fagotto, F. (2014). Variable Combinations of Specific Ephrin Ligand/Eph Receptor Pairs Control Embryonic Tissue Separation. *PLoS Biology* **12**,.

Roycroft, A., Szabó, A., Bahm, I., Daly, L., Charras, G., Parsons, M. and Mayor, R. (2018). Redistribution of Adhesive Forces through Src/FAK Drives Contact Inhibition of Locomotion in Neural Crest. *Developmental Cell* **45**, 565-579.e3.

Selhuber-Unkel, C., Erdmann, T., López-García, M., Kessler, H., Schwarz, U. S. and Spatz, J. P. (2010). Cell adhesion strength is controlled by intermolecular spacing of adhesion receptors. *Biophysical Journal* **98**, 543–551.

Shapiro, L., Fannon, A. M., Kwong, P. D., Thompson, A., Lehmann, M. S., Grübel, G., Legrand, J. F., Als-Nielson, J., Colma, D. R. and Hendricksonn, W. A. (1995). Hydrophobe Interaktions-Chromatographie Structural basis of cell-cell adhesion by cadherins. *Merck Spectrum* **2**, 24–25.

Shih, J., and Keller, R. (1992). Cell motility driving mediolateral intercalation in explants of Xenopus laevis. *Development* **116**, 901-914.

Shindo, A., and Wallingford, J.B. (2014). PCP and septins compartmentalize cortical actomyosin to direct collective cell movement. *Science* **343**, 649-52.

Smith, J. C., Symesh, K., Hynes, R. O. and Desimone, D. (1990). *Mesoderm induction and the control of gastrulation in Xenopus laevis: the roles of fibronectin and integrins*.

Stappert, J. and Kemler, R. (1994). A short core region of e-cadherin is essential for catenin binding and is highly phosphorylated. *Cell Communication and Adhesion* **2**, 319–327.

Symes, K. and Smith, J. C. (1987). *Gastrulation movements provide an early marker of mesoderm induction in Xenopus laevis*.

Takeichi, M. (2014). Dynamic contacts: Rearranging adherens junctions to drive epithelial remodelling. *Nature Reviews Molecular Cell Biology* **15**, 397–410.

Troyanovsky, R. B., Sokolov, E. P. and Troyanovsky, S. M. (2006). Endocytosis of cadherin from intracellular junctions is the driving force for cadherin adhesive dimer disassembly. *Molecular biology of the cell* **17**, 3484–3493.

Truong Quang, B. A., Mani, M., Markova, O., Lecuit, T. and Lenne, P. F. (2013). Principles of E-cadherin supramolecular organization in vivo. *Current Biology* **23**, 2197–2207.

Vu, V., Light, T., Sullivan, B., Greiner, D., Hristova, K. and Leckband, D. (2021). P120 catenin potentiates constitutive E-cadherin dimerization at the plasma membrane and regulates trans binding. *Current Biology* 1–11.

Wardle, F. C. and Smith, J. C. (2004). Refinement of gene expression patterns in the early Xenopus embryo. *Development* **131**, 4687–4696.

West, J. J. and Harris, T. J. C. (2016). Cadherin Trafficking for Tissue Morphogenesis: Control and Consequences. *Traffic* **17**, 1233–1243.

Wildenberg, G. A., Dohn, M. R., Carnahan, R. H., Davis, M. A., Lobdell, N. A., Settleman, J. and Reynolds, A. B. (2006). p120-Catenin and p190RhoGAP Regulate Cell-Cell Adhesion by Coordinating Antagonism between Rac and Rho. *Cell* **127**, 1027–1039.

Winklbauer, R. (2015). Cell adhesion strength from cortical tension - An integration of concepts. *Journal of Cell Science* **128**, 3687–3693.

Wu, Y., Jin, X., Harrison, O., Shapiro, L., Honig, B. H. and Ben-Shaul, A. (2010). Cooperativity between trans and cis interactions in cadherin-mediated junction formation. *Proceedings of the National Academy of Sciences of the United States of America* **107**, 17592–17597.

Wu, Y., Vendome, J., Shapiro, L., Ben-Shaul, A. and Honig, B. (2011). Transforming binding affinities from three dimensions to two with application to cadherin clustering. *Nature* **475**, 510–513.

Wu, Y., Kanchanawong, P. and Zaidel-Bar, R. (2015). Actin-Delimited Adhesion-Independent Clustering of E-Cadherin Forms the Nanoscale Building Blocks of Adherens Junctions. *Developmental Cell* **32**, 139–154.

Xiao, K., Allison, D. F., Buckley, K. M., Kottke, M. D., Vincent, P. A., Faundez, V. and Kowalczyk, A. P. (2003). Cellular levels of p120 catenin function as a set point for cadherin expression levels in microvascular endothelial cells. *Journal of Cell Biology* **163**, 535–545.

Yao, M., Qiu, W., Liu, R., Efremov, A. K., Cong, P., Seddiki, R., Payre, M., Lim, C. T., Ladoux, B., Mège, R. M., et al. (2014). Force-dependent conformational switch of α -catenin controls vinculin binding. *Nature Communications* **5**,.

Yap, A. S., Niessen, C. M. and Gumbiner, B. M. (1998). The juxtamembrane region of the cadherin cytoplasmic tail supports lateral clustering, adhesive strengthening, and interaction with p120(ctn). *Journal of Cell Biology* **141**, 779–789.

Yap, A. S., Gomez, G. A. and Parton, R. G. (2015). Adherens Junctions Revisualized: Organizing Cadherins as Nanoassemblies. *Developmental Cell* **35**, 12–20.

Yonemura, S., Wada, Y., Watanabe, T., Nagafuchi, A. and Shibata, M. (2010). α-Catenin as a tension transducer that induces adherens junction development. *Nature Cell Biology* **12**, 533–542.

Figures

Figure 3.1

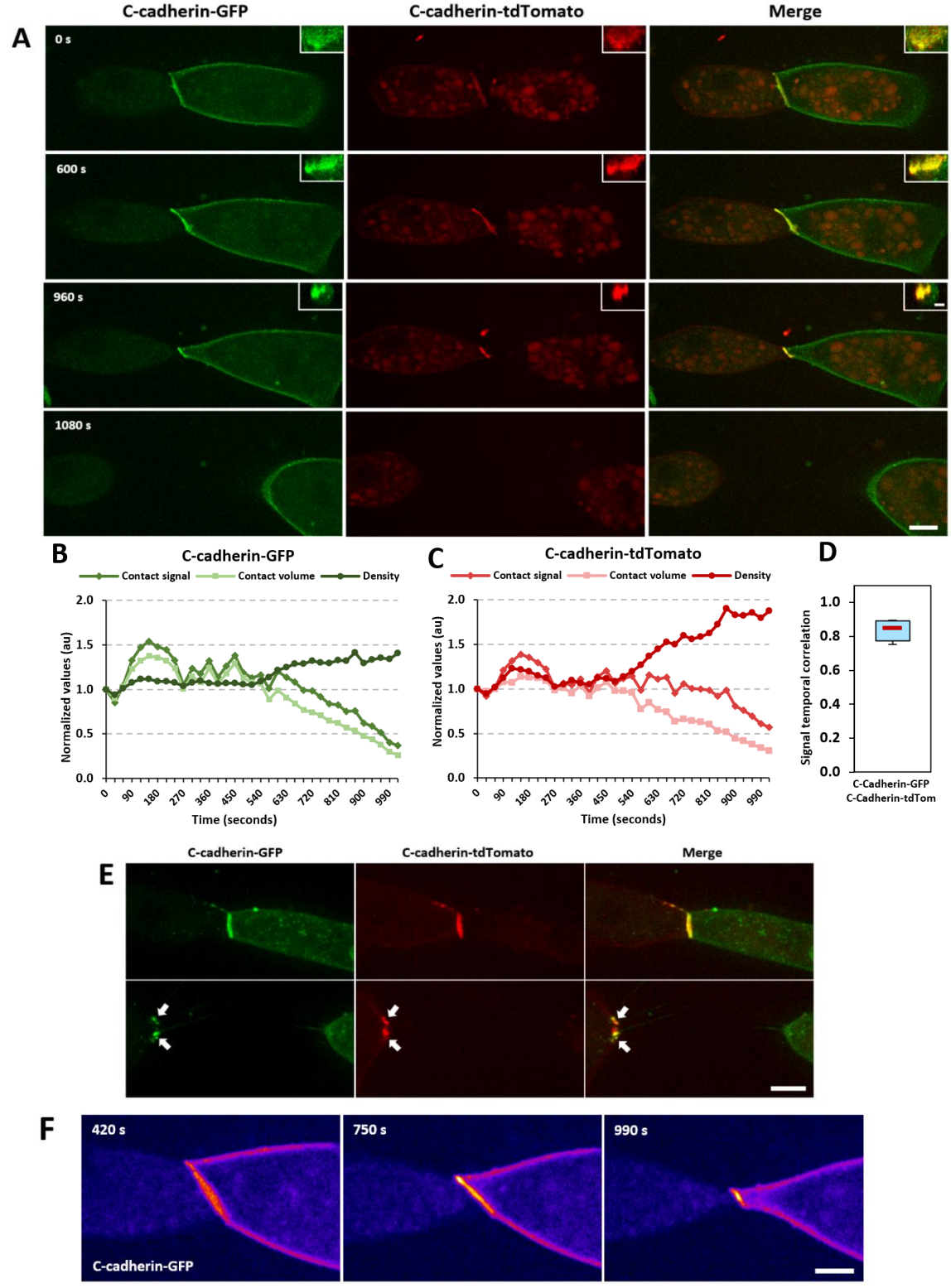

Figure 3.2

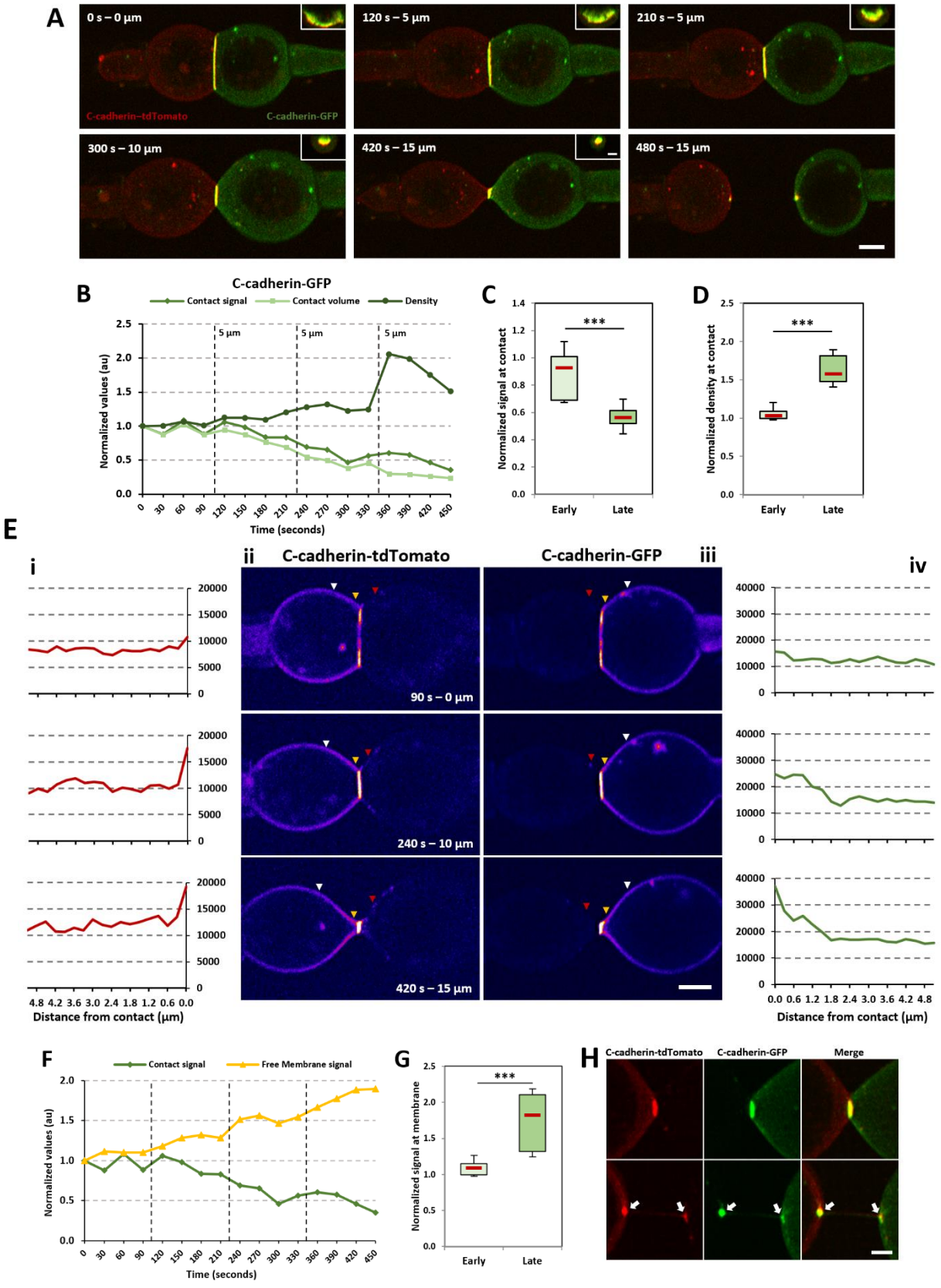
A
0 s – 0 µm
120 s – 5 µm
210 s – 5 µm
C-cadherin–tdTomato
C-cadherin-GFP
300 s – 10 µm
420 s – 15 µm
480 s – 15 µm
B
C-cadherin-GFP
Contact signal
Contact volume
Density
5 µm
Normalized values (au)
Time (seconds)
C
Normalized signal at contact
***
Early
Late
D
Normalized density at contact
***
Early
Late
E
i
ii C-cadherin-tdTomato
C-cadherin-GFP
iii
iv
90 s – 0 µm
240 s – 10 µm
420 s – 15 µm
Distance from contact (µm)
F
Contact signal
Free Membrane signal
Normalized values (au)
Time (seconds)
G
Normalized signal at membrane
***
Early
Late
H
C-cadherin-tdTomato
C-cadherin-GFP
Merge

Figure 3.3

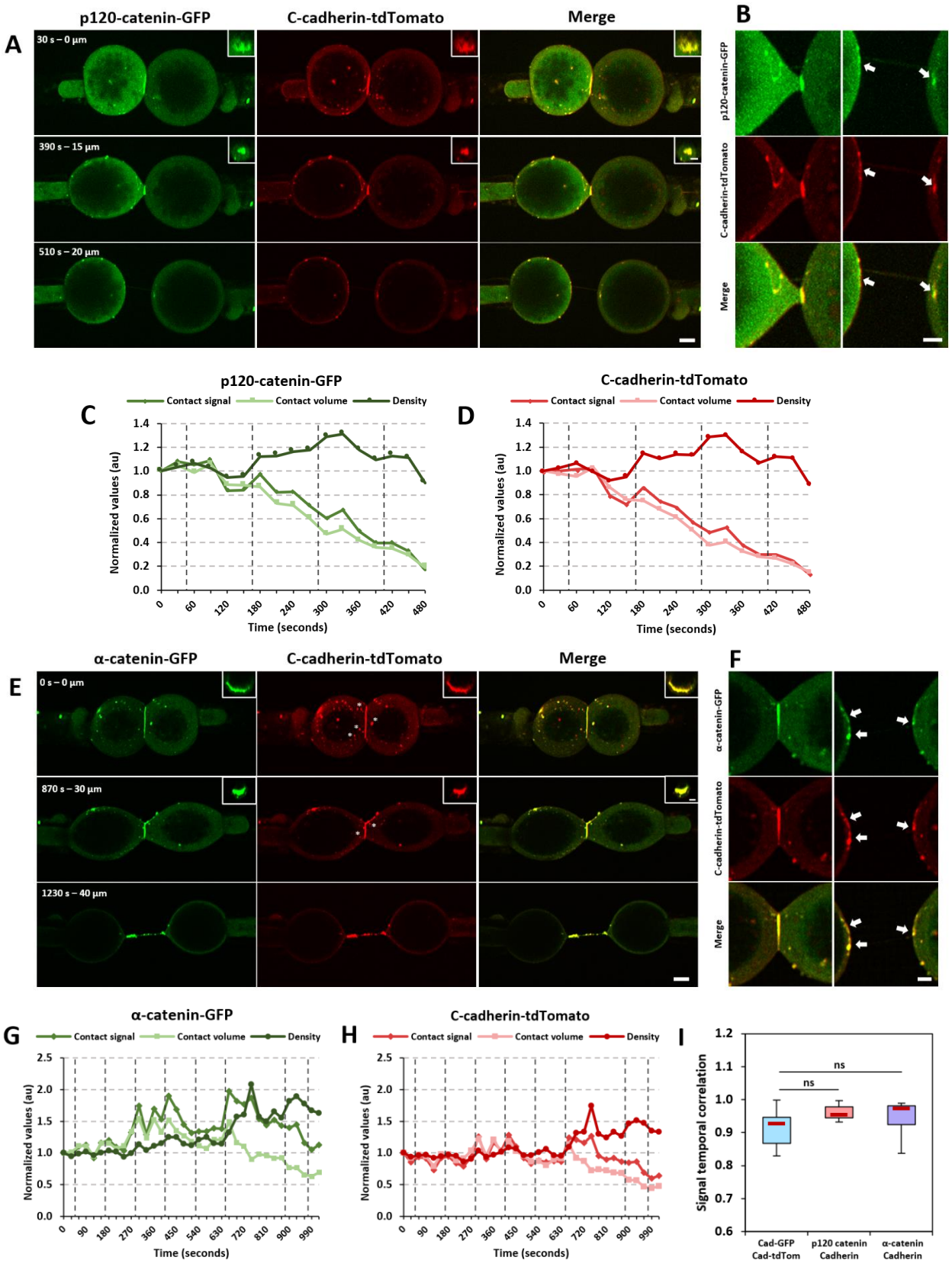
A
p120-catenin-GFP
C-cadherin-tdTomato
Merge
30 s – 0 µm
390 s – 15 µm
510 s – 20 µm
B
p120-catenin-GFP
C-cadherin-tdTomato
Merge
C
p120-catenin-GFP
Contact signal
Contact volume
Density
Normalized values (au)
Time (seconds)
D
C-cadherin-tdTomato
Contact signal
Contact volume
Density
Normalized values (au)
Time (seconds)
E
α-catenin-GFP
C-cadherin-tdTomato
Merge
0 s – 0 µm
870 s – 30 µm
1230 s – 40 µm
F
α-catenin-GFP
C-cadherin-tdTomato
Merge
G
α-catenin-GFP
Contact signal
Contact volume
Density
Normalized values (au)
Time (seconds)
H
C-cadherin-tdTomato
Contact signal
Contact volume
Density
Normalized values (au)
Time (seconds)
I
Signal temporal correlation
ns
ns
Cad-GFP
Cad-tdTom
p120 catenin
Cadherin
α-catenin
Cadherin

Figure 3.4

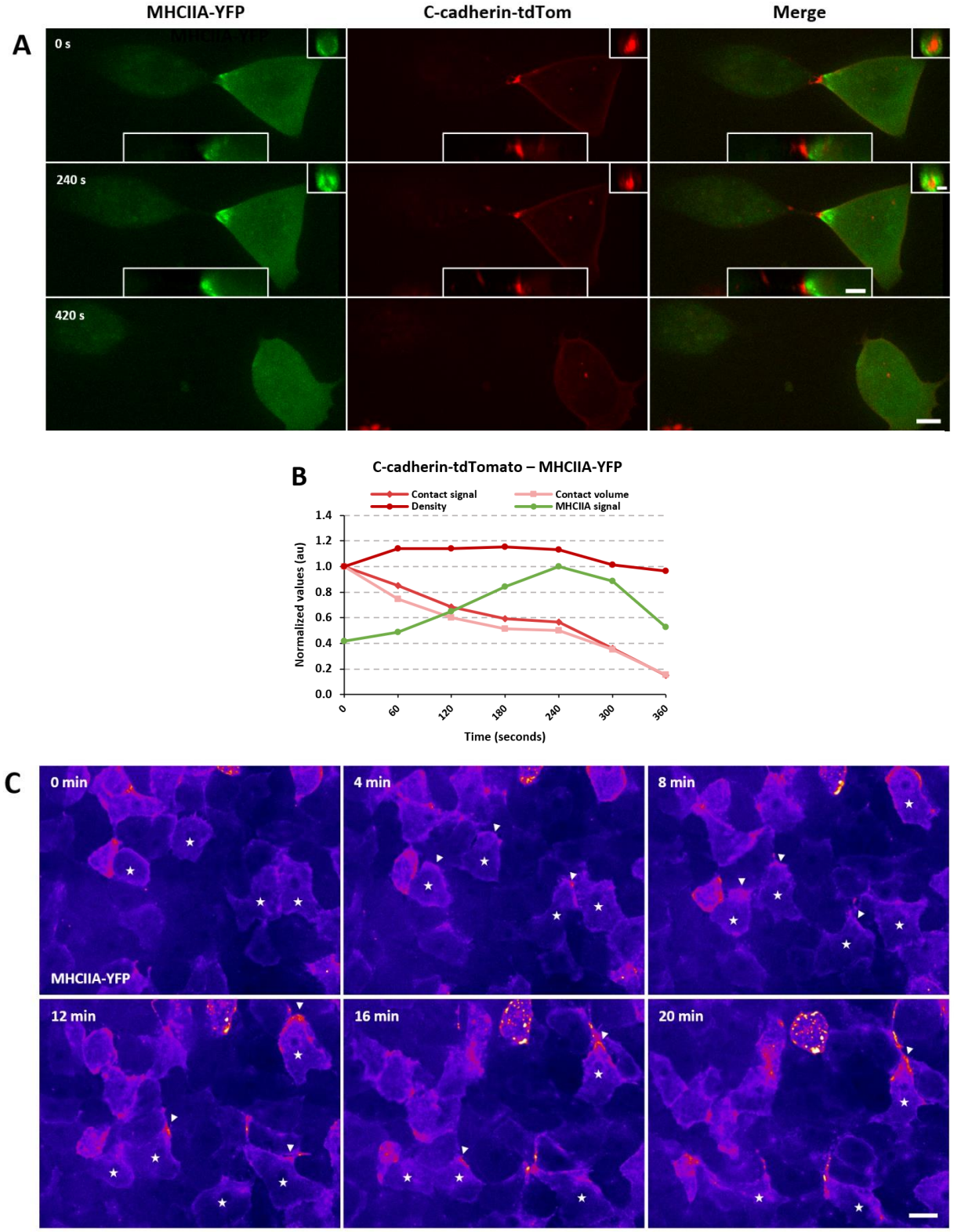
MHCIIA-YFP
C-cadherin-tdTom
Merge
A
0 s
240 s
420 s
B
C-cadherin-tdTomato – MHCIIA-YFP
Contact signal
Density
Contact volume
MHCIIA signal
Normalized values (au)
Time (seconds)
C
0 min
4 min
8 min
MHCIIA-YFP
12 min
16 min
20 min

Figure 3.5

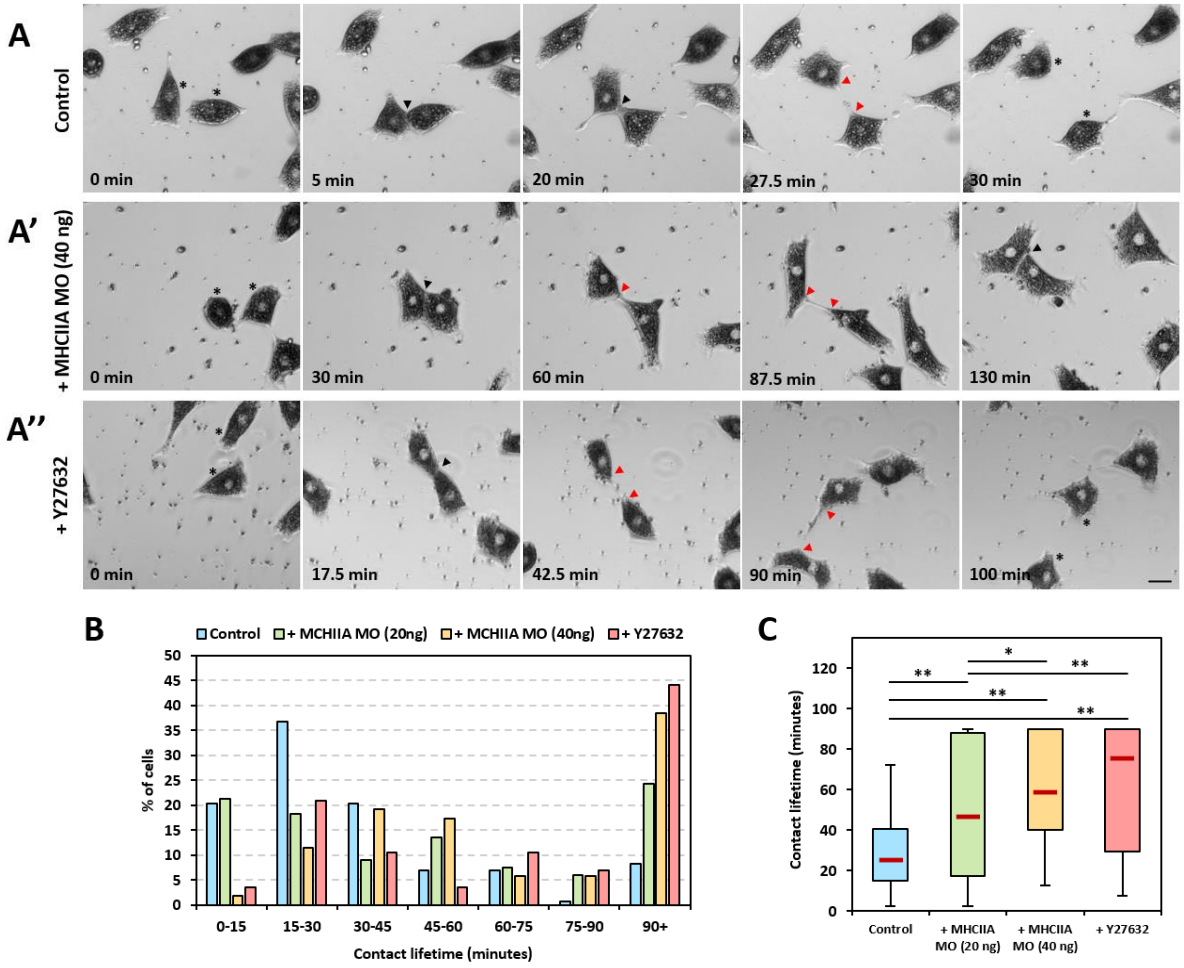
A
Control
0 min
5 min
20 min
27.5 min
30 min
A'
+ MHCIIA MO (40 ng)
0 min
30 min
60 min
87.5 min
130 min
A''
+ Y27632
0 min
17.5 min
42.5 min
90 min
100 min
B
Control
+ MCHIIA MO (20ng)
+ MCHIIA MO (40ng)
+ Y27632
% of cells
0-15
15-30
30-45
45-60
60-75
75-90
90+
Contact lifetime (minutes)
C
Contact lifetime (minutes)
Control
+ MHCIIA MO (20 ng)
+ MHCIIA MO (40 ng)
+ Y27632

Figure 3.6

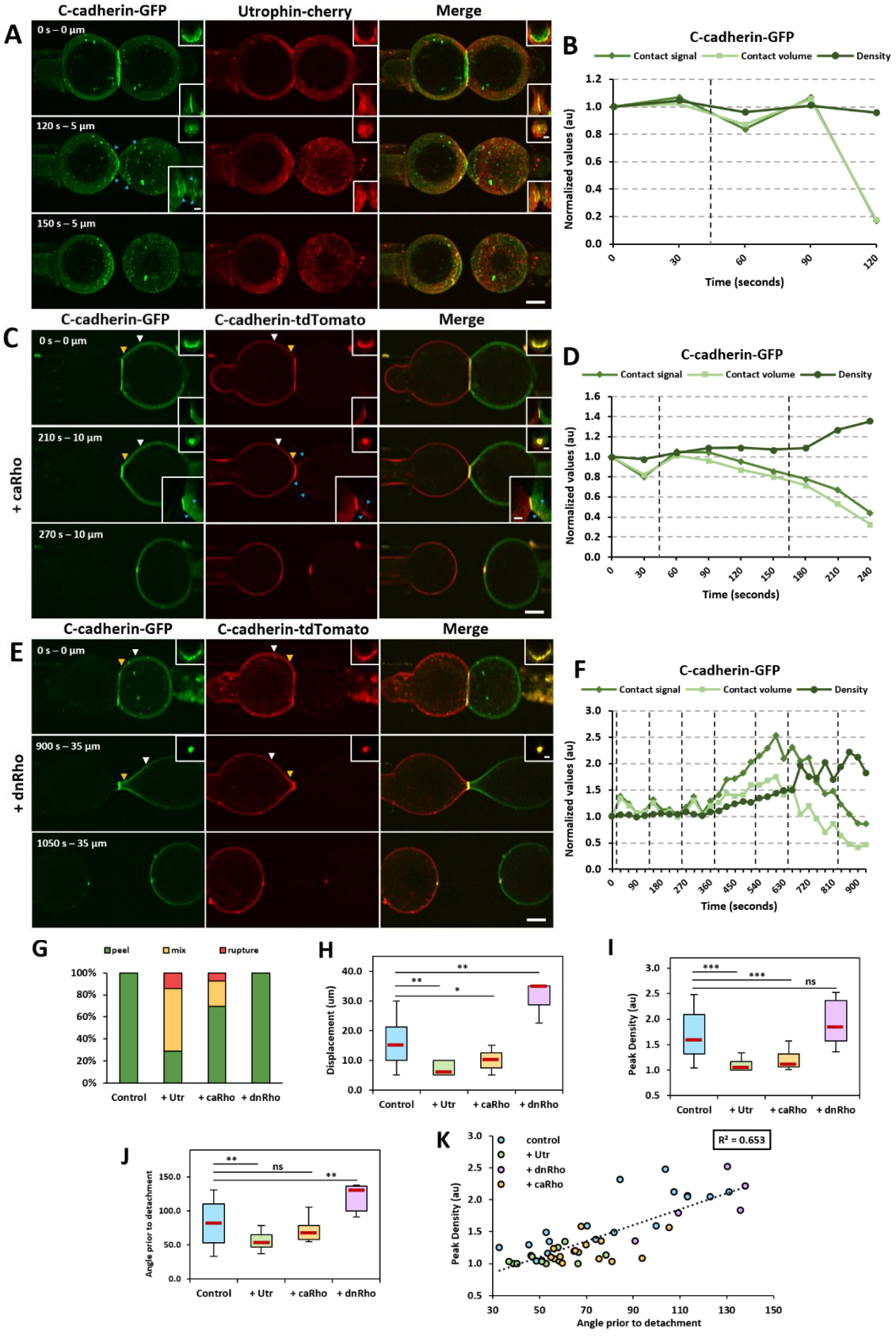
A
C-cadherin-GFP
Utrophin-cherry
Merge
0 s – 0 µm
120 s – 5 µm
150 s – 5 µm
B
C-cadherin-GFP
Contact signal
Contact volume
Density
Normalized values (au)
Time (seconds)
C
C-cadherin-GFP
C-cadherin-tdTomato
Merge
0 s – 0 µm
210 s – 10 µm
270 s – 10 µm
+ caRho
D
C-cadherin-GFP
Contact signal
Contact volume
Density
Normalized values (au)
Time (seconds)
E
C-cadherin-GFP
C-cadherin-tdTomato
Merge
0 s – 0 µm
900 s – 35 µm
1050 s – 35 µm
+ dnRho
F
C-cadherin-GFP
Contact signal
Contact volume
Density
Normalized values (au)
Time (seconds)
G
peel
mix
rupture
Control
+ Utr
+ caRho
+ dnRho
H
Displacement (um)
Control
+ Utr
+ caRho
+ dnRho
I
Peak Density (au)
ns
Control
+ Utr
+ caRho
+ dnRho
J
Angle prior to detachment
ns
Control
+ Utr
+ caRho
+ dnRho
K
control
+ Utr
+ dnRho
+ caRho
R² = 0.653
Peak Density (au)
Angle prior to detachment

Figure 3.7

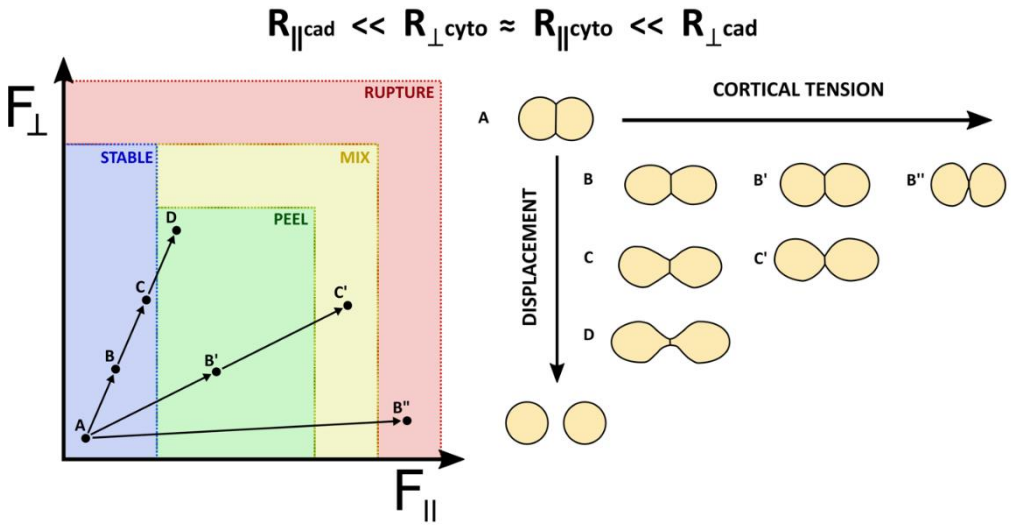
$R_{\parallel cad} << R_{\perp cyto} \approx R_{\parallel cyto} << R_{\perp cad}$
$F_\perp$
$F_\parallel$
RUPTURE
STABLE
MIX
PEEL
A
B
B'
B''
C
C'
D
CORTICAL TENSION
DISPLACEMENT

Figure Legends

Figure 3.1 – Contact remodelling during FN mediated cell migration shows a concomitant removal and condensation of cadherin from the cell contact. (A) A maximum intensity projection from a timelapse of a cell doublet plated on FN. The cell on the right is expressing C-cadherin-GFP and the cell on the left C-cadherin-tdTomato. A Z-stack of 12 µm was acquired every 30 seconds. The top right corner is a max projection of the YZ orthogonal view of the contact. Scale bar is 15 µm for Z projection and 5 µm for the YZ orthogonal view. (B,C) Quantification of total contact signal, volume, and average density for C-cadherin-GFP and C-cadherin-tdTomato of the cell double shown in (A). All values are normalized to the first timepoint. (D) Temporal correlation of the total cadherin signal comparing the slopes of C-cadherin-GFP and C-cadherin-tdTomato demonstrating that despite variations in magnitude of change, the overall patterns are consistent for both sides of the contact during remodelling. Comparison of seven doublets from five experiments. (E) Max intensity projection of a doublet prior and post detachment. White arrows highlight cadherin clusters containing cadherins from both cells after detachment of the cell contact, indicating that the contact ruptured cytoplasmically. Scale bar 15 µm. (F) A sum intensity projection of seven Z slices centred around the middle of the contact coloured with a fire LUT to emphasize changes in intensity. Examining the cytoplasm reveals no trace of intracellular cadherin. Scale bar is 10 µm.

Figure 3.2 – Displacement of cells using dual pipette aspiration reveals a consistent cell contact remodelling and detachment paradigm with cadherin removed from the contact diffusing on the free membrane.

(A-D) General description of cadherin remodelling

(A) Frames of a maximum intensity projection of a doublet being displaced using the DPA setup. The cell on the right is expressing C-cadherin-GFP and the cell on the left C-cadherin-tdTomato. A Z-stack of 25 µm was acquired every 30 seconds. The time and displacement are noted in the top left for each frame. The inset in the top right is a max projection of the YZ orthogonal view of

the contact. Scale bar is 15 µm for Z projection and 5 µm for the YZ orthogonal view. (B) Quantification of total contact signal, volume, and average density for C-cadherin-GFP and C-cadherin-tdTomato of the cell doublet shown in (A). All values are normalized to the first timepoint. Each vertical dashed line represents when the doublet was displaced by 5 µm. (C,D) Quantification of the total signal at the contact and average density of cadherin comparing average values from two minutes (four timepoints) of the early stages of remodelling to the two minutes immediately prior to detachment.

(E-G) Quantification of diffusion of cadherin onto lateral membrane

(E) (ii,iii) Sum intensity projections of seven Z slices centred around the middle of the cell contact, coloured with fire LUT to emphasize differences in intensity. Yellow arrowheads highlight increasing signal at the free membrane immediately adjacent to the contact, white arrowheads highlight the constant signal of the free membrane further from the contact suggesting increasing signal is coming from cadherin removed from the cell contact. Red arrowheads highlight the either lack of or very low levels of cadherin from one cell diffusing onto it's neighbour, suggesting that the adhesive trans bond of cadherin is ruptured. Scale bar is 15 µm (i, iv) Line scans of the 5 µm adjacent to the contact that reveal increasing signal intensity at the free membrane. (F) Comparison of the normalized signal at the contact and the free membrane of the doublet shown in (D), demonstrating that the membrane signal is enriched as the contact signal decreases. Vertical dashes indicate 5 µm displacements. (G) Pooled quantification of the membrane signal of multiple doublets comparing the early and late stages of remodelling as described above.

(H) Max intensity projection of the frames immediately prior to and following detachment of a cell contact. Arrows indicate clusters that contain cadherin from both cells, demonstrating that cadherin is ruptured cytoplasmically at the final step of detachment. Scale bar is 5 µm.

Statistical comparison for (C,D,G) using a paired students t-test. Nine doublets compared from six separate experiments. P-values < 0.001.

Figure 3.3 – Imaging p120 and α-catenin demonstrates that the entire cadherin-catenin complex is simultaneously remodelled. (A, E) Frames of a maximum intensity projection of doublets being displaced using the DPA setup. Cells co-express C-cadherin-tdTomato with p120 catenin (A) or α-catenin (E). 25 µm Z-stacks were acquired every 30 seconds. Time and displacement are noted in top left corner, while the top right is a maximum intensity projection of the YZ orthogonal view of the contact. Scale bars are 15 µm for Z projection and 5 µm for the YZ orthogonal view. (C,D,G,H) Quantification of total contact signal, volume, and average density for C-cadherin-tdTomato (D,H), p120 catenin-GFP (C), and α-catenin-GFP (G). Values are normalized to the first timepoint. (B, F) Max intensity projection of the frames immediately prior to and following detachment of a cell contact. Arrows indicate clusters that contain cadherin and p120 catenin (B) or cadherin and α-catenin (F), further supporting the idea that the final detachment involves the rupture of one of the CCCs cytoplasmic interactions. White asterisks denote clusters that may appear cytoplasmic that are in fact on the free membrane on lower Z planes of the image stack. See also Figure S3.1 (I) Temporal correlation of the slopes of the total contact signal comparing C-cadherin-tdTomato to either C-cadherin-GFP (n=9, 7 experiments), p120 catenin-GFP (n=10, 3 experiments), or α-catenin-GFP (n=10, 4 experiements). Statistical comparison using a one-way ANOVA with a post hoc Tukey test.

Figure 3.4 – MHCIIA is recruited adjacent to the cell contact after condensation of cadherin and prior to contact detachment. (A) Maximum intensity projection of a cell doublet plated on FN and co-expressing C-cadherin-tdTomato and MHCIIA-YFP, the right hand cell having much higher expression. YZ and XZ orthogonal views are shown in the top right and bottom, respectively. A Z-stack of 12 µm was acquired every 60 seconds. Scale bars are 15 µm for Z projection, 10 µm for XZ view, and 5 µm for YZ view. (B) Quantification of total cadherin contact signal, volume, average density, normalized to the first time point. MHCIIA-YFP signal is shown normalized to peak level. (C) An open faced Keller explant of involuting mesoderm plated on FN and expressing MHCIIA-YFP, imaged every 2 minutes. Cells marked with a white star will detach from their trailing neighbour and show increased levels of MHCIIA at their rear (white arrowheads) prior to doing so. Scale bar is 20 µm.

Figure 3.5 – A contact lifetime assay reveals that myosin mediated contractility enhances the ability of cells to detach from each other. Representative timelapses of dissociated cells plated on FN and imaged every 2.5 minutes. Time zero is the initiation of the cell contact and the final frame is the cells after they detach (or not in the case of A'). Timelapses of control cells (A), cells injected with 40 ng MHCIIA MO (A'), or cells treated with the ROCK inhibitor Y27632 (A'') are shown. Asterisks indicate which cells form the tracked cell contact, black arrowheads highlight the contact, while red arrowheads mark the extended membrane protrusions that form between cells at late stages of contact remodelling prior to contact detachment. Scale bar is 30 µm. (B) Distribution of contact lifetimes in 15 minute bins for different groups. (C) Average lifetime for different treatment groups. Control (n=158, 4 experiments), MHCIIA MO 20 ng (n=66, 2 experiments), MHCIIA MO 40 ng (n=40, 2 experiments), Y27632 (n=86, 2 experiments). Statistical comparisons using a one-way ANOVA with a post hoc Tukey test. * p-value <0.05, ** p-value < 0.01.

Figure 3.6 – Altering levels of cortical tension changes how cells remodel their contacts in response to force. (A) Max intensity projection of cell doublet co-expressing C-cadherin-GFP and utrophin-cherry. YZ and XZ orthogonal views are shown in top and bottom right corners, respectively. Blue arrowheads indicate clusters that ruptured cytoplasmically prior to the final detachment of the contact. (C,E) Sum intensity projections of cell doublets expressing C-cadherin-GFP (left cells) or C-cadherin-tdTomato (right cells) and caRho (C) or dnRho (E). YZ and XZ (in C) orthogonal views are shown in top and bottom right corners, respectively. Blue arrowheads in (C) highlight ruptured clusters both coloured cadherins. Comparison of signal at the lateral membrane highlighted by yellow and white arrowheads show increasing signal on lateral membrane adjacent to cell contact. (A,C,E) 25 µm Z-stacks acquired every 30 seconds. Scale bar for Z-projections is 15 µm and 5 µm for the orthogonal views. (B,D,E) Quantification of total cadherin signal, volume, and average density at the contact. All values normalized to the first time point. Vertical dashed lines represent 5 µm displacements. (G) Characterization of contact remodelling strategy showing the proportion of cells that remodelled via peeling, cytoplasmic rupture, or a mix of both. (H, I, J) Quantification of displacement required for detachment, peak

cadherin density prior to detachment, and angle between the cells prior to detachment. Control (n=17, 12 experiments), + utrophin (n=15, 6 experiments), + caRho (n=13, 5 experiments), + dnRho (n=5, 2 experiments). Statistical analysis using a one-way ANOVA with a post hoc Tukey test. * p-value <0.05, ** p-value < 0.01, *** p-value < 0.001. (K) Scatter plot showing the correlation between peak density and angle prior to detachment of the cell contact, all conditions combined.

Figure 3.7 – Explanation for different modes of detachment resulting from changing cortical tensions. We propose that the most efficient way to disrupt the CCC is through peeling the extracellular cadherin trans bond (cadherin resistance to parallel force: $R_{\parallel}$cad), which requires the application of a force parallel to the contact ($F_{\parallel}$), while the most difficult way to do so is through applying a force perpendicular to the cell contact ($F_{\perp}$; $R_{\perp}$cad). The force required to disrupt the CCCs cytoplasmic link to the actin cytoskeleton lies intermediate between these values and may or may not be sensitive to the orientation at which the force is applied ($R_{\perp}$cyto; $R_{\parallel}$cyto). As discussed, changing cortical tension likely impacts the magnitude of the force applied on the contact for each subsequent 5 um displacement, as well as altering the deformability of the cell in response to an applied force which would change the orientation of the applied force. On the right a representation of a doublet at equilibrium is shown (A), and different scenarios based on the levels of cortical tension are proposed. On the left, a phase diagram showing the resulting effect on the contact for the application of different magnitudes and combinations of $F_{\perp}$ and $F_{\parallel}$. As observed, a doublet with lower cortical tension requires a larger net displacement to stimulate contact remodelling. This stems from both the decreased total force applied on the contact (smaller force arrows between each step), as well as the force being applied at a more oblique angle causing a larger proportion of that force being applied perpendicular to the contact (A, B, C). Doublets with an intermediate cortical tension have a larger applied force per step of displacement, resulting in larger applied forces (larger arrows between B' and C'). The more acute angle provides an ideal orientation so that peeling may immediately commence (B'), though if another displacement step is taken or the cortical tension is slightly higher, the cell may shift into the mixed regime where some clusters may be prone to cytoplasmic rupture while others are still

able to peel (C'). If the cortex tension of the doublet is very high, a small displacement will result in a very large force applied on the contact (B''). Though the cell is resistant to deformation and an ideal angle for peeling is maintained, this has little impact as the applied force is so large that it likely would have stimulated cytoplasmic rupture regardless of the orientation at which it was applied (B''). This model applies only to the remodelling of the contact up to the final stage, at which case every contact is ruptured cytoplasmically. The phase diagram assumes a constant level of cadherin at the contact; once removal of cadherin begins, the boxes will begin to shrink proportionally so that even when the cell is in a favourable orientation to peel it will eventually require cytoplasmic rupture to completely resolve the contact. This simple model also doesn't display the effects of increasing cadherin density as the contact is remodelled, which would ostensibly make it harder to rupture the extracellular cadherin trans bond through peeling. This could potentially stabilize the contact as peeling is less effective (PEEL and MIX zones become STABLE) and make cytoplasmic rupture the only option for disruption of the adhesion.

Supporting Information

Supplemental Table S1

List of mRNA used in this study with injected amounts

Plasmid	mRNA injected per blastomere at 2 cell stage (pg)
Constitutively active Alk4	1000
β-catenin	100
C-cadherin-GFP	600
C-cadherin-dTomato	600
p120 catenin-GFP	400
α-catenin-GFP	500
Non-muscle myosin heavy chain 2A (NMHC2A)-YFP	500
Utrophin261-cherry	200
Constitutively active RhoA (caRho)	50
Dominant negative RhoA (dnRho)	150

Supplemental Table S2

List of morpholinos with injected amounts

Target	Sequence	Amount/injected blastomore
C-cadherin	CCACCGTCCCGAACGAAGCCTCAT	20ng
MHCIIA	GATACTTGTCCACATCTGTTTGTGC	20 or 40 ng
Control	CCTCTTACCTCAGTTAACAATTTATA	20 or 40 ng

Supplemental Figures
Figure S3.1

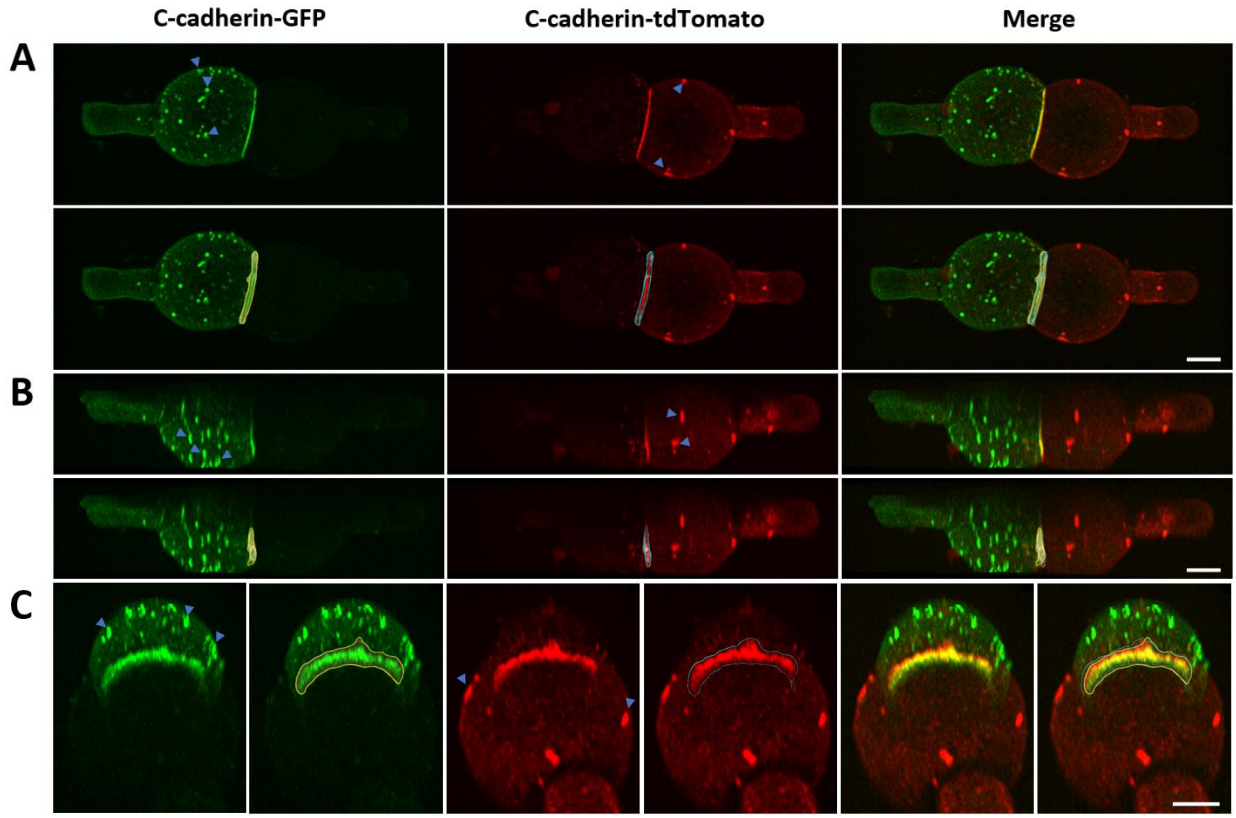

Figure S3.2

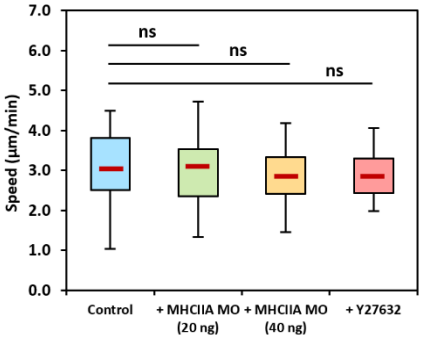

Figure S3.3

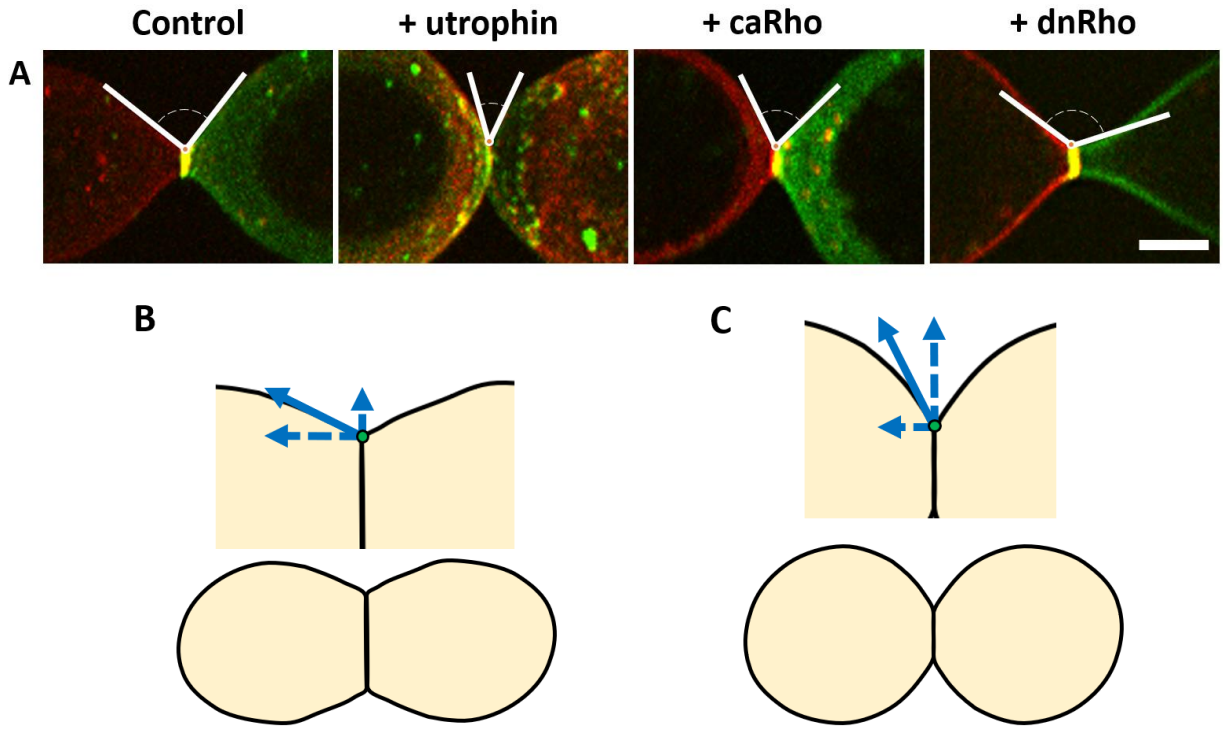

Supplemental Figure Legends

Figure S3.1 (related to Figure 3.1, 2, and 3) **– 3D segmentation of cadherin signal using Imaris –** Cells held using DPA assay visualized in the 3D imaging software, Imaris. Cell on left expressing C-cadherin-GFP, cell on right expressing C-cadherin-tdTomato (A) Top-down view view of cells. Bottom frame shows the segmentation output, yellow outline for C-cadherin-GFP and blue outline for C-cadherin-tdTomato. (B) Side view to highlight height of the contact. (C) View at angle to emphasize the shape of overall shape of the contact. Frames on right show segmentation output. Blue arrowheads highlight clusters that appear cytoplasmic from top-down or side views but are in fact clearly localized on the free membrane from the angled view. Scale bars are 10 μm.

Figure S3.2 (related to Figure 3.5) **– Migration speeds of single cells plated on FN –** Migration speeds of control, +MHCIIA MO (20ng), +MHCIIA MO (40ng), and +Y27632 treated single cells. No treatment had any effect on the rate of migration. Control: n=50(4); MHCIIA (20ng): n=39(2); MHCIIA (40ng): 35(2); Y27632: n=36(2). Statistical analysis using a one-way ANOVA with a post hoc Tukey test.

Figure S3 (related to Figure 3.6 and 7) **– Demonstration of angle measurements between two contact cells prior to detachment –** (A) Examples of cell-cell contacts immediately prior to detachment for control, +utrophin, +caRho, and +dnRho injected doublets. For control, caRho, and dnRho cells on the right are expressing C-cadherin-tdTomato and cells on the left are expressing C-cadherin-GFP. Utrophin injecting cells are co-expressing C-cadherin-GFP and utrophin-cherry. White lines show the tangent along the membranes that were used to calculate the angle. Control and +dnRho have oblique angles while +utrophin and +caRho show more acute angles. Scale bar 10 μm. (B,C) Graphics representing doublets who maintain oblique angles (B) or acute angles (C) upon displacement of the cells. Solid blue arrows show how the force would be applied tangential to the membrane. Dashed arrows show the perpendicular and parallel components of the applied force. Doublets that maintain oblique angles have a larger perpendicular component while doublets with acute angles have a larger parallel component.

Chapter IV – Final Discussion

Discussion

The work presented in this thesis sought to first understand how the migratory capacity of mesoderm was controlled, and next to explain how this migration drove cell-cell contact remodelling – both within the context of the *Xenopus laevis* gastrula. In this chapter, I will summarize the main findings, expand on the discussions, and address outstanding questions relevant to Chapters II and III, before discussing several interesting questions in the general field of cadherin biology.

Chapter II – Summary of findings

In Chapter II we directly compared the migratory properties of two tissues that display drastically different morphogenetic capabilities, the ectoderm and mesoderm of the *Xenopus* gastrula. After observing the dramatic transformation of the non-migratory ectoderm into a rapidly migrating cell type upon the chemical inhibition of ROCK induced myosin contractility, we searched for mesoderm specific negative regulators of RhoA. Our screen revealed two such regulators, Rnd1 and Shirin, whose depletion from the mesoderm completely blocked gastrulation. We systematically characterized the migratory and physical properties at both the single cell and tissue scale after overexpression in ectoderm or depletion in mesoderm, that revealed completely coherent results. Overexpression of Rnd1 or Shirin reduced cortical tension/surface tension of cells and tissues allowing them to spread and migrate. Strikingly, Shirin and Rnd1 each conferred a specific property of the collective migration of mesoderm: Shirin compromised cell-cell adhesion and induced a dispersive mode of migration, while Rnd1 is pro-adhesive and permits collective migration and rapid intercalation of cells. Though it was already established that downregulation of Rho-ROCK mediated contractility occurs to facilitate cell spreading, here we revealed a developmentally regulated downregulation that determines tissue-scale properties and is essential for morphogenesis. We termed this transition the 'ectoderm-to-mesoderm' transition and propose that it represents the most basal type of migratory switch, as the standard 'epithelial-to-mesenchymal' transition requires the alteration of more complex set of cell properties.

Chapter II – Outstanding questions and future directions

One of the most intriguing unexplored observations from this chapter is the latent contractility observed within the endogenous mesoderm. This is clearly demonstrated by the cycles of spreading and contracting of mesodermal explants on FN that are completely abolished upon ROCK inhibition. This suggests that the mesoderm likely expresses its own (set) positive regulator(s) of RhoA. Indeed, we unexpectantly found that the Rho GEF Plekhg5 is enriched in mesoderm. Initial characterization showed that depletion in the embryo blocked gastrulation, and overexpression in ectodermal explants increased the viscosity and tissue surface tension (data not shown). These preliminary results reveal that the mesoderm must maintain some contractility to generate and/or resist the forces that are exerted during gastrulation. Further characterization of the precise role of Plekhg5 is required to see if it has roles beyond the tuning of the physical properties of the mesoderm. It is tempting to speculate that it may be required for the recruitment of myosin that occurs prior to cell-cell detachment (Figure 3.4). Plekhg5 loss-of-function may then have similar effects to MHCIIA depletion or ROCK inhibition, compromising the efficiency of the final contact rupture (Figure 3.5). Such defect may well account for the strong inhibition of the global movement of involution.

While we showed that ectopic expression of either Rnd1 or Shirin was sufficient to induce spreading and migration of ectoderm, these regulators alone were clearly not able to fully reconstitute mesoderm behaviour. For instance, the migratory speed of single cells is lower than that of mesoderm (Figure 2.1G, 2.5I), even though collective spreading of explants is induced remarkably efficiently (Figure 2.9H). Along the same line, the differences in adhesive properties are not well recapitulated, neither by depletion in the mesoderm, nor expression in the mesoderm (Figure 2.4G,H). Note that we have systematically titrated the amounts of mRNA injected, thus the issue cannot simply be explained by insufficient expression or on the contrary overexpression. The obvious explanation is that the combined action of both regulators is required. We did attempt preliminary co-expression experiments, trying a few combinations (different amounts of injected mRNA) on the single cell migration assay, but did not obtain any significant increase in migration speed. Such experiments should certainly be pursued. Even if a systematic titration of both components may help, a better approach will be to establish the

actual levels of Rnd1 and Shirin expression in the mesoderm. So far, we only performed qPCR as antibodies were not available. The team has now been raising antibodies against the two proteins, which should allow in the near future to directly estimate protein levels, and thus also refine the design of experimental manipulations. The above-mentioned possibility to titrate injected mRNAs is a great advantage of the Xenopus embryo, which allows to achieve rather precise expression levels. However, another obvious possibility is that other regulators contribute to mesoderm properties. Besides Plekhg5, a few other candidates were identified in the original screen, which should be further investigated.

Related to this, determining the relative abundance of Rnd1 and Shirin in cells could help reveal more about their specific functions. Though not direct, one way to approach this would be to perform single molecule inexpensive FISH (smiFISH) to simultaneously image and quantify the amount of Shirin and Rnd1 transcripts (Tsanov et al., 2016). This would allow us to directly quantify the relative abundance of Shirin and Rnd1 within individual cells in fixed slices of the involuting mesoderm. It would be interesting to see if the relative abundance of these transcripts depending on where the cell is located within the tissue, or if expression levels are homogenous. There are three distinct mesodermal populations that involute at the dorsal blastopore, the leading edge mesendoderm (LEM), prechordal mesoderm (PCM), and the chordamesoderm (CM). Previous estimates of tissue surface tension and viscosity revealed that LEM and CM have very similar properties, these values are decreased by ~40% in the PCM (David et al., 2014). Using smiFISH we could directly compare if these transcripts are enriched in the PCM compared to the LEM and CM. Another hypothesis we could test is whether or not cells located at deeper layers (that are more likely to radially intercalate) express higher levels of Rnd1, which was associated with higher levels of intercalation in our explant spreading assay.

The implementation of the micropipette aspiration assay on embryonic tissue explants has been highly informative to understand the tissue rheology of the wild type tissues and dissect the unique properties of Rnd1 and Shirin. We extracted three values from these experiments: viscosity, tissue surface tension, and the size of the deformation during the initial passive response phase of aspiration. Surface tension and viscosity are well established parameters. Surface tension represents how fast a spherical tissue will return to a spherical state after a

deformation and is impacted by the cell-cell adhesion and cortical tension of the constituent cells (Guevorkian et al., 2011). Viscosity is a measure of how resistant the cells within a tissue are to cell-cell rearrangements (David et al., 2014), therefore tissues with low viscosity have a higher capacity to remodel cell-cell contacts or in general have weaker adhesions. Notably, these values vary with changing aspiration forces (Guevorkian et al., 2010), suggesting that these measurements also reflect the mechanosensitive response of tissues to applied forces and not necessarily the mechanical properties of these tissues at equilibrium. However, we believe that the size of the initial deformation reflects the equilibrium mechanical properties of the tissue. Intriguingly, this is the property that ectoderm and mesoderm displayed the largest differences (Figure 3.10D), with only modest differences in viscosity and tissue surface tension (Figure 3.10E,F). This suggests that mesoderm tissue at equilibrium is even more pliable then when it is under external stresses, though during gastrulation it is unlikely that it ever be allowed to reach equilibrium. All of this poses an intriguing opportunity to establish an assay where we can probe the range of stresses that tissues can dynamically respond to by titrating the aspiration pressures used during these measurements. If we are correct in our assumption and the size of the initial deformation is a measurement of equilibrium properties this value should scale proportionally to the applied force. On the other hand, viscosity and surface tension may show a different response to changing pressures. We could potentially establish the range of stresses that control tissues can respond to, and certain experimental perturbations may affect this mechanosensitve range, allowing a more nuanced analysis.

Chapter III – Summary of findings

In this chapter I provide the first detailed analysis of cell-cell contact remodelling in a model of mesenchymal morphogenesis. This in itself is significant, as the vast majority of existing literature pertaining to cell-cell rearrangement during morphogenesis has focused on epithelial models (Pinheiro and Bellaïche, 2018; Takeichi, 2014). Epithelial and mesenchymal tissues undergo cell-cell rearrangements through entirely different processes: contraction of junctional actomyosin in epithelia and differential cell migration in mesenchyme (Huang and Winklbauer,

2018; Pinheiro and Bellaïche, 2018). Unsurprisingly, I found that the mechanisms driving contact remodelling differed from previous studies focusing on epithelia. While epithelial studies stress the need to remove cadherin through endocytosis (de Beco et al., 2009; Iyer et al., 2019; Levayer et al., 2011; Peglion et al., 2014; Troyanovsky et al., 2006), I find here that simply peeling cadherin thus rupturing the cadherin trans bond suffices without any traces of endocytosis. The cadherin remaining at the contact condenses and must eventually rupture the CCC cytoplasmic link to actin, demonstrating for the first time that the weakest link of the CCC shifts at different stages of adhesive remodelling. Further, instead of contraction of a junctional actomyosin network we observed myosin recruitment adjacent to the contact that, along with the force applied on the contact through differential migration, facilitated the detachment of cells. Finally, while the important interplay between cortical tension and cell-cell adhesion is gaining more attention in terms of setting equilibrium adhesion strength (Maître et al., 2012; Winklbauer, 2015), here I explored how cortical tension influences the non-equilibrium situation of cell contact remodelling and detachment revealing a direct relationship between cortical tension and remodelling strategy.

Chapter III – Outstanding questions and future directions

Interestingly, despite the removal of cadherin from the cell contact, a sub-population persists and even concentrates leading to much denser packing of cadherin at the contact prior to detachment. Super-resolution studies have demonstrated that cadherin clusters have varying degrees of density (Truong Quang et al., 2013; Wu et al., 2015), with some reaching what is referred to as 'crystal lattice density', which refers to the maximal density when cadherin is optimally organized with minimal spacing and saturated trans and cis bonds (Boggon et al., 2002; Harrison et al., 2011). Though we could not determine the actual density of the clusters from our data, the fact that the peak densities of the dnRho injected cells and the densest controls reach very similar levels (2.0-2.5 fold relative increase; Figure 3.6K) could suggest that the clusters at the final stages of remodelling are at or near crystal lattice density. The increasing density as tension is applied could be the result of two processes. First, reorganization and condensation of

clusters of variable density as the contact shrinks as it has been demonstrated that nanoclusters constantly disassemble and reassemble (Indra et al., 2018). Alternatively, peeling may only remove the least dense clusters as denser clusters may require the simultaneous rupture of more adhesive bonds for disruption of the cluster to occur (i.e. the load is distributed across more bonds), so over time the average density increases as only the least dense clusters are removed from the contact. Whether the increase in density is an active or passive process - or a combination of both - remains to be seen.

Despite demonstrating the critical interplay of the actomyosin cytoskeleton and cell-cell adhesion, I was unfortunately unable to find conditions that allowed us to image these components without interfering with the mechanical properties of the cells. Injection of utrophin clearly increased cortical tension likely through enhancing the bundling of actin and its overall connectivity (Belin et al., 2014; Bendix et al., 2008; Ennomani et al., 2016). It may be worthwhile to test other actin probes to find one that will not alter cortical tension, though most are likely to interfere with actin or the recruitment of endogenous actin binding proteins in some way (Belin et al., 2014; Courtemanche et al., 2016; Kumari et al., 2020).

While there may be some hope to find an appropriate probe/conditions to image actin while manipulating cells with the DPA setup, attempts to image myosin were less encouraging. Despite our efforts to find conditions to image myosin (and actin) using our DPA setup we were unable to find conditions that didn't impact the cell cortex. Cortical tension is modulated primarily by myosin contractility (Chugh and Paluch, 2018), so it isn't surprising that injecting MHCIIA RNA or MOs may perturb the cortex. If any amount of MHCIIA MO was present the cells were in a constant state of blebbing that interfered with formation of contact formation and maturation. Attempts to inject MHCIIA-YFP RNA without co-injection of the MO also interfered with contact formation, and when contacts did form the cells appeared more rigid, similar to the utrophin injected cells. Additionally, the effects were inconsistent from experiment to experiment, leading us to rely on cells plated on FN or tissue explants of endogenous mesoderm where we didn't notice any extreme effects on cell behaviour. It is well established that cell-cell (David et al., 2014; Engl et al., 2014; Maître et al., 2012; Toret et al., 2014; Yamada and Nelson, 2007) and cell-matrix (Arthur and Burridge, 2001; Lawson and Burridge, 2014; Wakatsuki et al.,

2003) adhesion modulate the cortex at the site of adhesion via the remodelling of actin and regulation of actomyosin contractility. Though it is unclear if these effects can be propagated outside of the area of the contact, we believe that the extensive cell-cell (in explants) and cell-matrix adhesion (explants and FN plated cells) helped mitigate the effects we observed in isolated dissociated cells. Micropipette aspiration of single cells and doublets of S180 cells (Aladin et al., 2020) and the 8-cell mouse embryo (Maître et al., 2015) did not find differences in cortical tension between single cells and the larger configurations. On the other hand, the cortical tension of cell surfaces at interstitial gaps is decreased (Barua et al., 2017; Parent et al., 2017). Further, using micropatterns to vary the size of cell-matrix adhesions and then probing the stiffness of cells revealed that stiffness decreased with increasing FN adhesion (Al-Kilani et al., 2011). More thorough studies on cell-cell and cell-matrix adhesion modulating properties of the cortex outside of adhesion sites are required.

A previous study manipulating zebrafish progenitor cells also found that one of the cytoplasmic interactions of the CCC ruptures after cells are forced to detach (Maître et al., 2012). While their study implicated the β-catenin/α-catenin link, in our study α-catenin clearly persisted in cadherin clusters after detachment suggesting it was stably bound to the rest of the CCC. To gain further insight it would be helpful to know if in Xenopus the α-catenin/actin is indeed the link that ruptures or if it is part of the cytoskeleton itself. If it is the latter case, the difference could be due to the higher cortical tension – and potentially stronger cortex - of developing zebrafish tissues compared to tissues of the Xenopus gastrula (David et al., 2014; Schötz et al., 2008).

An important next step would be to extend these studies to imaging cadherin in endogenous mesoderm cells within tissue explants, as we have done for myosin. Though I expect it would be impossible to have the same detailed information that we get through the DPA experiments (lateral diffusion would likely be impossible to see), it will be important to demonstrate that the general process of removal of cadherin with a parallel condensation of the remnant holds under physiologically settings.

It will also be critical to get estimates on the cortical tension of utrophin, caRho, and dnRho injected cells to reinforce my indirect observations estimating cortical tension based on the holding pressures required to aspire the cells. It is possible to directly measure cortical tension using the micropipette aspiration (MPA) assay, which would require no changes to my experimental setup. Cortical tension can be calculated by measuring the aspiration pressure required to aspire a deformation of the cell that is equivalent to half the radius of the pipette (Guevorkian and Maître, 2017). However, during my initial attempts to use this technique it was clear that the membrane was detaching from the cortex, thus confounding any measurements as the pressure applied by the aspiration would be split between the membrane deformation and the cortex deformation. Therefore, I will use the doublet assay described in Chapter II (Appendix 2.1; Figure 2.7) to instead get relative estimates of cortical tension.

The pulling protocol used in the DPA experiments simulated the situation where a leading cell was migrating faster than its rear-neighbour, though it is clear that many other orientations occur within the embryo (Huang and Winklbauer, 2018). Radial intercalation of deep cells to more superficial layers and 'sliding' laterally across slower moving neighbours are particularly prominent within the mesoderm. While radial intercalation would be difficult to address, investigating lateral sliding would be attainable. I have briefly explored the following approaches, though did not pursue them further. Using the DPA setup, simply grasping the cells very close to the cell contact would likely be sufficient to emulate sliding. Further, using micropatterned linear FN substrates where one row is free to migrate beside rows of constrained cells. One would expect that the majority of the force applied on the contact during migration in this orientation would be applied parallel, an ideal orientation for peeling.

Chapter II and III – An integration of concepts

Finally, it would be exciting to merge the findings of Chapters II with the approaches in Chapter III by investigating how the cell-cell contacts of ectoderm respond to applied tensions using the DPA setup. Would ectoderm cells rapidly remodel their cell contacts in response to displacement due to their higher cortical tension similar to caRho and utrophin injected

mesoderm cells, or do they have other mechanisms to stabilize their contacts? Further, these assays could help us further characterize the specific roles of Rnd1 and Shirin with respect to cell-cell adhesion. It would be interesting to titrate the levels of Rnd1, Shirin, and dnRho (as a control for generic downregulation of cortex tension) where they all equally decrease the cortical tension so that there are no differences due to magnitude and orientation of applied forces. Shirin and dnRho should in theory have the same effect unless Shirin has a specific role at disrupting cell-cell contacts. The localization of Rnd1 at the contact suggests that it could be the agent responsible for downregulating cortical tension at the cell-cell contact, and thus enhancing the adhesive potential of the cells (Winklbauer, 2015). If this were the case, we would expect that Rnd1 doublets would be more resistant to remodelling as they may be starting from a stronger equilibrium adhesion than dnRho or Shirin injected cells. As ectoderm is still more adhesive than mesoderm, it is not clear whether or not they act through the same pathway to downregulate cortical tension at the contact. Notably, in epithelial cell lines it has been shown that p190 RhoGAP (the downstream effector of Rnd1 antagonism of RhoA) is actively suppressed at the adherens junctions through the myosin IIA dependent recruitment of ROCK1 (Priya et al., 2015; Priya et al., 2017). This maintains Rho-ROCK induced contractility which was required for epithelial integrity. Exploring how cortical tension is regulated at the cell-cell contact to favour adhesion, and how this may differ between tissues of different physical and adhesive properties is a very promising avenue of research.

Interesting questions in cadherin biology

After close to 45 years of intense research since the discovery of cadherins, they will likely be the focus of many decades more of scrutiny. Advancement in our understanding of cadherin has continued to accelerate in recent years, not only describing new phenomena but redefining old ones. Studies of cadherin span many different scales that I covered in Chapter I, and I will highlight some intriguing outstanding questions.

Structural studies have definitively elucidated the adhesive interfaces of type I and type II classic cadherins (Boggon et al., 2002; Brasch et al., 2018; Harrison et al., 2011; Patel et al.,

2006), and similar studies have begun to focus on other members of the cadherin superfamily, e.g. the CDHR15/CDHR23 interface (Sotomayor et al., 2012), and both clustered and non-clustered protocadherins (Cooper et al., 2016; Goodman et al., 2016; Nicoludis et al., 2015; Rubinstein et al., 2015). However, while some effort has been made to understand the extracellular organization of type III and IV classic cadherins (Jin et al., 2012), the adhesive interface is still unknown. This is crucial information, as they represent the classic cadherins for invertebrate model organisms, and many critical studies of cadherin have focused on they type IV classic dE-cadherin in Drosophila (Chandran et al., 2021; Kale et al., 2018; Truong Quang et al., 2013). While all classic cadherins share a common catenin binding cytoplasmic domain, it would be interesting to see if any adaptations are made to compensate for a potentially very different adhesive interface, and to see if similar principles exist for trans and cis interactions in forming clusters. Rigorous comparative studies of type I/II and III/IV classic cadherins would also provide insight into the form and function of the ancient CCC thought to have been present at the rise of multicellularity which was likely most similar to a type III cadherin (Hulpiau and van Roy, 2011).

Many cadherin associated proteins (CAPs) have been identified either directly or in proteomic screens (Guo et al., 2014; discussed above). Since higher fidelity crosslinking techniques have been demonstrated (Troyanovsky et al., 2021), direct comparison of the interactome of cadherin at different stages of a cell-cell contact lifetime (initial formation, maturation, equilibrium, under stress) could reveal new interactions or better explain already established interactors. Similarly, proteomic approaches could be used to better understand cadherin signalling, and even be used to compare the signalling potential of different classic cadherins, as they likely have different CAPs (Scarpa et al., 2015). This would complement the existing literature that compare the binding affinities and tension resistance of different classic cadherins (Thiery et al., 2012).

The recent discovery of E-clusters and C-clusters (Troyanovsky et al., 2021) raises several new avenues of research. The striking observation that vinculin cannot associate with the densely packed E-clusters was surprising, as it is typically assumed that they are the most adhesive clusters and bear much of the load applied on the contact. There is still the possibility that vinculin may be recruited to the periphery of E-clusters, and superresolution microscopy would be useful

here. An attempt to quantify the relative proportion of E to C clusters would be interesting, especially comparisons across the different stages of the contact lifetime, for example, are E-clusters enriched when the contact is under tension? Examination of the most common C-cluster forming CAPs is also important, as well as determining the specific roles they may play at organizing cadherin and the cytoskeleton at the contact.

Finally, the results presented in Chapter III provide a much-needed description of adhesion disassembly and remodelling during cell-cell rearrangements. While models have been proposed involving cadherin treadmilling and endocytic recycling during collective migration (Peglion et al., 2014), this is the only direct demonstration of how cadherin adhesions can be remodelled to facilitate cell rearrangements. Most existing literature perturbs some property important to cadherin regulation and uses indirect readouts of general impacts on cell-cell rearrangements or other morphogenetic processes, that while informative, do not speak to how the CCC is remodelled at the molecular level.

To conclude, the work presented in this thesis addressed two important questions, finding cortical tension and cell-cell adhesion at the root of each. First, how is motility differentially regulated between tissues in a developing embryo, and second, how do the stresses provided by cell motility stimulate the remodelling of cell contacts and the rearrangement of cells we see during morphogenesis.

References

Aladin, D. M. K., Chu, Y. S., Robinson, R. C., Dufour, S., Viasnoff, V., Borghi, N. and Thiery, J. P. (2020). Extracellular domains of E-cadherin determine key mechanical phenotypes of an epithelium through cell- And non-cell-autonomous outside-in signalling. *bioRxiv*.

Al-Kilani, A., de Freitas, O., Dufour, S. and Gallet, F. (2011). Negative feedback from integrins to cadherins: A micromechanical study. *Biophysical Journal* **101**, 336–344.

Arthur, W. T. and Burridge, K. (2001). RhoA inactivation by p190RhoGAP regulates cell spreading and migration by promoting membrane protrusion and polarity. *Molecular Biology of the Cell* **12**, 2711–2720.

Barua, D., Parent, S. E. and Winklbauer, R. (2017). Mechanics of Fluid-Filled Interstitial Gaps. II. Gap Characteristics in Xenopus Embryonic Ectoderm. *Biophysical Journal* **113**, 923–936.

Belin, B. J., Goins, L. M. and Mullins, R. D. (2014). Comparative analysis of tools for live cell imaging of actin network architecture. *BioArchitecture* **4**, 189–202.

Bendix, P. M., Koenderink, G. H., Cuvelier, D., Dogic, Z., Koeleman, B. N., Brieher, W. M., Field, C. M., Mahadevan, L. and Weitz, D. A. (2008). A quantitative analysis of contractility in active cytoskeletal protein networks. *Biophysical Journal* **94**, 3126–3136.

Boggon, T. J., Murray, J., Chappuis-Flament, S., Wong, E., Gumbiner, B. M. and Shapiro, L. (2002). C-cadherin ectodomain structure and implications for cell adhesion mechanisms. *Science* **296**, 1308–1313.

Brasch, J., Katsamba, P. S., Harrison, O. J., Ahlsén, G., Troyanovsky, R. B., Indra, I., Kaczynska, A., Kaeser, B., Troyanovsky, S., Honig, B., et al. (2018). Homophilic and Heterophilic Interactions of Type II Cadherins Identify Specificity Groups Underlying Cell-Adhesive Behavior. *Cell Reports* **23**, 1840–1852.

Chandran, R., Kale, G., Philippe, J. M., Lecuit, T. and Mayor, S. (2021). Distinct actin-dependent nanoscale assemblies underlie the dynamic and hierarchical organization of E-cadherin. *Current Biology* **31**, 1726-1736.e4.

Chugh, P. and Paluch, E. K. (2018). The actin cortex at a glance. *Journal of Cell Science* **131**, 1–9.

Cooper, S. R., Jontes, J. D. and Sotomayor, M. (2016). Structural determinants of adhesion by protocadherin-19 and implications for its role in epilepsy. *eLife* **5**, 1–22.

Courtemanche, N., Pollard, T. D. and Chen, Q. (2016). Avoiding artefacts when counting polymerized actin in live cells with LifeAct fused to fluorescent proteins. *Nature Cell Biology* **18**, 676–683.

David, R., Luu, O., Damm, E. W., Wen, J. W. H., Nagel, M. and Winklbauer, R. (2014). Tissue cohesion and the mechanics of cell rearrangement. *Development (Cambridge)* **141**, 3672–3682.

de Beco, S., Gueudry, C., Amblard, F. and Coscoy, S. (2009). Endocytosis is required for E-cadherin redistribution at mature adherens junctions. *Proceedings of the National Academy of Sciences of the United States of America* **106**, 7010–7015.

Engl, W., Arasi, B., Yap, L. L., Thiery, J. P. and Viasnoff, V. (2014). Actin dynamics modulate mechanosensitive immobilization of E-cadherin at adherens junctions. *Nature Cell Biology* **16**, 584–591.

Ennomani, H., Letort, G., Guérin, C., Martiel, J. L., Cao, W., Nédélec, F., de La Cruz, E. M., Théry, M. and Blanchoin, L. (2016). Architecture and Connectivity Govern Actin Network Contractility. *Current Biology* **26**, 616–626.

Goodman, K. M., Rubinstein, R., Thu, C. A., Mannepalli, S., Bahna, F., Ahlsén, G., Rittenhouse, C., Maniatis, T., Honig, B. and Shapiro, L. (2016). γ-Protocadherin structural diversity and functional implications. *eLife* **5**, 1–25.

Guevorkian, K. and Maître, J. L. (2017). Micropipette aspiration: A unique tool for exploring cell and tissue mechanics in vivo. *Methods in Cell Biology* **139**, 187–201.

Guevorkian, K., Colbert, M.-J., Durth, M., Dufour, S. and Brochard-Wyart, F. (2010). Aspiration of biological viscoelastic drops. *Physical review letters* **104**, 218101.

Guevorkian, K., Gonzalez-Rodriguez, D., Carlier, C., Dufour, S. and Brochard-Wyart, F. (2011). Mechanosensitive shivering of model tissues under controlled aspiration. *Proceedings of the National Academy of Sciences of the United States of America* **108**, 13387–13392.

Guo, Z., Neilson, L. J., Zhong, H., Murray, P. S., Zanivan, S. and Zaidel-Bar, R. (2014). E-cadherin interactome complexity and robustness resolved by quantitative proteomics. *Science Signalling* **7**, 1–13.

Harrison, O. J., Jin, X., Hong, S., Bahna, F., Ahlsen, G., Brasch, J., Wu, Y., Vendome, J., Felsovalyi, K., Hampton, C. M., et al. (2011). The extracellular architecture of adherens junctions revealed by crystal structures of type i cadherins. *Structure* **19**, 244–256.

Huang, Y. and Winklbauer, R. (2018). Cell migration in the Xenopus gastrula. *Wiley interdisciplinary reviews. Developmental biology* **7**, e325.

Hulpiau, P. and Van Roy, F. (2011). New insights into the evolution of metazoan cadherins. *Molecular Biology and Evolution* **28**, 647–657.

Indra, I., Choi, J., Chen, C. S., Troyanovsky, R. B., Shapiro, L., Honig, B. and Troyanovsky, S. M. (2018). Spatial and temporal organization of cadherin in punctate adherens junctions.

Proceedings of the National Academy of Sciences of the United States of America **115**, E4406–E4415.

Iyer, K. V., Piscitello-Gómez, R., Paijmans, J., Jülicher, F. and Eaton, S. (2019). Epithelial Viscoelasticity Is Regulated by Mechanosensitive E-cadherin Turnover. *Current Biology* **29**, 578-591.e5.

Jin, X., Walker, M. A., Felsövályi, K., Vendome, J., Bahna, F., Mannepalli, S., Cosmanescu, F., Ahlsen, G., Honig, B. and Shapiro, L. (2012). Crystal structures of Drosophila N-cadherin ectodomain regions reveal a widely used class of Ca 2+-free interdomain linkers. *Proceedings of the National Academy of Sciences of the United States of America* **109**,.

Kale, G. R., Yang, X., Philippe, J. M., Mani, M., Lenne, P. F. and Lecuit, T. (2018). Distinct contributions of tensile and shear stress on E-cadherin levels during morphogenesis. *Nature Communications* **9**,.

Kumari, A., Kesarwani, S., Javoor, M. G., Vinothkumar, K. R. and Sirajuddin, M. (2020). Structural insights into actin filament recognition by commonly used cellular actin markers. *The EMBO Journal* **39**, 1–13.

Lawson, C. D. and Burridge, K. (2014). The on-off relationship of Rho and Rac during integrin-mediated adhesion and cell migration. *Small GTPases* **5**,.

Levayer, R., Pelissier-Monier, A. and Lecuit, T. (2011). Spatial regulation of Dia and Myosin-II by RhoGEF2 controls initiation of E-cadherin endocytosis during epithelial morphogenesis. *Nature Cell Biology* **13**, 529–540.

Maître, J. L., Berthoumieux, H., Krens, S. F. G., Salbreux, G., Jülicher, F., Paluch, E. and Heisenberg, C. P. (2012). Adhesion functions in cell sorting by mechanically coupling the cortices of adhering cells. *Science* **338**, 253–256.

Maître, J. L., Niwayama, R., Turlier, H., Nedelec, F. and Hiiragi, T. (2015). Pulsatile cell-autonomous contractility drives compaction in the mouse embryo. *Nature Cell Biology* **17**, 849–855.

Nicoludis, J. M., Lau, S. Y., Schärfe, C. P. I., Marks, D. S., Weihofen, W. A. and Gaudet, R. (2015). Structure and Sequence Analyses of Clustered Protocadherins Reveal Antiparallel Interactions that Mediate Homophilic Specificity. *Structure* **23**, 2087–2098.

Parent, S. E., Barua, D. and Winklbauer, R. (2017). Mechanics of Fluid-Filled Interstitial Gaps. I. Modeling Gaps in a Compact Tissue. *Biophysical journal* **113**, 913–922.

Patel, S. D., Ciatto, C., Chen, C. P., Bahna, F., Rajebhosale, M., Arkus, N., Schieren, I., Jessell, T. M., Honig, B., Price, S. R., et al. (2006). Type II Cadherin Ectodomain Structures: Implications for Classical Cadherin Specificity. *Cell* **124**, 1255–1268.

Peglion, F., Llense, F. and Etienne-Manneville, S. (2014). Adherens junction treadmilling during collective migration. *Nature Cell Biology* **16**, 639–651.

Pinheiro, D. and Bellaïche, Y. (2018). Mechanical Force-Driven Adherens Junction Remodelling and Epithelial Dynamics. *Developmental Cell* **47**, 3–19.

Priya, R., Gomez, G. A., Budnar, S., Verma, S., Cox, H. L., Hamilton, N. A. and Yap, A. S. (2015). Feedback regulation through myosin II confers robustness on RhoA signalling at E-cadherin junctions. *Nature Cell Biology* **17**, 1282–1293.

Priya, R., Liang, X., Teo, J. L., Duszyc, K., Yap, A. S. and Gomez, G. A. (2017). ROCK1 but not ROCK2 contributes to RhoA signalling and NMIIA-mediated contractility at the epithelial zonula adherens. *Molecular Biology of the Cell* **28**, 12–20.

Rubinstein, R., Thu, C. A., Goodman, K. M., Wolcott, H. N., Bahna, F., Mannepalli, S., Ahlsen, G., Chevee, M., Halim, A., Clausen, H., et al. (2015). Molecular Logic of Neuronal Self-Recognition through Protocadherin Domain Interactions. *Cell* **163**, 629–642.

Scarpa, E., Szabó, A., Bibonne, A., Theveneau, E., Parsons, M. and Mayor, R. (2015). Cadherin Switch during EMT in Neural Crest Cells Leads to Contact Inhibition of Locomotion via Repolarization of Forces. *Developmental cell* **34**, 421–434.

Schötz, E. M., Burdine, R. D., Jülicher, F., Steinberg, M. S., Heisenberg, C. P. and Foty, R. A. (2008). Quantitative differences in tissue surface tension influence zebrafish germ layer positioning. *HFSP Journal* **2**, 42–56.

Sotomayor, M., Weihofen, W. A., Weihofen, W. A. and Corey, D. P. (2012). Structure of a force-conveying cadherin bond essential for inner-ear mechanotransduction. *Nature* **492**, 128–132.

Takeichi, M. (2014). Dynamic contacts: Rearranging adherens junctions to drive epithelial remodelling. *Nature Reviews Molecular Cell Biology* **15**, 397–410.

Thiery, J. P., Engl, W., Viasnoff, V. and Dufour, S. (2012). Biochemical and biophysical origins of cadherin selectivity and adhesion strength. *Current Opinion in Cell Biology* **24**, 614–619.

Toret, C. P., Collins, C. and Nelson, W. J. (2014). An Elmo-Dock complex locally controls rho gtpases and actin remodelling during cadherin-mediated adhesion. *Journal of Cell Biology* **207**, 577–587.

Troyanovsky, R. B., Sokolov, E. P. and Troyanovsky, S. M. (2006). Endocytosis of cadherin from intracellular junctions is the driving force for cadherin adhesive dimer disassembly. *Molecular biology of the cell* **17**, 3484–3493.

Troyanovsky, R. B., Sergeeva, A. P., Indra, I., Chen, C., Kato, R. and Shapiro, L. (2021). Sorting of cadherin – catenin-associated proteins into individual clusters. 1–11.

Truong Quang, B. A., Mani, M., Markova, O., Lecuit, T. and Lenne, P. F. (2013). Principles of E-cadherin supramolecular organization in vivo. *Current Biology* **23**, 2197–2207.

Tsanov, N., Samacoits, A., Chouaib, R., Traboulsi, A. M., Gostan, T., Weber, C., Zimmer, C., Zibara, K., Walter, T., Peter, M., et al. (2016). SmiFISH and FISH-quant - A flexible single RNA detection approach with super-resolution capability. *Nucleic Acids Research* **44**,.

Wakatsuki, T., Wysolmerski, R. B. and Elson, E. L. (2003). Mechanics of cell spreading: Role of myosin II. *Journal of Cell Science* **116**, 1617–1625.

Winklbauer, R. (2015). Cell adhesion strength from cortical tension - an integration of concepts. *Journal of cell science* **128**, 3687–3693.

Wu, Y., Kanchanawong, P. and Zaidel-Bar, R. (2015). Actin-Delimited Adhesion-Independent Clustering of E-Cadherin Forms the Nanoscale Building Blocks of Adherens Junctions. *Developmental Cell* **32**, 139–154.

Yamada, S. and Nelson, W. J. (2007). Localized zones of Rho and Rac activities drive initiation and expansion of epithelial cell-cell adhesion. *Journal of Cell Biology* **178**, 517–527.